

REGIONAL AND SPECIES LEVEL RESPONSES OF SCLERACTINIAN CORALS
UNDER GLOBAL CHANGE WITHIN THE CARIBBEAN SEA

Colleen Bove

A dissertation submitted to the faculty at the University of North Carolina at Chapel Hill in
partial fulfilment of the requirements for the degree of Doctor of Philosophy in the
Environment, Ecology, and Energy Program.

Chapel Hill
2020

Approved by:

Karl D. Castillo

Sarah W. Davies

Michael F. Piehler

Justin B. Ries

James Umbanhowar

© 2020
Colleen Bove
ALL RIGHTS RESERVED

ABSTRACT

Colleen Bove: Regional and species level responses of Scleractinian corals under global change within the Caribbean Sea
(Under the direction of Karl D. Castillo)

Human-induced global change has caused rapid increases in ocean temperature (warming) and declines in seawater pH (acidification), and are expected to have negative impacts on tropical reef-building corals globally. Abnormally high seawater temperatures disrupt the symbiosis between corals and their algal endosymbiont in a process known as ‘coral bleaching.’ During such bleaching events, calcification rates decline and physiological processes deteriorate. Additionally, corals rely heavily on elevated seawater pH in order to support and maintain production of their calcium carbonate skeletons. Together, changes in ocean temperatures and seawater pH pose serious threats to coral reefs, foundational ecosystems that provide habitat for countless essential fisheries, while also acting as natural buffers from storms and providing major economic support for tropical coastal communities. Identifying how these global scale stressors impact Caribbean coral reefs is critical in understanding community composition and coral abundance on future reefs.

This dissertation employs an interdisciplinary suite of techniques to assess the impacts of ocean acidification and warming on the growth and physiology of Caribbean corals to improve understandings of the responses of coral under projected global change, and provide a framework for similar future studies. Through the use of a meta-analysis (Chapter 1), I identified trends in coral calcification throughout the Greater Caribbean Sea in

response to experimental ocean acidification and warming, and performed quantitative assessment of experimental design effects on coral calcification rates. I then conducted a 93-day simulated ocean acidification and warming mesocosm experiment to identify growth (Chapter 2, 4) and physiological (Chapter 3) responses of several species of common Caribbean corals. The results from this work highlight the diversity of responses of Caribbean corals to projected global change at individual and species levels, as well as between the coral host and algal endosymbiont. Overall, the variation in growth and physiological responses of these important Caribbean coral species under ocean acidification and warming is critical in predicting the future ‘winners’ and ‘losers’ of Caribbean reefs as global change unfolds.

For my amazing husband and of course, for the corals.

ACKNOWLEDGEMENTS

I am so extremely thankful for all the support from everyone I have received throughout the years that has helped me get to this point. Thank you so much to my advisor Karl Castillo for recognizing and encouraging my excitement for research and coral reefs from the beginning. Thank you to James Umbanhowar and Mike Piehler for serving on my committee and providing extensive support and guidance over the last five years, and especially to committee members Justin Ries and Sarah Davies for hosting me in your labs, allowing me to conduct the research questions I sought to address. Additionally, thank you so much to my mentors Alina Szmant, Jaye Cable, John Bruno, and Emily Eidam who answered countless questions about being a scientist, a mentor, and an overall better person, you all helped me so much more than you know.

Thank you to all my wonderful Northeastern friends, Isaac Westfield, Amanda Dwyer, Francis Choi, Sara Williams, Louise Cameron, Sara Schaal and many others, for welcoming me into your community and supporting me along my entire journey. To all my colleagues and friends, JP Rippe, Justin Baumann, Kaylyn Gootman, Shelby Ziegler, and so many others, I thank you for being my sanity and sounding board for everything, and inspiring my love for my research and everything coral. To my family, Mom, Dad, Kate, Mary, Stuart, Chris, and Josie, thank you for all you have put up with and all the sacrifices you made to help me to get here. And finally, to Matt for all selflessness in supporting me and keeping me smiling, I could not be here without you.

TABLE OF CONTENTS

LIST OF TABLES	xi
LIST OF FIGURES	xii
LIST OF ABBREVIATIONS.....	xiii
INTRODUCTION	1
CHAPTER 1: META-ANALYSIS REVEALS REDUCED CORAL CALCIFICATION UNDER PROJECTED OCEAN WARMING BUT NOT UNDER ACIDIFICATION ACROSS THE CARIBBEAN SEA.....	5
Introduction.....	5
Methods.....	8
<i>Study selection</i>	8
<i>Data extraction and preparation</i>	8
<i>Calculation of effect size</i>	10
<i>Statistical analyses</i>	11
Results.....	12
<i>Overall calcification response</i>	12
<i>Calcification response of Florida Keys versus Belize corals</i>	13
<i>Temperature and aragonite saturation state impacts on calcification rates across studies</i>	13
<i>Experimental design impacts on coral calcification rate in studies</i>	13
Discussion.....	14
<i>Ocean warming, but not acidification, independently impairs calcification of Caribbean reef-building corals</i>	15

<i>Calcification responses to global change stressors vary by region within the Caribbean</i>	17
<i>Experimental design considerations and recommendations for future research</i>	20
Conclusions.....	23
CHAPTER 2: COMMON CARIBBEAN CORALS EXHIBIT HIGHLY VARIABLE RESPONSES TO FUTURE ACIDIFICATION AND WARMING	30
Introduction.....	30
Materials and methods	33
<i>Experimental design</i>	33
<i>Measured and calculated parameters</i>	34
<i>Quantification of calcification and linear extension</i>	34
<i>Colony-level effects of basal calcification rate on calcification response to stress</i>	35
<i>Statistical analyses</i>	36
Results.....	36
<i>Calcification rates</i>	36
<i>Colony-level calcification response to stress</i>	37
<i>Linear extension</i>	38
Discussion.....	38
<i>Caribbean corals exhibit nonlinear calcification responses to pCO₂ and temperature</i>	38
<i>Faster-growing colonies may be more vulnerable to pCO₂ and thermal stress</i>	41
<i>All coral species, except <i>S. siderea</i>, exhibited net skeletal dissolution under the highest pCO₂</i>	42
<i><i>Siderastrea siderea</i> and <i>P. astreoides</i> maintain constant rates of linear extension under pCO₂ and thermal stress</i>	44

<i>Experiments reveal corals' differential resilience to future oceanic change</i>	45
CHAPTER 3: GLOBAL CHANGE ALTERS CORAL HOLOBIONT PHYSIOLOGY AND SUGGESTS FUTURE SHIFTS IN CARIBBEAN CORAL REEF DIVERSITY.....	50
Introduction.....	50
Methods.....	54
<i>Experimental design</i>	54
<i>Host and symbiont physiological measurements</i>	55
<i>Statistical analysis of coral holobiont physiology</i>	57
<i>Siderastrea siderea transcriptome preparation and differential gene expression analysis</i>	58
<i>Weighted gene co-expression network analysis and module gene ontology enrichment</i>	59
Results.....	60
<i>Coral host and algal endosymbiont physiology</i>	60
<i>Principal component analysis of coral holobiont physiology</i>	61
<i>Siderastrea siderea host and algal endosymbiont transcriptomic responses to temperature and pCO₂</i>	62
<i>Weighted gene correlation network analysis</i>	63
Discussion	65
<i>Coral host total energy reserves show little change under simulated global change</i>	65
<i>Algal endosymbionts exhibit productivity loss under ocean acidification</i>	66
<i>Species-specific holobiont physiology highlights overall response to ocean acidification</i>	70
<i>Siderastrea siderea coral host exhibits greater transcriptomic response to global change stressors</i>	72

Conclusions.....	75
CHAPTER 4: EXTREME OCEAN ACIDIFICATION ALTERS SKELETAL MORPHOLOGY IN A CARIBBEAN REEF-BUILDING CORAL	82
Introduction.....	82
Methods.....	84
<i>Experimental design</i>	84
<i>Assessment of corallite height and infilling</i>	85
<i>Septa and septal peak rugosity</i>	86
<i>Statistical analyses</i>	86
Results.....	87
<i>Corallite height and percent skeletal infilling</i>	87
<i>Septal peak rugosity</i>	88
<i>Septal ridge rugosity</i>	88
<i>Qualitative assessment of septa alterations due to treatment</i>	88
Discussion	89
<i>Ocean acidification drives greater differences in corallite morphology than warming</i>	89
<i>Morphological plasticity of corallites determined by natal reef environment</i>	93
<i>Future directions and implications</i>	94
APPENDIX 1: SUPPLEMENTAL DESCRIPTIONS AND FIGURES – CHAPTER 1.....	103
APPENDIX 2: SUPPLEMENTAL DESCRIPTIONS AND FIGURES – CHAPTER 2.....	113
APPENDIX 3: SUPPLEMENTAL DESCRIPTIONS AND FIGURES – CHAPTER 3.....	150
APPENDIX 4: SUPPLEMENTAL DESCRIPTIONS AND FIGURES – CHAPTER 4.....	166
REFERENCES	178

LIST OF TABLES

Table 1.1 Experimental design effect sizes.....	29
Table 2.1 Average experimental treatment conditions	49
Table 2.1 Summary of <i>Siderastrea siderea</i> RNA libraries.....	81

LIST OF FIGURES

Figure 1.1 Map of meta-analysis study sites.....	24
Figure 1.2 Global effect size of meta-analysis treatments.....	25
Figure 1.3 Regional effect size of meta-analysis treatments.....	26
Figure 1.4 Magnitude analysis of temperature on calcification rates.....	27
Figure 1.5 Magnitude analysis of aragonite saturation state on calcification rates.....	28
Figure 2.1 Net coral calcification rates.....	46
Figure 2.2 Colony-level calcification response to treatment.....	47
Figure 2.3 Coral linear extension rates.....	48
Figure 3.1 Coral host and algal endosymbiont physiology.....	76
Figure 3.2 Coral holobiont physiology principal component analyses.....	77
Figure 3.3 <i>Siderastrea siderea</i> host and algal endosymbiont gene expression.....	78
Figure 3.4 WGCNA analysis of <i>Siderastrea siderea</i> host gene expression.....	79
Figure 3.5 Summary of physiological responses to treatment.....	80
Figure 4.1 Diagram of corallite height and infilling methodology.....	96
Figure 4.2 Representative SEM image of corallite morphology.....	97
Figure 4.3 Corallite height and infilling in response to temperature and $p\text{CO}_2$	98
Figure 4.4 Representative SEM images of control versus extreme treatment morphology ...	99
Figure 4.5 <i>Siderastrea siderea</i> septal peak rugosity in response to experimental treatment	100
Figure 4.6 <i>Siderastrea siderea</i> septal ridge rugosity in response to experimental treatment	101
Figure 4.7 Representative images of skeletal dissolution and pitting.....	102

LIST OF ABBREVIATIONS

SE	Standard error
AIC	Akaike's information criterion
ATP	Adenosine triphosphate
BP	Biological processes
C	Celsius
Ca ²⁺	Calcium
CaCO ₃	Calcium carbonate
CC	Cellular component
CO ₂	Carbon dioxide
DEG	Differentially expressed genes
DIC	Dissolved inorganic carbon
FDR	False discovery rate
GO	Gene ontology
H ⁺	Hydrogen / proton
HCO ₃ ⁻	Bicarbonate
IPCC	Intergovernmental Panel on Climate Change
MBRS	Mesoamerican Barrier Reef System
MF	Molecular function
N	Sample size
PC	Principal component
PCA	Principal component analysis
<i>p</i> CO ₂	Partial pressure of carbon dioxide

Q_E	Residual heterogeneity
Q_M	Test of moderators
s	Standard deviation
SEM	Scanning electron microscope
SMD	Standard mean difference
SST	Sea surface temperature
T0	Initial time point
T90	Final time point
TA	Total alkalinity
μatm	Micro atmospheres
WGCNA	Weighted gene co-expression network analysis
Y	Mean calcification response
Ω_{Arag}	Aragonite saturation state

INTRODUCTION

Increasing atmospheric carbon dioxide from anthropogenic sources is of growing concern as global average $p\text{CO}_2$ concentrations have now surpassed 400 μatm , and are rapidly approaching 410 μatm (Tans and Keeling 2017). Even with significant reductions in anthropogenic carbon emissions, associated atmospheric warming will likely exceed 2.0°C by the end of the century (Mauritsen and Pincus 2017, Raftery et al. 2017). This rapid change in atmospheric $p\text{CO}_2$ has resulted in negative and often irreversible impacts on both terrestrial and marine ecosystems worldwide (Solomon et al. 2009, Pecl et al. 2017). In terrestrial ecosystems, rising surface temperatures have posed serious threats to many animals that are unable to cope with increasingly common and abnormally high thermal stress events (Caruso et al. 2014, Gunderson and Stillman 2015, Urban 2015, Pacifici et al. 2017). Similarly, marine ecosystems around the world are under unprecedented threats from global change stressors, especially ocean warming and ocean acidification (Sabine et al. 2004, Hoegh-Guldberg et al. 2007, Doney et al. 2009, Burrows et al. 2011).

Ocean warming is a major concern for marine organisms, especially at lower latitudes due to the projected loss of species richness as they migrate to higher latitudes seeking cooler waters (Burrows et al. 2014, Stuart-Smith et al. 2015). Reef-building corals are especially threatened, as they currently live within a degree of their thermal maxima (Jokiel and Coles 1977, Kleypas et al. 1999). With increasing occurrence of record-breaking mass bleaching and mortality events, increasing SST will have huge consequences for the survival of corals

globally (Hughes et al. 2017b). Abnormally high seawater temperatures disrupt the symbiosis between corals and their endosymbiotic photosynthetic algal endosymbiont (*Symbiodiniaceae*) in a process known as ‘coral bleaching’ (Glynn 1991, Brown 1997). During thermal bleaching, calcification rates decline and physiological processes deteriorate (Jokiel and Coles 1977, Grottoli et al. 2006, Castillo et al. 2014, Davies et al. 2016). As a result, mortality rates increase due to the strong dependence of corals on their endosymbionts, which can contribute up to 100% of their daily metabolic requirements (Muscatine et al. 1981). The breakdown of this important symbiosis during acute ocean warming events impacts the ability of reef-building corals to counter additional environmental stressors.

Along with ocean warming, rising atmospheric $p\text{CO}_2$ drives an increase in CO_2 dissolution into the world’s oceans, increasing bicarbonate ion concentrations $[\text{HCO}_3^-]$ in seawater and reducing surface ocean pH, commonly referred to as ocean acidification (Orr et al. 2005). Calcifying marine organisms, especially reef-building corals, rely heavily on elevated seawater pH (relative to environmental seawater) and supersaturated aragonite saturation state (Ω_{ar}) at the site of calcification to precipitate their calcium carbonate (CaCO_3) skeletons and shells (Orr et al. 2005, Schneider and Erez 2006, Doney et al. 2009). Studies have shown negative growth responses (Reynaud et al. 2003, Jury et al. 2010, Krief et al. 2010, Ries et al. 2010, Comeau et al. 2013b, Bove et al. 2019), a parabolic calcification response (Castillo et al. 2014), and no growth response (Reynaud et al. 2003, Jury et al. 2010, Bove et al. 2019) to increasing $p\text{CO}_2$ concentrations.

Recently, focus has shifted towards understanding how the combination of increasing $p\text{CO}_2$ and temperature affect reef-building corals as these two climate stressors continue to co-occur. In general, temperature seems to pose a greater threat to reef-building corals than $p\text{CO}_2$

(Carricart-Ganivet et al. 2012, Chua et al. 2013, Castillo et al. 2014, Venti et al. 2014, Davies et al. 2016, Okazaki et al. 2017), however, the interaction of the two stressors may further complicate coral reef responses to climate change. For example, some studies have found the combination of $p\text{CO}_2$ and temperature to cause a more negative growth response in corals than either stressor alone (Reynaud et al. 2003, Agostini et al. 2013, Horvath et al. 2016, Prada et al. 2017), while other studies report no interactive response (Edmunds et al. 2012, Schoepf et al. 2013, Okazaki et al. 2017, Bove et al. 2019). Numerous explanations have been suggested for the wide array of responses, including differences in heterotrophy rates or food availability (Edmunds 2011, Towle et al. 2015, Brown et al. 2018), evolutionary divergence and its role in the calcification process (Brown and Edmunds 2016), minute physiological control of the chemistry in the calcifying fluid (Agostini et al. 2013, Holcomb et al. 2014, Barott et al. 2015, Cai et al. 2016), and differences in experimental design and manipulation (Cornwall and Hurd 2016).

Although significant research has been performed to elucidate the response of reef-building corals to ocean acidification and warming stress, several gaps in our knowledge still remain. For example, very few studies have been performed specifically on Caribbean reef-building coral species, and often the scope of these studies is limited to a single species or measured response (Castillo et al. 2014, Horvath et al. 2016, Okazaki et al. 2017, Bove et al. 2019). Additionally, fewer of these studies have measured multiple physiological and growth parameters in tandem (Grottoli et al. 2014, Towle et al. 2015). Understanding these studies in the context of one another provides the unique opportunity to identify potential regions or species more likely to persist under changing ocean condition, while identifying strengths or pitfalls in experimental design considerations. In order to fully understand the responses of

Caribbean reef-building corals under projected global change, it is imperative to build a region-wide understanding of the growth responses of corals under simulated global change conditions through synthesis of multiple comprehensive studies.

This PhD dissertation explores the responses of Caribbean corals under global change stressors, specifically ocean acidification and warming, using a variety of approaches to assess the future success of reef-building corals throughout the Greater Caribbean Sea. Chapter 1 combines traditional meta-analytical techniques with additional analyses to synthesize previously reported Caribbean coral calcification rates in response to experimentally-induced ocean acidification and warming treatments. Chapter 2 quantifies skeletal growth and survival of four common Caribbean coral species in a 93-day ocean acidification and warming mesocosm experiment. Chapter 3 builds upon the previous chapter by assessing the physiological responses of the coral host and algal endosymbiont of three of the coral species included in the 93-day mesocosm experiment, and further investigating those physiological responses in one species through transcriptomic analyses. Finally, Chapter 4 quantifies minute alterations to the coral skeleton after prolonged exposure to ocean acidification and warming conditions in *Siderastrea siderea* to better understand how coral calcification is being altered by these global change stressors. Together, this dissertation identifies species-specific responses under global change, as well as the role of the coral host and algal endosymbiont in such responses, to understand how future Caribbean coral reefs may cope with changing ocean conditions.

CHAPTER 1: META-ANALYSIS REVEALS REDUCED CORAL CALCIFICATION UNDER PROJECTED OCEAN WARMING BUT NOT UNDER ACIDIFICATION ACROSS THE CARIBBEAN SEA¹

Introduction

Reef-building corals provide the three-dimensional framework for tropical coral reef ecosystems across the globe, supporting many important ecological and economic goods and services (Costanza et al. 2014). However, coral reefs globally are experiencing declines in diversity and abundance (Pandolfi et al. 2003), raising concerns for the overall health of these essential ecosystems. Such changes in coral reef ecosystems are especially evident throughout the Caribbean Sea (Alvarez-Filip et al. 2009, Schutte et al. 2010). Declines in carbonate production rates (Perry et al. 2013) and reduced coral cover (Cote et al., 2005) on Caribbean reefs have shifted these ecosystems to less structurally complex reefs dominated by algae, sponges, and gorgonians (Norstrom et al. 2009). Over the past two decades, ocean warming and acidification have been identified as two of the primary stressors causing this shift and therefore there have been widespread efforts to better understand how coral reefs will likely respond to projected increases in these two human-induced global change stressors (Stoltenberg et al. , Kleypas et al. 1999, Doney et al. 2009, Enochs et al. 2016).

The Intergovernmental Panel on Climate Change (IPCC) has projected that sea surface temperatures in the Caribbean region could rise between 0.6 and 3.0°C by the end of

¹ This chapter previously appeared as an article in *Frontiers in Marine Science*. The original citation is as follows: Bove C.B., Umbanhowar J., and Castillo K.D. “Meta-analysis reveals reduced coral calcification under projected ocean warming but not under acidification across the Caribbean Sea” *Frontiers in Marine Science*, 7, no. 127 (February 2020): 1–11.

the 21st century (ocean warming), and atmospheric $p\text{CO}_2$ will surpass 600 μatm , causing surface ocean pH to decrease by 0.1–0.3 pH units (ocean acidification) (IPCC 2014). These projections pose significant threats to reef-building corals throughout the Caribbean, causing mass mortality events, reducing recruitment, deteriorating key physiological processes, and lowering coral calcification rates (Jokiel and Coles 1977, Grottoli et al. 2006, Davies et al. 2016, Okazaki et al. 2017). Despite the consensus that global change will negatively affect Caribbean reef-building corals, the extent of these impacts vary widely by species, region, or measured physiological response parameter (Harvey et al. 2013). A great example of such variation in coral responses to ocean acidification and warming is seen in Okazaki et al. (2017) where some species exhibited no response to ocean acidification or warming while other corals in the same experiment exhibited reduced calcification under one or both stressors. Furthermore, a study conducted by Kenkel et al. (2015) demonstrated a variety of physiological responses (i.e., calcification and Symbiodiniaceae physiology) of corals under ocean warming even within a single species. Understanding the variability in coral responses depicted in previous studies under projected ocean acidification and warming will improve our ability to predict how coral reef ecosystems will be impacted under global change stressors.

Meta-analyses are valuable tools for combining the findings from multiple studies to summarize results across the literature (Gurevitch and Hedges 1999). Although the use of meta-analyses to better understand biological responses to ocean acidification and warming are common (Kroeker et al. 2010, Harvey et al. 2013, Kelley and Lunden 2017), few have focused specifically on reef-building corals (Chan and Connolly 2013). Further, those analysing corals have not addressed the combined effects of ocean acidification and warming

(Harvey et al. 2013). Because these two stressors are not likely to act on reef-building corals independently from one another (Halpern et al. 2007), analyses that investigate the combined effects of acidification and warming provide a more realistic view of the future of tropical coral reefs. Caribbean coral reefs are experiencing region-wide declines more severely than reefs in the Red Sea and the Australian Great Barrier Reef (Pandolfi et al. 2003, Gattuso et al. 2014), highlighting the need to study coral reefs on more local scales. Because of projected further declines in Caribbean coral reefs, a better understanding of how these global stressors are impacting reef-building corals within this ocean basin is necessary for predicting the future success of these important marine ecosystems.

Here, we implement a meta-analysis approach of the peer-reviewed literature to investigate the impacts of experimentally induced ocean acidification, ocean warming, and the combination of acidification and warming on calcification responses of Caribbean corals under projected global change. This meta-analysis aims to address the following questions: (1) How do Caribbean corals respond to ocean acidification and ocean warming in isolation, and to the combined effects of acidification and warming? (2) How do coral calcification responses to these stressors vary by region within the Caribbean? In addressing these questions, this analysis will further the understanding of Caribbean-wide coral calcification responses under projected global change stressors, while providing future steps to improve this knowledge.

Methods

Study selection

Experimental studies conducted in the Caribbean Sea were identified using Google Scholar with the following search terms: "Caribbean coral," "ocean acidification," "ocean warming," "experiment," "manipulation," "control," and "calcification." Studies derived from the search were examined, and those that presented all of the following information were included in the meta-analysis: coral species, location of specimen collection, control and experimental temperature and/or control and experimental $p\text{CO}_2$ values, method of experimental manipulation, duration of exposure to treatment conditions, and calcification rate. Studies altering ocean acidification treatments with acid additions (i.e., hydrochloric acid) were excluded from this meta-analysis because these do not represent ecologically relevant changes in carbonate chemistry. Several other studies that met these criteria not present in the literature search were also included in the meta-analysis. Studies were collected for analysis until September 2018.

Data extraction and preparation

Detailed information on the location where coral colonies were collected and experimental design of each study was recorded (Table S1.1). Several studies included multiple species, collection sites, or experimental factors. In these cases, each species and/or collection site was considered as a separate experiment such that multiple comparisons were made against the one control treatment. Although the inclusion of all species and collection sites could reduce independence of some data points, all possible combinations were included to expand the extent of species and location responses. Additionally, studies with

other experimental parameters outside of acidification and warming were only utilized in this study when these external factors were considered to be under ambient conditions to prevent confounding results (Chan and Connolly 2013). In studies that reported calcification over time, only the final growth rate was used in this analysis.

For consistency in treatment analysis, only $p\text{CO}_2$ concentrations were used as the measure of acidification manipulation because of the potentially large variation in pH scale based on measurement methods (Zeebe and Wolf-Gladrow 2001). The wide variety of reported experimental $p\text{CO}_2$ values were categorized into one of the two categories: control or high. Below current-day or extreme $p\text{CO}_2$ treatments from selected studies were not included in this analysis. In experiments in which more than one elevated $p\text{CO}_2$ treatment was used to represent projected scenarios, the higher concentration treatment was selected for the meta-analysis. The $p\text{CO}_2$ treatment considered as current-day or ambient for each experiment was categorized in the ‘control’ group, despite variations in $p\text{CO}_2$ concentrations due to experimental design (380 – 513 μatm). Similarly, temperature treatments were categorized as either ‘control’ when reported to represent current-day or ambient conditions (26 – 30.6 °C), or as ‘elevated’ in experiments testing warming scenarios (30 – 32 °C). No study selected analysed the impact of multiple warming levels.

Calcification rate was chosen as the response parameter in this meta-analysis due to its common use as a stress response in manipulations experiments on Caribbean corals. Mean calcification rate, standard error, and sample size of each experiment was extracted from all included studies for the desired treatments. When raw data were not reported, values were mined from the literature using Web Plot Digitizer for analysis (<https://apps.automeris.io/wpd/>). Two coral species exhibited net dissolution in the control

treatments and therefore were excluded from this analysis because of potential bias from additional unknown stressors.

Calculation of effect size

Calcification rates in response to independent ocean acidification and warming treatments were measured for each experiment using standard mean differences (SMD), or Hedge's G, to establish the proportion of change between the treatment and control. SMDs were used in this analysis because of the presence of negative calcification rates in some treatments. Analyses were performed in the R (R Core Development Team 2016) package *metafor* (version 2.0–0) (Viechtbauer 2010) to calculate effect sizes (SMD) per experiment.

The interaction strength of ocean acidification and warming was determined using methods for factorial meta-analysis (Crain et al. 2008, Harvey et al. 2013). Only studies that reported outcomes for a fully factorial experiment including acidification (Y_{OA}), warming (Y_{OW}), the combination of the two (Y_{both}), and a control (Y_C) were used to calculate the interaction effect size. The interaction strength was calculated as

$$SMD_{both} = \left[\frac{(Y_{both} - Y_{OW}) - (Y_{OA} - T_C)}{2s} \right]$$

where Y is the mean calcification response for the denoted treatment, and s is the pooled standard deviation. Control values are denoted by subscript C , ocean acidification is denoted by subscript OA , warming is denoted by subscript OW , and the combination treatment is represented by subscript $both$. The sample variance of the effect size was calculated as

$$s_N^2(SMD_{both}) = \frac{1}{N_{OA}} + \frac{1}{N_{OW}} + \frac{1}{N_{both}} + \frac{1}{N_C} + \frac{SMD_{both}^2}{2(N_{OA} + N_{OW} + N_{both} + N_C)}$$

where N is the sample size of the indicated treatment.

Statistical analyses

A random effects model was implemented using the *metafor* package (function *rma.mv*) to calculate the mean effect of each treatment on calcification to account for variation in responses due to species and study design. To assess the effects of study design parameters on resulting calcification rates in either acidification or warming studies, two fully additive random effects models (function *rma.mv*) were fit with magnitude change between control and treatment, irradiance ($\mu\text{mol photons m}^{-2} \text{ s}^{-1}$), and duration (days) as continuous predictors, and seawater (natural versus artificial) and feeding (2 times a week, 3 times a week, or no data) were assessed as discrete predictors. An additional model was used to compare effect sizes of corals by region. For this model, only corals collected from the Florida Keys or Belize were considered because of the larger sample sizes from these regions. Random intercepts of study and species within treatment were included to account for potential correlation among results due to these factors. When the 95% confidence intervals of each estimated mean do not overlap zero, the effect size is considered clear statistical evidence. A test of moderators (Q_M) was used to determine differences between variables (temperature and/or region). Additionally, tests for residual heterogeneity (Q_E) were performed, with Q_E signifying that additional moderators not considered may be impacting the study results (Tables S1.2, S1.3).

To better understand the qualitative differences in calcification responses of corals from Florida and Belize to ocean acidification and warming, linear mixed effects models with observations weighted by sample size divided by standard error were fit using the *lme4* package (version 1.1–21) (Bates et al. 2015a). Using all warming studies, we compared models with measured calcification rates as response variable and coral collection region,

scaled temperature, and experiment duration as predictors with random slopes for study and species. We also fit a quadratic effect of temperature. Model selection using AICc was completed with random effects for species and study. A similar analysis was performed using reported aragonite saturation state (Ω_{Arag}) of each treatment to better assess ocean acidification on calcification rates.

Results

In total, eleven studies met the standards of this meta-analysis, including the responses of thirteen Caribbean coral species collected from five different countries across the Greater Caribbean Sea (Figure 1.1; Table S1.1). Of the studies selected, only four performed fully factorial ocean acidification and warming experiments, and one performed two independent acidification and warming experiments. The most studied coral species from the Caribbean region were *Porites astreoides* (5 studies), *Acropora cervicornis* (4 studies), and *Siderastrea siderea* (4 studies). Finally, the Florida Keys and Belize were the two most-studied regions within the wider Caribbean fitting the criteria of this meta-analysis.

Overall calcification response

Meta-analysis of the dataset revealed that calcification rates of Caribbean corals were reduced by ocean warming but not ocean acidification (Figure 1.2; Figure S1.2). However, the 95% confidence interval of the combination of ocean warming and acidification overlapped zero, indicating no statistically clear trend towards synergistic or antagonistic effects of these treatments (Figure 1.2; Table S1.2).

Calcification response of Florida Keys versus Belize corals

Corals from Belize only exhibited clearly reduced calcification rates under ocean warming (Figure 1.3A; Table S1.3), while acidification, warming, and the combination of both stressors did not clearly alter experimental calcification rates of corals from the Florida Keys (Figure 1.3B; Table S1.3). Further, the resulting Q_E suggests there is significant between-study variation (Table S1.3).

Temperature and aragonite saturation state impacts on calcification rates across studies

Secondary analysis of mean calcification rates ($\text{mg cm}^{-2} \text{ day}^{-1}$) against treatment temperature across all Florida and Belize studies revealed a parabolic response to temperature (Figure 1.4; Tables S1.4, S1.5). Similarly, mean calcification rates across Ω_{Arag} resulted in a nonlinear response to acidification (Figure 1.5; Tables S1.6, S1.7). Both nonlinear trends in response to temperature and Ω_{Arag} were a result of treatment rather than region (Tables S1.6, S1.7), suggesting regional differences identified in the meta-analysis were due to experimental designs employed to represent current regional environmental differences.

Experimental design impacts on coral calcification rate in studies

Quantification of experimental design parameters within warming studies identified that magnitude of treatment, irradiance, seawater type used, and feeding frequency all clearly impacted calcification rates (

Table 1.1). Specifically, studies that utilized natural seawater and those with a larger difference between the control and treatment temperatures within a study exhibited higher

effect sizes, suggesting a less negative effect of treatment. Studies that employed higher irradiance levels in their systems demonstrated more negative effects of treatment light level. Finally, studies that reported feeding their corals twice a week were less impacted by warming treatment than those feeding three times a week, however, studies with no data on feeding were the least affected by treatment. Duration of experiment was deemed redundant in the model and was thus dropped.

Within the acidification studies, irradiance, seawater type used, feeding frequency, duration, and the interaction of duration with treatment magnitude impacted effect sizes, while magnitude alone was not clearly different (

Table 1.1). Studies using natural seawater, employing higher irradiance levels, and those with longer durations resulted in great effect sizes, suggesting they lessened the effects of acidification treatment on calcification responses. Similar to warming studies, acidification studies in which feeding corals was conducted twice a week exhibited less negative responses to treatment than those feeding three times a week, with studies reporting no feeding data exhibiting the least negative responses to treatment. Finally, coral calcification responses were less impacted by acidification in studies with longer duration of exposure and a greater $p\text{CO}_2$ change.

Discussion

The current study utilized a meta-analytical approach to analyse the effects of ocean acidification, warming, and the combination of the two stressors on calcification rates of Caribbean corals. The two most-studied regions within the Greater Caribbean, the Florida

Keys and Belize, were further assessed for differences in calcification responses to ocean acidification, warming, and the combination of both stressors.

Ocean warming, but not acidification, independently impairs calcification of Caribbean reef-building corals

Ocean warming alone induced an overall adverse effect on calcification rates of the Caribbean corals analysed in this meta-analysis, contrasting a previous meta-analysis assessing coral calcification rates from multiple ocean basins (Harvey et al. 2013). However, increased bleaching, mortality, and declines in coral growth in response to warming is well-documented throughout the Caribbean Sea in field studies and reviews (Hughes et al. 2003, Hoegh-Guldberg et al. 2007, Carricart-Ganivet et al. 2012), supporting the overall reduced calcification rates to warming observed in the current meta-analysis. While there is evidence that suggests coral calcification rates, along with other physiological processes, increase along with warming seawater temperatures (Lough and Barnes 2000), the physiological advantages of warmer waters diminish when a thermal maxima is reached (Bahr et al. 2018, Silbiger et al. 2019). Ocean warming has also been closely associated with coral bleaching (Brown 1997) and since corals receive a significant proportion of their energetic need from their algal endosymbionts (Muscatine et al. 1981), it is likely that the loss of algal endosymbionts diminished energy reserves utilized in calcification. Thus, a significant number of corals in warming treatments from the included studies also likely exhibited signs of bleaching (i.e., reduced algal endosymbiont density) under elevated temperature, although bleaching was not assessed as a response variable in this meta-analysis due to low reporting and the diversity of bleaching metrics reported in the studies examined.

Ocean acidification did not clearly reduce calcification rates of Caribbean corals, contradictory to the findings of previous meta-analyses that have investigated the calcification response of tropical corals to ocean acidification from various other ocean basins (Kroeker et al. 2010, Chan and Connolly 2013, Harvey et al. 2013, Kroeker et al. 2013). Coral calcification is influenced by the Ω_{Arag} of seawater, with higher Ω_{Arag} (lower $p\text{CO}_2$) often promoting faster calcification rates (Langdon and Atkinson 2005). This aragonite-calcification relationship is most likely driven by corals' ability to control Ω_{Arag} at their calcification site by pumping Ca_2^+ into the calcifying fluid from the surrounding seawater, removing two protons (H^+) in the process, finally converting HCO_3^- to CO_3^{2-} (Cohen and McConnaughey 2003, Allemand et al. 2010, Ries 2011, Von Euw et al. 2017). Thus, even under low aragonite saturation (high $p\text{CO}_2$) corals that are able to elicit strong control over this process are likely to be more resilient against the effects of ocean acidification, although it may be energetically costly (Davies et al. 2016) and may impair other physiological processes. It is therefore likely that corals included in this meta-analysis that did not exhibit reduced calcification rates in association with simulated ocean acidification may have stronger control of their calcifying fluid to maintain comparable growth rates. Overall, corals from the studies included in the current meta-analysis exhibited variable responses under experimental seawater acidification, highlighting the diversity of responses to stress on the individual and species levels (Comeau et al. 2014, Okazaki et al. 2017, Bove et al. 2019).

Although ocean warming caused reduced calcification of Caribbean corals in the included studies, the combination of acidification with warming was not clearly different from the two independent stressors (Crain et al. 2008). Because only four studies tested the

combination of acidification and warming (Towle et al. 2015, Horvath et al. 2016, Okazaki et al. 2017, Bove et al. 2019), however, the sample size for the interaction term was very low. With this small samples size in conjunction with only about 17% of Caribbean reef-building coral species analysed in the current study, the potential for synergistic or additive effects should not be ignored. Because synergistic relationships can be unpredictable, especially when additional stressors are introduced (Harvey et al. 2013), it is important that additional combined stressor experiments be conducted to better understand the response of Caribbean reef-building corals to these interrelated stressors.

Calcification responses to global change stressors vary by region within the Caribbean

Coral calcification responses to ocean acidification, warming, and the combination of the two stressors varied between corals collected from the Florida Keys and those collected from Belize. Corals from the Florida Keys did not exhibit clearly reduced calcification rates under independent ocean acidification and warming, or the combination of ocean acidification and warming. However, corals from Belize reduced calcification rates from ocean warming treatments. This regional difference is likely due in part to adaptation of the corals in each region to their local environmental conditions (Oliver and Palumbi 2011, Putnam et al. 2017). Corals found off the coast of Belize experience a much narrower range of annual sea surface temperatures (*ca* 24–32°C) than corals located off the southern coast of Florida (*ca* 18–31°C) (Castillo and Lima 2010, Okazaki et al. 2017), resulting in a higher annual mean temperature in Belize than the Florida Keys. This difference in annual temperature variability has likely led to the adaptation of the corals in Florida to more extreme temperatures, resulting in different thermal susceptibilities than corals in Belize

(Marshall and Baird 2000, Guest et al. 2012) and may act as a potential pathways of adaptation or acclimatization to projected global change. Although statistically clear effect sizes may be due to variations in natal environments, differences in experimental treatment levels may also confound these results. Indeed, further analysis studies identified that treatment level predominately drove resulting calcification rates, not specifically collection region. Further, the resulting model fit to the calcification rates across temperature exhibited a quadratic fit, similar to what would be expected for a thermal performance curve (Portner et al. 2006). Reef-building corals generally exhibit a threshold response to ocean warming when a particularly high temperature or prolonged exposure to warming water causes bleaching, reduced growth rates, and mortality (Glynn 1996, Brown 1997). However, the treatment temperatures used in the Florida and Belize experiments represent warming scenarios specific to the corresponding region, highlighting already-present warming patterns of these regions. Indeed, elevated temperatures employed in studies using Belize corals were 1–2 °C higher than the elevated temperatures used in Florida experiments (31–32 versus 30 °C), reflecting differences in annual mean temperatures (Castillo and Lima 2010, Okazaki et al. 2017). Additionally, the temperatures employed in the Florida Keys studies were representative of the bleaching threshold for the region (Manzello et al. 2007), while the Belize studies used end-of-century projections. Corals are known to live within a narrow thermal range (Kleypas et al. 1999) and the Florida studies tested the upper end of that threshold, while the Belize studies pushed beyond that limit. Consequently, the clear effect of temperature on Belize corals is due largely to the selected treatment temperature employed in each study, although this is likely indicative of differing warming patterns between these regions.

Overall coral calcification rates in response to region and treatment Ω_{Arag} across ocean acidification studies was also assessed, again resulting in a nonlinear response to changing seawater chemistry. Because response of corals to ocean acidification is heavily dependent on extent of seawater chemistry change, duration, and individual colony susceptibility (Orr et al. 2005, Ries et al. 2010, Schoepf et al. 2017), it is not surprising that the nonlinear response quantified in the present meta-analysis is not as dramatic as the temperature response. Although studies based their acidification treatments on projected end-of-century concentrations relevant for the environment from which the corals were collected, this resulted in a wide range of experimental $p\text{CO}_2$ concentrations (Belize 600–900 μatm versus 750–1340 μatm Florida Keys). While the exact relationship between calcification and $p\text{CO}_2$ (or Ω_{Arag}) varies, the general relationship suggests increased $p\text{CO}_2$ reduces coral calcification (Langdon and Atkinson 2005, Chan and Connolly 2013). Indeed, calcification rates of Caribbean corals exhibit a general decline in response to reduced Ω_{Arag} , similar to the 15% decline in calcification reported by Chan and Connolly (2013) for every unit decrease in Ω_{Arag} . Although this is a significant decline in skeletal growth in terms of maintaining reef production, this reduction is much less dramatic than that of the measured calcification decline associated in the included ocean warming studies. This difference in threshold responses suggests that while acidification is going to be a chronic stressor continually impacting carbonate production and maintenance on coral reefs, increasing warming events will pose a more immediate and dramatic threat on the future of tropical coral reefs.

Experimental design considerations and recommendations for future research

With such variation in study implementation and lingering gaps in the literature, results from this meta-analysis may not capture all underlying causes of calcification responses to ocean acidification, warming, and the combination of stressors. Several gaps in simulated global change studies using corals were identified in this meta-analysis including coral collection sites, variety of species included, and experimental design differences. Although corals from the Florida Keys and Belize were heavily represented in the meta-analysis, only a single study collected corals from reefs south of Belize (Jury et al. 2010) and in the Eastern Caribbean (Bedwell-Ivers et al. 2017). This scattered sampling leaves much of the Caribbean understudied in regards to how coral reefs may respond to ocean acidification and warming as the two stressors continue to co-occur. Additionally, only about 17% of Caribbean coral diversity was represented, leaving out a significant percentage of coral species from the region, including several dominant reef-building species. Without having a better understanding of the calcification responses of other species within the Caribbean, meta-analyses like this will not be able to accurately predict potential reef-wide responses to global change. Future studies should consider what regions and species within the Caribbean have been extensively studied in similar ocean acidification and warming experiments and aim to expand outside of these regions and/or species in designing experiments.

In addition to ensuring that experimental treatments (temperature and $p\text{CO}_2$) represent ecologically relevant conditions, it is important to consider how experimental design dictates resulting coral calcification responses. For example, within all included studies in this meta-analysis experimental duration ranged from two hours (Jury et al. 2010) up to 95 days (Castillo et al. 2014), with additional variation in seawater type used, irradiance, and how

corals received nutrition throughout the experiments (see Table 1.1; Table S1.1). Upon further inspection of these design differences in both warming and acidification studies, the use of natural seawater was associated with higher effect sizes, suggesting less negative responses to treatment than when using artificial seawater, likely due to the different buffering capacity of natural seawater compared to many artificial seawater products (Atkinson and Bingman 1997). By using natural seawater, especially taken from experimental corals' native reef environments, mesocosm studies may also be able to accommodate more difficult to rear species to expand the range of species used in such experiments. However, the benefits of using artificial seawater (i.e., potential for more consistent results between studies) should also be weighed in the planning of mesocosm experiments. Additionally, reported feeding across both acidification and warming studies played a significant role in resulting coral calcification rates, with studies feeding corals twice weekly exhibiting less negative effects of treatment than in studies feeding three times. Although increased heterotrophy may alleviate stress associated with increasing temperatures and decreasing Ω_{Arag} (Towle et al. 2015, Brown et al. 2018), the higher nutrient load on the experimental systems as a result of increased feeding may harm physiological processes in the corals, reducing overall growth rates (D'Angelo and Wiedenmann 2014). Of the studies that did not report feeding frequency, all utilized natural seawater in their experimental systems, thus it is likely that the authors relied on natural nutrients and plankton abundances that were more beneficial for the corals. Efforts should be made to establish and report reasonable feeding practices (i.e., quantity, frequency, type of food) based on coral species, collection depth, and collection location for each study to reduce the impacts of starvation or overeating on measured coral responses.

Interestingly, the present meta-analysis identified that higher irradiance levels in warming studies were associated with more negative effects of warming on calcification rates, while higher irradiance in acidification studies potentially acted as a rescue effect in response to treatment, contrary to Chan and Connolly (2013). These results suggest that the combination of high light levels with warming seawater temperatures may exacerbate bleaching-associated reduced growth rates (Brown 1997), while higher light levels may alleviate the negative impacts of ocean acidification by stimulating photosynthesis of the coral algal endosymbionts (Suggett et al. 2013). In addition to different responses to irradiance between the two study types, experimental duration did not play a role in warming studies while longer acidification experiments exhibited slightly less negative responses to treatment, differing from the meta-analysis performed by Chan and Connolly (2013). However, longer acidification experiments with greater treatment magnitude exhibited more negative responses to treatment, likely indicative of ocean acidification being a chronic stressor while ocean warming is generally associated with acute stress events (Hoegh-Guldberg et al. 2007). As further experiments are designed, care should be taken to use ecologically-relevant experimental durations that appropriately address questions being addressed. In order to understand how corals respond under chronic acidification and acute warming stress, future experiments should consider conducting such research on the scale of months to years as possible. The recommendations put forth in this study should be considered when designing future Caribbean coral global change studies, even those outside acidification and warming treatments, along with other previously suggested (Widdicombe et al. 2010) to improve the overall understanding of Caribbean corals under projected global change.

Conclusions

Overall, results from this meta-analysis suggest the sensitivity of Caribbean corals to ocean warming, while also identifying several current knowledge gaps and potential opportunities for future research. Specifically, this analysis highlights the need for further studies including the combination of ocean acidification and warming, as well as expanding the research to additional Caribbean reef-building coral species and regions. Furthermore, although differences in calcification responses between the Florida Keys and Belize were detected in this meta-analysis, further analysis determined this difference was largely attributed to the treatments employed, highlighting the significance of experimental protocols in measured results. The studies reviewed in the current analysis exhibit a wide range of experimental designs, including variations in duration, feeding, irradiance, treatment levels, and even seawater. These variations in experimental implementation play a major role in the results of the current meta-analysis and suggest that consideration of previous experimental designs should be made when designing new experiments to make the results more comparable. Additionally, future meta-analyses of Caribbean corals should include additional parameters outside of calcification, such as bleaching, metabolism, and survival. The inclusion of additional responses will improve the overall understanding of how corals within the wider Caribbean may respond under projected ocean acidification and warming. Because ecosystem level experiments are difficult to conduct, meta-analyses are important tools for understanding the responses of a wide variety of species to projected global change stressors. This analysis provides valuable insight into the calcification response of corals throughout the Caribbean; however, further experiments must be conducted to expand understanding beyond the small selection of species and regions included in this meta-analysis.

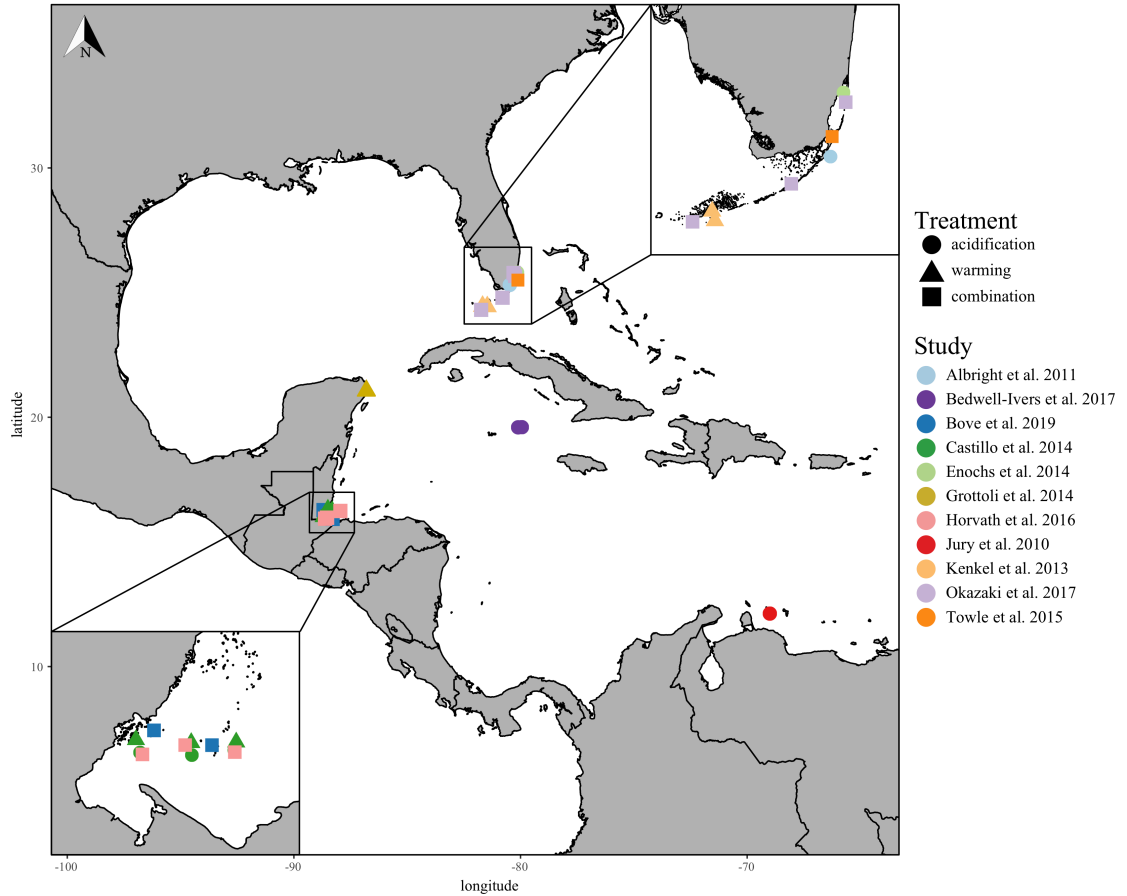


Figure 1.1 Map of meta-analysis study sites

Coral collection sites of all included studies with experimental study represented by colour and treatments represented by shape: acidification only (circle), warming only (triangle), and the combination of acidification and warming (square). The lower left insert displays close-up of the Belize collection sites and the upper right insert displays the Florida Keys collection sites.

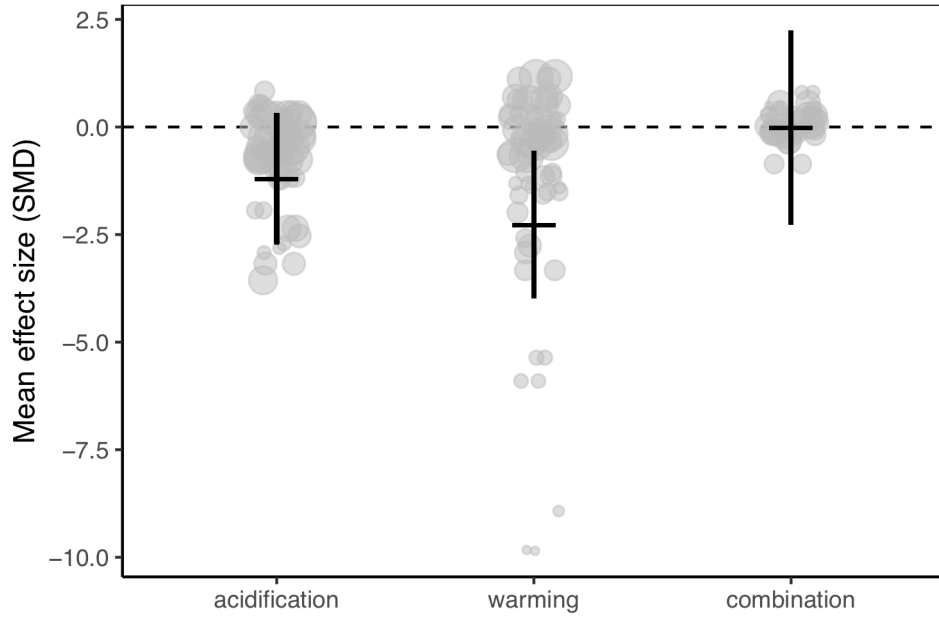


Figure 1.2 Global effect size of meta-analysis treatments

Mean effect (standard mean difference) and 95% confidence interval of ocean acidification, warming, and the combination of acidification and warming on calcification rate for all studies in the meta-analysis. Grey circles indicate the effect size of each individual study and the size of each circle represents the weight of each study (1/SE). Clear statistical evidence of a treatment effect is identified when the 95% confidence interval does not overlap zero.

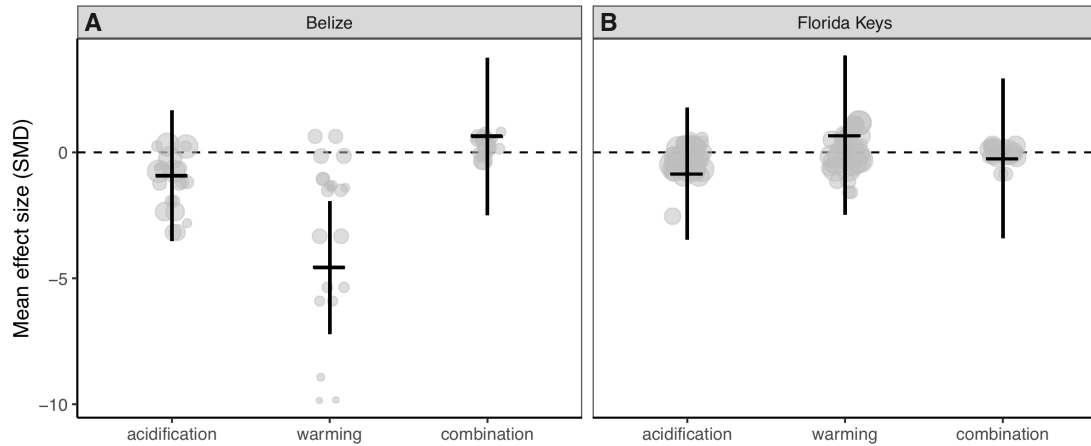


Figure 1.3 Regional effect size of meta-analysis treatments

Mean effect (standard mean difference) and 95% confidence interval of ocean acidification, warming, and the combination of acidification and warming on calcification rate for (A) Belize corals and (B) Florida Keys corals. Grey circles indicate the effect size of each individual study and the size of each circle represents the weight of each study ($1/SE$). Clear statistical evidence of a treatment effect is identified when the 95% confidence interval does not overlap zero.

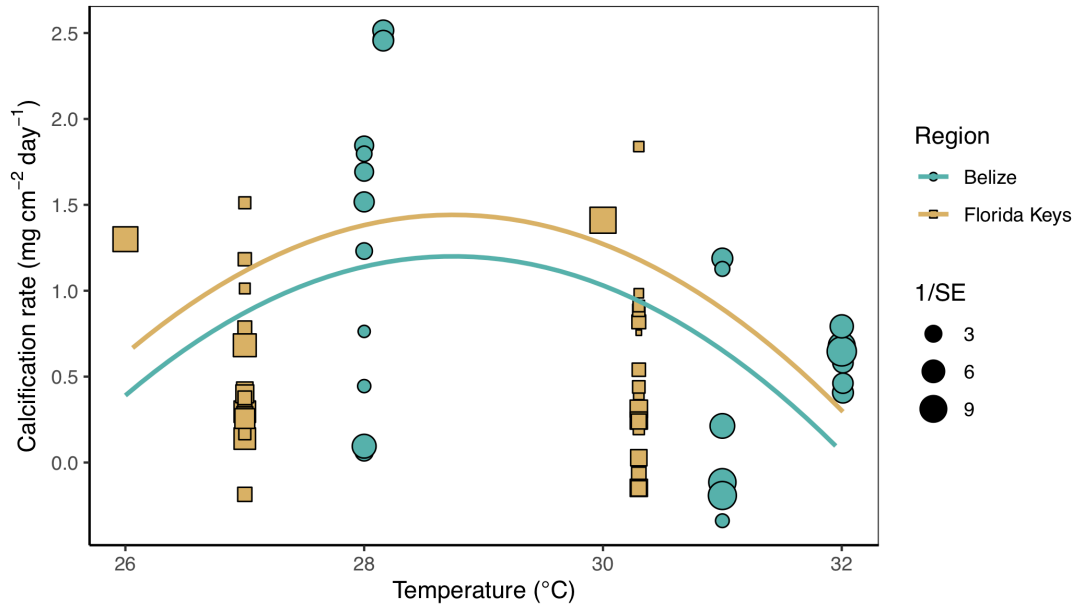


Figure 1.4 Magnitude analysis of temperature on calcification rates

Mean calcification rate (mg cm⁻² day⁻¹) of corals from each warming study by treatment temperature (°C) with the linear mixed effects model quadratic fit by region and experimental duration (mean duration = 59.8 days). Shape and colour of each point denotes study region (blue circle = Belize; brown square = Florida) and size of shape represents the weight (1/SE) of study.

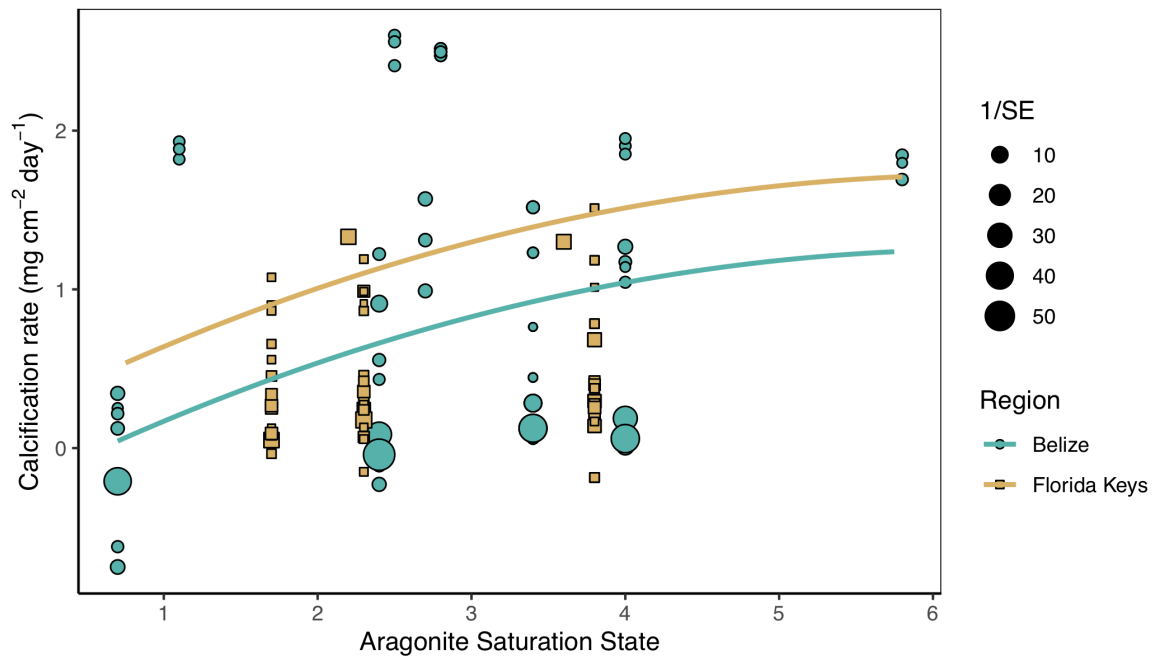


Figure 1.5 Magnitude analysis of aragonite saturation state on calcification rates

Mean calcification rate ($\text{mg cm}^{-2} \text{ day}^{-1}$) of corals from each acidification study by treatment aragonite saturation state (Ω_{Arag}) with the linear mixed effects model quadratic fit by region and experimental duration (mean duration = 66.5 days). Shape and colour of each point denote study region (blue circle = Belize; brown square = Florida Keys) and size of shape represents the weight ($1/\text{SE}$) of study.

	Estimate	Lower 95% CI	Upper 95% CI
<i>Warming Experiments</i>			
Intercept	-29.39	-39.56	-19.22
Magnitude (°C) *	10.34	5.58	15.1
Irradiance *	-0.24	-0.34	-0.14
Seawater (natural) *	29.77	19.72	39.82
Feeding (3x) *	-3.54	-4.97	-2.12
Feeding (N.D.) *	87.16	49.69	124.64
<i>Acidification Experiments</i>			
Intercept	-2.03	-2.78	-1.28
Magnitude ($\mu\text{atm } p\text{CO}_2$)	0.000	-0.003	0.003
Irradiance *	0.009	0.004	0.014
Seawater (natural) *	2.39	1.14	3.64
Feeding (3x) *	-15.04	-22.61	-7.48
Feeding (N.D.) *	3.61	0.28	6.94
Duration *	0.21	0.09	0.32
Magnitude x days *	-0.0005	-0.0007	-0.0003

Table 1.1 Experimental design effect sizes

Effect size estimate and 95% confidence intervals of experimental design parameters calculated for all warming and acidification experiments. Non-overlapping 95% confidence intervals of each design parameter were interpreted to indicate a significant influence on measured coral calcification response to treatment. Magnitude (difference between control and treatment condition), irradiance ($\text{mmol photons m}^{-2} \text{ s}^{-1}$), and duration (days) were evaluated as continuous predictors, while seawater (natural versus artificial) and feeding (2 times a week, 3 times a week, or no data) were assessed as factors. Parameters denoted with an asterisk (*) was determined to clearly impact calcification response to treatment.

CHAPTER 2: COMMON CARIBBEAN CORALS EXHIBIT HIGHLY VARIABLE RESPONSES TO FUTURE ACIDIFICATION AND WARMING²

Introduction

Increasing carbon dioxide (CO₂) from anthropogenic sources is of growing concern as global average atmospheric *p*CO₂ has now increased from a pre-industrial level of 280 μatm to 410 μatm (Tans and Keeling 2017). This rapid change has resulted in negative and often irreversible impacts on both terrestrial and marine ecosystems (Solomon et al. 2009, Pecl et al. 2017). In terrestrial ecosystems, rising surface temperatures pose serious threats to animals and plants that are unable to cope with hotter, longer, and more frequent thermal stress events (Fitter and Fitter 2002, Caruso et al. 2014). Marine ecosystems are under similarly intense pressure from ocean warming and acidification (Hoegh-Guldberg et al. 2007), affecting everything from biogeochemical cycling to habitat and population structure (Hoegh-Guldberg and Bruno 2010).

Ocean warming is a major concern for marine organisms, especially at lower latitudes where sea surface temperature is predicted by the Intergovernmental Panel on Climate Change (IPCC) to rise between 0.6 and 3.0°C by the end of the 21st century (Stocker et al. 2013). Reef-building corals in these low-latitude regions, including the Caribbean, are already living within a degree of their thermal maxima (Jokiel and Coles 1977) and are therefore considered to be at particular risk (Somero 2010). Abnormally high seawater

² This chapter previously appeared as an article in Proceedings of the Royal Society B – Biological Sciences. The original citation is as follows: Bove C.B., Ries J.B., Davies S.W., Westfield I.T., Umbanhowar J., and Castillo K.D. “Common Caribbean corals exhibit highly variable responses to future acidification and warming” *Proceedings of the Royal Society B – Biological Sciences*, 286, no. 1900 (April 2019): 1–9.

temperatures disrupt the symbiosis between the coral animal and its algal endosymbiont (Symbiodiniaceae) (LaJeunesse et al. 2018) through a process known as ‘coral bleaching’ (Glynn 1991), resulting in deterioration of corals’ physiological processes (Jokiel and Coles 1977, Grottoli et al. 2006, Castillo et al. 2014). Mortality rates increase due to the strong dependence of corals on their endosymbionts, which contribute up to 100% of their daily metabolic requirements (Muscatine et al. 1981), impacting the corals’ ability to withstand additional environmental stress.

Rising atmospheric $p\text{CO}_2$ is not only warming surface seawater, but also causing more CO_2 to dissolve into oceans, reducing carbonate ion concentration [CO_3^{-2}], pH, and aragonite saturation state (Ω_A) of seawater—a process known as ocean acidification (Orr et al. 2005). The IPCC projects that atmospheric $p\text{CO}_2$ will surpass 600 μatm by 2100, which would cause surface ocean pH to decrease by 0.1 – 0.3 (Stocker et al. 2013). Scleractinian corals rely heavily on elevated pH and Ω_A at their site of calcification to form calcium carbonate skeletons (Al-Horani et al. 2003, Cohen and McConnaughey 2003, Ries 2011, Venn et al. 2013), making it harder for some species to maintain conditions within these sites that are supportive of skeletal formation under acidification (McCulloch et al. 2012). However, previous research has revealed inconsistencies in scleractinian corals’ response to acidification (Ries et al. 2009, Comeau et al. 2013a). Simulations of past (Albright et al. 2016) and future (Albright et al. 2018) $p\text{CO}_2$ conditions in a natural reef system on the Great Barrier Reef revealed a decrease in net community calcification with increasing $p\text{CO}_2$, while *ex situ* experiments demonstrated negative (Reynaud et al. 2003, Jury et al. 2010, Comeau et al. 2013a), threshold (Ries et al. 2010), parabolic (Castillo et al. 2014), and no significant (Reynaud et al. 2003, Jury et al. 2010) response of corals to increased $p\text{CO}_2$. Numerous

explanations for the wide array of responses include differences in experimental design (Cornwall and Hurd 2016), evolutionary divergence amongst corals with respect to mechanisms of calcification and/or resilience to acidification (Brown and Edmunds 2016), and differences amongst coral species' physiological control of calcifying fluid chemistry (Ries 2011, Agostini et al. 2013, Holcomb et al. 2014, Barott et al. 2015). Moreover, although studies have investigated the effects of increasing $p\text{CO}_2$ on coral calcification and health, fewer have investigated the combined effects of temperature and $p\text{CO}_2$.

In isolation, warming has been shown to more negatively impact coral calcification than $p\text{CO}_2$ (Carricart-Ganivet et al. 2012, Castillo et al. 2014, Venti et al. 2014, Davies et al. 2016, Okazaki et al. 2017). However, numerous studies have observed that the combination of $p\text{CO}_2$ and temperature causes a more severe negative response in corals than either stressor alone (Edmunds et al. 2012, Agostini et al. 2013, Schoepf et al. 2013, Horvath et al. 2016, Okazaki et al. 2017), although few studies report a truly synergistic interaction between warming and acidification. This highlights the importance of studying the response of multiple coral species to global change scenarios under a common suite of conditions. Using multiple species in the same experiment minimizes differential outcomes that arise from differences in experimental design, allowing for direct comparison among species. The few studies that have investigated multiple coral species have yielded important insights into reef-community-level responses to acidification and warming, including projecting rates of whole-reef accretion under future IPCC scenarios (Okazaki et al. 2017).

Here we investigate the independent and combined effects of ocean acidification and warming on four abundant and widespread Caribbean scleractinian coral species—*Siderastrea siderea*, *Pseudodiploria strigosa*, *Porites astreoides*, and *Undaria*

tenuifolia—in a 93-day laboratory experiment. These four species were selected because they span a range of skeletal morphologies (foliate—domical), possess similar life history strategies (Szmant 1986), and occupy similar depth and geographic ranges (Veron 2000). Corals collected from the Belize Mesoamerican Barrier Reef System (MBRS) were reared under projected temperature and $p\text{CO}_2$ stress with the aim of characterizing the effects of future global change on a suite of genetically and morphologically diverse Caribbean coral species.

Materials and methods

Experimental design

Six colonies of *S. siderea*, *P. strigosa*, *P. astreoides*, and *U. tenuifolia* were collected from inshore and offshore reef environments along the southern portion of the Belize MBRS (see Appendix 2 for details of coral collection, Figure S2.1). Forty-eight coral colonies were transported to Northeastern University's Marine Science Centre in Nahant, Massachusetts, and sectioned into eight comparably sized fragments, and placed into aquaria for a recovery period of 23 days. After recovery, temperature and $p\text{CO}_2$ was adjusted gradually over a 20-day interval until target experimental conditions were approximately achieved for each treatment (temperature: 28 and 31°C; $p\text{CO}_2$: 280, 400, 700, 2800 μatm). Coral fragments were acclimated to treatment conditions for 30 days and then maintained in each experimental treatment for 93 days. Four $p\text{CO}_2$ treatments corresponding to pre-industrial (311/288 μatm), present-day ($p\text{CO}_2$ control; 405/447 μatm), end-of-century (701/673 μatm), and an extreme (3309/3285 μatm) $p\text{CO}_2$ were maintained at two temperatures corresponding to the corals' approximate present day mean annual temperature (28°C; determined by over

10 years of *in situ* records (Castillo and Lima 2010, Castillo et al. 2012, Baumann et al. 2016)) and projected end-of-century annual mean temperature (31°C) (Stocker et al. 2013). The extreme $p\text{CO}_2$ treatment was formulated at a value approaching that predicted for year 2500 (Stocker et al. 2013), and was selected to push the corals closer to their physiological limits. Experimental tanks were illuminated on a 10:14 h light:dark cycle with photosynthetically active radiation of *ca.* 300 $\mu\text{mol photons m}^{-2} \text{s}^{-1}$ (see Appendix 2 for detailed experimental conditions and maintenance; Figures S2.2, S2.3).

Measured and calculated parameters

Temperature, salinity, and pH were measured every other day throughout the experiment (Table 2.1). Water samples were obtained every ten days for measurement of total alkalinity (TA) and dissolved inorganic carbon (DIC) and analysed with a VINDTA 3C (Marianda Corporation, Kiel, Germany). Temperature, salinity, TA, and DIC were used to calculate carbonate parameters using CO₂SYS (Pierrot et al. 2006) with Roy et al. (1993) carbonic acid constants K_1 and K_2 (Roy et al. 1993), Mucci's (1983) value for the stoichiometric aragonite solubility product (Mucci 1983), and an atmospheric pressure of 1.015 atm (Table 2.1; Figure S2.4; Tables S2.2, S2.3). The two temperatures at a given $p\text{CO}_2$ level exhibited slight differences in carbonate chemistry because the solubility of CO₂ in seawater varies with temperature.

Quantification of calcification and linear extension

Net calcification rates were estimated from surviving coral fragments using a buoyant weight method (Davies 1989) performed at the beginning of the pre-acclimation period and

every 30 days throughout the experiment (see Appendix 2 for empirical derivation of buoyant weight–dry weight relationships for all four coral species and for survivorship; Figures S2.5, S2.6).

Extension was quantified from vertical cross sections of the corals as the total area of skeleton above the calcein dye line incorporated into coral skeletons at the beginning of the experiment, divided by the length of the region of active growth (see Appendix 2 for detailed methodology; Figure S2.7). Linear extension was not quantified for *U. tenuifolia* or *P. strigosa* because their irregular skeletal morphologies rendered the method too inaccurate.

Colony-level effects of basal calcification rate on calcification response to stress

Recent work has shown that coral species that calcify faster are generally more vulnerable to the effects of ocean acidification than slower calcifying species (Comeau et al. 2014)—raising the possibility that similar trends exist within species amongst colonies with differing calcification rates. Colony-specific relationships between basal calcification rate and response to $p\text{CO}_2$ and thermal stress were investigated by assessing correlation between the random effect of colony on each colony's calcification rate within the control treatment (pre-industrial $p\text{CO}_2$ at 28°C) versus each colony's calcification response to $p\text{CO}_2$ or thermal stress (i.e., change in calcification rate between the control treatment and the stress treatments). Small sample size prevented fitting a frequentist model to estimate these colony level effects, so a Bayesian hierarchical regression model was fit to calculate credible intervals of the corresponding extracted correlation coefficient using R package *brms* (version 2.7.0) with default priors (Bürkner 2017). Random effects relating colony-specific relationships between basal calcification rate and response to $p\text{CO}_2$ and thermal stress were

calculated for all species together, as the study lacked the statistical power to assess this correlation within individual species.

Statistical analyses

Three-way mixed-model analyses of variance selected using AIC (Table S2.4) were used to assess impacts of $p\text{CO}_2$ and temperature on calcification and linear extension (*lme4* (1.1-12)) (Bates et al. 2015b). Parametric bootstraps were performed to model 95% confidence intervals with 1500 iterations (Wilcox 2010). Significant differences between treatments were defined as non-overlapping 95% confidence intervals. Because reef environment was not a significant predictor of any parameter, colonies were pooled across reef environments and these effects were not further addressed (see Appendix 2 for detailed analyses; Tables S2.12, S2.13). To further evaluate the effects of acidification and warming on *U. tenuifolia*, survival rates were assessed using a Kaplan-Meier estimate of survival (*survfit, survival*, 2.39-5) (Therneau 2015b). Cox proportional hazard models, with colony nested within tank as a random effect, were performed using *coxme* (2.2-5) (Therneau 2015a).

Results

Calcification rates

All four coral species exhibited nonlinear declines in calcification rate with increasing $p\text{CO}_2$ (Figure 2.1). Notably, *S. siderea* maintained positive net calcification across all temperature and $p\text{CO}_2$ treatments (Figure 2.1A), while the other species exhibited net dissolution in at least one treatment. *Pseudodiploria strigosa* maintained net calcification at 28°C, but exhibited net dissolution in all but pre-industrial $p\text{CO}_2$ at 31°C (Figure 2.1B).

Porites astreoides yielded negligible net calcification or net dissolution in all treatments except under pre-industrial $p\text{CO}_2$ at 31°C (Figure 2.1C), and *U. tenuifolia* exhibited net calcification in all treatments except under the extreme $p\text{CO}_2$ treatment (Figure 2.1D). Temperature had no significant effect on *S. siderea* or *P. astreoides* calcification rates; however, elevated temperature significantly reduced calcification rate in *P. strigosa* under all $p\text{CO}_2$ conditions (Figure 2.1; Tables S2.5, S2.6). The effect of temperature on calcification rates of *U. tenuifolia* could not be quantified due to low survival in the elevated temperature treatments.

Colony-level calcification response to stress

A negative slope of the correlation between random effects of colony on calcification rate in the control treatment (pre-industrial $p\text{CO}_2$ at 28°C) versus those in the stress treatments (Figure 2.2) would support the hypothesis that faster calcifying colonies (relative to the treatment mean) under control conditions calcify slower (relative to the treatment mean) under $p\text{CO}_2$ and thermal stress (Figure 2.2). While the best estimates of these correlations were negative, only the 75% credible intervals, and not the 95% credible intervals, did not always overlap zero (Figure S2.8)--suggesting that the results of the current experiment provide weak evidence for the inverse correlations between basal calcification rate and calcification response to $p\text{CO}_2$ and thermal stress. However, the current study likely lacked the statistical power to confirm the statistical significance of this correlation owing to a combination of low within-colony replication and high mortality rate.

Linear extension

Siderastrea siderea and *P. astreoides* exhibited positive linear extension rates in all treatments. Neither temperature, nor $p\text{CO}_2$, nor their interaction had a significant impact on linear extension rates of *S. siderea* or *P. astreoides* (Figure 2.3; Tables S2.7, S2.8).

Discussion

Caribbean corals exhibit nonlinear calcification responses to $p\text{CO}_2$ and temperature

All four coral species exhibited nonlinear calcification responses to $p\text{CO}_2$ driven primarily by stability in calcification rates across the three lowest $p\text{CO}_2$ treatments, and major declines under extreme $p\text{CO}_2$ (Figure 2.1). One exception to this trend was *P. strigosa*, which exhibited an abrupt decline in calcification rate at present-day $p\text{CO}_2$. Similar nonlinear calcification responses have been reported in previous studies for several temperate (Ries et al. 2010, Rodolfo-Metalpa et al. 2010) and tropical corals (Jury et al. 2010, Castillo et al. 2014, Okazaki et al. 2017), indicating that such $p\text{CO}_2$ thresholds exist for a diverse range of coral species. Interspecific differences in corals' calcification responses to $p\text{CO}_2$ may be influenced by differences in a coral's ability to control Ω_A at their calcification site (Cohen and McConnaughey 2003, Ries 2011). It has been proposed that corals transport Ca^{2+} into the calcifying fluid from the surrounding seawater in exchange for two protons using the enzyme Ca^{2+} -ATPase (Cohen and McConnaughey 2003), increasing the Ω_A by elevating $[\text{Ca}^{2+}]$ and by converting HCO_3^- to CO_3^{2-} (Cohen and McConnaughey 2003, Ries 2011, Von Euw et al. 2017). However, this process requires energy (1 mole ATP consumed per mole of Ca^{2+} -ATPase (Al-Horani et al. 2003)), which should increase under more acidic conditions as more protons must be removed to deprotonate HCO_3^- . This suggests that the threshold $p\text{CO}_2$

for maintaining stable rates of calcification is determined, at least in part, by the energetic costs of regulating ionic concentrations at the coral's site of calcification (Ries 2011, Davies et al. 2016, Von Euw et al. 2017).

Increased temperature had no significant effect on calcification rates of either *S. siderea* or *P. astreoides* (Figures 2.1A, 2.1C). Similarly, in a prior study, *S. siderea* from the Florida Keys demonstrated stability in calcification rates with a temperature increase from 27°C to 30.3°C (Okazaki et al. 2017). However, two studies on *S. siderea* from the Belize MBRS reported reduced calcification rates with a temperature increase from 28°C to 32°C (Castillo et al. 2014, Horvath et al. 2016). Other studies have also reported reduced calcification for *P. astreoides* under thermal stress (Kenkel et al. 2013a, Okazaki et al. 2017), although the present study found that an increase in temperature from 28°C to 31°C did not significantly impact calcification rate of this species. These apparent discrepancies in coral species' calcification responses to warming may arise from evaluating temperature effects across different portions of these species' thermal performance curves. Rates of biological processes, including calcification, are known to increase with increasing temperature to a maximum before declining with continued temperature increases, resulting in a thermal performance curve (Portner et al. 2006), which are typically parabolic in shape. It is possible that the two temperatures investigated in the present experiment are symmetrically distributed about this species' optimal temperature, resulting in equivalent calcifications rates at both temperatures.

Notably, only *P. strigosa* exhibited reduced calcification rates under thermal stress (Figure 2.1B), contrasting previous work on this species showing no calcification response to thermal stress (Okazaki et al. 2017). Again, this discrepancy between studies may result from

assessing temperature effects across different portions of this species' thermal performance curve (28 – 31°C versus 27.0 – 30.3°C in prior study). Differences in populations may also contribute to these discrepancies amongst studies with respect to a species' calcification responses to temperature (Marshall and Baird 2000) and $p\text{CO}_2$ (Manzello et al. 2012, Melendez and Salisbury 2017).

The effect of temperature on *U. tenuifolia* calcification rate could not be fully evaluated due to low survival at 31°C, although these results highlight the thermal sensitivity of this species—as previously observed on the Belize MBRS after thermal bleaching events (Aronson et al. 2000, Aronson et al. 2002) (Figure S2.6D, Tables S2.9, S2.10, S2.11). Previous studies suggest that the susceptibility of *U. tenuifolia* to thermal stress arises from lack of compensatory stress responses (Lesser 1997, Feder and Hofmann 1999, Robbart et al. 2004, Seemann et al. 2012), including insufficient production of heat shock proteins to protect against thermal events (Robbart et al. 2004) and reduced endosymbiont photosynthesis due to oxidative stress induced by warming (Lesser 1997). Owing to its reliance on endosymbiont photosynthesis over heterotrophy for energy (Seemann et al. 2012), oxidative bleaching may effectively starve this species of nutrition.

The interaction between $p\text{CO}_2$ and temperature did not significantly impact calcification rates for any of the coral species. Absence of an interactive effect of $p\text{CO}_2$ and temperature on coral calcification rate is relatively common and has been observed for multiple species (Muehllehner and Edmunds 2008, Schoepf et al. 2013, Okazaki et al. 2017). A previous study that exposed *S. siderea* to elevated temperature (32°C), elevated $p\text{CO}_2$ (~900 μatm), and the combination of these two stressors found calcification rates were most negatively affected by the combined high- $p\text{CO}_2$ /high-temperature treatment, resulting in additive, but not

synergistic, effects on calcification rates (Horvath et al. 2016). Thus, the evidence to date suggests that scleractinian corals exposed to both $p\text{CO}_2$ and thermal stress rarely experience effects that are truly synergistic. Finally, calcification rates in the present study were generally comparable to those reported for corals from the Florida Keys (Okazaki et al. 2017) and Belize (Horvath et al. 2016).

Faster-growing colonies may be more vulnerable to $p\text{CO}_2$ and thermal stress

Colonies that exhibited faster calcification in the control treatment (pre-industrial $p\text{CO}_2$ at 28°C) tended to exhibit slower calcification in the elevated- $p\text{CO}_2$ and elevated-temperature treatments, suggesting a trade-off in which faster calcifying colonies may be more vulnerable to the negative impacts of $p\text{CO}_2$ and thermal stress on calcification. Unsurprisingly, this correlation was weakest when comparing pre-industrial to present-day $p\text{CO}_2$ treatments—the two most similar treatments. This variation in calcification rates was evident across the four coral species, which is consistent with previous literature suggesting that divergent calcification strategies exist across populations (Szmant and Gassman 1990, Rinkevich 1996, Metcalfe and Monaghan 2001, Arnott et al. 2006, Leong and Pawlik 2010). Our analysis provides preliminary support for two end-member strategies of calcification: (1) fast calcifying colonies that divert more energy towards flourishing during favourable environmental regimes but flounder during periods of environmental stress (potentially due to lack of energetic reserves) and (2) slower calcifying colonies that store more energy during environmentally favourable conditions, yet are able to continue calcifying under environmentally stressful conditions (potentially due to their ability to tap energy stored during environmentally favourable times).

These divergent calcification strategies within coral populations may confer stability to populations faced with environmental stress over both short and long timescales. Over short timescales, these strategies increase the probability that at least some colonies (faster calcifiers) flourish when conditions are favourable, while ensuring that there are also survivors (slower calcifiers) during unfavourable times that allow populations to persist (Conover and Schultz 1995). Over longer timescales, these divergent strategies may provide a high-degree of genotypic variability upon which natural selection can act, thereby facilitating the evolution of the population toward optimal weightings of these calcification strategies (Arnott et al. 2006), depending on the magnitude and duration of the environmental perturbation [e.g., short-term anthropogenic cycles (Hughes et al. 2003) vs. medium-term glacial cycles (Daly 1915) vs. longer-term secular trends in $p\text{CO}_2$ trends associated with tectonics (Honisch et al. 2012)]. Although populations of coral species that exhibit these divergent calcification strategies could become more tolerant of anthropogenic stressors in the future, they would also become slower growing through time. Although our current study was not designed to specifically address colony-level calcification responses, our analysis demonstrates a potential trade-off within species that may allow populations to persist under projected global change. This apparent relationship between a colony's basal calcification rate and its response to $p\text{CO}_2$ and thermal stress merits further investigation given its potentially far-reaching implications for corals' response to global change.

*All coral species, except *S. siderea*, exhibited net skeletal dissolution under the highest $p\text{CO}_2$*

Specimens of *S. siderea* maintained positive net calcification under all treatments (Figure 2.1A), suggesting greater resilience to $p\text{CO}_2$ and thermal stress compared to the other

species examined (Ries et al. 2010, Agostini et al. 2013, Von Euw et al. 2017). Indeed, correcting net calcification rates with empirically derived gross dissolution rates (Ries et al. 2016) yields high rates of gross calcification for *S. siderea* even in undersaturated seawater conditions (Figure S2.9a), providing support for the assertion that *S. siderea* is able to maintain conditions supportive of aragonite precipitation at its site of calcification, despite external seawater supporting dissolution of its aragonite skeleton (Castillo et al. 2014, Horvath et al. 2016, Okazaki et al. 2017). The combination of resilient calcification responses to thermal and $p\text{CO}_2$ stress with the high survival exhibited by *S. siderea* in the present study (Figure S2.6A, Tables S2.9, S2.10, S2.11), as well as in prior studies (Castillo et al. 2014, Horvath et al. 2016, Okazaki et al. 2017), suggests that *S. siderea* possesses unique physiological mechanisms for maintaining basic life processes under $p\text{CO}_2$ and thermal stress, and may contribute to its abundant distribution on reefs throughout the Caribbean (Alemu and Clement 2014).

Specimens of *P. strigosa*, *P. astreoides*, and *U. tenuifolia* exhibited net skeletal dissolution in at least one $p\text{CO}_2$ -temperature treatment, with the greatest net dissolution observed under the highest $p\text{CO}_2$ treatment (Figure 2.1; Figure S2.9B-D). *Pseudodiploria strigosa* exhibited the highest rates of net dissolution at the elevated temperature, likely owing, at least in part, to the loss of algal symbionts (i.e., partial bleaching; Figure S2.10) from which corals obtain a significant portion of their energy (Muscatine et al. 1981). Thus, under thermal stress, reduced symbiont densities may lead to diminished photosynthate, reducing energy available for calcification, and eventually leading to thermally-induced mortality as observed in the present study (Figure S2.6B, Tables S2.9, S2.10, S2.11) and previous experiments on juvenile corals (Bassim and Sammarco 2003). Under these

conditions, corals may be unable to produce enough new skeleton to counter the effects of skeletal dissolution in undersaturated conditions (Ries et al. 2016).

Siderastrea siderea and *P. astreoides* maintain constant rates of linear extension under $p\text{CO}_2$ and thermal stress

Increasing $p\text{CO}_2$ had no significant effect on linear extension rates of either *S. siderea* or *P. astreoides* (Figure 2.3), providing support for prior assertions that symbiotic corals exert strong control over the chemical milieu at their site of calcification (Cohen and McConnaughey 2003, Ries 2011, McCulloch et al. 2012, Venn et al. 2013). This constant rate of extension (i.e., volume addition) combined with the threshold decrease in net calcification (i.e., mass addition) with increasing $p\text{CO}_2$ suggests that both species produce less dense skeletons and/or that the gain in skeletal mass associated with the new linear extension is offset by the loss of previously formed skeletal mass via dissolution under extreme $p\text{CO}_2$ (Figure 2.3; Figure S2.9A). Additionally, the observation that *P. astreoides* exhibited net dissolution at both temperatures under several $p\text{CO}_2$ treatments, yet maintained constant rates of linear extension, suggests that dissolution, rather than decreasing skeletal density, is driving the decline in calcification rate of this species under increasing $p\text{CO}_2$ —as the addition of new, less-dense skeleton alone could not cause a net decrease in skeletal mass (i.e., net dissolution).

Linear extension of *S. siderea* and *P. astreoides* did not differ significantly across temperatures (Figure 2.3). This contrasts previous reports linking historical ocean warming to reductions in extension of wild specimens of *S. siderea*, although this decrease was observed only for forereef colonies along the southern MBRS (Castillo et al. 2012). Extension rates of *S. siderea* observed in the present study were generally comparable to those reported for wild

specimens in Belize (Castillo et al. 2012). Conversely, the lack of temperature effect on extension of *P. astreoides* is consistent with the measured calcification response, supporting prior observations that rates of net calcification within this species is driven by rate of linear extension, rather than by changes in skeletal density (Elizalde-Rendon et al. 2010, Carricart-Ganivet et al. 2012).

Experiments reveal corals' differential resilience to future oceanic change

Diverse responses to $p\text{CO}_2$ and warming exhibited by the corals investigated here reveal a spectrum of resilience to future global oceanic change. We confirm the relatively high resilience of *S. siderea* to thermal and $p\text{CO}_2$ stress (Okazaki et al. 2017), the moderate sensitivity of *P. astreoides*, and the relatively high sensitivity of *P. strigosa* (Alemu and Clement 2014, Pratte and Richardson 2014) and *U. tenuifolia* (Lesser 1997, Aronson et al. 2000, Robbart et al. 2004). The results also highlight the relative resilience of the investigated species (excluding *P. strigosa*) to moderate $p\text{CO}_2$ stress, while revealing their high sensitivity to extreme $p\text{CO}_2$. Faster-growing colonies tended to exhibit increased vulnerability to $p\text{CO}_2$ and thermal stress, suggesting variability in tolerance of $p\text{CO}_2$ and thermal stress within populations of these corals—a potential pathway for evolutionary resilience. Collectively, these results reveal the wide spectrum of responses exhibited by four common Caribbean corals in response to changes in ocean pH and temperature, a necessary step in understanding and forecasting the response of coral reef systems to future global change.

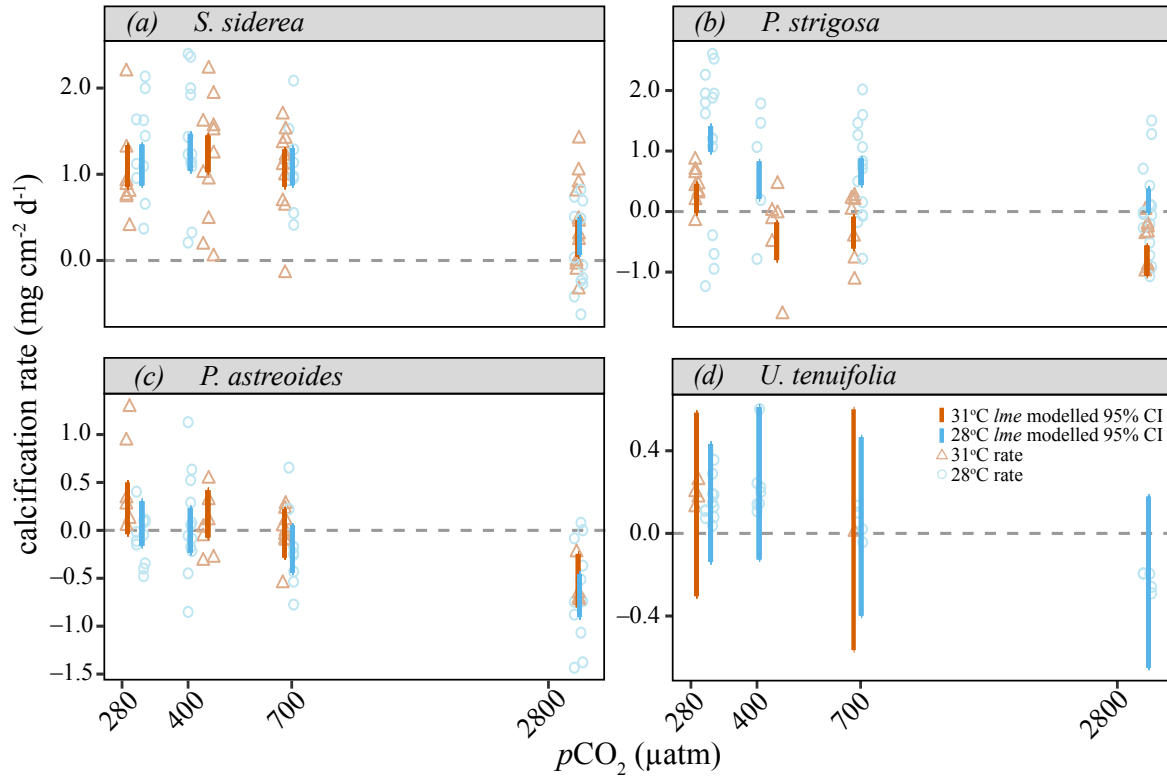


Figure 2.1 Net coral calcification rates

Net calcification rates ($\text{mg cm}^{-2} \text{ day}^{-1}$) for *S. siderea* (A), *P. strigosa* (B), *P. astreoides* (C), and *U. tenuifolia* (D) cultured over a range of $p\text{CO}_2$ and temperature conditions. Blue circles represent net calcification rates for fragments in the 28°C treatments and orange triangles represent net calcification rates for fragments in the 31°C treatments. Blue and orange vertical bars represent modelled 95% confidence intervals for each $p\text{CO}_2$ treatment at 28°C and 31°C , respectively.

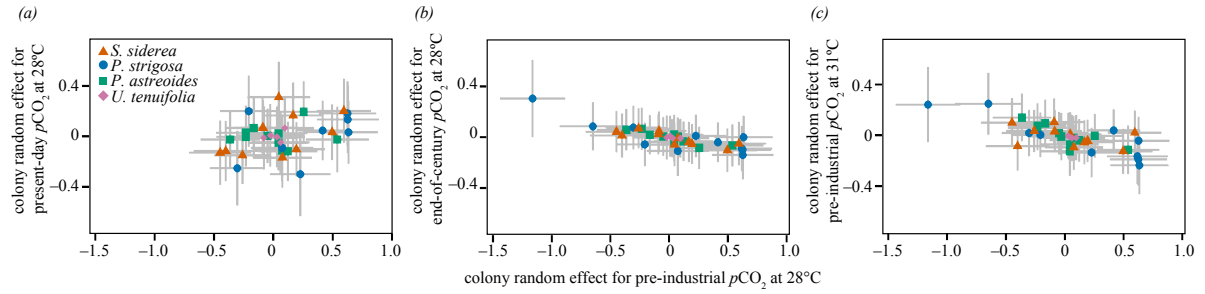


Figure 2.2 Colony-level calcification response to treatment

Estimated random effects and 95% credible intervals of colony on calcification rate of all four species under the control treatment (pre-industrial $p\text{CO}_2$ at 28°C) versus random effects of colony on calcification rate under stress treatments of present-day $p\text{CO}_2$ at 28°C (A), end-of-century $p\text{CO}_2$ at 28°C (B), and pre-industrial $p\text{CO}_2$ at 31°C (C).

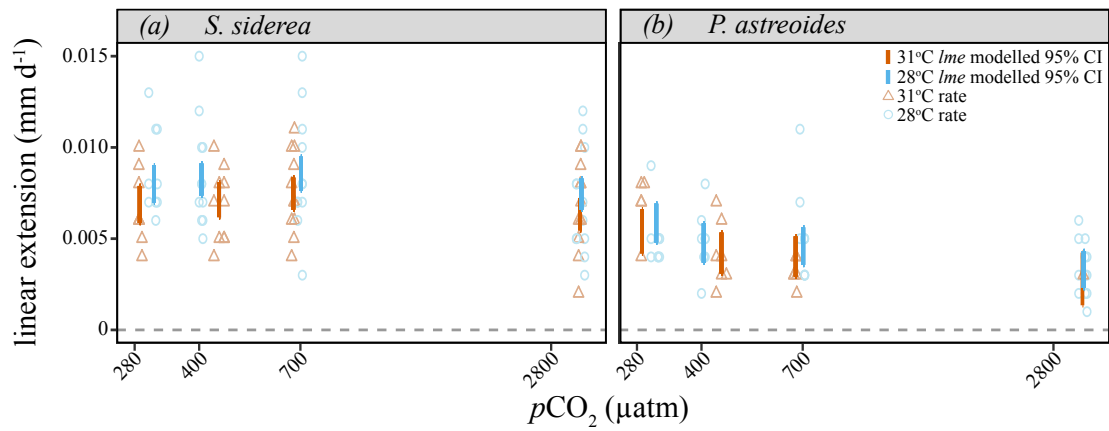


Figure 2.3 Coral linear extension rates

Linear extension rates (mm day⁻¹) for *S. siderea* (A) and *P. astreoides* (B) cultured over a range of pCO₂ and temperature conditions. Blue circles represent extension rates for fragments in the 28°C treatments and orange triangles represent extension rates for fragments in the 31°C treatments. Blue and orange vertical bars represent modelled 95% confidence intervals for each pCO₂ treatment at 28°C and 31°C, respectively.

Treatment	T (°C)	$p\text{CO}_2$ (μatm)	pH	TA (μM)	DIC (μM)	Ω_A	Salinity
1	27.9±0.04	311±18	8.30±0.01	2052±8	1708±15	4.0±0.1	31.7±0.02
2	28.0±0.04	405±17	8.20±0.01	2081±3	1788±10	3.4±0.1	31.8±0.02
3	28.1±0.05	701±17	8.01±0.03	2092±7	1901±8	2.4±0.1	31.7±0.02
4	28.1±0.02	3309±76	7.31±0.01	2131±5	2156±6	0.7±0.1	31.8±0.02
5	31.0±0.04	288±12	8.34±0.01	2101±6	1710±11	4.6±0.1	31.7±0.02
6	31.1±0.05	447±28	8.21±0.01	2077±6	1773±15	3.6±0.1	31.7±0.02
7	30.9±0.03	673±19	8.00±0.01	2082±6	1865±8	2.7±0.1	31.7±0.02
8	31.0±0.05	3285±99	7.29±0.01	2123±4	2135±5	0.8±0.1	31.7±0.02

Table 2.1 Average experimental treatment conditions

Treatment conditions measured either every other day (T, pH, salinity) or every ten days ($p\text{CO}_2$, TA, DIC, Ω_A).

CHAPTER 3: GLOBAL CHANGE ALTERS CORAL HOLOBIONT PHYSIOLOGY AND SUGGESTS FUTURE SHIFTS IN CARIBBEAN CORAL REEF DIVERSITY

Introduction

Human-induced global change is driving unprecedented variations in global ecosystems function, from increases in terrestrial dryness (Greve et al. 2018) and severe storm activity across lower latitudes (Hoegh-Guldberg et al. 2018), to reduced species ranges globally (Hoegh-Guldberg et al. 2019). Coral reefs are a prime example of an ecosystem heavily impacted by changing climate conditions and associated stressors, particularly by ocean acidification and warming (Knowlton 2001, Hoegh-Guldberg et al. 2007). Ocean acidification and warming are predicted to alter many marine ecosystems via oversimplification of ecosystem structure and function, especially for organisms with longer generational times and thus with fewer opportunities to adapt to changing conditions (Nagelkerken and Connell 2015). Thus, understanding the diversity of responses of tropical reef-building corals at both the species and individual levels is critical to predict the success of future populations.

Quantification of calcification rates of corals (i.e., rate of skeletal production) is an informative and common tool used to assess the overall health of corals under stress in both field and laboratory experiments (Allemand et al. 2010, Ries et al. 2010, Comeau et al. 2013b, Crook et al. 2013, Enochs et al. 2014, Kenkel et al. 2015). Understanding changes in calcification rates of corals is critical in evaluating how coral reefs will respond under global change due to the importance of production of new reef structure for the entire ecosystem to

thrive. Previous work quantifying coral calcification rates under global change stressors has demonstrated a diversity of growth responses under stress, including both maintained and suppressed calcification rates (Comeau et al. 2013b, Castillo et al. 2014, Horvath et al. 2016, Okazaki et al. 2017, Bove et al. 2019). Corals that are able to maintain calcification rates under stress are thought to accomplish this at a cost to other metabolic processes in order to continue skeletal growth (Cohen and Holcomb 2009, Davies et al. 2016, Von Euw et al. 2017). Although calcification rates are a valuable measure of coral response to stress, they do not provide insight into how the individual components of the coral holobiont (i.e., animal host versus dinoflagellate endosymbionts) respond to projected global change stressors. In order to address this gap, many studies are now quantifying physiological responses of the coral host and algal endosymbionts under stress in an attempt to understand coral responses more thoroughly (Rodolfo-Metalpa et al. 2010, Schoepf et al. 2013, Kenkel et al. 2015).

Coral tissue biomass and energy reserves (i.e., lipid, protein, carbohydrate) are important aspects of overall coral health (Rodrigues and Grottoli 2007, Schoepf et al. 2013) that provide insight into resilience and recovery capacity in response to environmental stressors (Rodrigues and Grottoli 2007). While energy reserves are extremely important in understanding the coral host response to stress, few studies have looked into how the combination of ocean acidification and warming influence these parameters (Schoepf et al. 2013, Towle et al. 2015). Coral tissue biomass is reliant on the equilibrium between energy sources and expenditures, thus corals with already low biomass (i.e., energy reserves) may experience heightened vulnerability under environmental stress (Thornhill et al. 2011) and may explain the variation of physiological responses to stress within and between species (Okazaki et al. 2017, Bove et al. 2019). However, recent studies have demonstrated that

corals do not consume energy reserves under environmental stress (Schoepf et al. 2013), nor do corals increase metabolic processes (Edmunds 2012). This suggests that corals may utilise other physiological mechanisms as coping tools to maintain growth and host energy reserves, such as relying more heavily on their associated algal endosymbionts for their metabolic needs.

Tropical reef-building corals rely heavily on the maintenance of an endosymbiotic relationship with photosynthetic dinoflagellates (family Symbiodiniaceae) for a significant portion of their energetic needs (Muscatine et al. 1981). However, this relationship often breaks down under times of severe or prolonged stress, especially with increasing seawater temperatures, resulting in the phenomenon referred to as ‘coral bleaching’ (Glynn 1996, Brown 1997, Anthony et al. 2008). As corals bleach in response to ocean acidification and especially warming, physiological processes, including calcification (De'ath et al. 2009, Cantin et al. 2010) and gametogenesis (Szmant and Gassman 1990), deteriorate. Thus, as the symbiosis between the coral host and algal endosymbiont breaks down, both components of the holobiont are likely to exhibit closely tied physiologies. Indeed, the highest measured coral tissue biomass values in several Caribbean reef-building coral species occurred immediately after the highest measured symbiont density and chlorophyll a content (Fitt et al. 2000), highlighting the importance of algal endosymbiont contribution of energy to the coral host.

Countless studies have been conducted to assess the impacts of current and future ocean acidification and warming on tropical coral reefs, however, the consensus of these studies suggests that responses to these stressors will be highly variable (Chan and Connolly 2013, Comeau et al. 2014, Albright et al. 2016, Bahr et al. 2018, Kornder et al. 2018).

Indeed, Barshis et al. (2013) identified potential frontloading of genes (i.e., genes less upregulated under stress than in control conditions) in heat-tolerant colonies of *Acropora hyacinthus* compared to heat-stressed colonies of the same species, identifying a potential explanation for within-species divergent physiological responses. Additionally, previous work has identified divergent gene expression profiles between the coral host and algal endosymbiont community in response to ocean acidification and warming, suggesting that the algal endosymbionts may be more susceptible to these stressors at the larval stage (Rivest et al. 2018), while the host may be more impacted in mature colonies (Leggat et al. 2011, Davies et al. 2018). These differences in transcriptomic responses of the different components of the coral holobiont are also likely highly species-specific, however, overall responses to these stressors appear to be similar across studies (Kaniewska et al. 2012, Moya et al. 2012, Davies et al. 2016). Specifically, corals may divert cellular energy toward processes that promote survival and recovery post-stress events, such as increased respiration and metabolism, at the expense of other physiological processes (Maor-Landaw et al. 2014, Davies et al. 2016). Understanding the molecular mechanisms underpinning the calcification and physiological responses of coral holobionts under projected global change may provide valuable insights into why such variation between species and individuals exist.

To assess the physiological responses of Caribbean coral holobionts to independent and combined ocean acidification (280–3200 μatm) and warming (28, 31 °C), we conducted a 93-day common-garden experiment on 3 species of corals (*Siderastrea siderea*, *Pseudodiploria strigosa*, and *Porites astreoides*) and quantified coral host energy reserves (total protein, carbohydrate, lipid), algal endosymbiont physiology (cell density and chlorophyll a concentration), and gene expression (*S. siderea* only). Based on previous

similar work, we hypothesized that 1) coral hosts would be more susceptible to acidification and warming stress than the associated algal endosymbionts, 2) coral holobionts will be more susceptible to thermal stress than acidification, and 3) physiological responses will be highly species-specific. Our results underline the diversity of physiological responses of Caribbean corals and identify varying susceptibilities of the studied species to projected global change that will drive changes in species abundance.

Methods

Experimental design

The experimental design and implementation is described in detail in Bove et al. (2019) and the specific details of the experimental treatments are included in Appendix 2. Briefly, in June 2015 six colonies each of four Caribbean reef-building corals (*Siderastrea siderea*, *Pseudodiploria strigosa*, *Porites astreoides*, *Undaria tenuifolia*) were collected from inshore and offshore reef environments from the southern portion of the Belize Mesoamerican Barrier Reef System. Corals were immediately transported to Northeastern University's Marine Science Center. Colonies were sectioned into eight equally-sized fragments and maintained in one of eight experimental treatments (three replicate tanks per treatment) for 93 days. The eight treatments encompassed four $p\text{CO}_2$ treatments corresponding to pre-industrial, current-day ($p\text{CO}_2$ control), end-of-century, and an extreme $p\text{CO}_2$ level and two temperatures corresponding to the corals' approximate present day mean (28°C) and projected next-century warming (31°C). These $p\text{CO}_2$ -temperature combinations resulted in eight triplicate (24 tanks total) treatments: 311 (± 96), 405 (± 91), 701 (± 94), 3309 (± 414) μatm at 28°C (± 0.4); and 288 (± 65), 447 (± 152), 673 (± 104), 3285 (± 484) μatm at

31.0°C (±0.4). At the completion of the experimental period, corals were immediately flash-frozen in liquid nitrogen and transported back to the University of North Carolina at Chapel Hill. Coral tissue was removed from the skeleton with an airbrush and stored in 50 mL conical tubes at –80°C until further processing. Due to reduced survivorship of *U. tenuifolia* in response to stress treatments (Bove et al. 2019) (see Appendix 2), this species was not further assessed for physiological analyses in this study.

Host and symbiont physiological measurements

Preserved tissue slurries were homogenized with a tissue tearer (BioSpec Products; Bartlesville, Oklahoma, USA) for several minutes and vortexed for 5 seconds, after which, 1.0 mL of slurry was aliquoted for algal endosymbiont density analysis. Algal endosymbiont aliquots were dyed with 200 µL of a 1:1 Lugol's iodine and formalin solution and cell densities were quantified by performing at least 3 replicate counts of 10 µL samples using a hemocytometer (1 x 1 mm; Hausser Scientific, Horsham, Pennsylvania, USA) and a compound microscope. Algal endosymbiont densities were standardized to total tissue volume and previously measured coral surface area (10⁶ cells per cm²) (Bove et al. 2019).

Remaining tissue slurry was centrifuged at 4400 rpm for 3 minutes to separate the coral host and algal endosymbiont fractions, and the host fraction was poured off from the endosymbiont pellet. Chlorophyll a pigment was extracted from the algal pellet by adding 40 mL of 90% acetone to the conical tube at –20°C for 24 hours. Samples were diluted by adding 0.1 mL of extracted chlorophyll a sample to 1.9 mL of 90% acetone. If samples were too high or too low to read on the fluorometer, samples were reanalysed by either diluting or concentrating the sample, respectively. Extracted chlorophyll a content was measured using a

Turner Design 10-AU fluorometer with the acidification method (Parsons et al. 1984) and expressed as the μg of pigment per cm^2 of coral tissue surface area.

Coral host supernatant was aliquoted (1 mL each) for total protein, carbohydrate, and lipid analysis, and stored at $-80\text{ }^\circ\text{C}$. Glass beads were added to total protein aliquots, vortexed for 15 minutes, and centrifuged for 3 minutes at 4000 rpm. Duplicate samples were prepared with 235 μL of seawater, 15 μL of protein aliquot, and 250 μL of Bradford reagent (*Thermo Scientific*) and left for ca. 20 minutes. Coral host total protein samples were read at 562 nm on a spectrophotometer (Eppendorf BioSpectrometer® basic; Hamburg, Germany) in duplicates and were expressed as mg per cm^2 coral tissue surface area. For coral host carbohydrate, 25 μL of phenol was added to 1000 μL of diluted coral host slurry and vortexed for 3 seconds before immediately adding 2.5 mL concentrated sulphuric acid (H_2SO_4). Samples were incubated at room temperature for 1 minute and then transferred to a room temperature water bath for 30 minutes (Masuko et al. 2005). Finally, 200 μL of each standard and sample was pipetted into a 96-well plate in triplicate and read on a spectrophotometer at 485nm (BMG LABTECH POLARstart Omega; Cary, North Carolina, USA). Total carbohydrate was expressed as mg per cm^2 coral tissue surface area. Finally, coral host lipids were extracted following the Folch Method (Folch et al. 1956) by adding 600 μL of chloroform (CHCl_3) and methanol (CH_3OH) in a 2:1 ratio to 600 μL of host slurry and placed on a plate shaker for 20 minutes before adding 160 μL of 0.05M sodium chloride (NaCl). Tubes were inverted twice and then centrifuged at 3000 rpm for 5 minutes. Finally, the lipid layer was removed and 100 μL was pipetted in triplicate into a 96-well plate for colorimetric assay. The lipid assay was performed by adding 50 μL of CH_3OH to each well before evaporating the solvent at $90\text{ }^\circ\text{C}$ for 10 minutes. Next, 100 μL of H_2SO_4 was added to

every well, incubated at 90 °C for 20 minutes, and cooled on ice for 2 minutes before transferring 75 µL of each sample into a new 96-well plate. Background absorbance of the new plate was read at 540 nm on a spectrophotometer before adding 34.5 µL of 0.2 mg/mL vanillin in 17% phosphoric acid to each well. The plate was read again at 540 nm and coral host lipid concentrations were normalised to coral surface area (mg per cm²) (Cheng et al. 2011).

Statistical analysis of coral holobiont physiology

Three separate three-way mixed-model analyses of variance selected using Akaike information criterion were used to construct modelled 95% confidence intervals of the T0 coral holobiont physiologies and to assess impacts of $p\text{CO}_2$ (factor) and temperature (factor) on total host energy reserves, algal endosymbiont densities, and algal endosymbiont chlorophyll a content for each species after 93 days in the experimental conditions (lme4 (1.1-21)) (Bates et al. 2015a). Parametric bootstraps were performed to model 95% confidence intervals with 2000 iterations (Wilcox 2010). Significant differences between treatments were defined as non-overlapping 95% confidence intervals (see Appendix 3; Tables S3.1 – S3.6). Because reef environment was not a significant predictor of any parameter, colonies were pooled across reef environments and these effects were not further addressed. Principal component analyses (PCA) (function *prcomp*) of scaled and centered physiological parameters (calcification rates are those reported previously for the same samples in Bove et al. (2019)), host carbohydrate, host lipid, host protein, algal endosymbiont chlorophyll a, algal endosymbiont cell density) were employed to further assess the relationship between physiological parameters and treatment conditions for each

species. Main effects (temperature, $p\text{CO}_2$, and the combination of temperature with $p\text{CO}_2$) were evaluated using the *adonis* function (see Appendix 3; Tables S3.7 – S3.9). All statistical analyses were performed in R (version 3.5.2) (R Core Development Team 2016).

Siderastrea siderea transcriptome preparation and differential gene expression analysis

A subset of 42 *S. siderea* fragments was selected for transcriptomic analysis at the completion of the experiment. These fragments were selected to represent all treatments and both reef environments to better understand how this species responds under independent and combined ocean acidification and warming (Table 1.1). Coral RNA was isolated with the RNAqueous-Micro Total RNA Isolation Kit (*Invitrogen*) following the manufacturer's protocols with some additional steps. Prior to RNA isolation, samples were thawed on ice and placed in a bead beater for 1 min with a small number of beads and 150 μL of lysis buffer before proceeding with the manufacturer's protocol. Trace DNA contamination was eliminated with DNase I (*Invitrogen*) digestion for 20 min at 37°C. Total RNA was transcribed into first-strand cDNA and the complementary DNA was PCR amplified. Each library received an individual barcode adapter through a secondary PCR and samples were sequenced across two lanes of *Illumina HiSeq 2500* at Tufts Genomics, which yielded pair-ended (PE) 50 base pair (bp) reads.

Total raw reads across libraries ranged from 17,481 to 15,746,927 PE 50 bp sequences (Table 3.1). Quality filtered reads (filtered using *Fastx_toolkit*) were mapped to the coral holobiont transcriptome (*S. siderea* combined with *Symbiodinium goreauii*). Mapped reads were then subset as either coral host or algal endosymbiont for downstream analysis, and ranged from 664 to 791,604 in the coral host and 233 to 382,453 in the algal

endosymbiont (Table 3.1). Differential gene expression analysis was performed on the separated coral host and algal endosymbiont counts with *DESeq2* [1.22.2; (Love et al. 2014)] in R (R Core Development Team 2016) by treatment (each temperature crossed with $p\text{CO}_2$ treatments). Because sampling across reef environments was uneven, samples were pooled by reef environment for all downstream analyses. Raw counts were *vst* (variance stabilizing transformation) transformed and then normalised for size factor differences using the median ratio method. A principal component analysis (*prcomp* function) and the *adonis* function were employed to test for overall expression differences across treatments. Pairwise Wald tests were conducted for each of the seven treatments through comparison to the control treatment (400 μatm ; 28 °C). The number of differentially expressed genes (DEGs) identified in each pairwise comparison were corrected for false positives using the Benjamini and Hochberg false discovery rate (FDR) correction for multiple testing (Benjamini and Hochberg 1995). A contig was considered significantly differentially expressed if it met a FDR adjusted $P < 0.05$.

Weighted gene co-expression network analysis and module gene ontology enrichment

Correlation structure within the transformed gene expression and physiological data was examined using a Weighted Gene Co-expression Network Analysis (WGCNA) (Langfelder and Horvath 2008) to identify groups of genes (“modules”) that are co-regulated within temperature and $p\text{CO}_2$ treatments across *S. siderea* samples. Expression of genes within each module is summarized by the overall expression and represented by the eigengene, which can then be correlated *post-hoc* with provided traits, in this case treatment, natal reef environment, and holobiont physiology (calcification rate, host carbohydrate, host

lipid, host protein, algal endosymbiont chlorophyll a, algal endosymbiont cell density). Resulting correlations with provided traits were assessed to identify modules that capture pathways correlating with response to treatment conditions (temperature, and $p\text{CO}_2$) as well as with other physiological parameters. Gene Ontology (GO) enrichment analysis was also applied to WGCNA modules to identify GO enrichment within each selected module.

Results

Coral host and algal endosymbiont physiology

Coral host total tissue energy reserves (mg cm^{-2}) was calculated as the sum of each protein, lipid, and carbohydrate value per coral host. No overall effect of $p\text{CO}_2$ was quantified in any of the three species examined (Figure 3.1A). Elevated temperature (31°C) resulted in a clear reduction in total coral host energy reserves in only *P. strigosa* across all $p\text{CO}_2$ treatments (Figure 3.1A). Total host energy reserves of *P. astreoides* at T0 were clearly greater than the total energy reserves quantified in coral hosts maintained under control treatment at T90 (Figure 3.1A). There was no difference in total energy reserves between T0 and T90 control coral hosts in either *S. siderea* or *P. strigosa*.

Neither $p\text{CO}_2$ nor temperature exhibited a statistically clear overall effect on algal endosymbiont cell densities ($10^6 \text{ cells cm}^{-2}$) quantified at T90 in any of the three coral species (Figure 3.1B). Algal endosymbiont cell density in *P. astreoides* T0 densities were clearly lower than those measured under all treatments at T90 (Figure 3.1B). Algal endosymbiont cell densities did not exhibit a statistically clear difference between T0 fragments and T90 fragments maintained at the control treatment in *S. siderea* or *P. strigosa*.

All species exhibited reduced algal endosymbiont chlorophyll a ($\mu\text{g cm}^{-2}$) in the highest $p\text{CO}_2$ treatment, while elevated temperature (31°C) only clearly reduced chlorophyll a in the algal endosymbionts associated with *P. strigosa* (Figure 3.1C). Algal endosymbiont chlorophyll a content of *S. siderea* and *P. strigosa* at T0 was lower than the measured chlorophyll a in fragments maintained in the control treatment at T90 (Figure 3.1C). Conversely, chlorophyll a measured at T0 was not clearly different than in fragments reared in the control treatment at T90 for *P. astreoides*.

Principal component analysis of coral holobiont physiology

Two principal components (PCs) explained approximately 69% of the variance in physiological responses of the *S. siderea* holobiont to ocean acidification and warming treatments (Figure 3.2A). Treatment $p\text{CO}_2$ predominantly drove physiological responses ($P = 0.026$), while temperature and reef environment were not significant ($P > 0.05$). Samples with higher host energy reserves (lipid, protein, carbohydrate) separated out from samples with higher calcification rates, while samples with greater endosymbiont physiology (chlorophyll a, cell density) were more similar to samples with higher calcification rates. Further, samples with greater endosymbiont physiology and calcification rates were more present in low $p\text{CO}_2$ treatments (Figure 3.2A). For *P. strigosa*, 78% of the variance in the holobiont responses to treatments was explained by two PCs (Figure 3.2B). Both treatment temperature ($P = 0.013$) and $p\text{CO}_2$ ($P = 0.013$) drove coral holobiont physiology, however native reef environment again did not impact overall physiology ($P = 0.07$). Samples within the elevated temperature treatment clustered closely together at the low end of all measured parameters, however, samples from each $p\text{CO}_2$ treatment were less clearly similar (Figure

3.2B). Finally, two PCs explained about 63% of the total variance of the *P. astreoides* holobiont response to treatment (Figure 3.2C). Again, temperature ($P = 0.039$) and $p\text{CO}_2$ ($P = 0.011$) drove separations in holobiont physiology, while reef environment was nonsignificant ($P = 0.744$). Coral holobiont samples separated most clearly along PC1 (43.6%) with overall greater physiology, while PC2 (19.8%) exhibited separation of samples with higher protein, carbohydrate, and calcification rates from those with higher endosymbiont physiology and lipid content (Figure 3.2C).

Siderastrea siderea host and algal endosymbiont transcriptomic responses to temperature and $p\text{CO}_2$

Transcriptomic analysis of *S. siderea* host expression of significant DEGs (FDR = 0.05) in response to $p\text{CO}_2$ alone exhibited a total of 867 DEGs, representing a total of 5.7% of the entire transcriptome responding to treatment (Figure 3.3A). Temperature drove few DEGs in the coral host (399) to only represent 1.98% of the total host transcriptome responding to experimental treatments (Figure 3.3A). Finally, the combination of $p\text{CO}_2$ with temperature resulted in 122 significant DEGs, only about 0.8% of the host transcriptome (Figure 3.3A). Similarly, transcriptomic analysis of *S. siderea* algal endosymbiont (*Cladocopium goreau*) expression in response to $p\text{CO}_2$ resulted in 6.65% (1567) of the endosymbiont transcriptome expressing significant DEGs (FDR = 0.05) (Figure 3.3B). Within $p\text{CO}_2$ DEGs, the majority of the significant DEGs were enriched (99%) in higher $p\text{CO}_2$ treatments. Both temperature and the combination of $p\text{CO}_2$ with temperature resulted in no significant transcriptomic responses in the algal endosymbionts, highlighting the sensitivity of the endosymbionts to $p\text{CO}_2$ but not temperature (Figure 3.3B).

Principal component analysis (PCA) of the overall vst-transformed expression profiles of the coral host explained approximately 58% of the expression differences with two PCs (Figure 3.3C). Treatment $p\text{CO}_2$ ($P = 0.001$) and temperature ($P = 0.015$) significantly drove differences in *S. siderea* host expression profiles. Conversely, two PCs explained approximately 95% of the overall expression profile differences in *C. goreau*, with $p\text{CO}_2$ ($P = 0.002$), but not temperature ($P = 0.083$), driving expression differences (Figure 3.3D).

Weighted gene correlation network analysis

WGCNA assigned 8,791 of the coral host vst-transformed isogroups to four modules (merging of 0.62) (Figure 3.4). The “brown” module (1047 genes) was significantly correlated with several treatments and physiological parameters, including upregulation with algal endosymbiont cell density ($r = 0.44$) and chlorophyll a concentration ($r = 0.34$), while the genes were downregulated with $p\text{CO}_2$ ($r = 0.41$). The “green yellow” module (2159 genes) was upregulated in algal endosymbiont cell density ($r = 0.35$) while the “blue” module (2527 genes) was downregulated ($r = 0.41$). Genes in the “midnight blue” module (334) were upregulated with $p\text{CO}_2$ ($r = 0.60$) and downregulated with calcification rate ($r = 0.36$) and temperature ($r = 0.39$). Temperature was associated with the upregulated genes in both the “cyan” ($r = 0.34$) and “dark red” ($r = 0.63$) modules, while the genes in the “dark turquoise” ($r = 0.50$) module were downregulated. Finally, the “blue” module (2527 genes) was significantly downregulated with algal endosymbiont cell density ($r = 0.40$) and the “dark green” module (179 genes) was significantly upregulated with carbohydrates ($r = 0.32$) (Figure 3.4B).

Gene Ontology (GO) enrichment analysis of the “blue” and “green yellow” modules correlating with algal endosymbiont density identified several pathways for “cellular component” (CC), “biological processes” (BP), and “molecular function” (MF) (Figures 3.4B, S3.9). Analysis of the “dark green” module associated with coral host carbohydrate content identified several CC, BP, and MF pathways correlating with the module (Figures 3.4B, S3.10). While modules significantly correlated with algal endosymbiont chlorophyll a (“brown”), calcification (“midnight blue”), $p\text{CO}_2$ (“brown”, “midnight blue”), temperature (“midnight blue”, “cyan”, “dark red”, “dark turquoise”), and algal endosymbiont cell density (“brown”), no significant GO terms were identified in these modules associated with the traits (Figure 3.4B).

GO enrichment of the “blue” module identified significantly downregulated terms associated with oxidative metabolism, cell growth, and proton transport in the CC category, while both BP and MF categories identified downregulation of terms relating to homeostasis, metabolism, oxidative and heat stress, and immune responses (Figures 3.4B, S3.9). The “green yellow” module identified upregulation of several terms within the CC, BP, and MF categories associated with response to environmental stimuli, cellular communication, metabolic processes, and cytoskeleton maintenance (Figures 3.4B, S3.9). Finally, the “dark green” module exhibited significantly upregulated GO enrichment terms associated with protein synthesis in the CC and MF categories, while the BP process exhibited terms associated with growth and metabolism (Figures 3.4B, S3.10).

No significant GO terms were identified through GO enrichment analysis in any of the algal endosymbiont modules correlating significantly with treatments or physiological parameters (Figure S3.11).

Discussion

Coral host total energy reserves show little change under simulated global change

Ocean acidification, warming, and the combination of the two stressors is expected to considerably reduce coral abundance and cover throughout the Greater Caribbean due to the physiological strain placed on the corals under these stressors (Hughes et al. 2017a, Drury 2019). Here, we demonstrate the variety of physiological responses, both at the coral host and the algal endosymbiont levels, to simulated ocean acidification and warming scenarios. Increasing $p\text{CO}_2$ did not elicit a reduction in the total host energy reserves (sum of protein, carbohydrate, and lipid concentrations per sample) in any of the three species examined, even under extreme $p\text{CO}_2$ or at the elevated temperature. Further, the lack of a clear response to $p\text{CO}_2$ was observed in the separate host lipid, protein, and carbohydrate concentrations for each species (Figures S3.1 – S3.3), suggesting all of the host energy reserves quantified were similarly unaffected by $p\text{CO}_2$. When compared with previously measured calcification rates (Figure S3.4), these results demonstrate that the corals in the current study do not consume tissue energy reserves as a mechanism to sustain net calcification under ocean acidification, as have been seen previously in similar studies (Edmunds 2012, Schoepf et al. 2013, Towle et al. 2015).

Conversely, total host energy reserves of only *P. strigosa* were clearly reduced under warming conditions regardless of $p\text{CO}_2$, likely driven by decline in protein concentrations (Figure S3.3B), and this species similarly exhibited slower calcification rates (Figure S3.4B). Indeed, *P. strigosa* is known to be a more thermally sensitive coral species (Scheufen et al. 2017, Rippe et al. 2018), especially compared with *S. siderea* and *P. astreoides*, and it is likely that the combination of reduced calcification rates with consumption of host energy

reserves is indicative of the fragments moving towards mortality. Thermal events on coral reefs are generally considered more acute stress events (on the scale of hours to weeks) (Hughes et al. 2018), thus exposure of these corals to more than 90 days of constant elevated temperatures may have elicited a more severe response to elevated temperature in *P. strigosa*. Although host energy reserves in *S. siderea* were not clearly different under elevated temperatures, the quantified values exhibited a trend towards lower total host energy reserves under warming compared to conspecifics reared at ambient temperature. Thus, it is possible that if the experiment were prolonged beyond the 93 days or employed a higher treatment temperature (i.e., greater than 31°C) that host energy reserves would be reduced for this species as well (Fitt et al. 1993). Indeed, calcification rates of these *S. siderea* fragments were not impacted by elevated temperature (31 °C), while corals collected from a similar region exhibited clearly reduced calcification rates when maintained at a slightly higher temperature for a similar duration (32 °C for 95 days) (Castillo et al. 2014). Because warming predominantly impacts the symbiosis between the coral host and algal endosymbiont (Brown 1997, Coles and Brown 2003, Baird et al. 2009), algal endosymbiont community and physiology likely play a significant role in both the calcification and host physiological responses of the three coral species examined.

Algal endosymbionts exhibit productivity loss under ocean acidification

While $p\text{CO}_2$ did not clearly alter the coral host energy reserves in any species examined in this study, *S. siderea* exhibited clear reductions in algal endosymbiont chlorophyll a concentration along with increasing $p\text{CO}_2$ and both *P. strigosa* and *P. astreoides* demonstrated trends suggestive of reduced chlorophyll a concentration under high

$p\text{CO}_2$, contrasting previous work (Hii et al. 2009, Crawley et al. 2010, Schoepf et al. 2013). Chlorophyll a concentrations are representative of the efficiency of the algal endosymbionts living within the coral tissue (Jones 1997), thus higher chlorophyll a content is generally interpreted to represent more productive endosymbiont communities (Prezelin 1987). The observed decline of chlorophyll a within fragments of *S. siderea*, along with the similar trends in *P. strigosa* and *P. astreoides*, in response to increasing $p\text{CO}_2$ may suggest that symbiont communities within the coral holobiont may become less efficient at photosynthesizing, consequently providing less autotrophically-derived carbon to the coral host (Muscatine et al. 1981, Anthony and Fabricius 2000). However, chlorophyll a alone does not fully represent algal endosymbiont physiology within a coral holobiont and thus should also be interpreted in the context of overall endosymbiont cell density.

While chlorophyll a concentration exhibited a clear reduction (*S. siderea* only) or declining trends (*P. strigosa* and *P. astreoides*) suggestive of sensitivity to increasing $p\text{CO}_2$, algal endosymbiont cell density only resulted in a trend in *S. siderea* with increasing $p\text{CO}_2$ and no clear effect on either *P. strigosa* or *P. astreoides*. This is consistent with previous work that demonstrated no change in algal cell density in several species of corals collected from Fiji (Schoepf et al. 2013), as well as in *Acropora cervicornis* collected from the Florida Keys (Towle et al. 2015). However, another study found clear decreases in algal endosymbiont cell densities in *Acropora millepora* from the Great Barrier Reef when exposed to elevated $p\text{CO}_2$ for 28 days (Edmunds 2011), a similar timescale to Schoepf et al. (2013) but shorter than both the current experiment (93 days) and Towle et al. (2015) (~56 days). The variable impacts of $p\text{CO}_2$ across species, regions, and experimental durations suggests that responses of the algal endosymbiont densities are highly variable and complex

when taken out of context of other algal endosymbiont physiology parameters (Fitt et al. 2000).

Experimental warming did not elicit a clear response in algal endosymbiont physiology (chlorophyll a or cell density) in *S. siderea* or *P. astreoides*. However, chlorophyll a concentration in *P. strigosa* was clearly reduced in all warming treatments and cell density exhibited a similar trend, although not significant. These algal endosymbiont physiology trends are not unexpected for the three species examined due to similar calcification and host physiology responses observed on the same fragments, and highlight the relative resilience of both *P. astreoides* and *S. siderea* under warming conditions (Okazaki et al. 2017, Bove et al. 2019). While warming is generally associated with bleaching, especially during prolonged exposure to elevated temperatures, *S. siderea* did not show signs of bleaching while *P. strigosa* was clearly bleached, especially over time (Figure S3.5). Interestingly, previous studies using colonies of *S. siderea* collected from a similar region on the Belize MBRS exhibited bleaching in warming experiments when the species was maintained at 32 °C for either 60 (Horvath et al. 2016) or 95 days (Castillo et al. 2014). The present study and those conducted previously only differ in temperature treatments by 1 °C, highlighting the potential consequences of even slight temperature increases on the symbiosis between the coral host and the algal endosymbiont. Additionally, the three species are known to host varying algal endosymbiont communities. Indeed, *S. siderea* is known to predominately host Symbiodiniaceae from the genus *Cladocopium*, while *P. strigosa* hosts both *Cladocopium* spp and *Breviolum* spp and *P. astreoides* hosts the genera *Breviolum* and *Symbiodinium* (LaJeunesse 2002). Previous studies have demonstrated variable thermal tolerances of different algal endosymbiont species (Suggett et al. 2008, Gregoire et al. 2017),

potentially driving the different trends in cell density and chlorophyll a concentration observed. Because of the major role these differing algal endosymbiont communities play in the coral holobiont, the algal communities should be assessed in the future.

Consideration of both cell density and chlorophyll a concentration together provides further insight into the overall physiology of algal endosymbionts hosted within the coral holobiont by understanding the efficiency per algal cell within each fragment (Mason 2018). For example, *S. siderea* fragments from the present study exhibited declines in both algal endosymbiont chlorophyll a and cell density with increasing $p\text{CO}_2$, but not temperature, suggesting that the algal endosymbiont communities within this species may be more sensitive to projected ocean acidification, exhibiting less dense, less efficient algal communities. Indeed, several other studies have demonstrated bleaching in corals, via reduced endosymbiont densities and chlorophyll a concentration, however the reasons behind the bleaching remains unclear (Anthony et al. 2008, Kaniewska et al. 2012, Mason 2018). Conversely, fragments of both *P. strigosa* and *P. astreoides* exhibited declining trends in chlorophyll a concentration accompanied by no clear change in algal endosymbiont cell density with increasing $p\text{CO}_2$, likely indicative of declining endosymbiont photosynthetic efficiencies (Prezelin 1987). Overall, these results confirm the diversity of algal endosymbiont responses under projected global change scenarios among coral species and highlight the need to better understand the mechanisms driving bleaching responses in the coral holobiont.

Species-specific holobiont physiology highlights overall response to ocean acidification

Understanding the individual physiological responses of the coral host and the algal endosymbionts provides valuable insight into the relationships within the coral holobiont, however, it is equally important to assess the two in conjunction to investigate potential drivers of the coral holobiont responses under global change stressors. Indeed, while simulated ocean acidification conditions only altered some parameters within the coral holobiont in some species, $p\text{CO}_2$ treatment clearly drove sample differences in principal component analyses on all three coral holobiont species. The significance of $p\text{CO}_2$ on the holobiont response highlights the complexity of the coral holobiont under stress (Weis 2010, Schoepf et al. 2013, Hoadley et al. 2019) and suggests that by only assessing a few physiological parameters, studies may be missing important changes to the coral holobiont. Unsurprisingly, the coral holobiont physiology of *P. strigosa* was also clearly explained by temperature treatment, with fragments reared at the elevated temperature clustering closely together at the low end of all physiological measurements. All measured physiological parameters within *P. strigosa* exhibited similar trends in the principal component analysis, with higher physiologies occurring in the control temperature, regardless of $p\text{CO}_2$ treatment. This is likely representative of the overall holobiont deterioration in response to thermal stress which would have likely led to total mortality if the experiment had been conducted longer, as is seen during mass bleaching events *in situ* (Eakin et al. 2010). Temperature also impacted *P. astreoides* holobiont physiology, with higher physiologies generally in the warmer treatment, while temperature did not clearly affect *S. siderea* holobiont physiology. This difference in coral holobiont physiology temperature responses is not surprising given that *P. astreoides* is generally considered a weedier coral that can persist in less-desirable

conditions (Green et al. 2008, Darling et al. 2012, Grottoli et al. 2014, Manzello et al. 2015), while *S. siderea* and *P. strigosa* are classified as ‘stress tolerant’ species with varying levels of susceptibility and resilience to environmental stressors (Alemu and Clement 2014, Castillo et al. 2014, Venti et al. 2014, Davies et al. 2016, Horvath et al. 2016, Neal et al. 2017, Okazaki et al. 2017).

Within the *S. siderea* holobiont physiology, host energy reserves drove similar physiological responses while algal endosymbiont parameters were more similar to one another. Interestingly, fragment calcification rate was more similar to algal endosymbiont physiology, highlighting the importance of retaining a healthy algal endosymbiont community for the maintenance of net calcification rates of *S. siderea*, especially under global change. This relationship suggests that *S. siderea* is able to maintain net calcification primarily due to carbon allocation from the associated algal endosymbionts (Muscatine and Cernichiari 1969). Indeed, previous work with *S. siderea* reported significant reductions in calcification rates accompanied by bleaching under warming scenarios (Castillo et al. 2014, Horvath et al. 2016). Conversely, *P. astreoides* exhibited similar protein, carbohydrate, and calcification physiology, highlighting the importance of maintaining protein and carbohydrate for sustained calcification rates (Allemand et al. 2004, Grottoli et al. 2004, Allemand et al. 2010). Additionally, lipid content within the *P. astreoides* host drove similar physiology patterns to both algal endosymbiont cell density and chlorophyll a concentration, indicative of a positive relationship between algal endosymbionts and coral host lipid content (Yamashiro et al. 2005, Chen et al. 2017). Together, these trends suggest that host energy reserves are important for maintaining calcification rates in *P. astreoides*, however, protein and carbohydrate are likely not being acquired/maintained via symbiosis with the algal

endosymbionts. Conversely, fragments with higher lipid content and algal endosymbiont physiology may be allocating energy away from skeletal growth towards other metabolic processes to promote a healthier coral holobiont (Grottoli et al. 2004). Overall, it is clear that coral holobiont responses to ocean acidification and warming cannot be easily explained through assessment of host or algal endosymbiont alone, emphasizing the importance of quantifying as many response parameters as possible in similar studies to gain accurate perspectives of future coral reefs.

Siderastrea siderea coral host exhibits greater transcriptomic response to global change stressors

Differential gene expression after exposure to ocean acidification and warming scenarios for 93 days highlight a greater transcriptomic response in the *S. siderea* coral host than in the algal endosymbionts. These findings suggest that the coral host may be responding more to acidification, and especially warming and the combination of stressors, than their associated algal endosymbionts as suggested previously (Leggat et al. 2011, Barshis et al. 2013, Davies et al. 2018). Further, both the coral host and algal endosymbionts exhibited a greater transcriptomic response to ocean acidification than warming, suggesting that the temperature employed in this study was not high enough to elicit symbiotic breakdown as seen previously (Davies et al. 2018), with the extreme $p\text{CO}_2$ treatment driving similar overall expression profiles in both the coral host and algal endosymbiont. Previous work has demonstrated transcriptomic responses of the coral host (Kaniewska et al. 2012, Moya et al. 2012, Davies et al. 2018) and algal endosymbionts (Rivest et al. 2018) to changes in seawater $p\text{CO}_2$, attributing the responses to changes in ion transportation, respiration, and oxidative stress response. The differences between the coral host and algal endosymbiont

differential expression highlight the need to further investigate the molecular underpinnings behind the symbiosis between the coral host and algal endosymbionts.

While WGCNA identified several coexpression modules of genes in both the *S. siderea* coral host and algal endosymbionts, Gene Ontology (GO) enrichment only identified significant terms associated with identified modules in the coral host, again highlighting the strong transcriptomic response of the coral host. Several coexpression modules within the coral host exhibited upregulation of genes corresponding to responses to environmental stimuli, growth, protein synthesis, and metabolic processes (Mayfield et al. 2010, Kaniewska et al. 2012, Moya et al. 2012, Davies et al. 2016) in association with algal endosymbiont cell densities and coral host carbohydrate content. This combined with downregulation of genes within the “blue” module corresponding to oxidative metabolism, immune response, and proton transport (Kaniewska et al. 2012, Moya et al. 2012, Granados-Cifuentes et al. 2013, Davies et al. 2016) suggest that fragments with greater endosymbiont densities were overall growing more and exhibited less stress signals. This agrees with the extensive evidence highlighting the importance of algal endosymbionts for the coral holobiont in order to maintain growth and survival, especially under stress (Brown 1997, Anthony et al. 2008, Baird et al. 2009, Leggat et al. 2011, Rivest et al. 2018). It is possible that the healthy association with the algal endosymbionts allow the coral host to allocate resources away from processes that are not necessary during times of homeostasis, such as immune response, towards increased growth to take advantage of the favorable conditions (Metcalf and Monaghan 2001, Bove et al. 2019). Conversely, some coral holobionts may actually allocate energy towards increasing metabolism as an adaptative strategy of survival indicating a stress

response (Moya et al. 2012), however, further evidence of these stress signals were not identified within these gene expression modules.

WGCNA identified several modules associated with temperature and $p\text{CO}_2$ treatment in the host, but not in the algal endosymbionts. While no significant GO terms were identified within any of these modules in the coral host, these results suggest that these treatments elicited a stress response in the coral host. Similar responses within the coral holobiont have been reported in response to elevated $p\text{CO}_2$ (Kaniewska et al. 2012, Moya et al. 2012) and temperature (Davies et al. 2016). Alone, warming has been shown in *S. siderea* to increase catabolic processes and reduce responses to environmental stimuli after long-term exposure (Davies et al. 2016), however, the same signs of physiological shutdown were not seen in the current study highlighting the significance that ocean warming of a single degree can have on Caribbean corals. Additionally, many previous studies identified significant increases in genes associated with proton transport or respiration in response to changing $p\text{CO}_2$ (Kaniewska et al. 2012, Moya et al. 2012, Davies et al. 2018), no similar responses were identified in the current study. Proton transport has been associated with increased calcification in corals through proton pumps to remove protons from the calcifying fluid (Cohen and McConnaughey 2003, Ries 2011), and has been proposed as a sign of acclimation of corals to elevated $p\text{CO}_2$ (Davies et al. 2016). To better understand the role of proton transport in coral calcification, it would be valuable to pair skeletal growth rates and gene expression with a measure of calcifying fluid saturation state.

Conclusions

As global change continues to persist, it is critical to understand species-specific coral holobiont responses under ocean acidification and warming scenarios in order to predict the future state of Caribbean coral reef assemblages. Results from the present study suggest that *S. siderea* may become dominant reef builders across the Caribbean due to their maintenance of tissue energy reserves, minimal transcriptomic response to stress, and relatively unaltered symbiosis with their algal endosymbionts (Figure 3.5). Conversely, *P. strigosa* was unable to maintain any holobiont physiological parameters under warming, suggesting that this species will be particularly vulnerable to thermal stress, likely resulting in widespread bleaching and mortality (Figure 3.5). Finally, *P. astreoides* exhibited shifts in host and algal endosymbiont physiology throughout the experiment, however, $p\text{CO}_2$ and temperature did not clearly elicit a response indicating this species may also fair better than most under global change (Figure 3.5). These results also demonstrate that while ocean warming is a severe acute stressor that will have dire consequences for coral reefs globally, chronic exposure to increasing $p\text{CO}_2$ may be impacting the coral holobiont physiology to a greater extent than previously assumed.

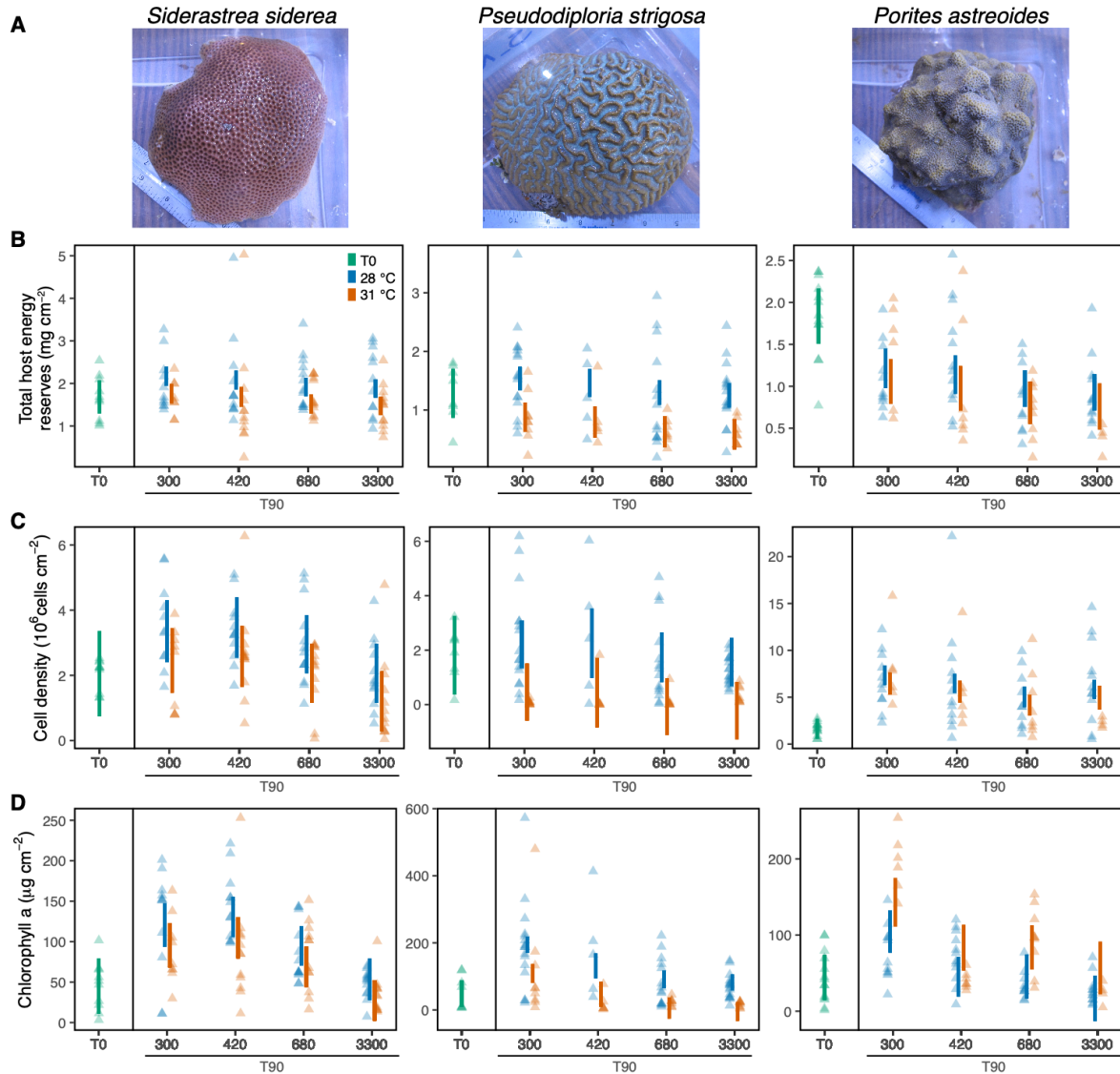


Figure 3.1 Coral host and algal endosymbiont physiology

Representative coral colony images (A) and modelled 95% confidence interval of (B) total host energy reserves (mg cm⁻²), (C) cell density (10⁶ cells cm⁻²), and (D) Chlorophyll a (μg cm⁻²) for *S. siderea*, *P. strigosa*, and *P. astreoides* at T0 (green) or T90 (red/blue), with individual coral fragment physiology denoted by points. Blue denotes 28°C and red denotes 31°C, with pCO₂ treatment along the x axis.

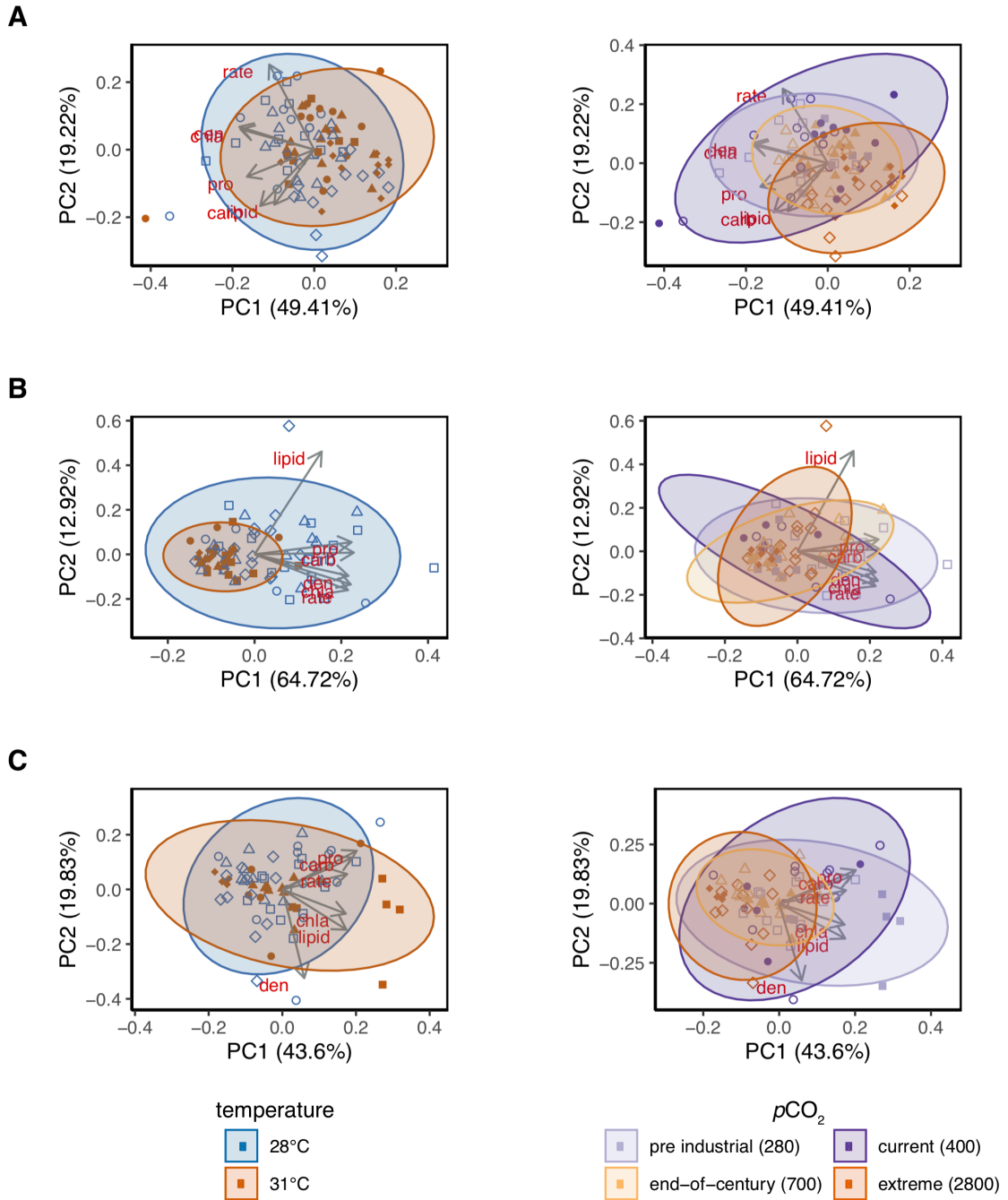


Figure 3.2 Coral holobiont physiology principal component analyses

Principal component analyses of overall holobiont physiology for (A) *S. siderea*, (B) *P. strigosa*, and (C) *P. astreoides*. Left column within each panel represents the data separated by temperature treatment (blue = 28 °C; red = 31 °C) and the right panel colours depict $p\text{CO}_2$ treatment (light purple = pre industrial/280; dark purple = current day/400; light orange = end of century/700; dark orange = extreme/2800).

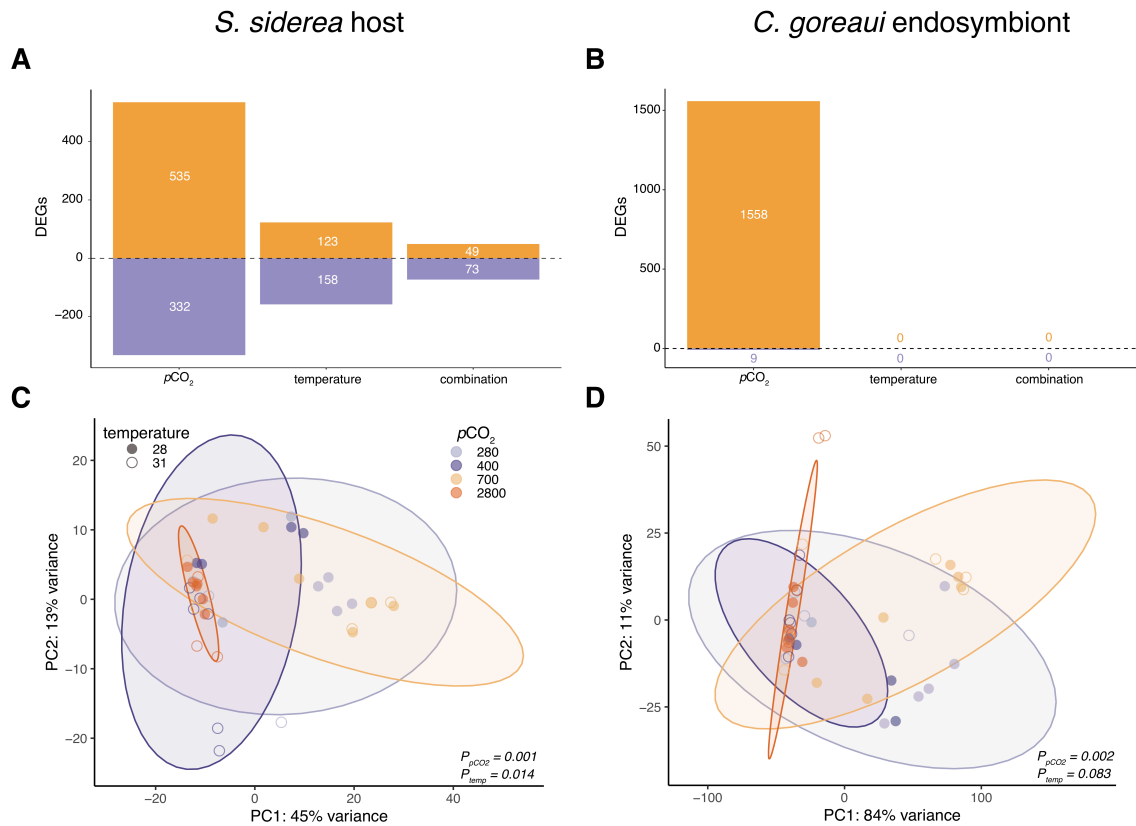


Figure 3.3 *Siderastrea siderea* host and algal endosymbiont gene expression

Bar plot depicting the numbers of significantly ($P < 0.05$) differentially expressed genes (DEGs) for *S. siderea* coral host (A) and algal endosymbionts (*C. goreau*; B) in response to $p\text{CO}_2$, temperature, or the combination of $p\text{CO}_2$ with temperature stress. Principal component analysis of the vst transformed isogroup clusters by $p\text{CO}_2$ and temperature treatment in both the coral host (C) and algal endosymbiont (D). $p\text{CO}_2$ drove significant profiles in both the host and endosymbionts, while temperature only elicited differences in the coral host.

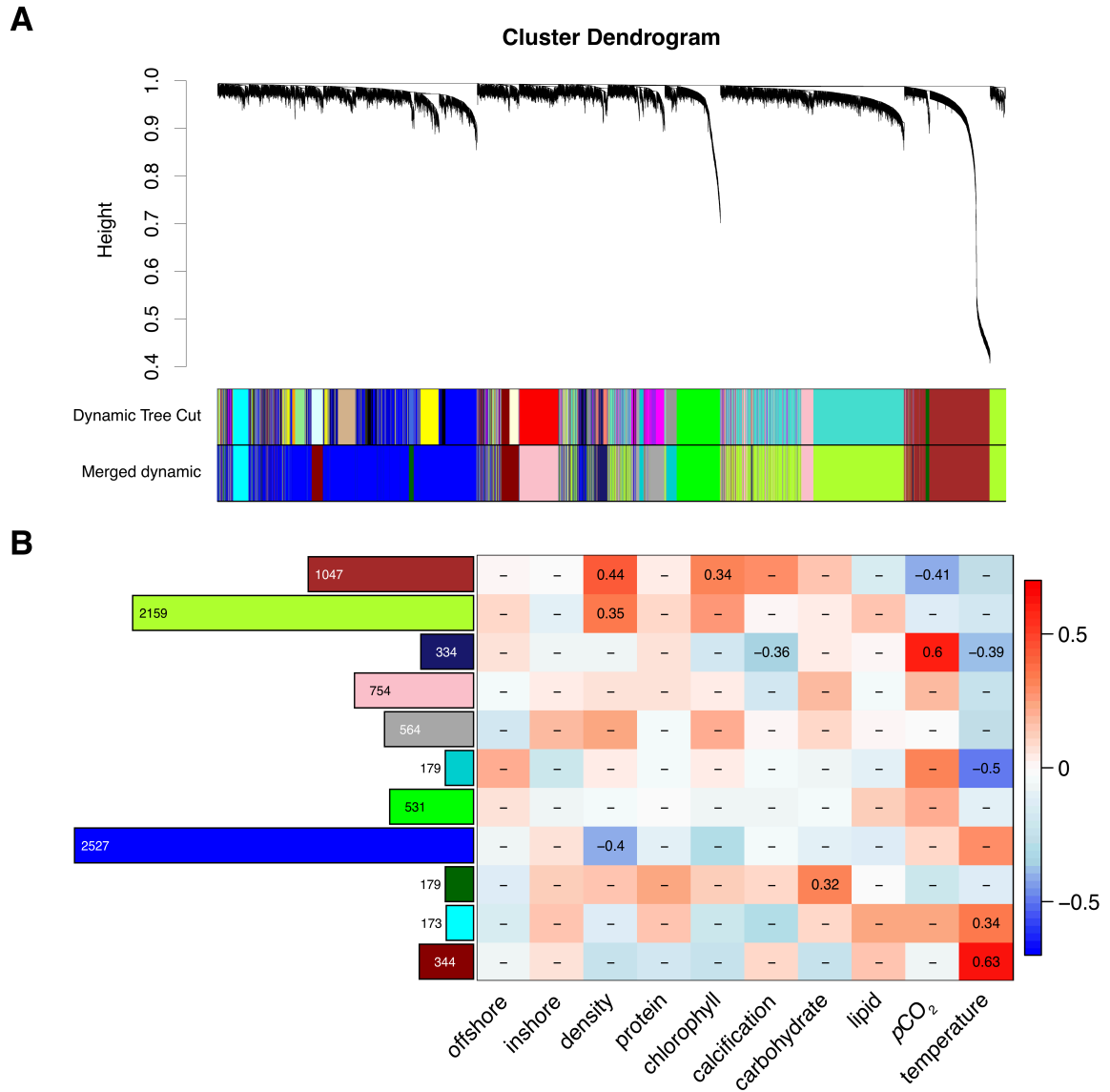


Figure 3.4 WGCNA analysis of *Siderastrea siderea* host gene expression

Dendrogram of gene clustering based on similar expression patterns (A). Coloured bars in the top depict co-expression modules before clustering of modules (Dynamic Tree Cut), and the coloured bars below depict modules based on clustering (Merged Dynamic). Correlations between module eigengenes and treatment or physiological parameters (B). The bar graph (left) depicts the number of genes corresponding to each module. Significant modules are denoted by values for Pearson's correlation coefficients within each cell.

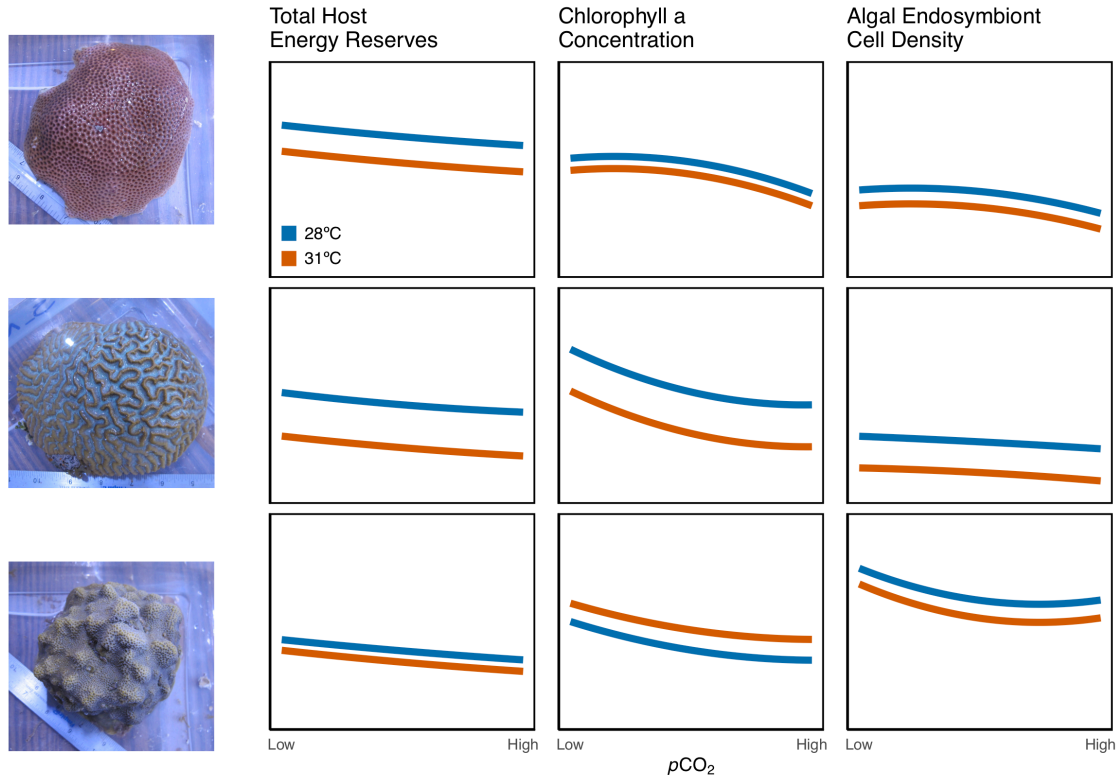


Figure 3.5 Summary of physiological responses to treatment

Summary of coral host and algal endosymbiont physiology trends in response to $p\text{CO}_2$ and temperature treatments. Each row represented the physiology of a single species and the columns correspond to the different physiological parameters. Temperature is depicted by colour (blue = 28 °C; red = 31 °C) and $p\text{CO}_2$ is represented along the x axis. Separation of blue and red lines represent effects of temperature, while lines with slopes deviating from a flat line represent $p\text{CO}_2$ effects. Overall, *S. siderea* appears more susceptible to changes in $p\text{CO}_2$, *P. strigosa* exhibits thermal sensitivity, and *P. astreoides* only shows moderate physiological response to temperature and $p\text{CO}_2$.

Sample	pCO ₂	Temp	# PE reads	Trimmed	Mapped (symbiont)	Mapped (host)	% mapped (symbiont)	% mapped (host)
CFSA1	280	31	8,340,331	2,350,680	111,510	451,153	4.7	19.2
CFSA10	2800	28	4,923,247	1,124,825	48,472	226,245	4.3	20.1
CFSA14	280	28	7,560,790	2,184,974	127,079	415,282	5.8	19.0
CFSA2	400	28	7,559,407	2,142,984	235,867	367,802	11.0	17.2
CFSA3	400	31	3,477,839	1,071,563	62,040	209,170	5.8	19.5
CFSA5	700	31	9,297,430	2,606,417	128,458	495,742	4.9	19.0
CFSA6	700	28	5,297,093	316,590	17,608	51,777	5.6	16.4
CFSA7	2800	31	7,325,024	2,009,615	34,730	404,788	1.7	20.1
CFSB1	280	31	6,028,486	1,673,102	174,147	283,293	10.4	16.9
CFSB10	400	31	8,309,773	2,074,975	144,215	385,694	7.0	18.6
CFSB13	400	28	9,315,996	2,355,221	229,362	479,857	9.7	20.4
CFSB2	280	28	3,644,957	898,462	57,371	138,180	6.4	15.4
CFSB3	2800	28	4,148,173	1,093,218	30,696	215,827	2.8	19.7
CFSB5	700	31	10,271,033	2,529,758	197,184	497,108	7.8	19.7
CFSB6	700	28	11,543,969	2,766,331	147,438	592,224	5.3	21.4
CFSB7	2800	31	9,227,113	2,289,967	34,630	377,864	1.5	16.5
CFSD11	280	28	5,007,517	1,269,669	99,749	196,608	7.9	15.5
CFSD3	400	31	8,524,744	1,689,962	106,544	286,126	6.3	16.9
CFSD5	700	31	15,746,927	3,658,550	283,765	791,604	7.8	21.6
CFSD6	700	28	5,507,256	1,610,552	130,713	308,209	8.1	19.1
CFSD7	2800	31	12,056,903	1,505,616	74,111	253,101	4.9	16.8
CFSD8	2800	28	7,068,598	1,964,633	150,906	387,577	7.7	19.7
CFSD9	400	28	8,397,205	2,143,893	265,788	366,642	12.4	17.1
CFSF16	2800	28	14,922,916	3,571,119	159,400	738,582	4.5	20.7
CFSF2	280	28	6,537,468	1,742,159	107,988	317,315	6.2	18.2
CFSF3	400	31	6,882,645	755,210	40,545	111,594	5.4	14.8
CFSF5	700	31	12,012,025	2,475,681	106,247	427,341	4.3	17.3
CFSF6	700	28	4,666,596	1,427,632	87,936	275,139	6.2	19.3
CFSF7	2800	31	7,177,091	1,676,428	113,655	267,673	6.8	16.0
CNSB1	280	31	9,815,280	2,566,080	133,619	421,547	5.2	16.4
CNSB2	280	28	11,230,948	3,358,859	382,453	620,212	11.4	18.5
CNSB20	2800	31	5,707,712	378,221	8,805	56,580	2.3	15.0
CNSB3	400	31	7,345,760	1,624,653	84,077	328,681	5.2	20.2
CNSB5	700	31	9,736,434	2,427,004	206,302	433,646	8.5	17.9
CNSB6	700	28	6,068,999	1,598,762	119,154	308,914	7.5	19.3
CNSB7	400	28	7,719,211	2,193,616	203,680	418,799	9.3	19.1
CNSB8	2800	28	5,202,678	1,153,371	47,355	246,329	4.1	21.4
CNSD1	280	31	11,451,779	3,290,594	286,474	668,958	8.7	20.3
CNSD2	280	28	17,481	6,148	233	723	3.8	11.8
CNSD5	700	31	8,554,185	2,499,249	172,317	553,441	6.9	22.1
CNSD8	2800	28	18,282	5,951	236	664	4.0	11.2

Table 2.1 Summary of *Siderastrea siderea* RNA libraries

Sample ID, pCO₂ (µatm) and temperature (°C) treatment, total number of raw 50 bp paired-end (PE) reads (“# PR Reads”), unpaired reads remaining after trimming and quality control (“Trimmed”), reads that mapped to the algal endosymbiont (“Mapped (symbiont)”) or coral host (“Mapped (host)”) transcriptome, and mapping efficiency of both the algal endosymbiont (% mapped (symbiont)) and coral host (% mapped (host)).

CHAPTER 4: EXTREME OCEAN ACIDIFICATION ALTERS SKELETAL MORPHOLOGY IN A CARIBBEAN REEF-BUILDING CORAL

Introduction

Coral calcification on tropical reefs produces the three-dimensional framework necessary to support a significant proportion of the world's ocean biodiversity. However, recent increases in atmospheric carbon dioxide (CO₂) concentrations from anthropogenic sources have caused dramatic global change phenomena, namely ocean warming and acidification (Hoegh-Guldberg et al. 2007, Doney et al. 2009, Hoegh-Guldberg and Bruno 2010), that are affecting the ability of scleractinian corals to maintain skeletal production. Ocean warming, caused by CO₂ trapping heat in the atmosphere and consequently driving warmer oceanic temperatures (IPCC 2019), is leading to more frequent and severe coral bleaching events globally (Hughes et al. 2017b) in which the symbiosis between the coral animal and algal endosymbionts breaks down (Brown 1997). Because reef-building corals rely on their algal endosymbionts for up to 100% of their nutritional needs (Muscatine et al. 1981), especially for calcification, colonies experiencing such dysbiosis often exhibit reduced skeletal growth and partial or total mortality (Cantin et al. 2010, DeCarlo et al. 2017, Prada et al. 2017). In addition to threats from warming sea surface temperatures, excess atmospheric CO₂ is being dissolved into the world's ocean causing declines in seawater pH and alterations to carbonate chemistry (Doney et al. 2009). Coral calcification has been shown to be closely linked with carbonate chemistry (Jury et al. 2010, Albright et al. 2016, Comeau et al. 2017, Schoepf et al. 2017, Albright et al. 2018, DeCarlo et al. 2018) through several field and

experimental studies, suggesting that changes to the carbonate system on coral reefs will further alter the way corals produce reef structures.

Although significant research has been performed to elucidate the calcification response of corals to ocean acidification and warming (Anthony et al. 2008, Agostini et al. 2013, Holcomb et al. 2014, Barott et al. 2015, Comeau et al. 2017, Bove et al. 2019, DeCarlo et al. 2019), little is known about the specific mechanisms that cause the observed declines in calcification rates. One theory behind the reduction in coral calcification is that coral skeletons are becoming less dense while maintaining extension rates in response to global change stressors (Mollica et al. 2018, Rippe et al. 2018). Conversely, others have suggested that changes in calcification rates are a result of dissolution of previously-formed skeletal material (Bove et al. 2019, Chou et al. 2020) or through morphological modifications to the skeleton (Marubini et al. 2003, Tambutte et al. 2015). Indeed, previous work has quantified declines in the structural complexity of *Siderastrea siderea* corallites under experimental ocean acidification and warming, potentially impacting the coral polyp's ability to anchor and retract within the corallite (Horvath et al. 2016).

Here, I investigate the effects of experimental ocean acidification and warming on skeletal morphology of the coral *S. siderea* from inshore and offshore reefs on the Mesoamerican Barrier Reef System (MBRS). In *S. siderea*, corallites contain a predictable pattern of septal disposition following hexameral symmetry (Neves et al. 2016), making it a great candidate for corallite morphological assessment. Corallite height and skeletal infilling were assessed using stereomicroscopy and complimented with scanning electron microscopy of septal ridge and peak rugosity to quantify alterations of the corallite after experimental treatment conditions. Fragments of *S. siderea* were previously exposed to one of eight

treatments for 93 days: two temperatures [present day (28°C) and an end-of-century (31°C)] fully crossed with four $p\text{CO}_2$ treatments [pre-industrial (~280 μatm), present-day (~400 μatm), end-of-century (~700 μatm), and extreme value (~3200 μatm)]. These data assist in the understanding of how ocean acidification and warming alter calcification rates of *S. siderea* by attempting to identify where changes in skeletal morphology may be occurring.

Methods

Experimental design

The experimental design and implementation is described in detail in Bove et al. (2019) and the specific parameters of the experimental treatments are included in the supplemental information. Briefly, six colonies of the common Caribbean reef-building coral *Siderastrea siderea* were collected from inshore and offshore reef environments in June 2015 from the southern portion of the Belize Mesoamerican Barrier Reef System. Corals were immediately transported to Northeastern University's Marine Science Center. Colonies were sectioned into eight equally sized fragments and maintained in one of eight experimental treatments (3 replicate tanks per treatment) for 93 days. The eight treatments encompassed four $p\text{CO}_2$ treatments corresponding to pre-industrial, current-day ($p\text{CO}_2$ control), end-of-century, and an extreme $p\text{CO}_2$ level and two temperatures corresponding to the corals' approximate present day mean (28°C) and projected next-century warming (31°C). These $p\text{CO}_2$ -temperature combinations resulted in eight triplicate (24 tanks total) treatments: 288 (± 65), 447 (± 152), 673 (± 104), 3285 (± 484) μatm at 28°C (± 0.4); and 311 (± 96), 405 (± 91), 701 (± 94), 3309 (± 414) μatm at 28°C at 31.0°C (± 0.4). At the completion of the experimental, coral tissue was removed from the skeleton with a seawater sprayer and

skeletons and air-dried for skeletal morphology assessment (see Appendix 2 for details on experimental design and maintenance).

Assessment of corallite height and infilling

All fragments of *S. siderea* (n = 87) were imaged for corallite height and infilling analyses via stereomicroscopy (Figure 4.1). Corallite height was quantified following Horvath et al. (2016), using a stereomicroscope (Nikon SMZ 1500) to determine the difference in vertical position of the microscope's z-stage between the in-focus basal plate and top of the septal ridge of each corallite (Figure 4.1B). Images were taken starting with the top of the basal plate fully-focused, then continued until the top of the septal ridge was fully in focus to result in corallite height. This was performed on 5 intact corallites away from the edge of the fragments, as this was the number determined to be needed in order to represent the fragment's true mean corallite height. In addition to height, area of each corallite was measured due to the phenotypic observation that larger corallites had greater heights.

Fully-focused images of all 5 corallites quantified were created using NIS Elements Basic Research (Nikon) using the z-series step images taken to produce the fully-focused image (Figure 4.1A). The final image was cropped along the top of the septal ridge and then the colour threshold was changed to white (skeleton) and black (space) using GIMP (GIMP Development Team 2019). White pixels in each image were then changed to red in order to calculate the ratio of red to black (skeleton to space) pixels in each corallite using a custom Python script to determine the percent corallite infilling (Figure 4.1C).

Septa and septal peak rugosity

A subset of *S. siderea* samples (n = 14) was selected to represent all treatments present in the experimental design and based on their previous assessment of transcriptomic responses to experimental stressors (see Appendix 3). Coral fragments were submerged for 3 hours in 8.25% sodium hypochlorite solution to remove organic residue and then rinsed with 95% ethanol and air-dried for at least 24 hours. Samples were then mounted and sputter coated in platinum (4.0 nm thickness; Leica EM ACE600; Buffalo Grove, Illinois, USA) and imaged using scanning electron microscopy (30 kV, 10.0 BI; Tescan Vega3; Brno - Kohoutovice, Czech Republic). For every coral fragment, a total of three corallites were analysed with the following images: full corallite, basal plate, 2 first order septa, 2 fourth order septa, 3 peaks per first order septa, and 3 peaks per fourth order septa (Neves et al. 2016) (see Figure 4.2 for representative images of corallite (A), septal ridge (B), and septal peak (C)). For images of the septa and septal peaks, the coral sample was angled in the SEM so that images could be taken of the septa from the side (Figure 4.2B–C). Septal ridge and septal peak rugosity were measured using IMAGEJ (Schindelin et al. 2012). Tracing along the peaks along the septa and then dividing it by the length quantified resulted in the septa rugosity. Similarly, the length of tracing each peak was divided by the length of a segmented line drawn from the base to the peak and then down to the base again to obtain the peak rugosity (Figure S4.1).

Statistical analyses

Linear mixed effects models selected using AIC were used to assess the impacts of $p\text{CO}_2$ and temperature on *S. siderea* corallite morphology (corallite height, infilling, septal

peak rugosity, and septal ridge rugosity), with a random effect of colony (*lme4* (1.1-12)) (Bates et al. 2015b) (see Tables S4.1–S4.4 for model selection). Parametric bootstraps were performed to model 95% confidence intervals with 2500 iterations (Wilcox 2010). Significant differences between treatments were defined as non-overlapping 95% confidence intervals. All statistical analyses were performed in R (3.5.2) (R Core Development Team 2016).

Results

Corallite height and percent skeletal infilling

Corallite height (mm) of *S. siderea* after 93-days of exposure to elevated temperature and $p\text{CO}_2$ exhibited no clear differences due to treatment effects (Figure 4.3A; Tables S4.5, S4.6). However, corallite height in the extreme $p\text{CO}_2$ treatment at both temperatures trended towards smaller heights, suggesting moderate effects of elevated $p\text{CO}_2$. Conversely, the percent of corallite skeletal infilling was lower in the control treatment (447 μatm ; 28 °C) compared to infilling of fragments reared under elevated temperature alone (447 μatm ; 31 °C) or compared to fragments reared at pre-industrial and end-of-century $p\text{CO}_2$ treatments at both temperatures (Figure 4.3B,; Tables S4.7, S4.8). Corallite skeletal infilling in fragments reared in the extreme $p\text{CO}_2$ treatment at both temperatures was clearly reduced compared to all other treatment. Natal reef environment did not clearly impact corallite height or skeletal infilling and was not assessed further for these parameters (Tables S4.1, S4.2).

Septal peak rugosity

Both 1st and 4th order septal peaks exhibited similar responses to temperature and $p\text{CO}_2$ after 93-days in experimental treatments (Figure 4.5; Tables S4.9, S4.10). Septal peak rugosity of both the 1st and 4th order peaks exhibited higher peak rugosity in inshore samples than in offshore sample in the pre-industrial and extreme $p\text{CO}_2$ treatments. Finally, temperature and $p\text{CO}_2$ treatment did not clearly impact septal peak rugosity of either 1st or 4th order peaks (Figure S4.2). While the 95% confidence intervals overlap, data suggest that both types of septal peaks trended toward the lower rugosity in the control treatment (447 μatm ; 28 °C) when compared to all other temperature and $p\text{CO}_2$ treatment combinations.

Septal ridge rugosity

Ridge rugosity of both 1st and 4th order septa do not exhibit clear impacts of experimental $p\text{CO}_2$ or temperature (Figure 4.6; Tables S4.11, S4.12). While 95% confidence intervals between natal reef environments were not clearly different, trends suggest that inshore fragments had more complex septal ridges than fragments originating in the offshore environment. Temperature and $p\text{CO}_2$ treatment did not clearly alter the 1st or 4th order septal ridge rugosity, however the lowest quantified complexity was in the end-of-century (673 μatm) $p\text{CO}_2$ treatment at current-day temperature (28 °C) (Figure S4.3).

Qualitative assessment of septa alterations due to treatment

Visual assessment was conducted on all septal peak and ridge SEM images to identify minute alterations to the skeleton that were not quantified through other measurements. Signs

of septal peak and ridge dissolution were observed on several corallite from different colonies maintained in the extreme $p\text{CO}_2$ treatment at both temperatures (Figure 4.7A–C). Septal peaks on corals maintained in the higher $p\text{CO}_2$ treatments (both end-of-century and extreme) were also generally smoother than peaks assessed on corals maintained at pre-industrial and control $p\text{CO}_2$ treatments. Additionally, skeletal pitting was observed on most corallites assessed in the elevated temperature treatment across $p\text{CO}_2$ levels (Figure 4.7D).

Discussion

Changes to seawater chemistry on coral reefs is expected to cause widespread reductions in net coral calcification rates, however, how ocean acidification alters these growth rates remains relatively unknown. The purpose of the current study was to assess changes to corallite morphology of *S. siderea* under simulated acidification and warming scenarios in order to quantify alterations that may be leading to reduced calcification rates. Assessment of experimental *S. siderea* fragments suggests that ocean acidification causes more detectable differences in corallite morphology than ocean warming, and colonies from different reef environments may exhibit varying levels of morphological plasticity to seawater conditions.

Ocean acidification drives greater differences in corallite morphology than warming

Substantial research has shown that increasing seawater $p\text{CO}_2$ causes declines in coral calcification rates across reef-building coral species (Cohen and Holcomb 2009, Ries et al. 2010, Albright and Langdon 2011, Comeau et al. 2014, Horvath et al. 2016, Bahr et al. 2018, Bove et al. 2019). Whiles these declines in calcification rates are often attributed to

physiological changes brought on by changing seawater chemistry, such as reduced efficiency of the proton pump (Cohen and Holcomb 2009) or reduction in energy reserves (Horvath et al. 2016), it is unclear if these changes are accompanied with alterations to skeletal structure and morphology. However, recent work has aimed to quantify the effects of ocean acidification on calcification rates and resulting morphology in tandem to better understand how coral calcification is changing with seawater chemistry (Marubini et al. 2003, Tambutte et al. 2015, Horvath et al. 2016).

Siderastrea siderea corallite morphology (height and infilling) patterns from the present study were similar to the previously reported calcification rates for these fragments, with reduced values under the extreme $p\text{CO}_2$ treatment (Bove et al. 2019). However, these findings contrast previous work on the same species that show clear reductions in both calcification rates and corallite morphology with increased $p\text{CO}_2$ (~ 900 μatm) on a shorter time scale (Horvath et al. 2016). Corallite height values were similar in the present study to those measured by Horvath et al. (2016), while percent corallite infilling was much lower (ca. 50-60% in the present study versus 80-90% in Horvath et al. (2016)). This difference in total skeletal infilling is likely due to varying colony corallite size or differences in experimental systems (i.e., light level, water flow, seawater source) (Foster 1979, Bove et al. 2020).

The assessment of corallite height and infilling were used as proxies for linear extension and skeletal density, respectively. These two parameters are commonly used to quantify growth rates in corals (Lough and Barnes 2000, Castillo et al. 2011, Carricart-Ganivet et al. 2012, Rippe et al. 2018), however, they represent two distinct growth mechanisms with extension (corallite height) preceding skeletal thickening (corallite

infilling) (Barnes and Lough 1993). Previous work has demonstrated that skeletal thickening is susceptible changing seawater chemistry, resulting in reduced skeletal density (Tambutte et al. 2015, Horvath et al. 2016, Mollica et al. 2018). Results from the present study only exhibit a reduction in skeletal infilling at the control treatment and under the most extreme $p\text{CO}_2$. This may be due to the relatively robust nature of *S. siderea* under acidification and warming stress (Davies et al. 2016, Bove et al. 2019), or because the coral tissue maintains contact with the skeleton after being precipitated, thus continuously modifying the top level of the skeleton (Mollica et al. 2018). Either way, understanding the role of skeletal extension versus thickening in response to changing seawater chemistry may provide beneficial insight into the calcification mechanisms impacts by ocean acidification.

The preliminary assessment of corallite septal ridge and peak rugosity in the present study was intended to determine a quantifiable approach to identify minute alterations to the skeletal morphology of *S. siderea* that may be responsible for declines in calcification rate facilitated by global change stressors. While previous studies have identified minute alterations to skeletal precipitation and morphology, these are generally very qualitative assessments (Marubini et al. 2003, Rodolfo-Metalpa et al. 2011, Tambutte et al. 2015), highlighting the need for new methodologies. Results from the limited sample size assessed in the present study suggest that measurement of septal ridge and peak rugosity may begin to explain changes in net calcification rates, however, other aspects of the skeleton are also likely being altered (Marubini et al. 2003, Tambutte et al. 2015). Additionally, the increase in septal peak rugosity in the extreme $p\text{CO}_2$ treatment suggests that higher rugosity of septal peaks does not necessarily translate to more ideal skeletal production. Visual assessment of septa in this and other studies (Marubini et al. 2003) suggest that elevated $p\text{CO}_2$ conditions

may result in more disorganized aragonite precipitation (i.e. higher rugosity) that may be a consequence of maintained growth rate or reduced control of the center of calcification (Holcomb et al. 2009, Allemand et al. 2010). Further, several signs of septal peak and ridge dissolution were observed in the present study, suggesting that some of the increased septal rugosity quantified may be attributed to active removal of previously deposited skeletal material. This is in contrast to previous work that identified no skeletal dissolution in response to elevated $p\text{CO}_2$, suggesting that tissue protects the skeleton from dissolution (Marubini et al. 2003, Rodolfo-Metalpa et al. 2011). However, the extent of acidification impacts on aragonite crystallization and dissolution is likely highly species-specific (Marubini et al. 2003) and *S. siderea* has exhibited alterations to septal peaks previously (Horvath et al. 2016) suggesting that it may be more susceptible to such external seawater changes, despite likely having a strong biological control of calcification (Davies et al. 2016).

Along with acidification, ocean warming causes even more dramatic declines in calcification rates in corals across ocean basins; however, alterations of skeletal morphology is not generally detected as a result of increasing temperatures (Foster et al. 2016, Horvath et al. 2016). Indeed, while some skeletal pitting was observed on septal peaks of *S. siderea* reared under warming treatments in the present study, temperature did not clearly alter any quantified morphological parameters. This suggests that while ocean acidification may alter how corals are precipitating their skeletons under acidification (Marubini et al. 2003, Tambutte et al. 2015, Foster et al. 2016, Horvath et al. 2016), declines in growth rates associated with warming may simply be due to resource limitation preventing continuous growth rates (Anthony et al. 2007). Indeed, previous work has demonstrated downregulation of genes associated with calcification in coral exhibiting thermally-induced bleaching,

resulting in lower calcification rates associated with algal endosymbiont loss (Kenkel et al. 2013b). Reduced calcification rates recorded in response to increasing ocean temperature is thus likely reflecting a biological response to the global change stressor, while acidification may also cause physical changes to coral skeletons.

Morphological plasticity of corallites determined by natal reef environment

Siderastrea siderea skeletal morphology is known to be highly responsive to environmental conditions, with corallite morphology (Foster 1980) and historic growth rates (Castillo et al. 2012, Rippe et al. 2018) varying based on reef location. Thus, it is not surprising fragments from the inshore exhibited higher septal rugosity than the offshore counterparts in some treatments in the present study. It is interesting, however, that inshore colonies of *S. siderea* are generally thought of being more resilient to less favourable conditions (i.e., temperature variation (Castillo and Lima 2010) and wave energy (Lugo-Fernandez et al. 1998)) while the inshore colonies from this study exhibited significant deviations from the control septal peak rugosity measurements, suggesting negative responses to experimental treatment. Alternatively, the increased septal peak rugosity identified in the inshore colonies may simply reflect changes in the growth strategy employed by this species to cope with changing seawater chemistry (Tambutte et al. 2015).

Similarly, *S. siderea* has been previously shown to produce thicker columella and synapticalae as a form of protection from the higher wave energy associated with more inshore environments (Foster 1980). While no clear differences in corallite height or infilling were detected between fragments from the different reef environments in the present study, this could be due to responses to the experimental conditions and water flow driving similar

morphologies over the total six-month period in the system. If this is the case, this suggests the plasticity of *S. siderea* skeletal morphology to environmental conditions (Foster 1979, 1980), even on the scale of months, that should be assessed further on shorter time scales. Additionally, the skeletal plasticity of *S. siderea* may be a valuable response employed by this species to thrive in various reefs environments (Baumann et al. 2016) and under environmental stressors (Davies et al. 2016, Bove et al. 2019).

Future directions and implications

Results from this study provide valuable insight into the morphological alterations accompanying calcification rates of the Caribbean coral *S. siderea* under projected global change stressors. Moving forward, additional experimental samples should be analysed for septal peak and ridge rugosity to better understand these minute skeletal alterations on more of a population level. These rugosity measurements could then be better compared with calcification rates, linear extension rates, and corallite height and infilling values in order to understand how these parameters are related. Indeed, preliminary analysis of the corallite parameters assessed here on a subset of fragments reveals potential relationships between parameters (Figure S4.4), including corallite height with first order septal ridge rugosity and linear extension with fourth order septal ridge rugosity. Additionally, further assessment of corallite morphology may lead to a better understanding of the phenotypic response of *S. siderea* to global change stressors. Another possible next step in assessing the thickening of corallites could be to directly measure the width of septa from images and count the total number of septa within each order as these are known to vary by colony or population in *S. siderea* (Foster 1980).

While concern over declining coral calcification rates in response to global change is increasing, our understanding behind the consequences of these changes on the coral skeleton is also improving. Ocean warming drives more dramatic declines in coral calcification rates, however, these declines appear to be associated with biological slowdown of growth (Anthony et al. 2007), leaving the structure of coral skeletons relatively unimpacted (Horvath et al. 2016). Conversely, ocean acidification is driving dissolution and morphological alterations to the coral skeleton that may explain why calcification rates are declining even though other physiological processes are less impacted (Schoepf et al. 2013). Together, these results highlight the potential changes in coral skeleton phenotypes that may occur on future reefs as oceans continue to experience rapid environmental transformations.

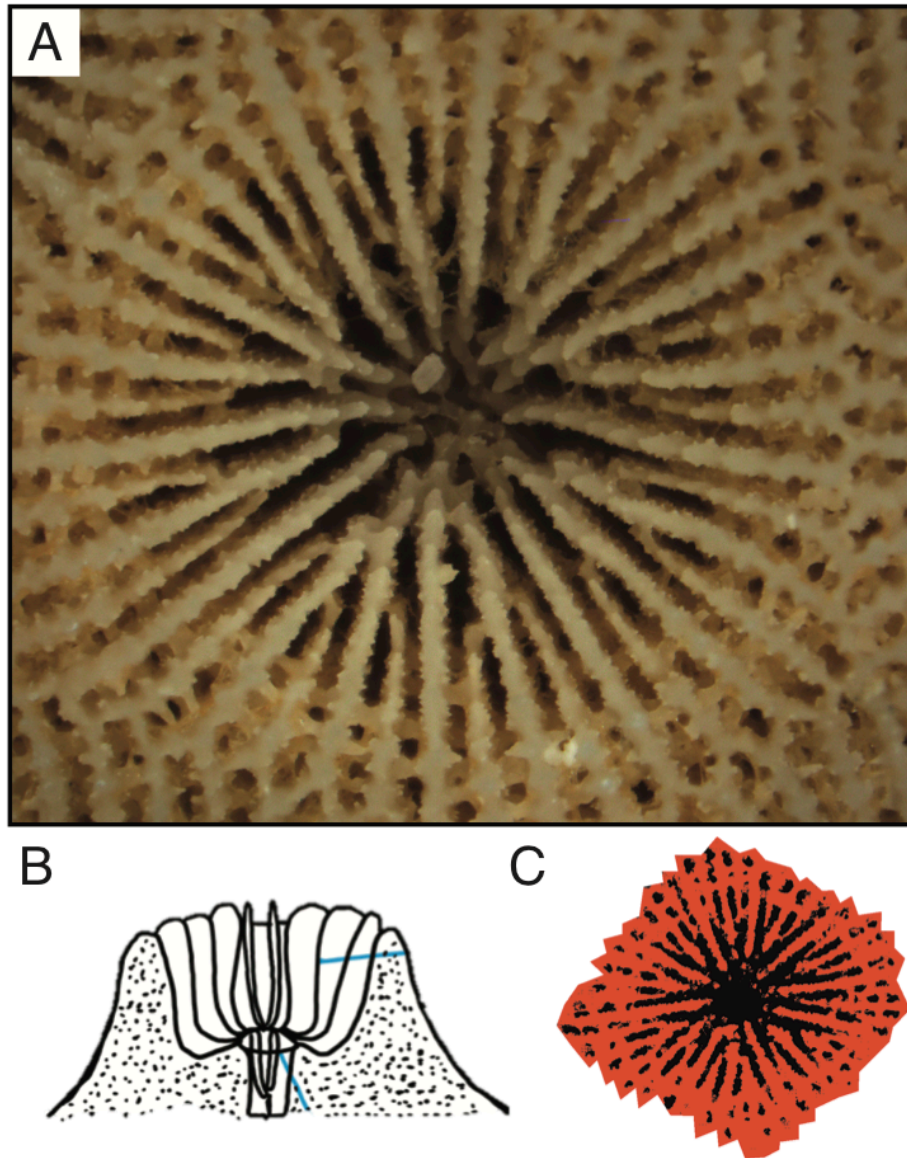


Figure 4.1 Diagram of corallite height and infilling methodology

Example of fully-focused image of corallite (A) taken to quantify corallite height (B) and then corallite skeletal infilling (C). Distance between the basal plate and the top of the septal ridge determined corallite height (B). Corallite image was converted to red (skeleton) and black (space) pixels and percent of red pixels was calculated for % infilling (C).

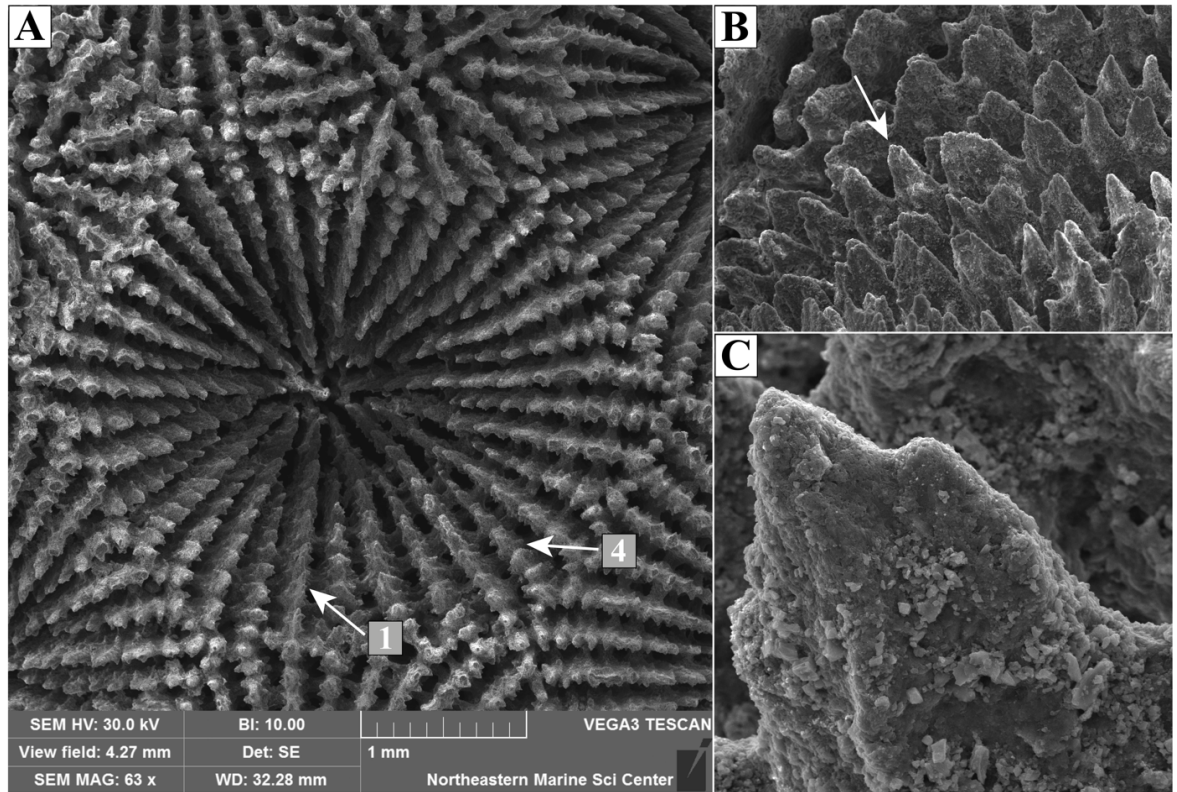


Figure 4.2 Representative SEM image of corallite morphology

Example images taken using a scanning electron microscope (SEM) of *S. siderea* corallite (A), septal ridge (B), and septal peak (C). Arrows denoted with the number ‘1’ and ‘2’ in panel A indicate the first and fourth order septa selected for SEM imaging and analyses, respectively. The arrow in panel B indicates the targeted septal ridge.

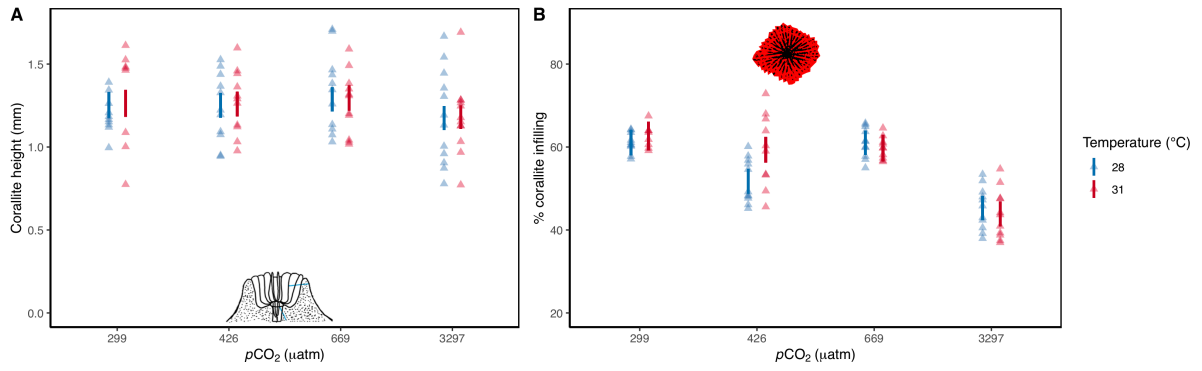


Figure 4.3 Corallite height and infilling in response to temperature and $p\text{CO}_2$

Modelled 95% confidence interval of *S. siderea* corallite height (mm) (A) and % skeletal infilling (B) in response to experimental $p\text{CO}_2$ and temperature conditions. Blue triangles represent values for fragments in the 28°C treatments and red triangles represent values for fragments in the 31°C treatments. Blue and red vertical bars represent modelled 95% confidence intervals for each $p\text{CO}_2$ treatment at 28°C and 31°C, respectively.

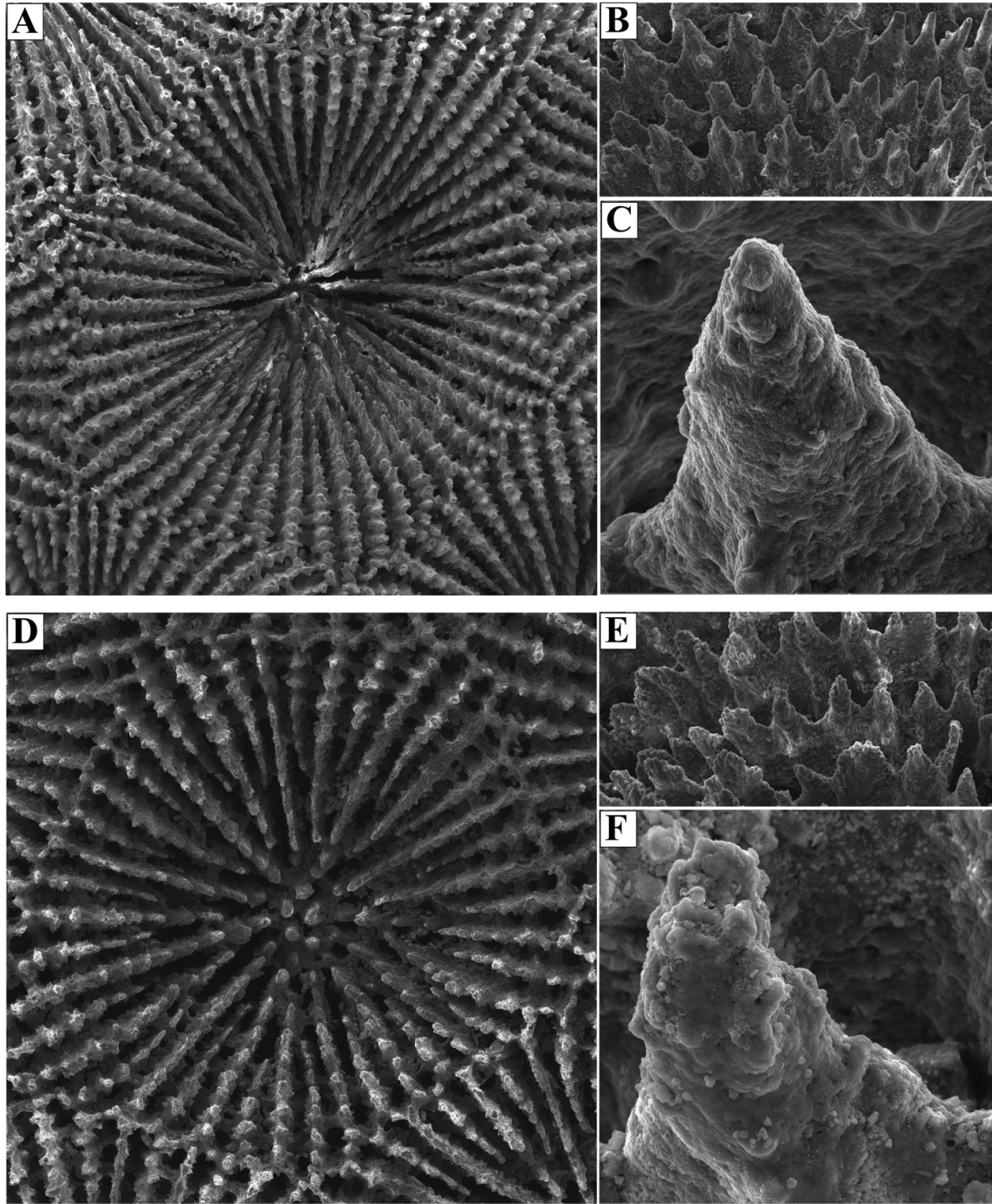


Figure 4.4 Representative SEM images of control versus extreme treatment morphology

Example images taken of fragments of *S. siderea* in the control (400 μatm; 28 °C) treatment (A-C) and the most extreme (2800 μatm; 31 °C) treatment (D-F). Full corallite (A, D), septal ridge (B, E), and septal peak (C, F) images demonstrate changes to corallite morphology as a result of exposure to 93-day of experimental acidification and warming.

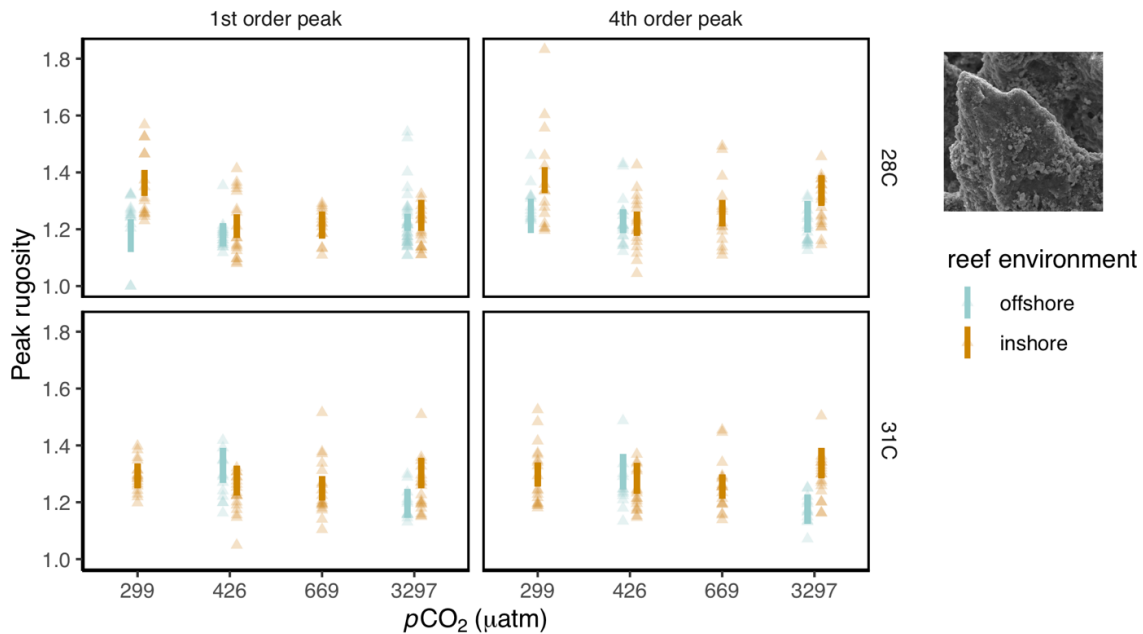


Figure 4.5 *Siderastrea siderea* septal peak rugosity in response to experimental treatment

Modelled 95% confidence interval of *S. siderea* 1st (left panels) and 4th (right panels) order septal peak rugosity in response to experimental $p\text{CO}_2$ and temperature conditions (28°C top panels; 31°C bottom panels). Light blue triangles represent values for fragments collected from the offshore reef environment and brown triangles represent values for fragments collected from the inshore reef environment. Light blue and brown vertical bars represent modelled 95% confidence intervals for each corresponding reef environment and treatment condition.

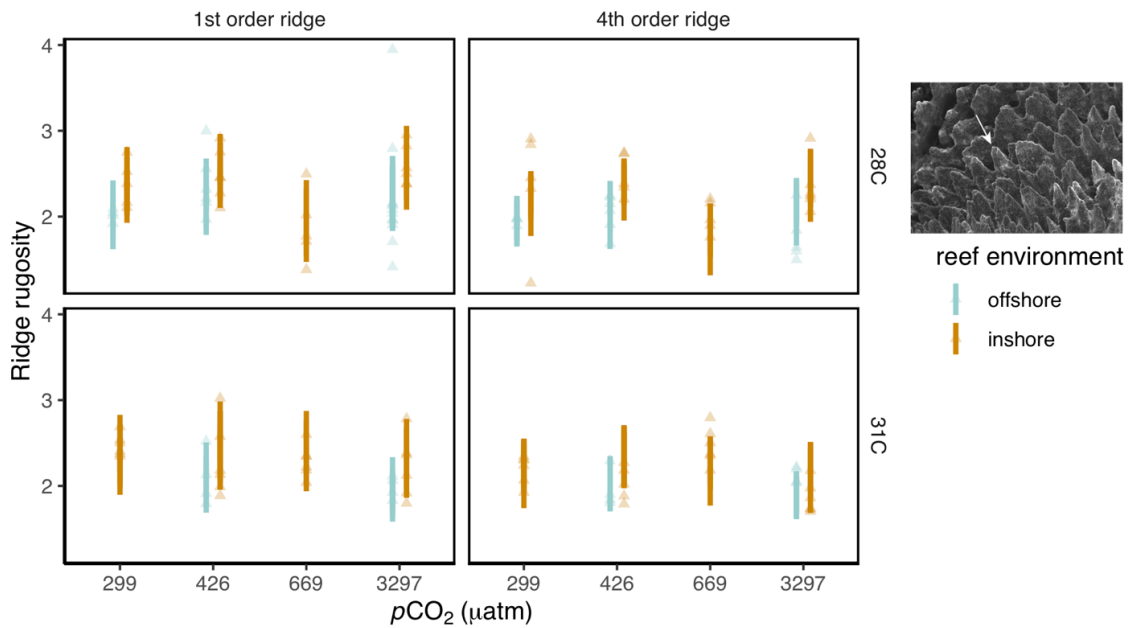


Figure 4.6 *Siderastrea siderea* septal ridge rugosity in response to experimental treatment

Modelled 95% confidence interval of *S. siderea* 1st (left panels) and 4th (right panels) order septal ridge rugosity in response to experimental $p\text{CO}_2$ and temperature conditions (28°C top panels; 31°C bottom panels). Light blue triangles represent values for fragments collected from the offshore reef environment and brown triangles represent values for fragments collected from the inshore reef environment. Light blue and brown vertical bars represent modelled 95% confidence intervals for each corresponding reef environment and treatment condition.

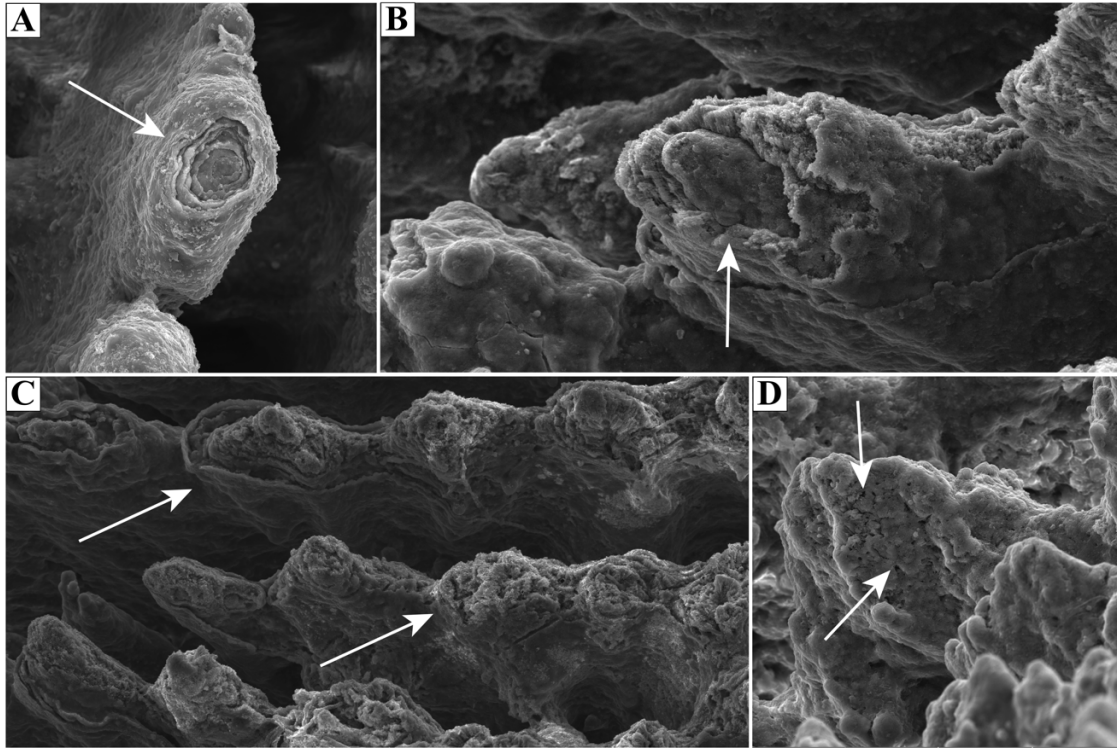


Figure 4.7 Representative images of skeletal dissolution and pitting

Example images of skeletal dissolution (A-C) and skeletal pitting (D) observed on *S. siderea* corallites. Skeletal dissolution (A-C) was observed only on fragments reared in one of the extreme $p\text{CO}_2$ treatments, while pitting (D) was observed across treatments, however, it was primarily documented in elevated seawater temperatures.

APPENDIX 1: SUPPLEMENTAL DESCRIPTIONS AND FIGURES – CHAPTER 1

Supplementary Table S1.1. List of included studies in meta-analysis with experimental design parameters. Treatment temperature and $p\text{CO}_2$ reported are for treatment levels used in this analysis. Missing data from studies is denoted by N.D.

Study	Location	Collection Sites	Species	Treatment	Duration	Feeding	Seawater	Irradiance	Control temperature	Treatment temperature	Control $p\text{CO}_2$	Treatment $p\text{CO}_2$
Albright and Langdon (2011)	Florida	Little Grecian Key Largo	<i>Porites astreoides</i>	$p\text{CO}_2$	49 d	N.D.	Natural seawater	N.D.	28	N.D.	380	800
Bestwell-Ivers et al. (2017)	Little Cayman	Cayman Research Center	<i>Acropora cervicornis</i> <i>Porites divaricata</i>	$p\text{CO}_2$	28 d	N.D.	Natural seawater	800 $\mu\text{mol photons m}^{-2} \text{ s}^{-1}$ at midday	30	N.D.	487	791
Beve et al. (2019)	Belize	Snake Cayes, Smadilla Cayes	<i>Porites astreoides</i> , <i>Pseudodiploria strigosa</i> , <i>Siderastrea sidera</i> , <i>Undaria tenuifolia</i>	warming $p\text{CO}_2$ combination	93 d	Frozen and newly hatched <i>Artemia</i> every other day	Filtered non-native seawater	300 $\mu\text{mol photons m}^{-2} \text{ s}^{-1}$	28	31	405	701
Castillo et al. (2014)	Belize	Nearshore, Backreef, Forereef	<i>Siderastrea sidera</i>	warming $p\text{CO}_2$	95 d	Frozen <i>Artemia</i> every other day	Artificial seawater	250 $\mu\text{mol photons m}^{-2} \text{ s}^{-1}$	28	32	472	704
Enos et al. (2014)	Florida	Dade County	<i>Acropora cervicornis</i>	$p\text{CO}_2$	42 d	N.D.	Natural seawater	178 $\mu\text{mol photons m}^{-2} \text{ s}^{-1}$	28	N.D.	513	870.9
Grotoli et al. (2014)	Mexico	Puerto Morelos	<i>Porites divaricata</i> , <i>Porites astreoides</i> , <i>Orbicella faveolata</i>	warming combination	15 d	N.D.	Natural seawater	600 $\mu\text{mol photons m}^{-2} \text{ s}^{-1}$	30.6	31.6	N.D.	N.D.
Horvath et al. (2016)	Belize	Nearshore, Backreef, Forereef	<i>Siderastrea sidera</i>	warming $p\text{CO}_2$ combination	60 d	Frozen <i>Artemia</i> twice weekly	Artificial seawater	250 $\mu\text{mol photons m}^{-2} \text{ s}^{-1}$	28	31	426	890
Jury et al. (2010)	Curacao	Sesquarium	<i>Madracis auretenra</i> <i>Acropora cervicornis</i> , <i>Agaricia agaricites</i> , <i>Dichocoenia stokesii</i> , <i>Montastraea cavernosa</i> , <i>Orbicella faveolata</i> , <i>Porites astreoides</i> , <i>Porites divaricata</i> , <i>Pseudodiploria strigosa</i> , <i>Siderastrea sidera</i> , <i>Siderastrea radians</i> , <i>Solenastrea hyades</i>	$p\text{CO}_2$ warming $p\text{CO}_2$ combination	2 h	<i>Artemia</i> nauplii twice weekly	Natural seawater	200 $\mu\text{mol photons m}^{-2} \text{ s}^{-1}$	28	N.D.	391	1480
Okazaki et al. (2017)	Florida	Key Biscayne, Biscayne National Park, Key West	<i>Orbicella faveolata</i> , <i>Porites astreoides</i> , <i>Porites divaricata</i> , <i>Pseudodiploria strigosa</i> , <i>Siderastrea sidera</i> , <i>Siderastrea radians</i> , <i>Solenastrea hyades</i>	$p\text{CO}_2$ combination	42 d	Live rotifers and larval twice weekly	Natural seawater	327 $\mu\text{mol quanta m}^{-2} \text{ s}^{-1}$	27	30.3	400	1340
Towle et al. (2015)	Florida	South Florida	<i>Acropora cervicornis</i>	warming $p\text{CO}_2$ combination	56 d	Dried zooplankton twice weekly	Natural seawater	353 $\mu\text{mol photons m}^{-2} \text{ s}^{-1}$	26	30	390	800
Kenkel et al. (2013)	Florida	Inshore and Offshore Sugarloaf Key	<i>Porites astreoides</i>	warming combination	43 d	N.D.	Natural seawater	70% Photosynthetically active radiation	27.2	30.9	N.D.	N.D.

Supplementary Table S1.2. Global meta-analysis mixed effects model (function *rma.mv*) output by treatment only, with random effects of study and species, used in Figure 1.2. The test for residual heterogeneity and significance is represented by Q_E (P -value) and the test of moderators is Q_M (P -value).

Treatment	Estimate	SE	Z-value	P-value
acidification	-1.2	0.78	-1.55	0.122
warming	1.19	1.41	0.84	0.399
combination	-1.07	1.19	-0.89	0.369
Variance Components				
Q_E (P -value)	823.95 (< 0.0001)			
Q_M (P -value)	2.4 (0.30)			

Supplementary Table S1.3. Meta-analysis mixed effects model (function *rma.mv*) output of treatment by region (Belize versus Florida Keys), with random effects of study and species, used in Figure 1.3. The test for residual heterogeneity and significance is represented by Q_E (P -value) and the test of moderators is Q_M (P -value).

Treatment	Estimate	SE	Z-value	P-value
<i>Belize</i>				
acidification	-0.93	1.32	-0.70	0.48
warming	1.56	2.24	0.70	0.49
combination	-3.64	2.07	-1.76	0.08
<i>Florida</i>				
acidification	0.09	1.88	0.05	0.96
warming	-0.96	3.18	-0.30	0.76
combination	5.17	3.06	1.69	0.09
Variance Components				
Q_E (P -value)	504.39 (< 0.0001)			
Q_M (P -value)	9.37 (0.09)			

Supplementary Table S1.4. Temperature and region linear mixed effects model section using AICc. All models were run with random effects for study and species and a weight of 1/SE. The asterisk (*) denotes the selected model run for the final analysis.

Model	DF	AICc
scaled temperature	6	107.84
scaled temperature + scaled temperature ²	7	72.85
scaled temperature + region	7	109.99
scaled temperature + region + scaled temperature ² *	8	75.39 *
region	6	125.18

Supplementary Table S1.5. Temperature and region best fit linear mixed effects model output and 95% confidence intervals of the calcification rates in response to treatment temperature plotted in Figure 1.4.

Predictors	Estimate	SE	Lower 95% CI	Upper 95% CI
intercept	0.74	1.26	-1.72	3.21
scaled temperature	-0.23	0.04	-0.31	-0.16
region	0.24	0.66	-1.05	1.53
scaled temperature ²	-0.36	0.05	-0.44	-0.27
days	0.01	0.01	-0.02	0.04
Random Effects				
variance species	0.20			
variance study	0.18			
residual	0.28			
N	60			
N _{study}	5			
N _{spec}	11			
AIC	75.39			

Supplementary Table S1.6. Aragonite saturation state and region linear mixed effects model section using AICc. All models were run with random effects for study and species and a weight of 1/SE. The asterisk (*) denotes the bet fit model.

Model	DF	AICc
scaled aragonite	6	56.39
scaled aragonite + scaled aragonite ²	7	47.98
scaled aragonite + region	7	57.97
scaled temperature + region + scaled aragonite ² *	8	49.85
region	6	105.28

Supplementary Table S1.7. Aragonite saturation state (Ω_{Arag}) and region best fit linear mixed effects model output and 95% confidence intervals of the calcification rates in response to treatment Ω_{Arag} plotted in Figure 1.5.

Predictors	Estimate	SE	Lower 95% CI	Upper 95% CI
intercept	-0.19	1.47	-3.06	2.69
scaled aragonite	0.10	0.02	0.07	0.14
region	0.47	0.75	-1.00	1.95
scaled aragonite ²	-0.04	0.01	-0.07	-0.02
days	0.02	0.02	-0.02	0.05
Random Effects				
variance species	0.17			
variance study	0.25			
residual	0.20			
N	140			
N _{study}	5			
N _{spec}	12			
AIC	49.85			

Figure S1.1 Forest plot depicting individual standard mean difference (SMD) and confidence interval of each species-site-study combination included in the meta-analysis of ocean acidification only studies. Studies with confidence intervals not overlapping zero (dotted line) denote either a significant increase (positive values) or decrease (negative values) in calcification response under experimental acidification compared to the corresponding control treatment.

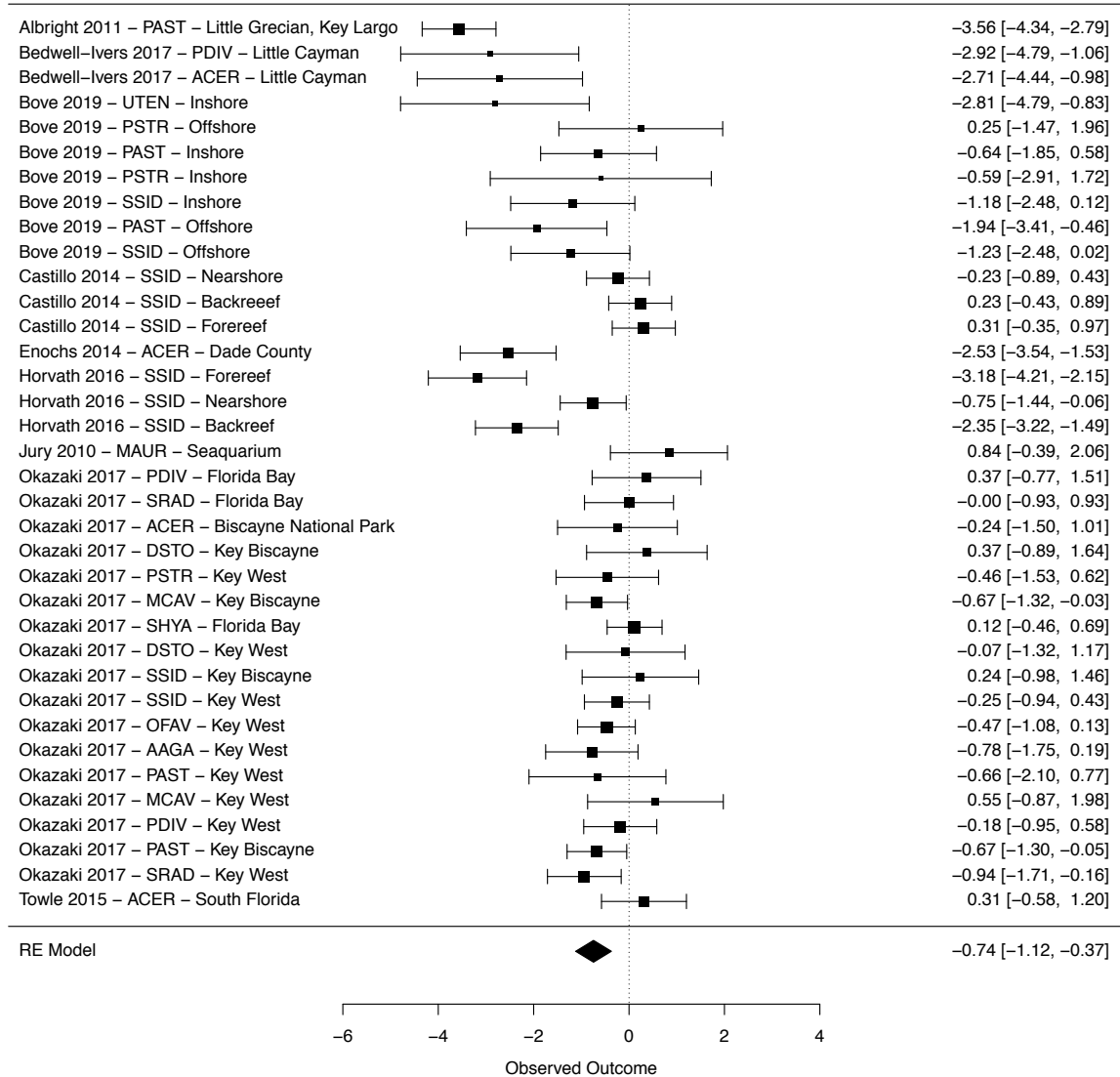


Figure S1.2. Funnel plot of the standard mean difference (SMD) against standard error of each species-site-study combination included in the meta-analysis of ocean acidification only studies. Dotted lines represent confidence intervals of all studies, background plot colour represents statistical significance of individual study, the black vertical line denotes the overall effect of all included ocean acidification studies.

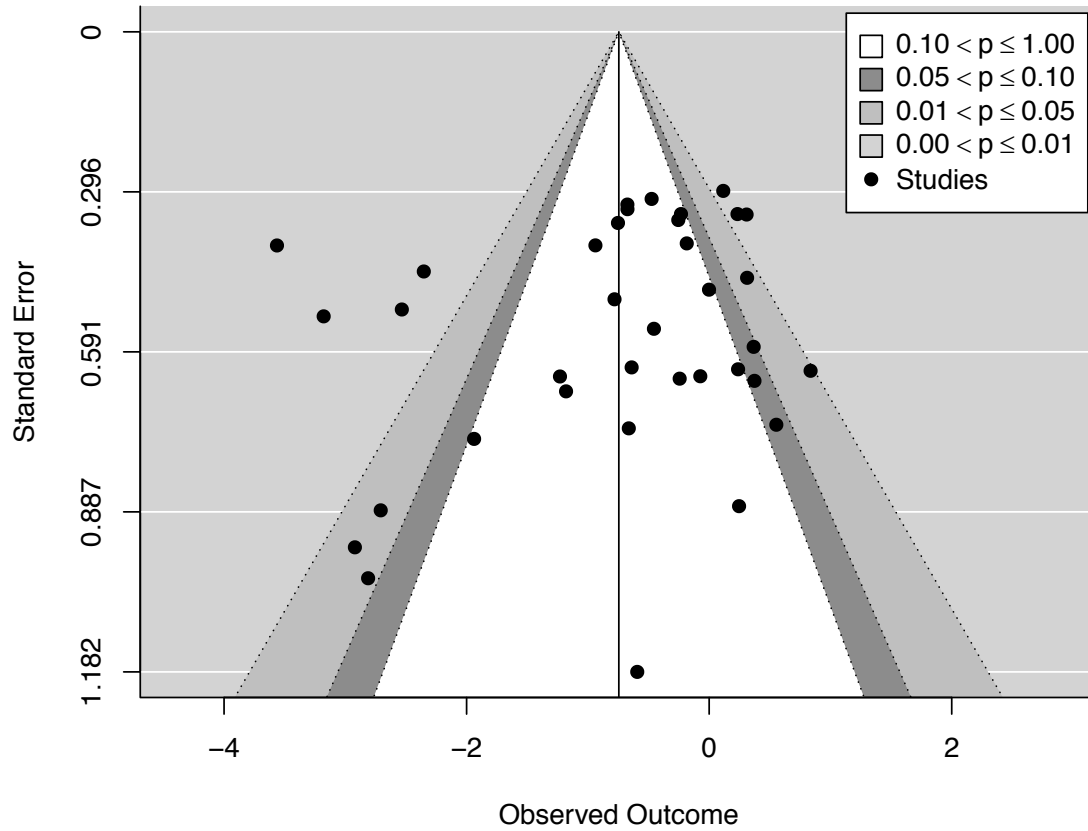


Figure S1.3. Forest plot depicting individual standard mean difference (SMD) and confidence interval of each species-site-study combination included in the meta-analysis of ocean warming only studies. Studies with confidence intervals not overlapping zero (dotted line) denote either a significant increase (positive values) or decrease (negative values) in calcification response under experimental warming compared to the corresponding control treatment.

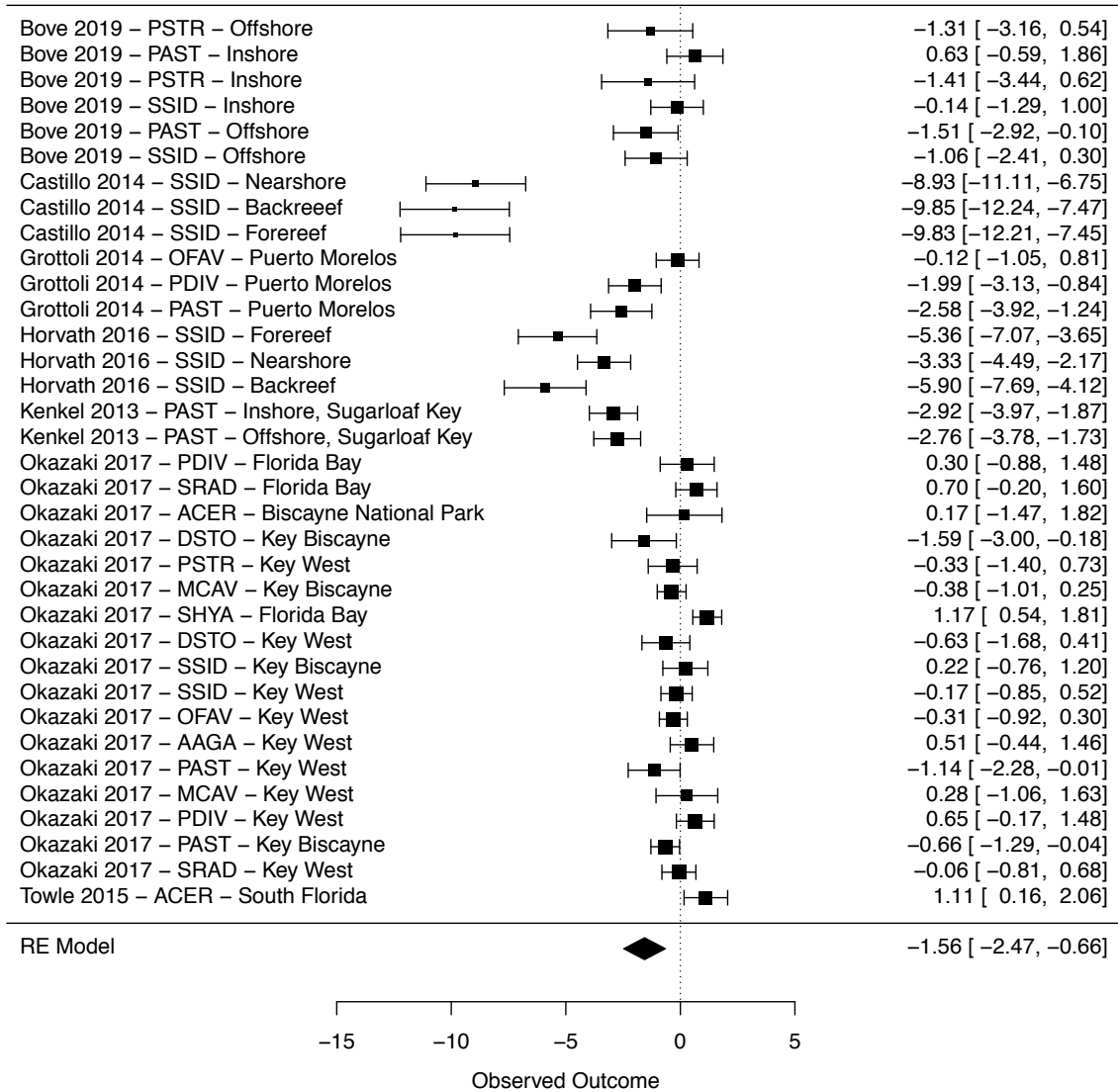


Figure S1.4. Funnel plot of the standard mean difference (SMD) against standard error of each species-site-study combination included in the meta-analysis of ocean warming only studies. Dotted lines represent confidence intervals of all studies, background plot colour represents statistical significance of individual study, the black vertical line denotes the overall effect of all included ocean acidification studies.

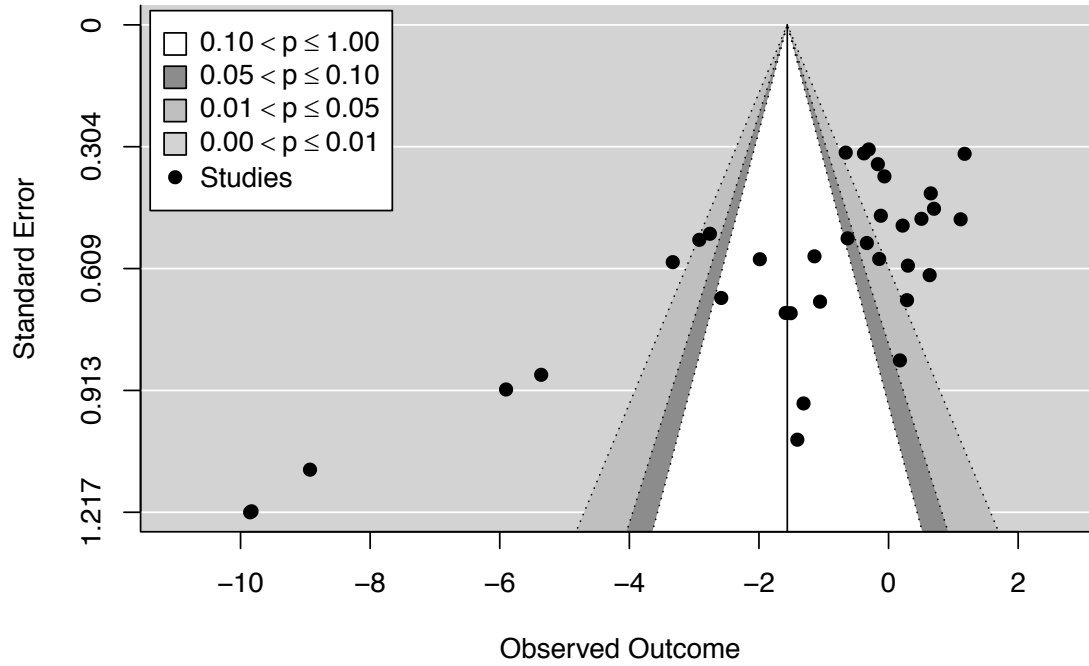


Figure S1.5. Forest plot depicting individual standard mean difference (SMD) and confidence interval of each species-site-study combination included in the meta-analysis of the combination of ocean acidification and warming studies.

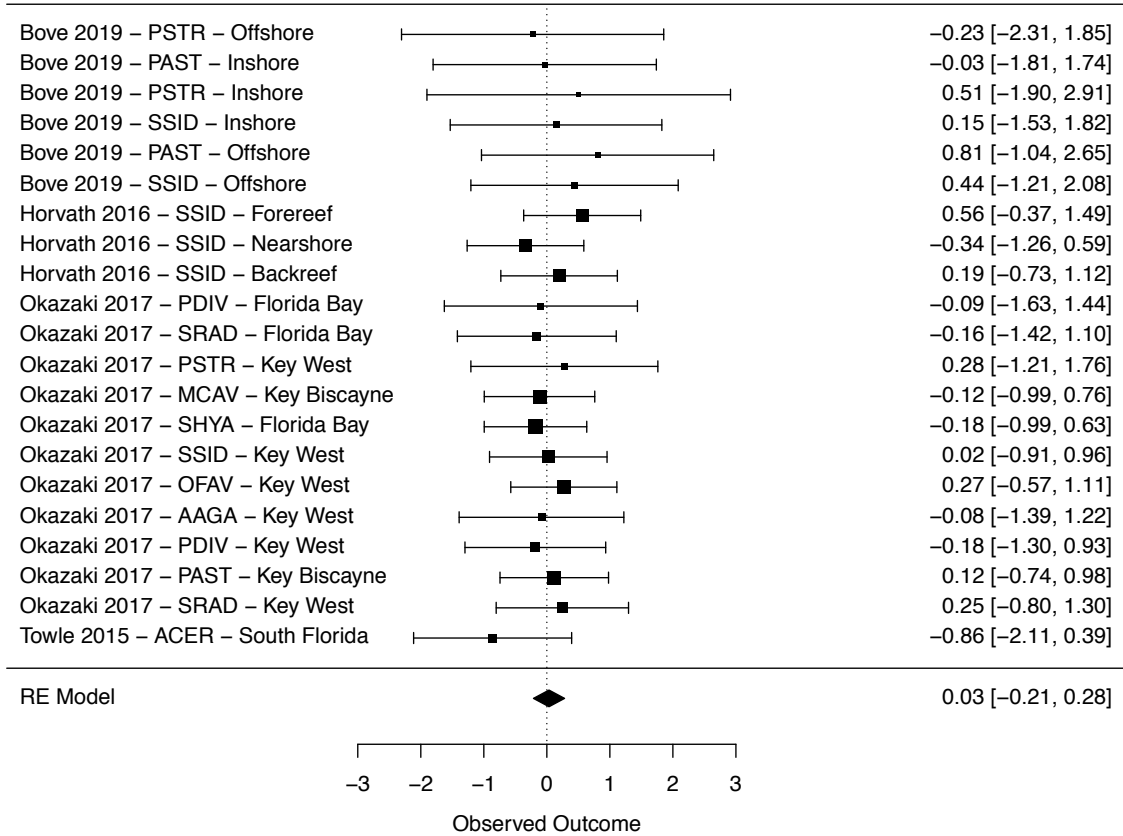
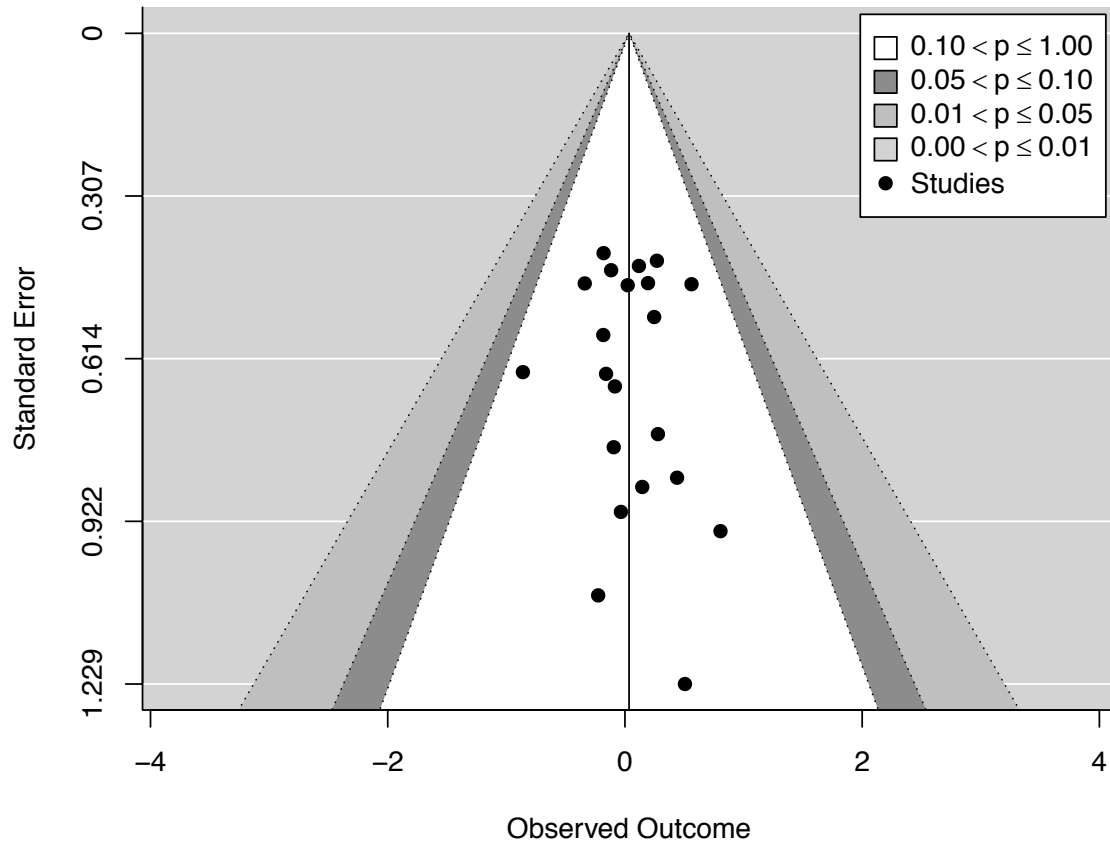


Figure S1.6. Funnel plot of the standard mean difference (SMD) against standard error of each species-site-study combination included in the meta-analysis of combined ocean acidification and warming only. Dotted lines represent confidence intervals of all studies, background plot colour represents statistical significance of individual study, the black vertical line denotes the overall effect of all included ocean acidification studies.



APPENDIX 2: SUPPLEMENTAL DESCRIPTIONS AND FIGURES – CHAPTER 2

Further explanation of methods

Coral collection

In June 2015, 6 colonies each of 4 reef-building coral species (*Siderastrea siderea*, *Pseudodiploria strigosa*, *Porites astreoides*, and *Undaria tenuifolia*; Figure S2.1) were collected from an inshore reef (Port Honduras Marine Reserve; 16°11'23.5314"N, 88°34'21.9360"W) and 6 colonies of each of the 4 coral species were collected from an offshore reef (Sapodilla Cayes Marine Reserve; 16°07'00.0114"N, 88°15'41.1834"W) along the Belize Mesoamerican Barrier Reef System (MBRS) at a depth of 3 to 5 m. A total of 48 coral colonies were collected from both reef environments (2 reef environments x 4 species x 6 colonies). The inshore reef is 9 km from the mainland of Belize, while the offshore reef is approximately 37 km from the mainland.

Experimental design and setup

Corals were transported to Northeastern University's natural flow-through seawater system located at the Marine Science Centre, where corals were sectioned with a seawater-cooled tile-cutting saw. Each sectioned coral fragment (approximate surface area: 5 cm x 3 cm = 15 cm²; approximate thickness: 2 cm) was mounted on to the outer surface of a 47 mm polystyrene petri dish (EMD Millipore; Billerica, Massachusetts, USA) using Loctite[®] cyanoacrylate adhesive (Düsseldorf, Germany). All 384 coral fragments (i.e., 48 colonies x 8 fragments) were placed into 1 of 8 treatments (4 fragments per species per tank; 16 fragments per tanks; 384 fragments in total; Figure S2.2) filled with 5 µm-filtered seawater obtained from Massachusetts Bay off the coast of Boston, Massachusetts (see Table S2.1 for *in situ*

water chemistry data from Belize) (Hyde et al. 2007, Soto et al. 2009). Corals were maintained in natural seawater at a salinity (\pm SD) of 30.7 (\pm 0.8) and temperature (\pm SD) of 28.2°C (\pm 0.5) for a recovery period of 23 days. After recovery, temperature and $p\text{CO}_2$ were adjusted every other day over a 20-day interval until target experimental conditions were approximately achieved for each treatment (temperature: 28 and 31°C; $p\text{CO}_2$: 280, 400, 700, 2800 μatm). Seawater temperatures in experimental tanks were incrementally increased by 0.4°C every 3 days and experimental $p\text{CO}_2$ was adjusted by $-12 \mu\text{atm}$ (pre-industrial), 0 μatm (current-day), $+30 \mu\text{atm}$ (end-of-century), and $+240 \mu\text{atm}$ (extreme) during the 20-day adjustment interval before starting the 30-day acclimation period. Four $p\text{CO}_2$ treatments corresponding to pre-industrial (311/288 μatm), current-day ($p\text{CO}_2$ control; 405/447 μatm), end-of-century (701/673 μatm), and an extreme (3309/3285 μatm) $p\text{CO}_2$ were maintained at two temperatures corresponding to the corals' approximate present day mean annual temperature (28°C; determined by over 10 years of *in situ* records) (Castillo and Lima 2010, Castillo et al. 2012, Baumann et al. 2016) and projected end-of-century annual mean temperature (31°C) (Stocker et al. 2013).

Experimental 42 L acrylic tanks were illuminated by full spectrum LED lights (Euphotica; 120W, 20000K) on a 10:14 h light:dark cycle with photosynthetically active radiation (PAR) of ca. 300 $\mu\text{mol photons m}^{-2} \text{ s}^{-1}$ to simulate natural light cycles occurring within the corals' native habitat (Castillo et al. 2014). PAR was regularly measured within each tank using a LI-COR LI-1500 data logger affixed with a LI-COR LI-192 2π underwater quantum sensor (LI-COR; Lincoln, Nebraska, USA; Figure S2.3). Experimental tanks were covered with an acrylic lid and wrapped in cellophane plastic to facilitate equilibrium between the gas mixtures and the experimental seawaters and to minimize evaporative water

loss. Circulation and turbulence in the experimental tanks were maintained with a Maxi-Jet[®] 400 L h⁻¹ powerhead (Marineland; Blacksburg, Virginia, USA), which have been used in previous common garden experiments on corals from Belize (Castillo et al. 2014, Horvath et al. 2016). Freshly filtered natural seawater was added via the flow-through system so that the water in each tank was replenished *ca.* 1.3 times per day.

Experimental $p\text{CO}_2$ gas mixtures were measured using Qubit S151 (range 0-2000 μatm ; accuracy $\pm 1 \mu\text{atm}$) and S153 (range 0-10%; accuracy $\pm 0.3\%$) infrared $p\text{CO}_2$ analyzers (Qubit Systems; Kingston, Ontario, Canada) calibrated with certified air- CO_2 gas standards. High-precision digital solenoid-valve mass flow controllers (*Aalborg Instruments and Controls*; Orangeburg, NY, USA) were used to bubble air alone (401; 447 μatm), or in combination with CO_2 -free air (311; 288 μatm) or CO_2 gas (701; 673; 3309; 3285 μatm) with compressed air to achieve gas mixtures of the desired $p\text{CO}_2$, and bubbled into each tank and sump via flexible air bubblers (Table 2.1; Figure S2.4). Because temperature affects the solubility of CO_2 in seawater, the two temperature treatments averaged different carbonate parameters for each of the $p\text{CO}_2$ treatments, despite being sparged with the same gas mixture ratios (Figure S2.4). These eight $p\text{CO}_2$ -temperature combinations were replicated three-fold (24 tanks total) and yielded the following treatment conditions ($\pm\text{SD}$): 311 (± 96), 405 (± 91), 701 (± 94), 3309 (± 414) $\mu\text{atm } p\text{CO}_2$ at 28°C (± 0.4); and 288 (± 65), 447 (± 152), 673 (± 104), 3285 (± 484) $\mu\text{atm } p\text{CO}_2$ at 31.0°C (± 0.4). The temperature of both the 28 and 31°C treatments were maintained using 50W glass aquarium heaters within each tank and 75W glass aquarium heaters (EHEIM; Deizisau, Germany) in each sump. Temperature, salinity, and pH were measured every other day and water samples were taken using 250 mL ground-glass-stoppered borosilicate glass bottles around 13:00 Eastern Time every 10 days

throughout the 93-day experimental period (9 September – 17 December 2015). Total alkalinity was determined by closed-cell potentiometric Gran titration and DIC was determined by coulometry (UIC 5400), with both methods calibrated with certified Dickson Laboratory standards for seawater CO₂ measurements (Scripps Institution of Oceanography; San Diego, California, USA). Measured temperature, salinity, TA, and DIC were used to calculate carbonate parameters using CO₂SYS (Pierrot et al. 2006) with Roy et al. (1993) carbonic acid constants K₁ and K₂ (Roy et al. 1993), the Mucci (1983) value for the stoichiometric aragonite solubility product (Mucci 1983), and an atmospheric pressure of 1.015 atm (Figure S2.4; Tables S2.2, S2.3). Moderate deviations between calculated and targeted parameters throughout the duration of the experiment resulted largely from biological activity within the aquaria and from minor seasonal changes in source water chemistry. Temperature was measured using a high precision partial-immersion glass thermometer (precision ±0.3%; accuracy ±0.4%). Salinity (±SD) was measured using a YSI 3200 (Yellow Springs, Ohio, USA) conductivity meter with a 10.0 cm⁻¹ cell and maintained at 31.7 (±0.2), with slight natural seasonal variation as expected in Massachusetts Bay waters. An AccuFet™ Solid-State pH probe (Fisher Scientific™; Waltham, Massachusetts, USA) calibrated with 7.00 and 10.01 NBS buffers maintained at experimental temperatures was used to measure pH in each tank (Table S2.2; Figure S2.4). Coral fragments within each tank were fed every other day with a mixture of *ca.* 6 g frozen adult *Artemia* sp. and 250 mL concentrated newly hatched live *Artemia* sp. (500 mL⁻¹) to satisfy any heterotrophic feeding by each species (Lewis and Price 1975, Winston 1983).

Buoyant weight quantification

Coral fragments were suspended in a 38 L aquarium 4 cm below the surface in seawater (temperature, 28.2°C; salinity, 32.4) using an aluminum wire hanging from a Nimbus NBL 423e Precision Balance (± 0.0002 precision, ± 0.002 accuracy; AE Adam[®]; Oxford, Connecticut, USA). A standard of a known mass was weighed three times before weighing corals in each tank to monitor any deviations in the balance over the course of the experiment. Each coral fragment was weighed three times, averaged, and normalized to surface area. Surface area was quantified in triplicate from photos of each nubbin taken at corresponding intervals using imaging software (IMAGE J).

A subsample of fragments from each coral species was selected for constructing the linear regression that relates the coral species' buoyant weight to their dry weight. Buoyant weight ('BW') and dry weight of the fragments are highly correlated for each species ($R^2_{S. siderea} = 0.970$, $p < 0.001$; $R^2_{P. strigosa} = 0.900$, $p < 0.001$; $R^2_{P. astreoides} = 0.980$, $p < 0.001$; $R^2_{U. tenuifolia} = 0.983$, $p < 0.001$), therefore the change in buoyant weight should be proportional to the corresponding change in dry weight (Figure S2.5).

$$S. siderea: \text{Dry weight (mg)} = 1.9 * \text{BW} + 3.47, R^2 = 0.970$$

$$P. strigosa: \text{Dry weight (mg)} = 1.78 * \text{BW} + 5.47, R^2 = 0.900$$

$$P. astreoides: \text{Dry weight (mg)} = 1.93 * \text{BW} + 4.51, R^2 = 0.980$$

$$U. tenuifolia: \text{Dry weight (mg)} = 1.66 * \text{BW} + 5.04, R^2 = 0.983$$

Linear Extension

A calcein horizon was emplaced into coral skeletons at the beginning of the experiment to establish a marker from which linear extension throughout the experiment could be measured (Venti et al. 2014). Each experimental tank was dosed with 213.4 g of a 1% calcein solution for 5 days. During this period, the light cycle was increased to 14 h light in all tanks to ensure sufficient uptake of fluorescent marker into skeletons. At the completion of the experiment, tissue was removed from all coral fragments using a precision seawater sprayer (PointZero; Sunrise, Florida, USA). Sections 5mm thick were cut from the middle of each fragment using a DB-100 ReefKeeper™ diamond band saw (Inland; Madison Heights, Michigan, USA). The full thin sections were imaged under a stereo microscope outfitted with a blue fluorescent adapter with excitation 440–460nm (NIGHTSEA™; Lexington, Massachusetts, USA). Linear extension was measured as the total area of new growth above the calcein line (Figure S2.7) measured using imaging software (IMAGE J) divided by the measured length of the coral's lateral growth surface. Extension was then divided by the number of months in the experimental treatments resulting in linear extension per month (mm month^{-1}).

Estimation of gross calcification rates

Gross calcification rates were estimated by subtracting the corals' calculated gross dissolution rates from their net calcification rates at the aragonite saturation states of each treatment. Gross dissolution was calculated using gross dissolution regression equations derived in Ries et al. (Ries et al. 2016) for two coral species. The gross dissolution equation ('y') for the massive coral *S. siderea* was used to estimate gross dissolution of the massive

corals *S. siderea*, *P. strigosa*, and *P. astreoides* from the current experiment, while the gross dissolution equation for the branching coral *O. arbuscula* was used to estimate gross dissolution of the branching coral *U. tenuifolia* (Ries et al. 2016) (Figure S2.9).

$$S. siderea: \quad y (\% \text{-wt/day}) = 0.055 - 0.638 * e^{(-6.187 * \Omega_A + 2.039 * \Omega_A)}$$

$$O. arbuscula: \quad y (\% \text{-wt/day}) = 0.073 - 0.638 * e^{(-5.632 * \Omega_A + 2.039 * \Omega_A)}$$

Survival quantification and analysis

Coral fragments were assessed for mortality every 30 days and considered dead when no living tissue remained. Impacts of $p\text{CO}_2$ and temperature on survival rates were assessed using a Kaplan-Meier estimate of survival (*survfit*, *survival*, 2.39-5) (Therneau 2015b). Cox proportional hazard models, with colony nested within tank as a random effect, were performed using *coxme* (2.2-5) (Therneau 2015a).

Further explanation of statistical analyses

Linear mixed effects models were fit to the calcification and linear extension data. Models were run to include species, $p\text{CO}_2$ (factor), and temperature (factor) as fixed effects with colony (genotype) as a random effect:

$$\text{lmer}(\text{rate} \sim \text{species} * (p\text{CO}_2 + \text{temperature}) + (1 | \text{colony}))$$

This model was selected using AIC and log likelihood tests to determine the best fit for the data. A parametric bootstrap of the data was run 1500 times for each model, resulting

in the modelled mean and 95% confidence intervals. Colonies were pooled by natal reef environment in all analyses because this was not a significant predictor of any measured parameter. All statistical analyses were performed using R 3.3.2 for OS X (R Core Development Team 2016).

A Bayesian hierarchical regression model was fit to calculate credible intervals of the corresponding extracted correlation coefficients using Hamiltonian MCMC, using default uninformative priors. Four chains were run for 1000 iterations after a 1000-iteration warmup. Chains mixed well and all Rhats were less than 1.0. The model was fit with species, $p\text{CO}_2$ (factor), and temperature (factor) as fixed effects with colony (genotype) as a random intercept and temperature and $p\text{CO}_2$ as random slopes:

```
brms(rate ~ species * (pCO2 + temperature) + ( 1 + pCO2 + temperature | colony), family = gaussian())
```

Additional results

Coral survivorship

Siderastrea siderea maintained nearly 100% survival across treatments, resulting in no significant effect of temperature ($p = 0.23$), $p\text{CO}_2$ ($p = 0.60$), or their interaction ($p = 1.0$) on survival (Figure S2.6a). Survival of *P. strigosa*, *P. astreoides*, and *U. tenuifolia* reared at 31°C was significantly reduced compared to conspecifics reared at 28°C ($p < 0.01$, $p < 0.01$, $p < 0.01$, respectively; Figure S2.6). No *U. tenuifolia* fragments under extreme $p\text{CO}_2$ conditions at 31°C survived the acclimation period, indicating that this species is extremely sensitive to these conditions. Increasing $p\text{CO}_2$ had no effect on survival of *P. astreoides* or *U. tenuifolia* ($p = 0.09$ and $p = 0.22$, respectively), while increasing $p\text{CO}_2$ significantly increased survivorship of *P. strigosa* ($p < 0.01$), a trend driven by relatively low survival at present-day $p\text{CO}_2$. Finally, the interaction between $p\text{CO}_2$ and temperature had no significant effect on

survivorship of *P. strigosa*, *P. astreoides*, or *U. tenuifolia* ($p < 0.08$, $p < 0.25$, $p < 0.21$, respectively; Figure S2.6B-D; Tables S2.9, S2.10, S2.11).

Effects of exposure duration on calcification rate

Differences in calcification rates for the four species were also examined across three 30-day observation intervals (T0-T30, T31-60, and T61-T90) to assess the impact of duration of exposure to treatment conditions on coral calcification rates. Although responses are complex, some general patterns emerged.

Specimens of *S. siderea* exhibited a slight increase in calcification rates from the first (T0-T30) to second (T31-T60) intervals in most treatments, followed by a decline from the second to third (T61-T90) interval (Figure S2.13a). In addition, calcification rates for coral reared at 28°C and 31°C under extreme $p\text{CO}_2$ are lower at each interval when compared with the lower $p\text{CO}_2$ treatments.

Calcification rates of *P. strigosa* were generally higher at 28°C than at 31°C at every 30-day interval, regardless of $p\text{CO}_2$ treatment. Excluding specimens reared under current-day $p\text{CO}_2$ at 28°C, calcification rates progressively declined across the three 30-day observational intervals of the experiment (Figure S2.13b).

Porites astreoides calcification rates demonstrated a declining trend across observational intervals within most temperature- $p\text{CO}_2$ treatment combinations, and exhibited net dissolution during the final interval (Figure S2.13C). However, some specimens failed to exhibit net calcification during any of the three intervals at either temperature.

Calcification rates of *U. tenuifolia* exhibited a decreasing trend across the three observational intervals for all $p\text{CO}_2$ and temperature treatment combinations (Figure S2.13d).

Missing data from the 31°C treatment in both the current-day and extreme $p\text{CO}_2$ treatments reflects the low survival rates in these treatments.

Additional discussion

Corals' natal reef environment does not influence resilience to $p\text{CO}_2$ or thermal stress

Rates of calcification, linear extension, and survival were not significantly impacted by natal reef environment (i.e., inshore vs. offshore) of the four coral species investigated here (Figures S2.11, S2.12; Tables S2.11, S2.12, S2.13). This result is consistent with previous laboratory experiments on some of the same and other species of zooxanthellate corals, which found no difference in responses to thermal and $p\text{CO}_2$ stress due to natal reef environment (Castillo et al. 2014, Horvath et al. 2016), but inconsistent with historical growth records of *S. siderea* obtained from century-scale coral cores that showed that the extension rate of forereef colonies has declined much faster than that of backreef and nearshore colonies (Castillo et al. 2011). However, it is possible that natal-reef-environment differences in resilience to thermal stress may emerge with more prolonged exposure to acidification and warming stress, as well as with larger sample sizes.

Reef environment	T (°C)	$p\text{CO}_2$ (μatm)	pH	TA (μM)	DIC (μM)	Ω_A	Salinity
Inshore	26.7	346.7	8.05	2495.9	2112	4.56	32.8
Inshore	26.7	326.0	8.04	2485.9	2090	4.68	32.7
Offshore	27.5	302.5	8.06	2572.8	2124	5.2	34.8
Offshore	27.5	298.1	8.06	2579.3	2126	5.25	34.8
Offshore	27.5	287.5	8.06	2583.8	2120	5.37	34.8

Table S2.1. Carbonate system parameters of seawater samples obtained in December 2016 from inshore and offshore locations in southern Belize near coral sampling sites demonstrating similarity to experimental seawater treatments (see Table 2.1 in the main text).

MEASURED PARAMETERS										
pCO₂ (gas-e)	(μ atm-v)	311	405	701	3309	288	447	673	3285	
Sal	(psu)	31.72	31.77	31.69	31.77	31.74	31.72	31.69	31.74	
SD		0.21	0.22	0.22	0.23	0.25	0.25	0.24	0.21	
Range		31.26 - 32.06	31.26 - 32.13	31.23 - 32.03	31.26 - 32.06	31.19 - 32.12	31.03 - 32.16	31.16 - 32.12	31.23 - 32.06	
n		120	120	120	120	120	120	120	120	
Temp	(°C)	27.9	28.0	28.1	28.1	31.0	31.1	30.9	31.0	
SD		0.4	0.4	0.5	0.2	0.4	0.5	0.3	0.5	
Range		27.2 - 29.6	27.0 - 29.0	27.1 - 30.2	27.7 - 28.7	30.0 - 32.2	30.4 - 32.5	30.1 - 31.7	30.0 - 33.0	
n		120	120	120	120	120	120	120	120	
pH_{M-NBS}		8.30	8.20	8.01	7.31	8.34	8.21	8.00	7.29	
SD		0.11	0.09	0.34	0.07	0.12	0.11	0.12	0.10	
Range		8.03 - 8.46	7.93 - 8.33	7.62 - 11.62	7.13 - 7.45	7.97 - 8.55	7.94 - 8.51	7.61 - 8.20	7.12 - 7.53	
n		120	120	120	120	120	120	120	120	
TA	(μ M)	2052	2081	2092	2131	2101	2077	2082	2123	
SD		43	17	37	25	32	32	35	22	
Range		1947 - 2104	2053 - 2121	2012 - 2128	2076 - 2160	2048 - 2152	2010 - 2125	2021 - 2134	2071 - 2148	
n		29	30	30	30	29	30	30	30	
DIC	(μ M)	1708	1788	1901	2156	1710	1773	1865	2135	
SD		78	52	46	34	57	80	42	28	
Range		1551 - 1829	1702 - 1859	1830 - 1981	2082 - 2217	1611 - 1795	1625 - 1905	1757 - 1917	2084 - 2194	
n		29	30	30	30	29	30	30	30	

Table S2.2.2. Average measured parameters for all treatments: salinity (Sal), temperature (Temp), pH, total alkalinity (TA), and dissolved inorganic carbon (DIC). ‘SD’ represents standard deviation and ‘n’ is the sample size.

CALCULATED PARAMETERS												
$p\text{CO}_2$ (gas-e)	($\mu\text{atm-v}$)	311	405	701	3309	288	447	673	3285			
SD		96	91	94	414	65	152	104	484			
Range		165 - 520	252 - 553	555 - 981	2442 - 4299	214 - 416	236 - 792	462 - 879	2681 - 4438			
n		29	30	30	30	29	30	30	30			
$\text{pH}_{\text{e-NBS}}$		8.27	8.18	7.97	7.37	8.29	8.15	7.99	7.38			
SD		0.10	0.08	0.05	0.05	0.07	0.11	0.06	0.06			
Range		8.07 - 8.45	8.06 - 8.33	7.85 - 8.05	7.25 - 7.48	8.16 - 8.38	7.93 - 8.34	7.89 - 8.11	7.25 - 7.46			
n		29	30	30	30	29	30	30	30			
$[\text{CO}_3^{2-}]$	(μM)	241	209	145	42	274	217	162	47			
SD		39	28	12	5	31	40	18	6			
Range		173 - 312	170 - 260	115 - 164	32 - 54	217 - 315	144 - 288	129 - 195	34 - 57			
n		29	30	30	30	29	30	30	30			
$[\text{HCO}_3^-]$	(μM)	1459	1568	1737	2029	1429	1545	1687	2009			
SD		109	77	51	29	82	114	51	23			
Range		1235 - 1643	1435 - 1666	1652 - 1841	1967 - 2076	1301 - 1553	1332 - 1742	1551 - 1748	1965 - 2052			
n		29	30	30	30	29	30	30	30			
$[\text{CO}_2]_{\text{(SW)}}$	(μM)	8	10	18	85	7	11	16	79			
SD		2	2	2	11	2	4	2	12			
Range		4 - 13	7 - 14	14 - 25	63 - 111	5 - 10	6 - 19	11 - 21	64 - 109			
n		29	30	30	30	29	30	30	30			
Ω_A		4.0	3.4	2.4	0.7	4.6	3.6	2.7	0.8			
SD		0.6	0.5	0.2	0.1	0.5	0.7	0.3	0.1			
Range		2.8 - 5.1	2.8 - 4.3	1.9 - 2.7	0.5 - 0.9	3.6 - 5.2	2.4 - 4.8	2.2 - 3.3	0.6 - 0.9			
n		29	30	30	30	29	30	30	30			

Table S2.3. Average measured parameters for all treatments: $p\text{CO}_2$ of the mixed gases in equilibrium with seawaters ($p\text{CO}_2$ (gas-e)); calculated pH (pH_{e}); carbonate ion concentration ($[\text{CO}_3^{2-}]$); bicarbonate ion concentration ($[\text{HCO}_3^-]$); dissolved carbon dioxide ($[\text{CO}_2]_{\text{SW}}$); and aragonite saturation state (Ω_A). ‘SD’ represents standard deviation and ‘n’ is the sample size.

Model	AIC	df
Temperature * Reef	508.5704	6
Reef	506.5132	4
Temperature	505.4378	4
Species * Reef	481.4342	10
Species	477.2899	6
Reef * $p\text{CO}_2$ * Temperature	476.3029	18
$p\text{CO}_2$ * Reef	475.0965	10
$p\text{CO}_2$	473.5468	6
Temperature * $p\text{CO}_2$	471.7448	10
Species * Temperature * Reef	470.4927	17
Species * Temperature	459.8295	10
Species * $p\text{CO}_2$ * Reef	458.286	34
Species * $p\text{CO}_2$ * Reef + Temperature	457.005	35
Species * $p\text{CO}_2$ + Temperature + Reef	451.5823	20
Species * $p\text{CO}_2$	451.1012	18
Species * $p\text{CO}_2$ + Temperature	449.6505	19
Species * $p\text{CO}_2$ * Temperature * Reef	449.1111	59
$p\text{CO}_2$ * Temperature * Reef + Species	448.8439	21
Species + $p\text{CO}_2$ * Temperature + Reef	446.5169	14
Species * Reef + $p\text{CO}_2$ + Temperature	446.3451	14
Species + $p\text{CO}_2$ + Temperature * Reef	445.5166	12
$p\text{CO}_2$ * Temperature + Species	444.6838	13
Species + $p\text{CO}_2$ + Temperature + Reef	444.5401	11
$p\text{CO}_2$ * Reef + Species + Temperature	443.6495	14
Species + $p\text{CO}_2$ + Temperature	442.6241	10
Species * $p\text{CO}_2$ * Temperature + Reef	440.0991	33
Species * $p\text{CO}_2$ * Temperature	438.1393	32
Species * Temperature * Reef + $p\text{CO}_2$	438.0031	20
Species * ($p\text{CO}_2$ + Temperature)	432.9082	22
Species * Temperature + Reef + $p\text{CO}_2$	430.5345	14
Species * Temperature + $p\text{CO}_2$	428.5378	13

Table S2.4. Summary of AIC and degrees of freedom (df) for all model combinations. The model combination in bold is the final model used in this analysis.

Species	Treatment		N	Mean Calcification (mg cm ² day ⁻¹)	Lower 95% CI	Upper 95% CI
<i>S. siderea</i>	28°C	311 µatm	10	1.106	0.872	1.342
		405 µatm	12	1.256	1.038	1.468
		701 µatm	11	1.084	0.875	1.302
		3309 µatm	12	0.280	0.070	0.492
	31°C	288 µatm	8	1.093	0.854	1.335
		447 µatm	11	1.243	1.026	1.448
		673 µatm	11	1.071	0.856	1.286
		3285 µatm	12	0.267	0.047	0.468
<i>P. strigosa</i>	28°C	311 µatm	15	1.198	0.989	1.408
		405 µatm	5	0.504	0.209	0.828
		701 µatm	14	0.665	0.443	0.871
		3309 µatm	16	0.181	-0.015	0.374
	31°C	288 µatm	9	0.202	-0.023	0.450
		447 µatm	6	-0.493	-0.801	-0.184
		673 µatm	7	-0.332	-0.606	-0.088
		3285 µatm	8	-0.815	-1.058	-0.564
<i>P. astreoides</i>	28°C	311 µatm	11	0.072	-0.159	0.304
		405 µatm	12	0.010	-0.233	0.231
		701 µatm	10	-0.196	-0.438	0.050
		3309 µatm	12	-0.680	-0.903	-0.456
	31°C	288 µatm	6	0.229	-0.039	0.497
		447 µatm	8	0.166	-0.073	0.419
		673 µatm	9	-0.039	-0.280	0.219
		3285 µatm	4	-0.523	-0.803	-0.246
<i>U. tenuifolia</i>	28°C	311 µatm	11	0.147	-0.138	0.432
		405 µatm	7	0.237	-0.125	0.611
		701 µatm	4	0.029	-0.398	0.465
		3309 µatm	5	-0.241	-0.650	0.177
	31°C	288 µatm	4	0.129	-0.304	0.583
		447 µatm	0	NA	NA	NA
		673 µatm	1	0.011	-0.565	0.601
		3285 µatm	0	NA	NA	NA

Table S2.5. Bootstrapped modelled mean calcification rate for each species in all $p\text{CO}_2$ and temperature treatments reported in $\text{mg cm}^2 \text{ day}^{-1}$. Sample sizes (N) and 95% confidence intervals (CI) are reported for each modelled mean calcification rate (Figure 2.1).

Fixed effect	Value	SE	<i>t</i> -value
(Intercept)	1.089	0.163	6.664
Species (PSTR)	0.106	0.224	0.471
Species (PAST)	-1.020	0.231	-4.412
Species (UTEN)	-0.947	0.251	-3.769
<i>p</i> CO ₂ - current	0.163	0.148	1.102
<i>p</i> CO ₂ - end-of-century	-0.002	0.150	-0.013
<i>p</i> CO ₂ - extreme	-0.809	0.146	-5.522
Temperature (31°C)	-0.011	0.100	-0.113
Species (PSTR) * <i>p</i> CO ₂ - current	-0.887	0.228	-3.886
Species (PAST) * <i>p</i> CO ₂ - current	-0.224	0.215	-1.039
Species (UTEN) * <i>p</i> CO ₂ - current	-0.074	0.280	-0.263
Species (PSTR) * <i>p</i> CO ₂ - end-of-century	-0.523	0.205	-2.558
Species (PAST) * <i>p</i> CO ₂ - end-of-century	-0.267	0.220	-1.216
Species (UTEN) * <i>p</i> CO ₂ - end-of-century	-0.121	0.295	-0.410
Species (PSTR) * <i>p</i> CO ₂ - extreme	-0.189	0.199	-0.950
Species (PAST) * <i>p</i> CO ₂ - extreme	0.063	0.221	0.284
Species (UTEN) * <i>p</i> CO ₂ - extreme	0.420	0.298	1.409
Species (PSTR) * Temperature (31°C)	-1.066	0.154	-6.923
Species (PAST) * Temperature (31°C)	0.166	0.153	1.080
Species (UTEN) * Temperature (31°C)	-0.013	0.273	-0.048
Colony (intercept)	0.147		
Residual	0.215		

Table S2.6. Summary output of the linear mixed effects model used to determine the relationship between calcification rates, *p*CO₂, and temperature for all four coral species (PSTR = *P. strigosa*; PAST = *P. astreoides*; UTEN = *U. tenuifolia*). Temperature and *p*CO₂ were treated as factors.

Species	Treatment		N	Mean LE (mm day ⁻¹)	Lower 95% CI	Upper 95% CI
<i>S. siderea</i>	28°C	311 µatm	11	0.0080	0.0070	0.0090
		405 µatm	9	0.0082	0.0074	0.0091
		701 µatm	11	0.0086	0.0076	0.0095
		3309 µatm	12	0.0075	0.0066	0.0083
	31°C	288 µatm	10	0.0069	0.0059	0.0079
		447 µatm	8	0.0071	0.0062	0.0081
		673 µatm	11	0.0075	0.0066	0.0083
		3285 µatm	12	0.0063	0.0055	0.0072
<i>P. astreoides</i>	28°C	311 µatm	9	0.0059	0.0048	0.0069
		405 µatm	9	0.0047	0.0037	0.0058
		701 µatm	9	0.0046	0.0036	0.0056
		3309 µatm	12	0.0033	0.0023	0.0043
	31°C	288 µatm	7	0.0054	0.0042	0.0066
		447 µatm	5	0.0042	0.0031	0.0053
		673 µatm	6	0.0041	0.0029	0.0051
		3285 µatm	1	0.0028	0.0014	0.0042

Table S2.7. Bootstrapped modelled mean linear extension for each species in all $p\text{CO}_2$ and temperature treatments reported in mm day^{-1} . Sample sizes (N) and 95% confidence intervals (CI) are reported for each mean extension rate (Figure 2.3).

Fixed effect	Estimate	SE	<i>t</i> -value
Intercept	7.86E-03	6.31E-04	12.5
Species (PAST)	-1.95E-03	9.14E-04	-2.14
<i>p</i> CO ₂ - current	3.62E-04	6.24E-04	0.058
<i>p</i> CO ₂ - end-of-century	7.32E-04	6.11E-04	1.20
<i>p</i> CO ₂ - extreme	-4.50E-04	6.01E-04	-0.075
Temperature (31°C)	-1.08E-03	4.12E-04	-2.62
Species (PAST) * <i>p</i> CO ₂ - current	-1.51E-03	9.35E-04	-1.62
Species (PAST) * <i>p</i> CO ₂ - end-of-century	-2.01E-03	9.38E-04	-2.15
Species (PAST) * <i>p</i> CO ₂ - extreme	-2.15E-03	9.60E-04	-2.24
Species (PAST) * Temperature (31°C)	5.01E-04	6.94E-04	0.072
Colony	1.68E-06		
Residual	3.46E-06		

Table S2.8. Summary output of the linear mixed effects model used to determine the relationship between linear extension, *p*CO₂ and temperature for *S. siderea* and *P. astreoides* (PAST). Temperature and *p*CO₂ were treated as factors.

Species	Treatment	T0	T30	T60	T90	
<i>S. siderea</i>	28°C	311 µatm	10	10	10	10
		405 µatm	12	12	12	12
		701 µatm	11	11	11	11
		3309 µatm	12	12	12	12
	31°C	288 µatm	8	8	8	8
		447 µatm	11	11	11	11
		673 µatm	12	11	11	11
		3285 µatm	12	12	12	12
<i>P. strigosa</i>	28°C	311 µatm	16	16	15	15
		405 µatm	8	6	5	5
		701 µatm	14	14	14	14
		3309 µatm	16	16	16	16
	31°C	288 µatm	14	11	9	9
		447 µatm	13	11	6	6
		673 µatm	15	13	7	7
		3285 µatm	13	11	8	8
<i>P. astreoides</i>	28°C	311 µatm	11	11	11	11
		405 µatm	12	12	12	12
		701 µatm	12	11	10	10
		3309 µatm	12	12	12	12
	31°C	288 µatm	11	8	6	6
		447 µatm	9	8	8	8
		673 µatm	12	12	9	9
		3285 µatm	10	6	4	4
<i>U. tenuifolia</i>	28°C	311 µatm	12	11	11	11
		405 µatm	7	7	7	7
		701 µatm	8	5	4	4
		3309 µatm	8	6	5	5
	31°C	288 µatm	8	8	4	4
		447 µatm	1	0	0	0
		673 µatm	4	2	1	1
		3285 µatm	0	0	0	0

Table S2.9. Sample size surviving for each species at each time point per treatment that was used for constructing survival curves (Figure S2.6).

Species	Fixed Effect	Hazard rate	Hazard ratio	Hazard ratio SE	<i>z</i>	<i>P</i>
<i>S. siderea</i>	<i>p</i> CO ₂	-5.39E-06	1.00	0.00	0	1.00
	Temperature (31°C)	22.09	3.92E09	0.00	Inf	0.00
	<i>p</i> CO ₂ * Temperature (31°C)	-5.87E-04	1.00	0.00	-Inf	0.00
<i>P. strigosa</i>	<i>p</i> CO ₂	-3.72E-03	1.00	0.00	-1.02	0.31
	Temperature (31°C)	0.58	1.79	1.51	0.39	0.70
	<i>p</i> CO ₂ * Temperature (31°C)	3.54E-03	1.00	0.00	0.97	0.33
<i>P. astreoides</i>	<i>p</i> CO ₂	3.12E-04	1.00	0.00	1.20	0.23
	Temperature (31°C)	0.47	1.60	1.17	0.40	0.69
	<i>p</i> CO ₂ * Temperature (31°C)	3.28E-03	1.00	0.00	1.52	0.13
<i>U. tenuifolia</i>	<i>p</i> CO ₂	3.41E-04	1.00	2.66E-04	1.28	0.20
	Temperature (31°C)	0.52	1.68	1.17	0.44	0.66
	<i>p</i> CO ₂ * Temperature (31°C)	3.26E-03	1.00	2.17E-03	1.51	0.13

Table S2.10. Cox mixed effects proportional hazards analysis for survival of all four species. The ‘hazard rate’ represents the modelled risk of death, so that positive values represent increased risk. The ‘hazard ratio’ indicates the hazard in the treatment compared to the control.

Species	Fixed Effect	loglik	χ^2	DF	P
<i>S. siderea</i>	NULL	-4.48			
	pCO ₂	-4.34	0.27	1	0.6
	Temperature (31°C)	-3.61	1.47	1	0.23
	Reef environment	-2.94	1.35	1	0.225
	pCO ₂ * Temperature (31°C)	-3.61	0	1	1
<i>P. strigosa</i>	NULL	-131.95			
	pCO ₂	-121.63	20.64	1	5.53E-06 ***
	Temperature (31°C)	-113.32	16.61	1	4.60E-05 ***
	Reef environment	-113.29	0.07	1	0.79
	pCO ₂ * Temperature (31°C)	-111.80	3.06	1	0.08
<i>P. astreoides</i>	NULL	-74.67			
	pCO ₂	-73.25	2.84	1	0.09
	Temperature (31°C)	-66.06	14.38	1	1.49E-04 ***
	Reef environment	-64.55	3.02	1	0.08
	pCO ₂ * Temperature (31°C)	-65.41	1.3	1	0.25
<i>U. tenuifolia</i>	NULL	-59.12			
	pCO ₂	-58.36	1.5	1	0.22
	Temperature (31°C)	-54.28	8.18	1	4.24E-03 **
	Reef environment	-54.16	0.24	1	0.63
	pCO ₂ * Temperature (31°C)	-53.49	1.56	1	0.21

Table S2.11. Statistical outcomes for coral survival analyses of all four species, using Cox mixed effects proportional hazards models.

Species	Reef Environment	Treatment	N	Mean Calcification (mg cm ² day ⁻¹)	Lower 95% CI	Upper 95% CI	
<i>S. siderea</i>	Offshore	28°C	311 µatm	6	1.045	0.803	1.284
			405 µatm	6	1.192	0.974	1.411
			701 µatm	6	1.023	0.808	1.252
			3309 µatm	6	0.217	-0.002	0.441
		31°C	288 µatm	4	1.031	0.789	1.275
			447 µatm	5	1.177	0.956	1.398
			673 µatm	6	1.008	0.789	1.228
			3285 µatm	6	0.202	-0.022	0.405
	Inshore	28°C	311 µatm	4	1.173	0.926	1.421
			405 µatm	6	1.320	1.094	1.539
			701 µatm	5	1.151	0.926	1.374
			3309 µatm	6	0.345	0.129	0.564
		31°C	288 µatm	4	1.159	0.905	1.407
			447 µatm	6	1.305	1.073	1.522
<i>P. strigosa</i>	Offshore	28°C	311 µatm	10	1.141	0.935	1.354
			405 µatm	3	0.444	0.146	0.778
			701 µatm	8	0.605	0.387	0.822
			3309 µatm	10	0.124	-0.078	0.322
		31°C	288 µatm	5	0.144	-0.088	0.386
			447 µatm	3	-0.553	-0.859	-0.233
			673 µatm	4	-0.392	-0.672	-0.141
			3285 µatm	5	-0.874	-1.136	-0.621
	Inshore	28°C	311 µatm	5	1.269	1.042	1.488
			405 µatm	2	0.572	0.265	0.904
			701 µatm	6	0.733	0.495	0.952
			3309 µatm	6	0.252	0.044	0.466
		31°C	288 µatm	4	0.272	0.036	0.527
			447 µatm	3	-0.425	-0.744	-0.107
		673 µatm	3	-0.264	-0.544	-0.006	
		3285 µatm	3	-0.746	-0.997	-0.482	

Species	Reef Environment	Treatment	N	Mean Calcification (mg cm ² day ⁻¹)	Lower 95% CI	Upper 95% CI	
<i>P. astreoides</i>	Offshore	28°C	311 µatm	6	0.012	-0.226	0.255
			405 µatm	6	-0.053	-0.296	0.171
			701 µatm	5	-0.259	-0.496	-0.010
			3309 µatm	6	-0.749	-0.991	-0.508
		31°C	288 µatm	3	0.163	-0.119	0.435
			447 µatm	4	0.098	-0.146	0.353
			673 µatm	4	-0.108	-0.356	0.155
			3285 µatm	0	NA	NA	NA
	Inshore	28°C	311 µatm	4	0.140	-0.102	0.385
			405 µatm	6	0.075	-0.180	0.301
			701 µatm	5	-0.131	-0.379	0.121
			3309 µatm	6	-0.621	-0.853	-0.399
31°C		288 µatm	4	0.291	0.015	0.574	
		447 µatm	6	0.226	-0.020	0.485	
		673 µatm	5	0.020	-0.221	0.280	
		3285 µatm	6	-0.470	-0.758	-0.192	
<i>U. tenuifolia</i>	Offshore	28°C	311 µatm	3	0.060	-0.233	0.361
			405 µatm	2	0.152	-0.233	0.539
			701 µatm	1	-0.062	-0.513	0.380
			3309 µatm	1	-0.337	-0.773	0.099
		31°C	288 µatm	0	NA	NA	NA
			447 µatm	0	NA	NA	NA
			673 µatm	0	NA	NA	NA
			3285 µatm	0	NA	NA	NA
	Inshore	28°C	311 µatm	8	0.188	-0.099	0.479
			405 µatm	5	0.280	-0.071	0.650
			701 µatm	3	0.066	-0.369	0.515
			3309 µatm	4	-0.209	-0.621	0.210
31°C		288 µatm	4	0.150	-0.284	0.597	
		447 µatm	0	NA	NA	NA	
		673 µatm	1	0.028	-0.536	0.622	
		3285 µatm	0	NA	NA	NA	

Table S2.12. Bootstrapped modelled mean calcification rate for each species by reef environment in all $p\text{CO}_2$ and temperature treatments reported in $\text{mg cm}^{-2} \text{day}^{-1}$. Sample sizes (N) and 95% confidence intervals (CI) are reported for each mean calcification rate (Figure S2.11).

Species	Reef Environment	Treatment	N	Mean LE (mm day ⁻¹)	Lower 95% CI	Upper 95% CI	
<i>S. siderea</i>	Offshore	28°C	311 µatm	6	0.0076	0.0066	0.0087
			405 µatm	6	0.0078	0.0069	0.0088
			701 µatm	6	0.0082	0.0072	0.0091
			3309 µatm	6	0.0071	0.0062	0.0080
		31°C	288 µatm	4	0.0065	0.0054	0.0076
			447 µatm	4	0.0067	0.0057	0.0077
			673 µatm	6	0.0071	0.0061	0.0080
			3285 µatm	6	0.0059	0.0050	0.0069
	Inshore	28°C	311 µatm	3	0.0084	0.0073	0.0096
			405 µatm	5	0.0086	0.0077	0.0096
			701 µatm	5	0.0090	0.0080	0.0100
			3309 µatm	6	0.0079	0.0069	0.0088
		31°C	288 µatm	4	0.0073	0.0063	0.0084
			447 µatm	6	0.0075	0.0065	0.0085
<i>P. astreoides</i>	Offshore	28°C	311 µatm	5	0.0055	0.0043	0.0066
			405 µatm	3	0.0043	0.0031	0.0055
			701 µatm	5	0.0042	0.0031	0.0053
			3309 µatm	6	0.0029	0.0018	0.0040
		31°C	288 µatm	2	0.0049	0.0037	0.0062
			447 µatm	3	0.0038	0.0026	0.0050
			673 µatm	3	0.0037	0.0025	0.0048
			3285 µatm	0	NA	NA	NA
	Inshore	28°C	311 µatm	4	0.0063	0.0052	0.0074
			405 µatm	6	0.0051	0.0040	0.0062
			701 µatm	4	0.0050	0.0039	0.0061
			3309 µatm	6	0.0037	0.0027	0.0048
		31°C	288 µatm	3	0.0057	0.0046	0.0070
			447 µatm	4	0.0045	0.0034	0.0057
		673 µatm	3	0.0045	0.0033	0.0056	
		3285 µatm	1	0.0032	0.0017	0.0046	

Table S2.13. Bootstrapped modelled mean linear extension for each species by reef environment in all $p\text{CO}_2$ and temperature treatments reported in mm day^{-1} . Sample sizes (N) and 95% confidence intervals (CI) are reported for each mean extension rate (Figure S2.12).

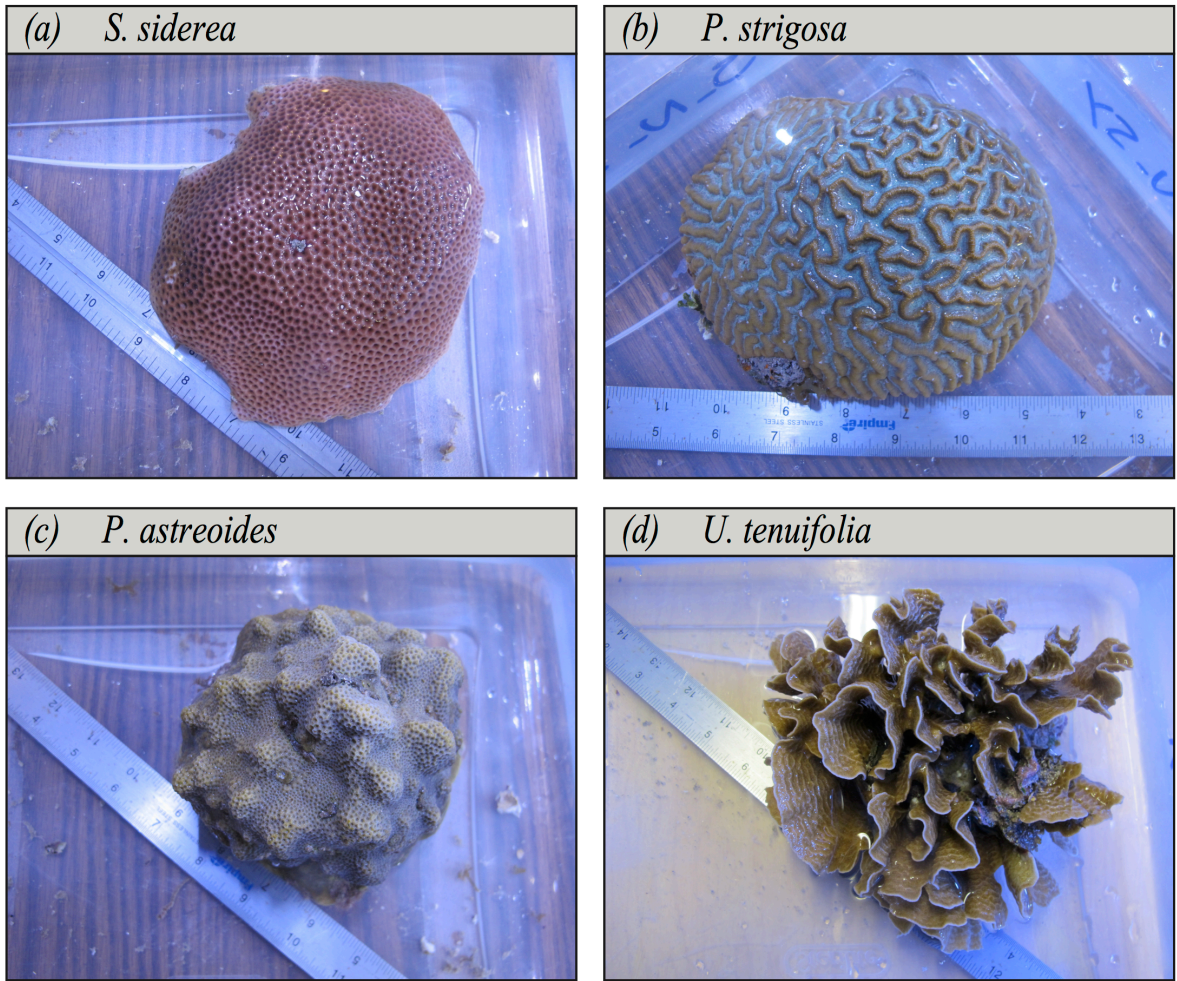


Figure S2.1. Representative specimens of the collected colonies of (a) *S. siderea*, (b) *P. strigosa*, (c) *P. astreoides*, and (d) *U. tenuifolia* from the Belize Barrier Reef System prior to sectioning.

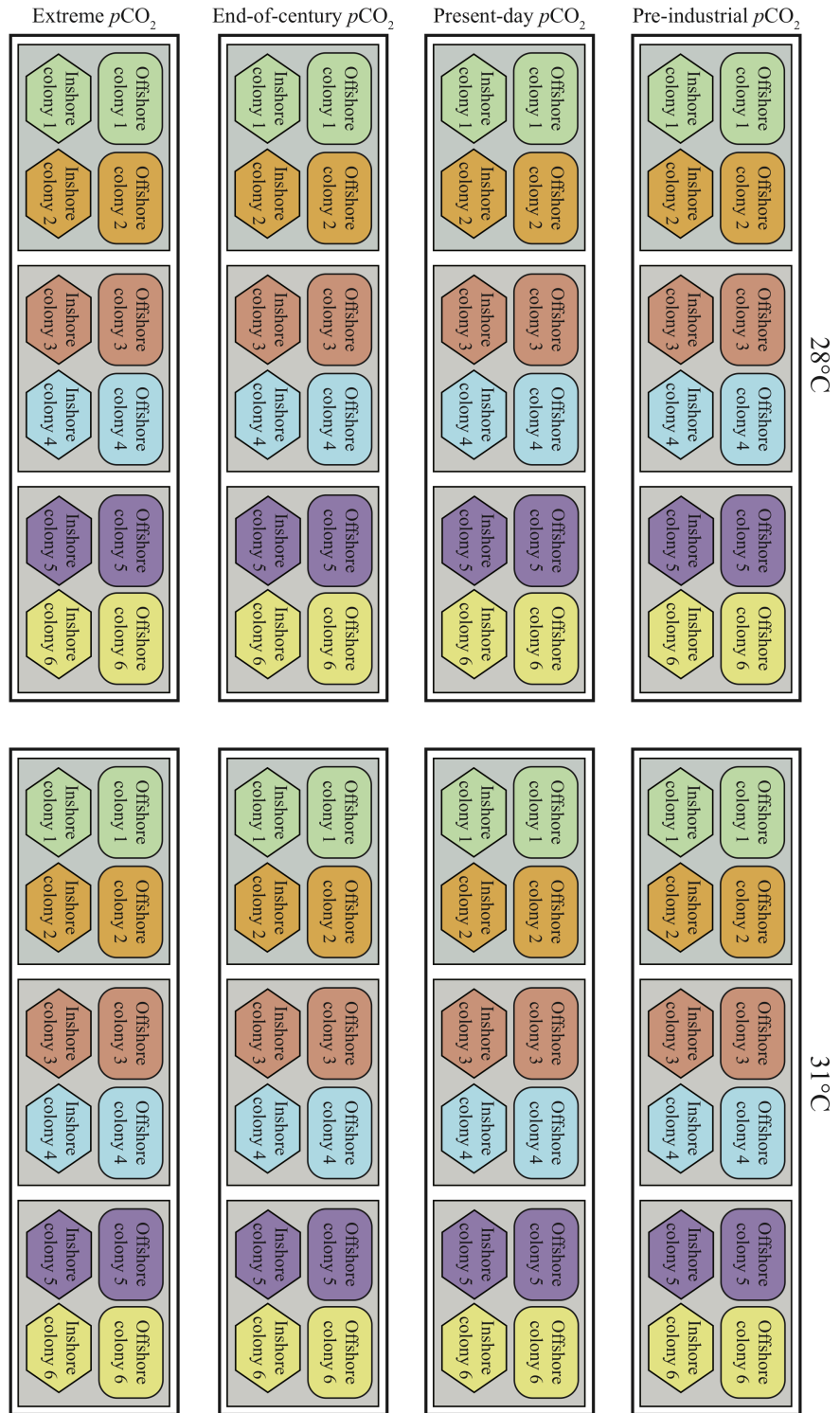


Figure S2.2. Diagram showing allocation of coral fragments for a single species throughout experimental tank array. Colour represent a different colony and shape represents reef environment. Four colonies (two from each reef environment) are reared within each tank (grey box), with three tanks comprising a treatment (white box). This is repeated for each

$p\text{CO}_2$ treatment at both temperatures. This same experimental design was used for all four species.

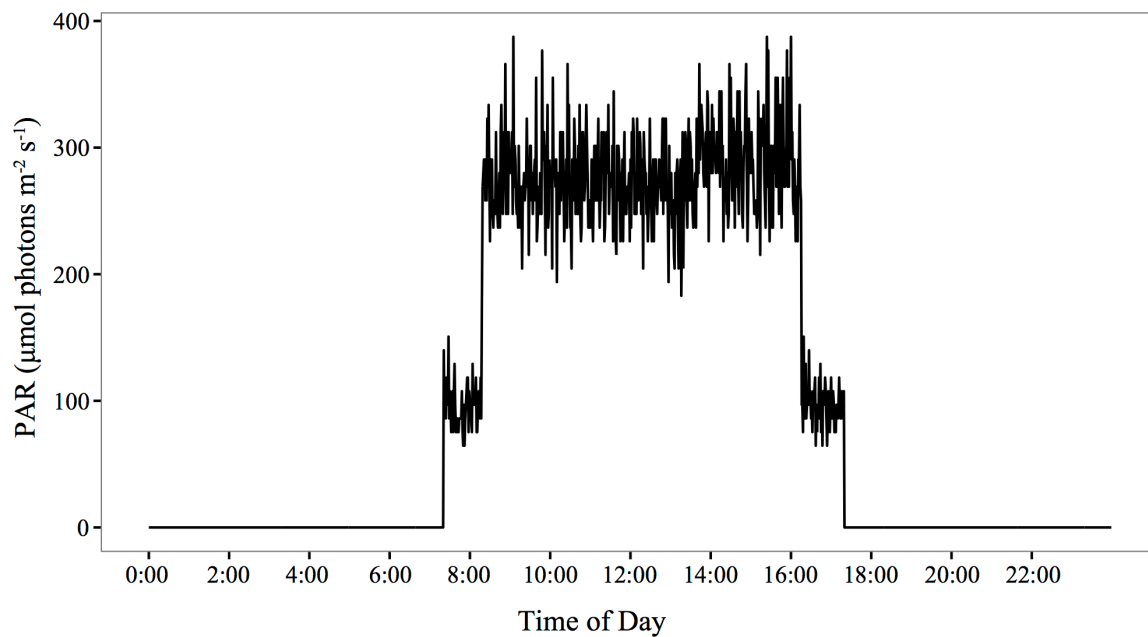


Figure S2.3. Ten hour light cycle for all 24 experimental treatment tanks reported in PAR (photosynthetically active radiation; $\mu\text{mol photons m}^{-2} \text{s}^{-1}$).

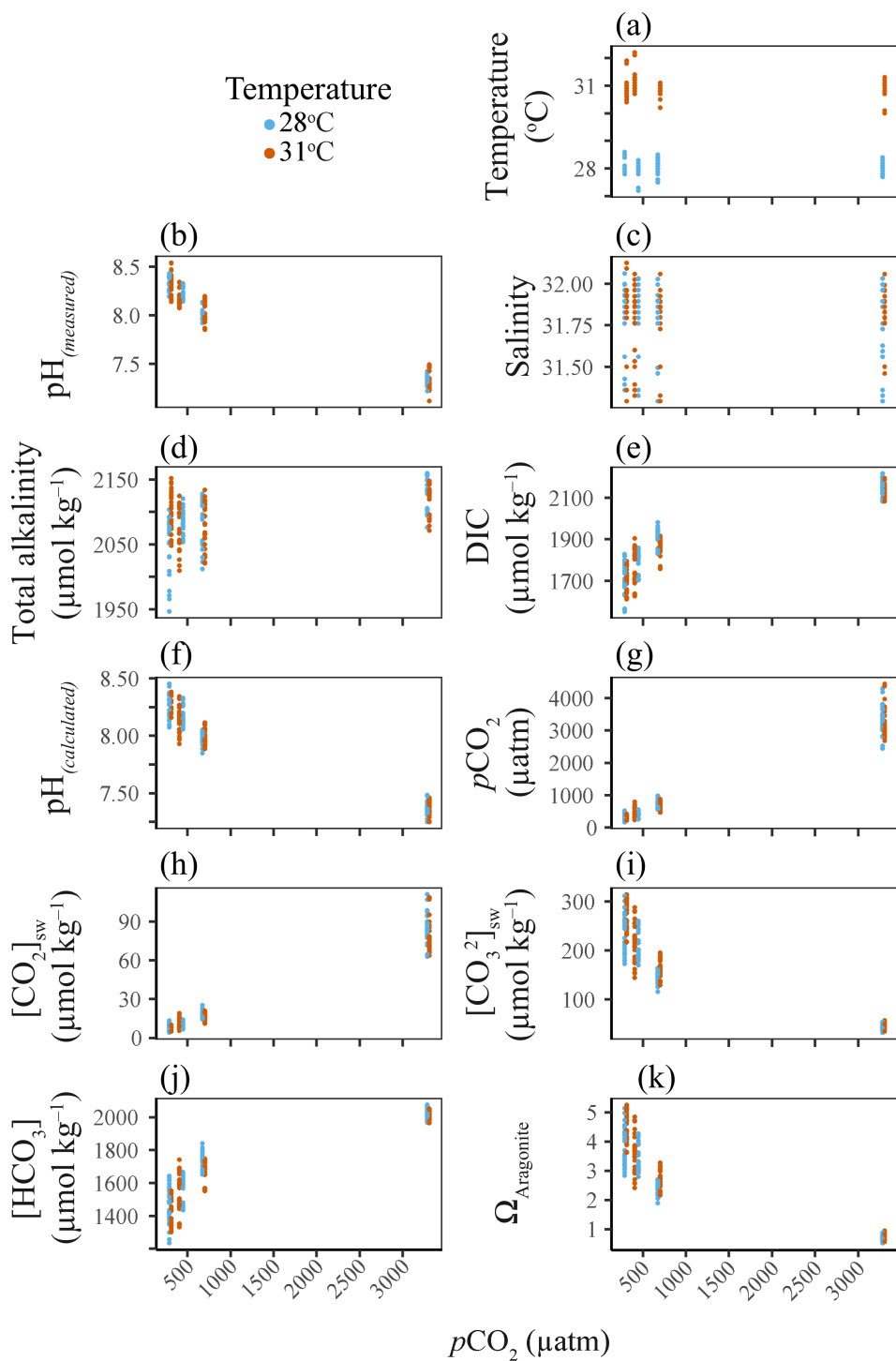


Figure S2.4. Calculated and measured parameters for all 24 experimental tanks over the 93-day experimental interval: (a) measured temperature; (b) measured pH; (c) measured salinity; (d) measured total alkalinity; (e) measured dissolved inorganic carbon; (f) calculated pH; (g) calculated $p\text{CO}_2$ of the mixed gases in equilibrium with the experimental seawaters; (h) calculated dissolved carbon dioxide; (i) calculated carbonate ion concentration; (j) calculated bicarbonate ion concentration; and (k) calculated aragonite saturation state.

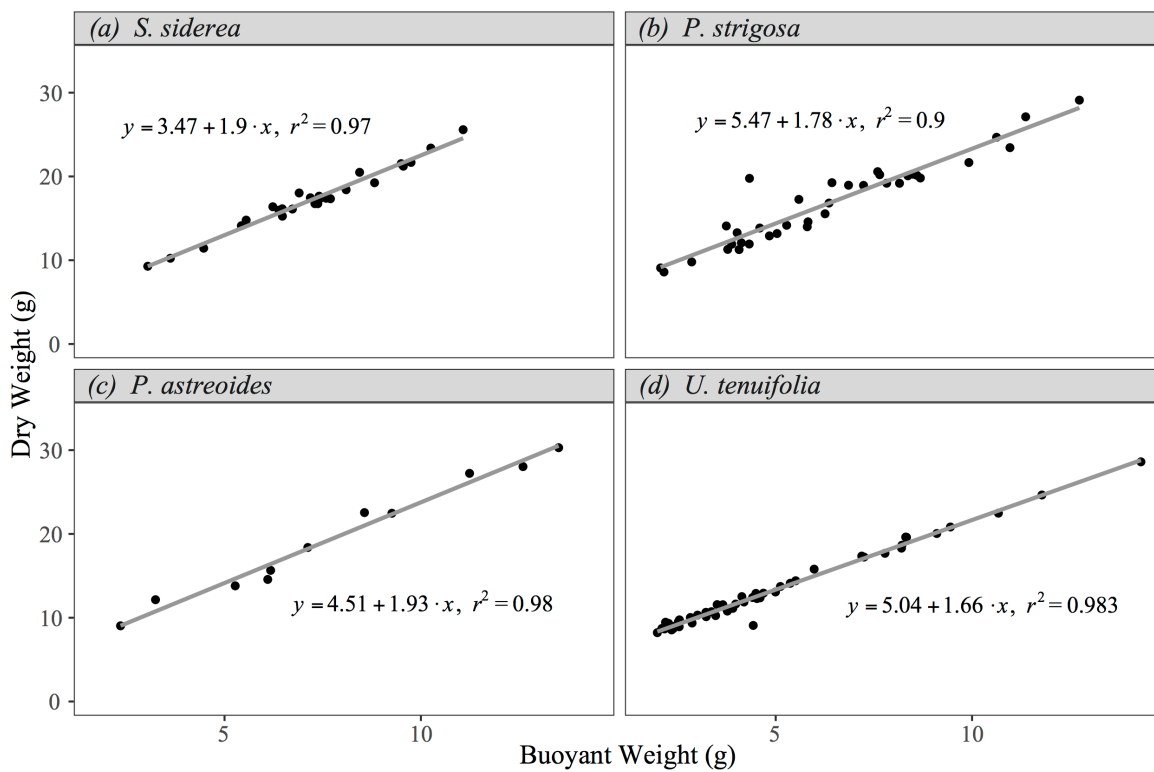


Figure S2.5. Linear relationship between buoyant weight (mg) and dry weight (mg) for (a) *S. siderea*, (b) *P. strigosa*, (c) *P. astreoides*, and (d) *U. tenuifolia*.

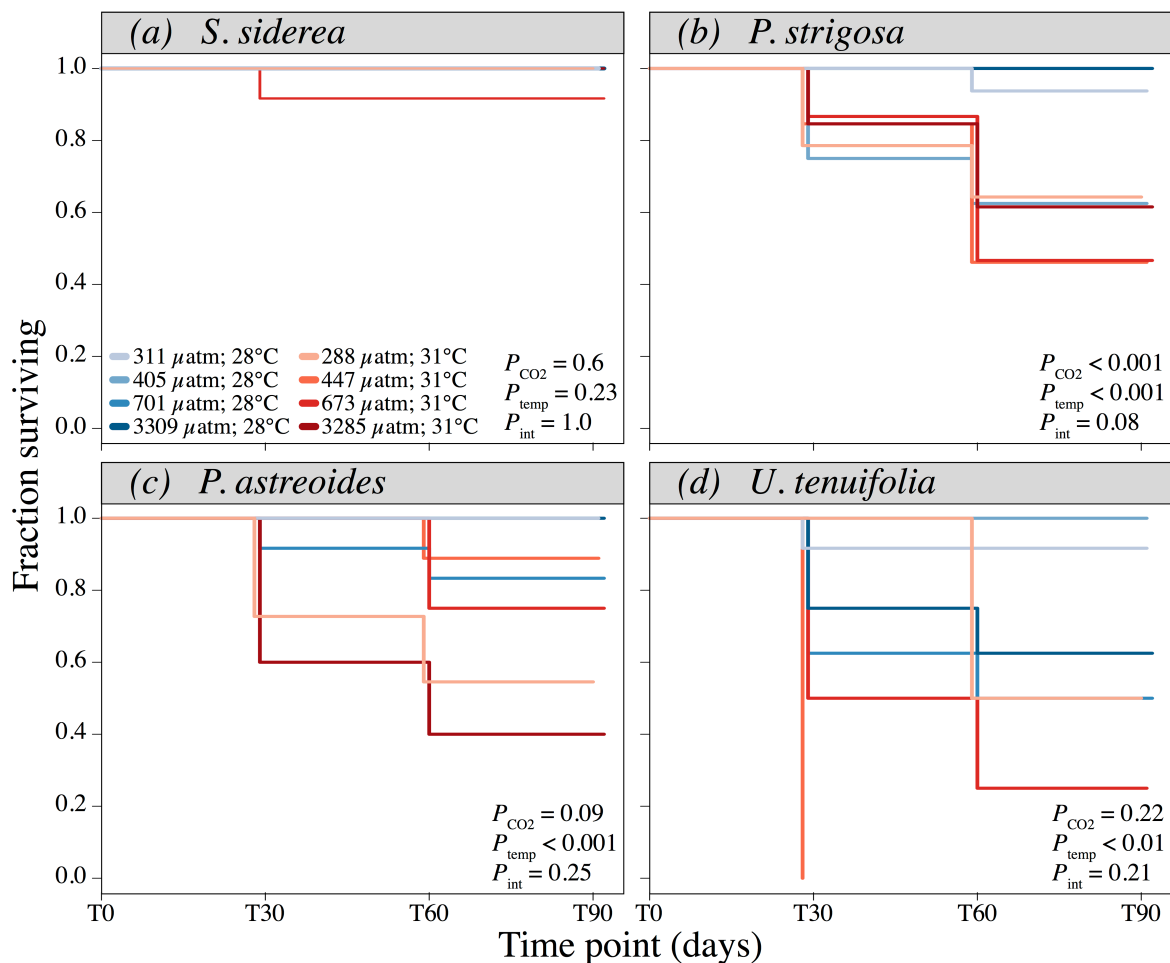


Figure S2.6. Fraction of fragments surviving from the start of the experiment for *S. siderea* (a), *P. strigosa* (b), *P. astreoides* (c), and *U. tenuifolia* (d). Blue represents 28°C treatments and red represents 31°C treatments. Colour intensity corresponds to pCO₂ level, with the lowest intensity representing pre-industrial pCO₂ and the highest intensity representing an extreme pCO₂ condition.

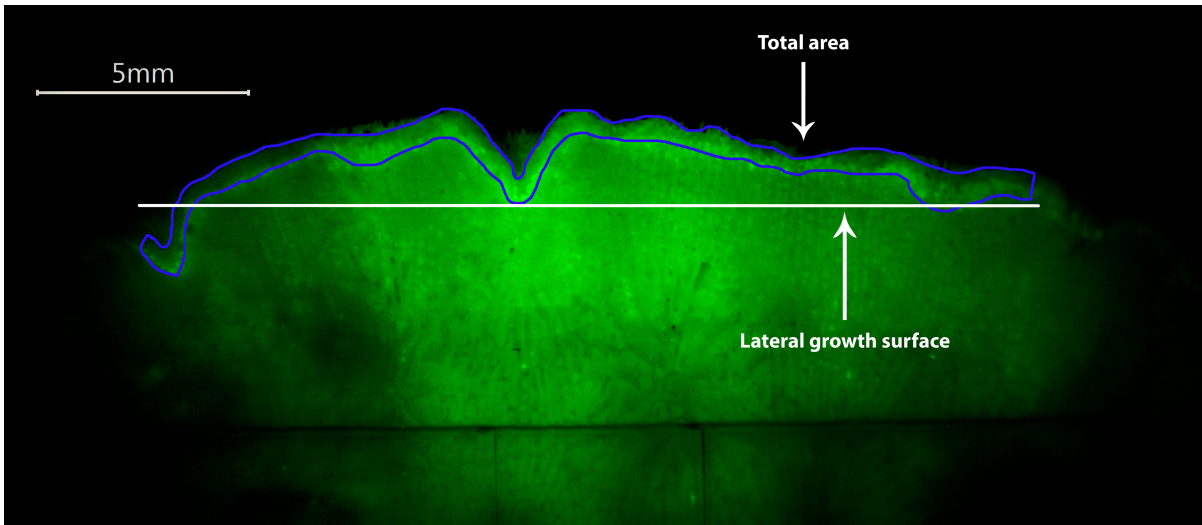


Figure S2.7. Example of linear extension measurement for *S. siderea* sample, indicating total growth area and lateral growth surface determination using image analysis software (IMAGE J). Linear extension was calculated by dividing total growth area by lateral growth surface

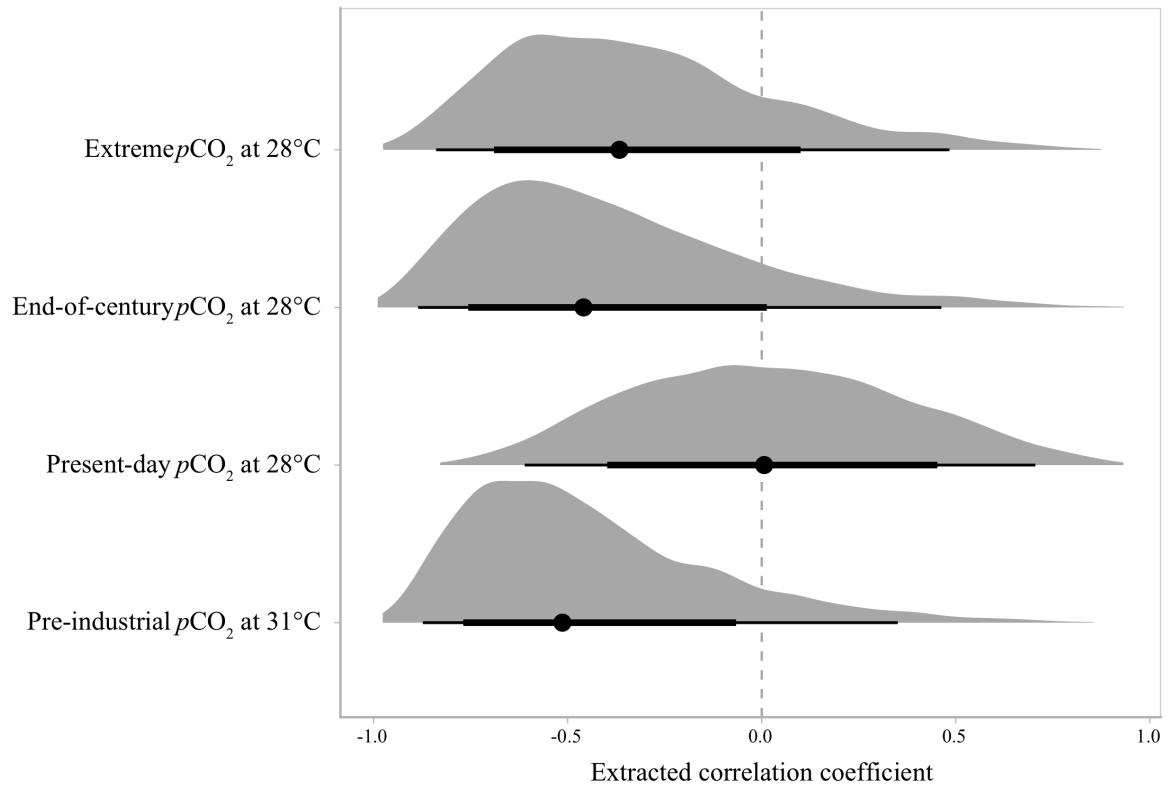


Figure S2.8. Density plot of the extracted correlation coefficients describing the correlation between the Bayesian random effects of colony on calcification rate under the control treatment (pre-industrial $p\text{CO}_2$ at 28°C) versus each stress treatment. The black circle represents the estimated mean, the thick black bar is the 75% credible interval, the thin black bar is the 95% credible interval, and the grey area represents the range of the Bayesian model output of the extracted correlation coefficients. Intervals that do not overlap zero denote significant effects of colony basal calcification rate on colony-level calcification response to $p\text{CO}_2$ or thermal stress.

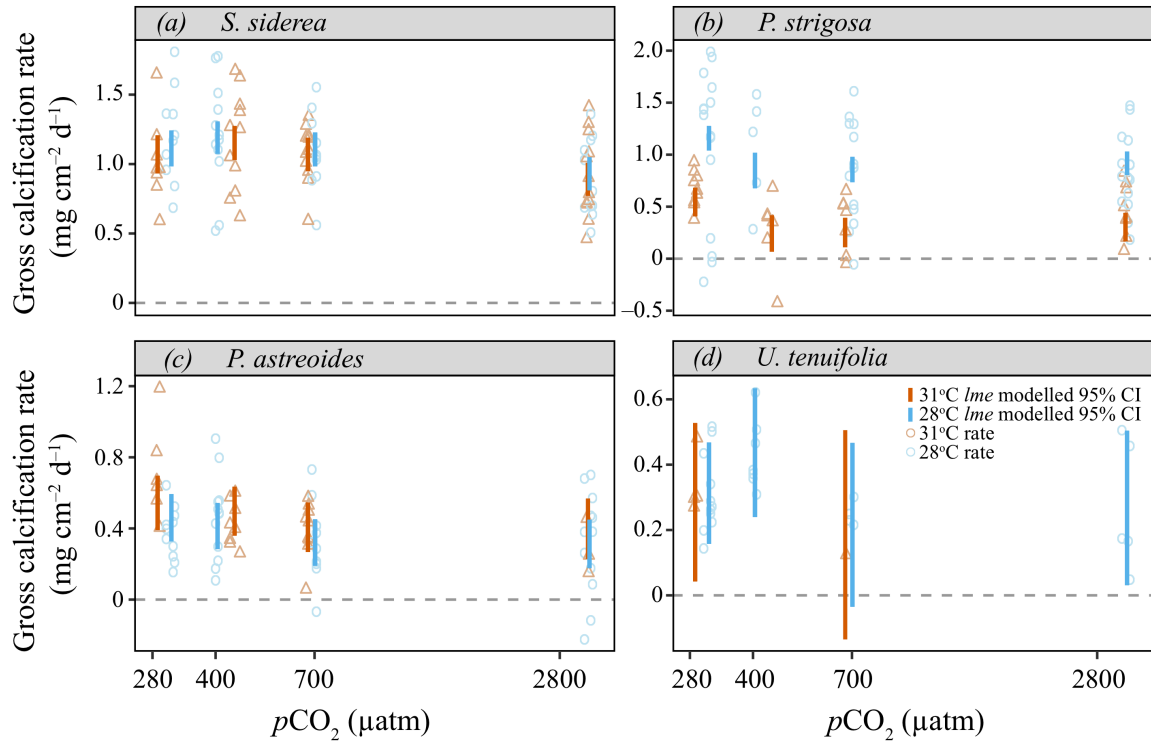


Figure S2.9. Modelled 95% confidence intervals of gross calcification rate for the 90-day experimental period in $\text{mg cm}^{-2} \text{day}^{-1}$ for (a) *S. siderea*, (b) *P. strigosa*, (c) *P. astreoides*, and (d) *U. tenuifolia*. Blue bars represent 28°C treatment 95% confidence intervals and orange bars represent 31°C treatment 95% confidence intervals, with $p\text{CO}_2$ along the x-axis (μatm). Blue open circles represent gross calcification rates for individual fragments in the 28°C treatment, and orange open circles represent gross calcification rates for individual fragments in the 31°C treatment.

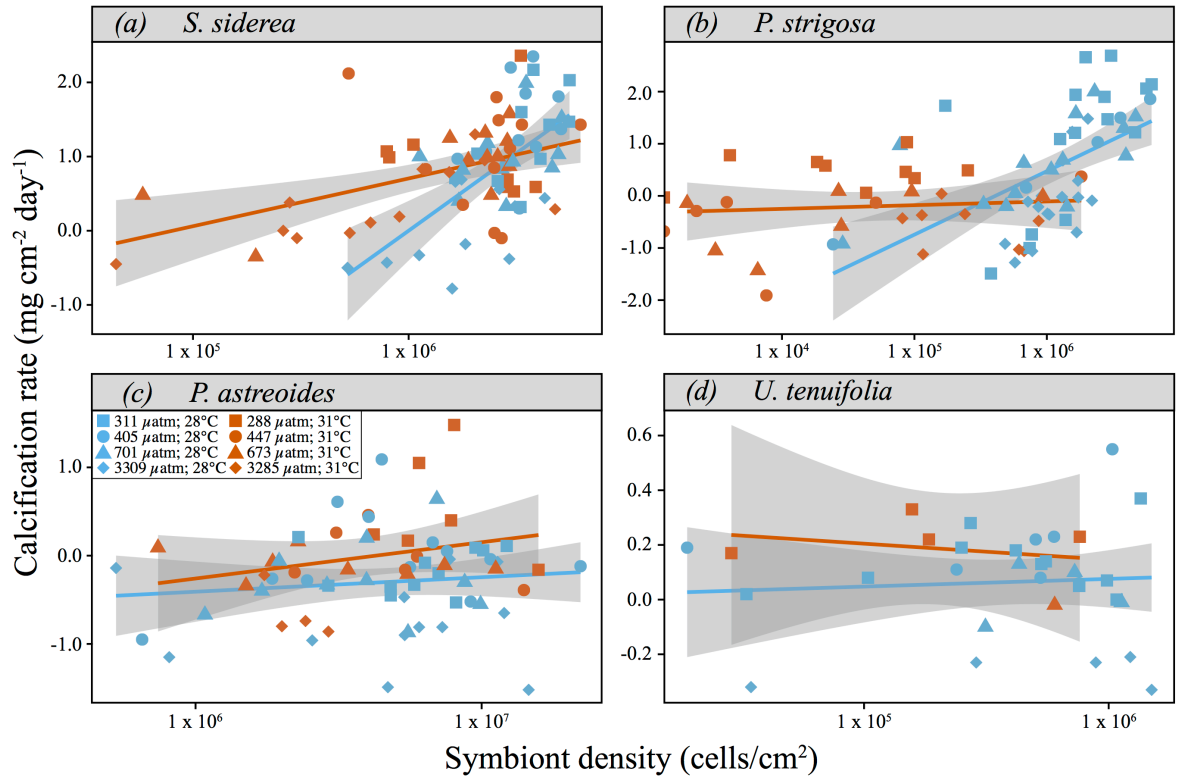


Figure S2.10. Relationship between calcification rate and symbiont density (cell counts cm⁻²) for (a) *S. siderea*, (b) *P. strigosa*, (c) *P. astreoides*, and (d) *U. tenuifolia*. Shape represents *p*CO₂ treatments and colour represents temperature treatments. The line denotes a simple linear regression with standard error denoted by grey shading.

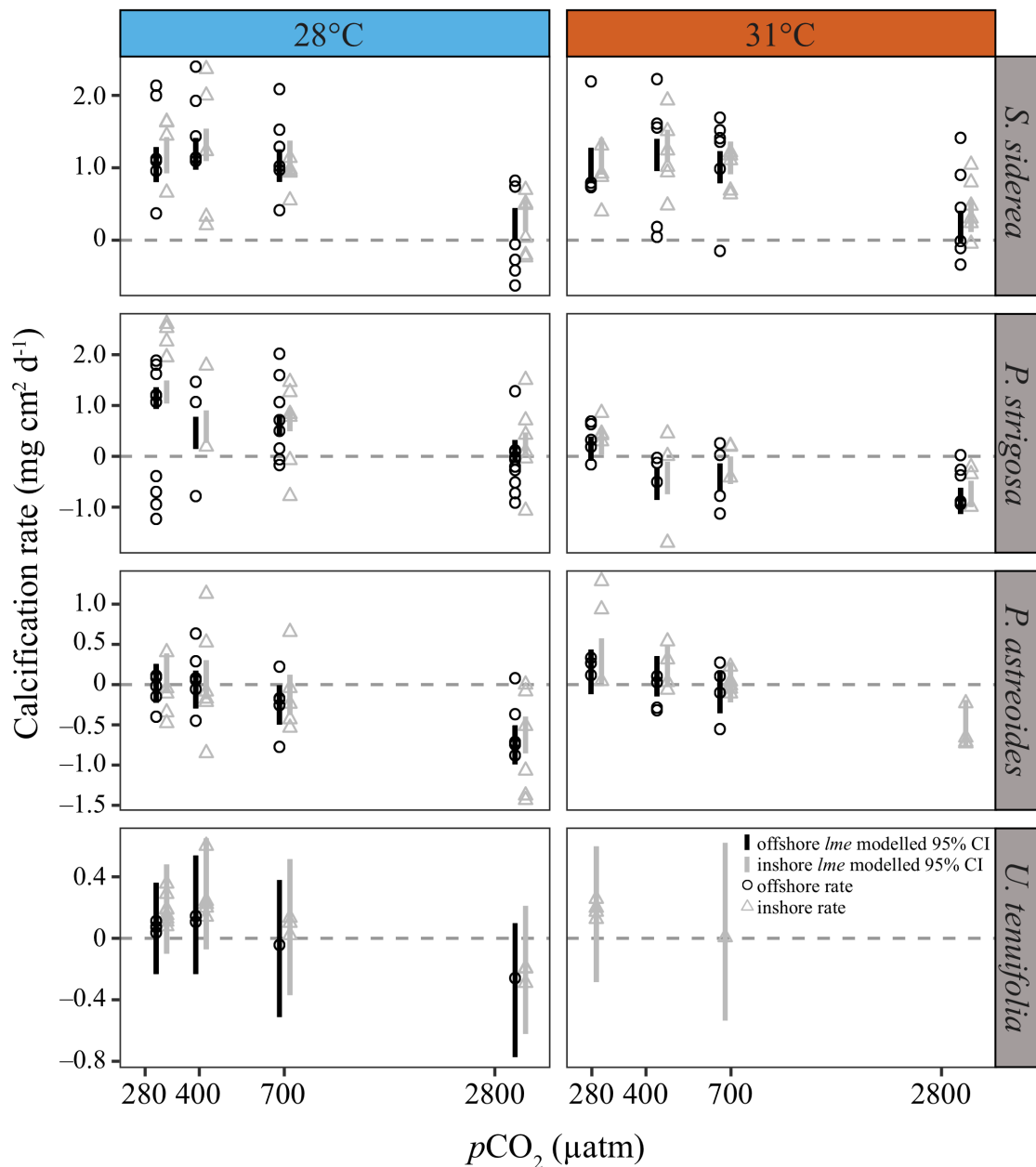


Figure S2.11. Modelled mean calcification rate for the 93-day experimental period in mg cm⁻² day⁻¹ separated by reef environment for (a) *S. siderea*, (b) *P. strigosa*, (c) *P. astreoides*, and (d) *U. tenuifolia*. Grey triangles denote inshore corals and black circles denote offshore corals. Left panel demonstrates mean calcification rate at 28°C and the right panel shows calcification at 31°C, with pCO₂ along the x-axis (μatm) on a log scale. Error bars denote 95% confidence intervals of each estimated mean.

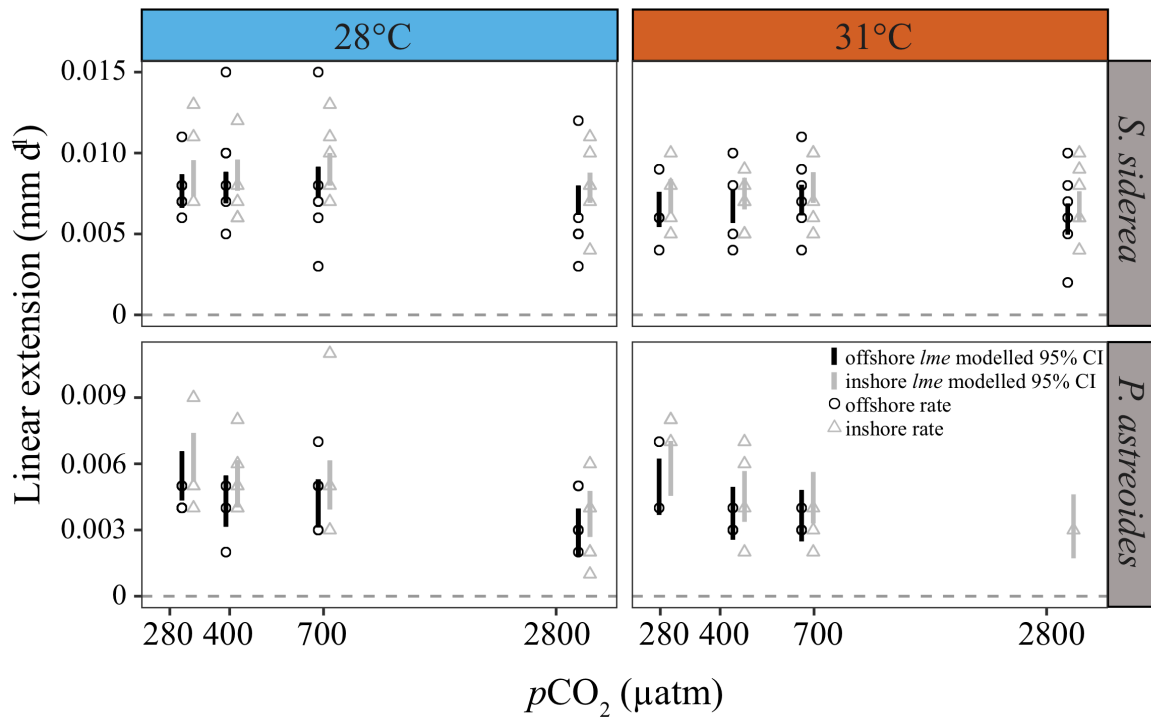


Figure S2.12. Modelled mean linear extension rate for the 93-day experimental period in $\text{mm cm}^{-2} \text{ day}^{-1}$ separated by reef environment for (a) *S. siderea* and (b) *P. astreoides*. Grey triangles denote inshore corals and black circles denote offshore corals. Left panel demonstrates mean calcification rate at 28°C and the right panel shows calcification at 31°C, with $p\text{CO}_2$ along the x-axis (μatm) on a log scale. Error bars denote 95% confidence intervals of each estimated mean.

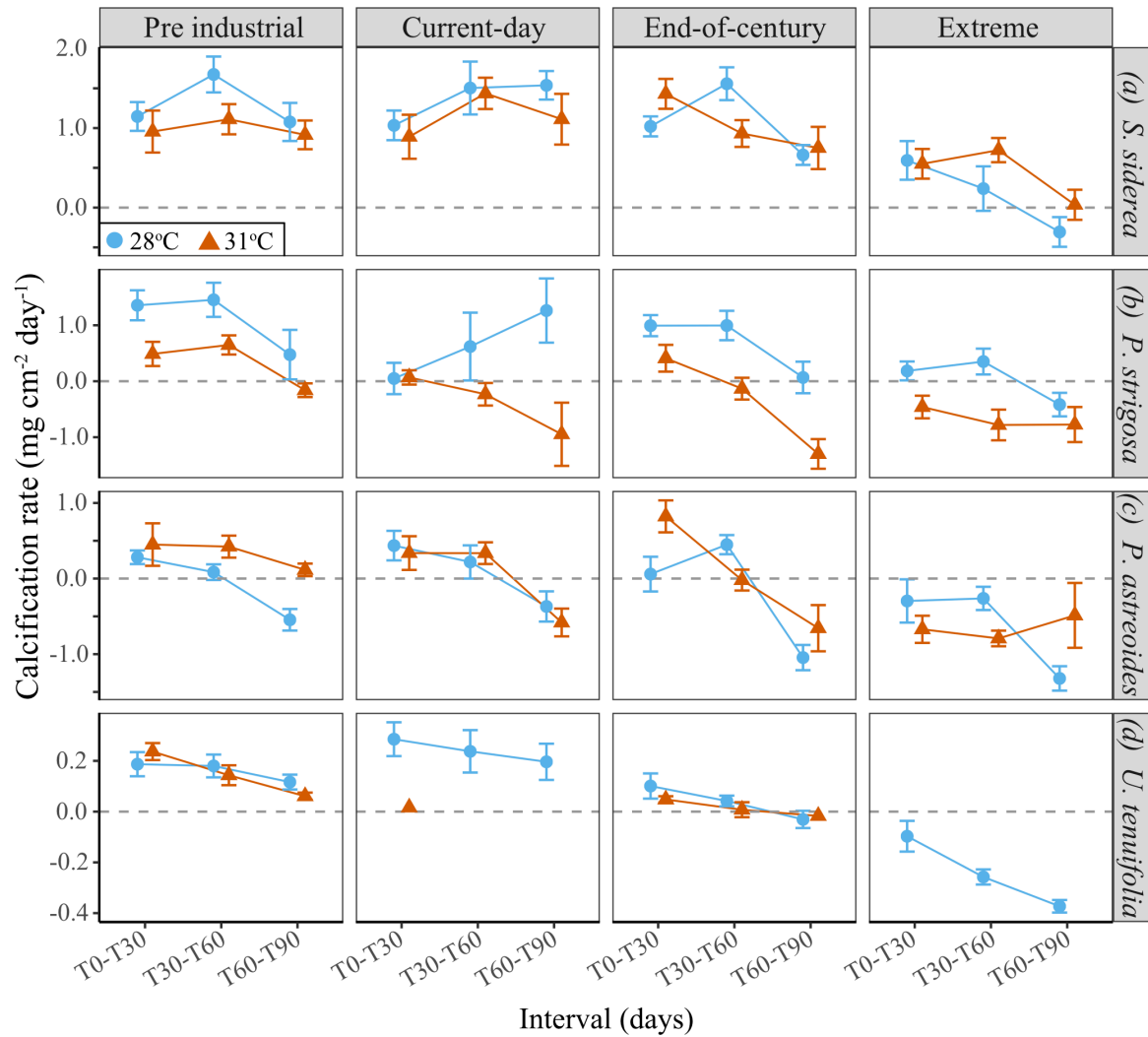


Figure S2.13. Mean calcification rate (mg cm⁻² day⁻¹) at each 30-day experimental interval at all pCO₂ treatments for (a) *S. siderica*, (b) *P. strigosa*, (c) *P. astreoides*, and (d) *U. tenuifolia*. Blue circles represent 28°C treatments and orange triangles represent 31°C treatments, with time interval along the x-axis. Error bars denote standard error of each mean.

APPENDIX 3: SUPPLEMENTAL DESCRIPTIONS AND FIGURES – CHAPTER 3

Species	Treatment	N	Modelled mean	Lower 95%	Upper 95%
SSID	288_28	11	0.4	0.3	0.48
SSID	311_31	9	0.4	0.28	0.47
SSID	3285_28	12	0.4	0.28	0.46
SSID	3309_31	12	0.4	0.26	0.44
SSID	405_31	12	0.4	0.3	0.47
SSID	447_28	12	0.4	0.32	0.49
SSID	673_28	13	0.3	0.24	0.41
SSID	701_31	12	0.3	0.22	0.39
SSID	T0	10	0.1	-0.05	0.19
PSTR	288_28	16	0.3	0.19	0.36
PSTR	311_31	9	0.1	0.04	0.23
PSTR	3285_28	15	0.2	0.13	0.3
PSTR	3309_31	8	0.1	-0.02	0.18
PSTR	405_31	5	0.1	-0.01	0.24
PSTR	447_28	5	0.3	0.13	0.38
PSTR	673_28	14	0.2	0.13	0.3
PSTR	701_31	7	0.1	-0.02	0.17
PSTR	T0	8	0.1	-0.05	0.22
PAST	288_28	11	0.2	0.11	0.31
PAST	311_31	6	0.3	0.15	0.37
PAST	3285_28	12	0.1	0.03	0.23
PAST	3309_31	4	0.2	0.06	0.3
PAST	405_31	7	0.2	0.12	0.33
PAST	447_28	12	0.2	0.08	0.27
PAST	673_28	10	0.1	0.01	0.21
PAST	701_31	9	0.2	0.06	0.26
PAST	T0	13	0.1	0	0.2

Table S3.1 Modelled mean host lipid and 95% confidence intervals

Bootstrapped modelled mean coral host lipid content (mg cm⁻²) for each species (SSID = *S. siderea*; PSTR = *P. strigosa*; PAST = *P. astreoides*) by treatment (T0 denotes samples taken at the start of the experiment and all others were assessed at T90). Sample sizes (N) and 95% confidence intervals are reported for each mean (Figure S3.1).

Species	Treatment	N	Modelled mean	Lower 95%	Upper 95%
SSID	288_28	11	1.2	0.95	1.35
SSID	311_31	8	0.8	0.62	1.02
SSID	3285_28	12	1.1	0.93	1.29
SSID	3309_31	12	0.8	0.6	0.96
SSID	405_31	12	0.8	0.57	0.93
SSID	447_28	12	1.1	0.91	1.26
SSID	673_28	13	1.3	1.1	1.44
SSID	701_31	12	0.9	0.76	1.1
SSID	T0	10	1.1	0.82	1.31
PSTR	288_28	16	0.8	0.6	0.93
PSTR	311_31	9	0.5	0.3	0.7
PSTR	3285_28	16	0.6	0.45	0.78
PSTR	3309_31	8	0.4	0.15	0.54
PSTR	405_31	6	0.4	0.16	0.65
PSTR	447_28	5	0.7	0.42	0.93
PSTR	673_28	14	0.6	0.39	0.75
PSTR	701_31	7	0.3	0.09	0.49
PSTR	T0	8	0.8	0.57	1.1
PAST	288_28	11	0.8	0.61	1.03
PAST	311_31	6	0.7	0.42	0.88
PAST	3285_28	12	0.6	0.38	0.78
PAST	3309_31	4	0.4	0.17	0.65
PAST	405_31	7	0.7	0.52	0.94
PAST	447_28	12	0.9	0.71	1.08
PAST	673_28	10	0.6	0.4	0.81
PAST	701_31	9	0.4	0.23	0.65
PAST	T0	14	1.4	1.2	1.61

Table S3.2 Modelled mean host carbohydrate and 95% confidence intervals

Bootstrapped modelled mean coral host carbohydrate content (mg cm^{-2}) for each species (SSID = *S. siderea*; PSTR = *P. strigosa*; PAST = *P. astreoides*) by treatment (T0 denotes samples taken at the start of the experiment and all others were assessed at T90). Sample sizes (N) and 95% confidence intervals are reported for each mean (Figure S3.2).

Species	Treatment	N	Modelled mean	Lower 95%	Upper 95%
SSID	288_28	11	0.5	0.41	0.58
SSID	311_31	9	0.4	0.35	0.52
SSID	3285_28	12	0.5	0.37	0.53
SSID	3309_31	12	0.4	0.31	0.47
SSID	405_31	12	0.5	0.38	0.54
SSID	447_28	12	0.5	0.44	0.6
SSID	673_28	13	0.5	0.39	0.54
SSID	701_31	12	0.4	0.33	0.49
SSID	T0	10	0.5	0.42	0.63
PSTR	288_28	16	0.6	0.49	0.64
PSTR	311_31	9	0.3	0.23	0.4
PSTR	3285_28	16	0.4	0.35	0.49
PSTR	3309_31	8	0.2	0.08	0.26
PSTR	405_31	6	0.2	0.06	0.29
PSTR	447_28	5	0.4	0.31	0.54
PSTR	673_28	14	0.5	0.37	0.54
PSTR	701_31	7	0.2	0.11	0.3
PSTR	T0	8	0.4	0.24	0.48
PAST	288_28	11	0.2	0.15	0.33
PAST	311_31	6	0.2	0.09	0.29
PAST	3285_28	12	0.1	0.01	0.2
PAST	3309_31	4	0.1	-0.05	0.17
PAST	405_31	7	0.2	0.07	0.25
PAST	447_28	12	0.2	0.13	0.29
PAST	673_28	10	0.2	0.07	0.25
PAST	701_31	9	0.1	0.02	0.2
PAST	T0	14	0.3	0.21	0.4

Table S3.3 Modelled mean host protein and 95% confidence intervals

Bootstrapped modelled mean coral host protein content (mg cm⁻²) for each species (SSID = *S. siderea*; PSTR = *P. strigosa*; PAST = *P. astreoides*) by treatment (T0 denotes samples taken at the start of the experiment and all others were assessed at T90). Sample sizes (N) and 95% confidence intervals are reported for each mean (Figure S3.3).

Species	Treatment	N	Modelled mean	Lower 95%	Upper 95%
SSID	288_28	11	2.16	1.95	2.39
SSID	311_31	8	1.76	1.53	1.99
SSID	3285_28	12	1.88	1.67	2.1
SSID	3309_31	12	1.48	1.26	1.69
SSID	405_31	12	1.68	1.45	1.91
SSID	447_28	12	2.09	1.86	2.3
SSID	673_28	13	1.92	1.71	2.12
SSID	701_31	12	1.52	1.3	1.74
SSID	T0	10	1.67	1.3	2.07
PSTR	288_28	16	1.54	1.34	1.73
PSTR	311_31	9	0.88	0.63	1.13
PSTR	3285_28	15	1.25	1.05	1.45
PSTR	3309_31	8	0.59	0.32	0.85
PSTR	405_31	5	0.8	0.53	1.06
PSTR	447_28	5	1.46	1.23	1.7
PSTR	673_28	14	1.3	1.09	1.5
PSTR	701_31	7	0.63	0.37	0.9
PSTR	T0	8	1.28	0.87	1.7
PAST	288_28	11	1.21	0.98	1.44
PAST	311_31	6	1.05	0.79	1.32
PAST	3285_28	12	0.93	0.71	1.15
PAST	3309_31	4	0.76	0.48	1.03
PAST	405_31	7	0.97	0.71	1.24
PAST	447_28	12	1.14	0.91	1.36
PAST	673_28	10	0.97	0.75	1.19
PAST	701_31	9	0.8	0.55	1.06
PAST	T0	13	1.83	1.51	2.16

Table S3.4 Modelled mean total host energy reserve and 95% confidence intervals

Bootstrapped modelled mean total coral host energy reserves (mg cm⁻²) for each species (SSID = *S. siderea*; PSTR = *P. strigosa*; PAST = *P. astreoides*) by treatment (T0 denotes samples taken at the start of the experiment and all others were assessed at T90). Sample sizes (N) and 95% confidence intervals are reported for each mean (Figure 3.1B).

Species	Treatment	N	Modelled mean	Lower 95%	Upper 95%
SSID	288_28	11	3.34	2.4	4.31
SSID	311_31	9	2.46	1.47	3.44
SSID	3285_28	12	2.07	1.16	2.97
SSID	3309_31	12	1.19	0.28	2.13
SSID	405_31	12	2.59	1.65	3.51
SSID	447_28	12	3.47	2.55	4.38
SSID	673_28	13	2.96	2.07	3.85
SSID	701_31	12	2.08	1.17	2.96
SSID	T0	10	2.07	0.74	3.35
PSTR	288_28	16	2.21	1.34	3.09
PSTR	311_31	9	0.43	-0.59	1.51
PSTR	3285_28	16	1.55	0.67	2.44
PSTR	3309_31	8	-0.23	-1.27	0.82
PSTR	405_31	6	0.46	-0.84	1.72
PSTR	447_28	5	2.23	0.98	3.52
PSTR	673_28	14	1.72	0.83	2.64
PSTR	701_31	7	-0.06	-1.11	0.97
PSTR	T0	8	1.8	0.37	3.25
PAST	288_28	11	7.33	6.31	8.38
PAST	311_31	6	6.44	5.29	7.62
PAST	3285_28	12	5.83	4.86	6.85
PAST	3309_31	4	4.94	3.67	6.23
PAST	405_31	6	5.58	4.45	6.75
PAST	447_28	12	6.47	5.44	7.48
PAST	673_28	10	5.02	3.97	6.09
PAST	701_31	8	4.13	3.03	5.25
PAST	T0	14	1.66	0.55	2.7

Table S3.5 Modelled mean algal endosymbiont cell density and 95% confidence intervals

Bootstrapped modelled mean algal endosymbiont cell density (10^6 cells cm^{-2}) for each species (SSID = *S. siderica*; PSTR = *P. strigosa*; PAST = *P. astreoides*) by treatment (T0 denotes samples taken at the start of the experiment and all others were assessed at T90). Sample sizes (N) and 95% confidence intervals are reported for each mean (Figure 3.1C).

Species	Treatment	N	Modelled mean	Lower 95%	Upper 95%
SSID	288_28	11	120.8	93.95	147.27
SSID	311_31	9	95.78	68.08	122.9
SSID	3285_28	12	53.23	27.81	78.85
SSID	3309_31	12	28.22	2.2	52.44
SSID	405_31	12	104.9	79.27	130.43
SSID	447_28	12	129.9	105.49	155.19
SSID	673_28	13	94.59	70.29	118.96
SSID	701_31	12	69.58	43.99	93.96
SSID	T0	10	46.17	11.01	79.02
PSTR	288_28	16	193.8	170.37	217.87
PSTR	311_31	9	108.8	81.57	136.4
PSTR	3285_28	16	81.43	57.99	105.14
PSTR	3309_31	8	-3.49	-32.26	24.19
PSTR	405_31	6	47.02	9.81	83.7
PSTR	447_28	5	131.9	94.83	168.34
PSTR	673_28	14	90.82	65.27	116.53
PSTR	701_31	7	5.91	-25.4	36.83
PSTR	T0	8	49.04	9.22	88.2
PAST	288_28	11	104.2	77.16	132.35
PAST	311_31	6	142.4	110.92	175.02
PAST	3285_28	12	17.71	-12.59	46.48
PAST	3309_31	4	55.9	22.29	91.31
PAST	405_31	7	83.73	53.52	113.12
PAST	447_28	12	45.54	19.14	71.25
PAST	673_28	10	44.91	16.96	74.43
PAST	701_31	9	83.1	55.13	112.3
PAST	T0	14	43.4	14.9	73.72

Table S3.6 Modelled mean algal endosymbiont chlorophyll a and 95% confidence intervals

Bootstrapped modelled mean algal endosymbiont chlorophyll a concentration (mg cm^{-2}) for each species (SSID = *S. siderica*; PSTR = *P. strigosa*; PAST = *P. astreoides*) by treatment (T0 denotes samples taken at the start of the experiment and all others were assessed at T90). Sample sizes (N) and 95% confidence intervals are reported for each mean (Figure 3.1D).

Parameter	Df	Sums of squares	Mean squares	F model	R ²	Pr (>F)
Temperature	1	3111	3111.1	2.0968	0.00376	0.15
pCO ₂	3	14260	4753.4	3.2037	0.01722	0.019 *
Reef	1	736	736.2	0.4962	0.00089	0.455
Residuals	546	810104	1483.7	0.97814		
Total	551	828211	1			

Table S3.7 PERMANOVA model output for *S. siderea* holobiont physiology

Assessment of the main effects of treatment pCO₂, temperature, and natal reef environment on the similarity/dissimilarity of *S. siderea* holobiont physiology as visualized in the PCA in Figure 3.2A. Parameters with an asterisk (*) denote significant main effects.

Parameter	Df	Sums of squares	Mean squares	F model	R ²	Pr (>F)
Temperature	1	18776	18775.5	6.0027	0.01231	0.011 *
pCO ₂	3	31998	10666.2	3.41	0.02098	0.019 *
Reef	1	10809	10809.2	3.4558	0.00709	0.059
Residuals	468	1463839	3127.9	0.95963		
Total	473	1525422	1			

Table S3.8 PERMANOVA model output for *P. strigosa* holobiont physiology

Assessment of the main effects of treatment pCO₂, temperature, and natal reef environment on the similarity/dissimilarity of *P. strigosa* holobiont physiology as visualized in the PCA in Figure 3.2B. Parameters with an asterisk (*) denote significant main effects.

Parameter	Df	Sums of squares	Mean squares	F model	R ²	Pr (>F)
Temperature	1	4401	4401.1	4.1153	0.00972	0.038 *
pCO ₂	3	12017	4005.7	3.7456	0.02654	0.007 *
Reef	1	116	116.4	0.1089	0.00026	0.754
Residuals	408	436336	1069.5	0.96349		
Total	413	452871	1			

Table S3.9 PERMANOVA model output for *P. astreoides* holobiont physiology

Assessment of the main effects of treatment pCO₂, temperature, and natal reef environment on the similarity/dissimilarity of *P. astreoides* holobiont physiology as visualized in the PCA in Figure 3.2C. Parameters with an asterisk (*) denote significant main effects.

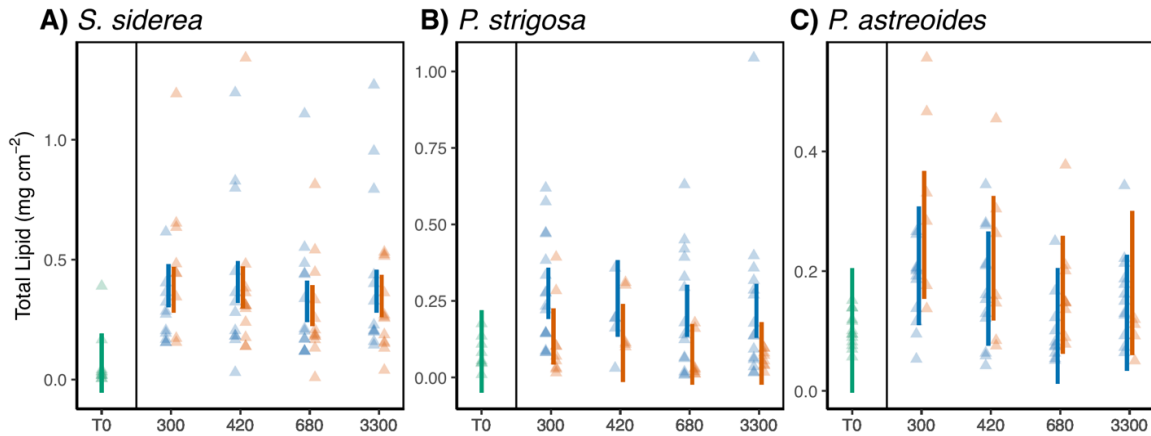


Figure S3.1 Total coral host lipid content. Modelled 95% confidence interval of total host lipid concentrations (mg cm⁻²) for (A) *S. siderea*, (B) *P. strigosa*, and (C) *P. astreoides* at T0 (green) or T90 (red/blue), with individual coral fragment physiology denoted by points. Blue denotes 28°C and red denotes 31°C, with *p*CO₂ treatment along the x axis.

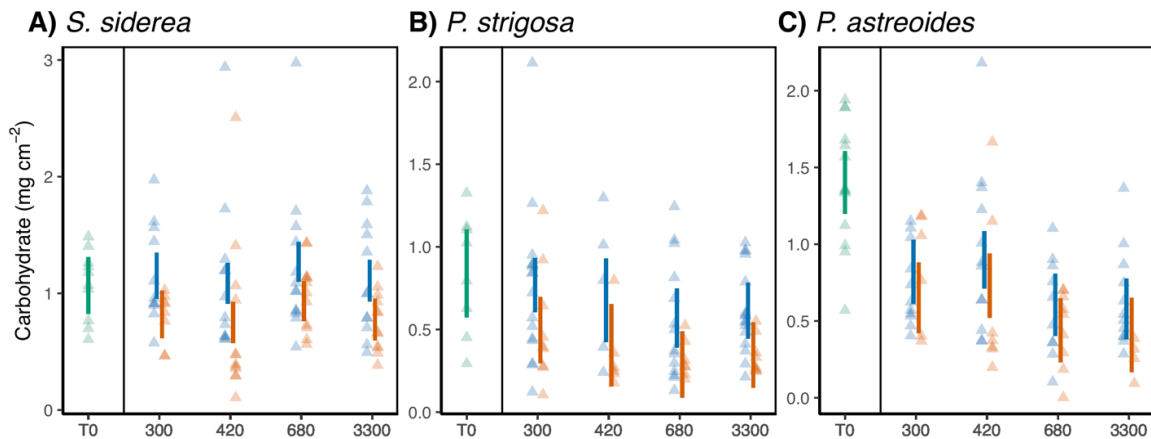


Figure S3.2 Total coral host carbohydrate content. Modelled 95% confidence interval of total host carbohydrate concentrations (mg cm⁻²) for (A) *S. siderea*, (B) *P. strigosa*, and (C) *P. astreoides* at T0 (green) or T90 (red/blue), with individual coral fragment physiology denoted by points. Blue denotes 28°C and red denotes 31°C, with *p*CO₂ treatment along the x axis.

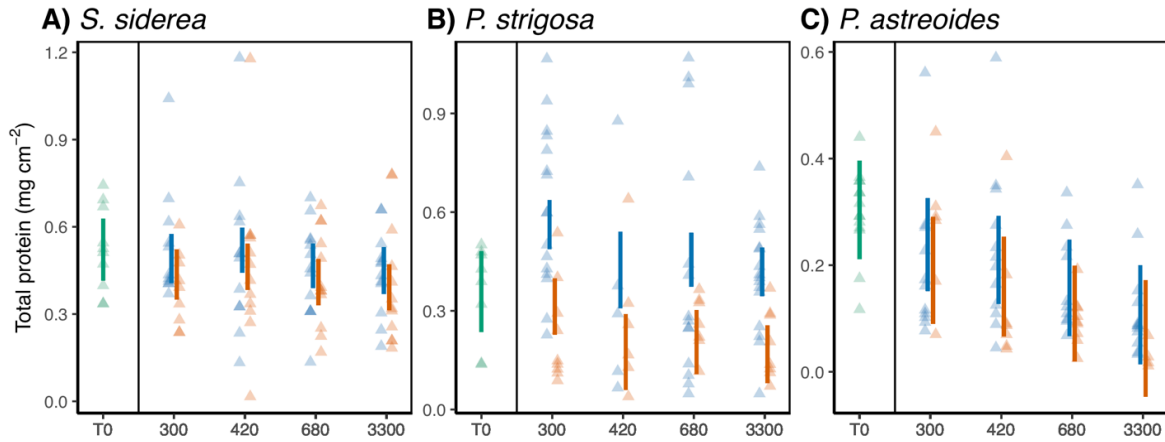


Figure S3.3 Total coral host protein content. Modelled 95% confidence interval of total host protein concentrations (mg cm⁻²) for (A) *S. siderea*, (B) *P. strigosa*, and (C) *P. astreoides* at T0 (green) or T90 (red/blue), with individual coral fragment physiology denoted by points. Blue denotes 28°C and red denotes 31°C, with pCO₂ treatment along the x axis.

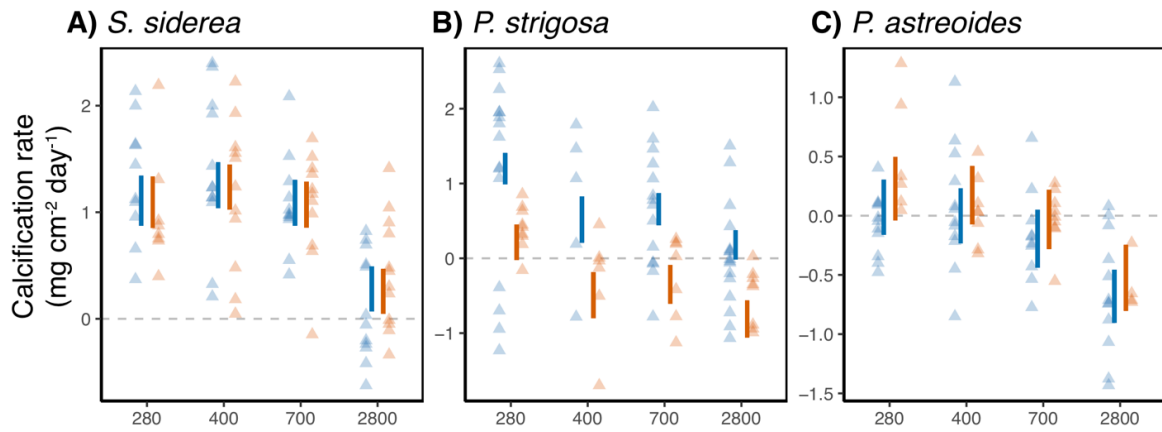


Figure S3.4 Coral calcification rates. Modelled 95% confidence interval of coral calcification rates (mg cm⁻² day⁻¹) previously reported in Bove et al. (2019) for (A) *S. siderea*, (B) *P. strigosa*, and (C) *P. astreoides* T90 only, with individual coral fragment rates denoted by points. Blue denotes 28°C and red denotes 31°C, with pCO₂ treatment along the x axis. The dashed grey line at 0 highlights confidence intervals exhibiting net calcification (above 0) or net dissolution (below 0).

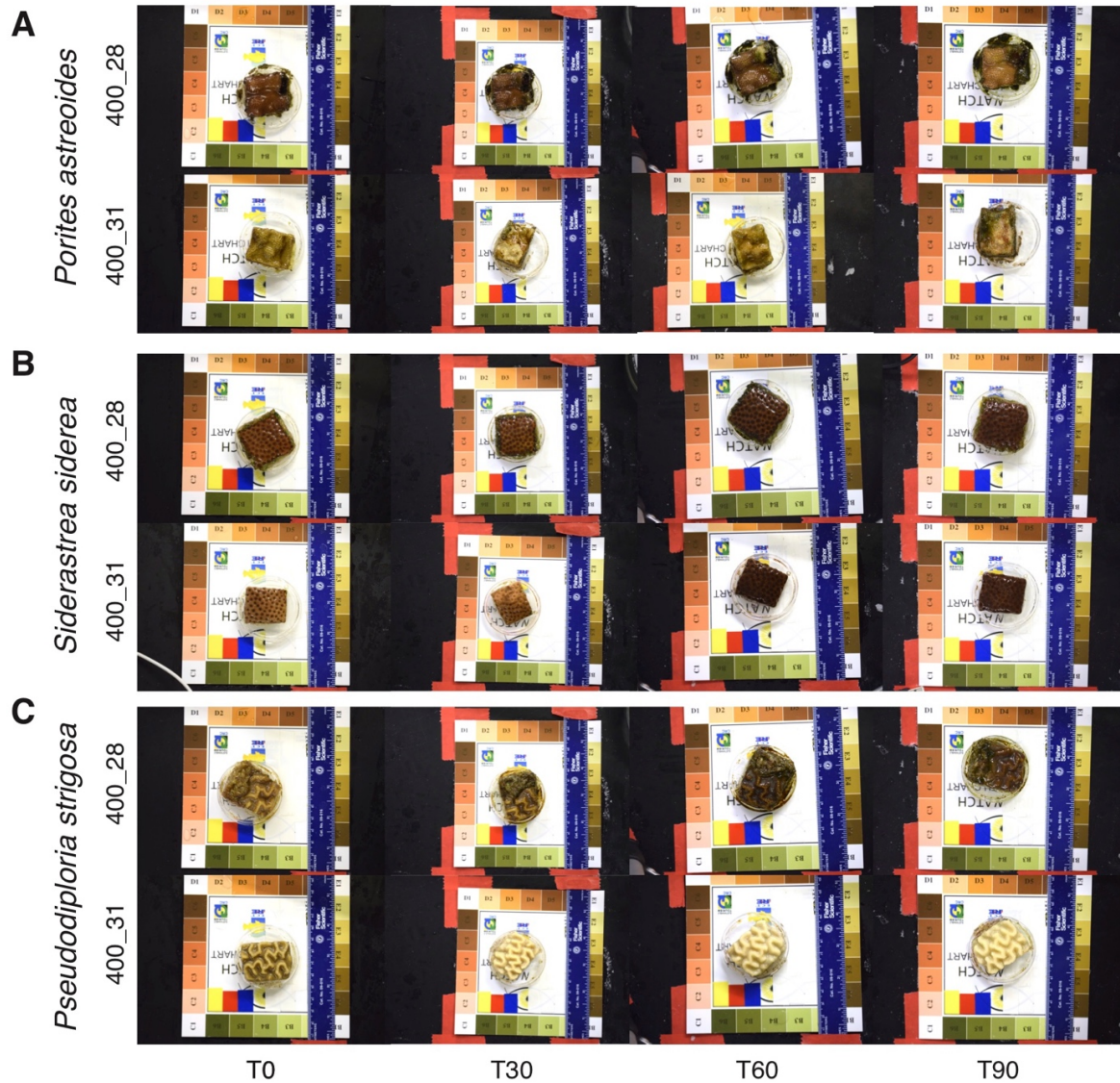


Figure S3.5 Coral colour change over experimental period. Representative images of *P. astreoides* (A), *S. siderea* (B), and *P. strigosa* from the same colonies demonstrating change in coral colour over time in either control (400_28) or warming (400_31) treatments from the start of the experiment (T0) to the end (T90).

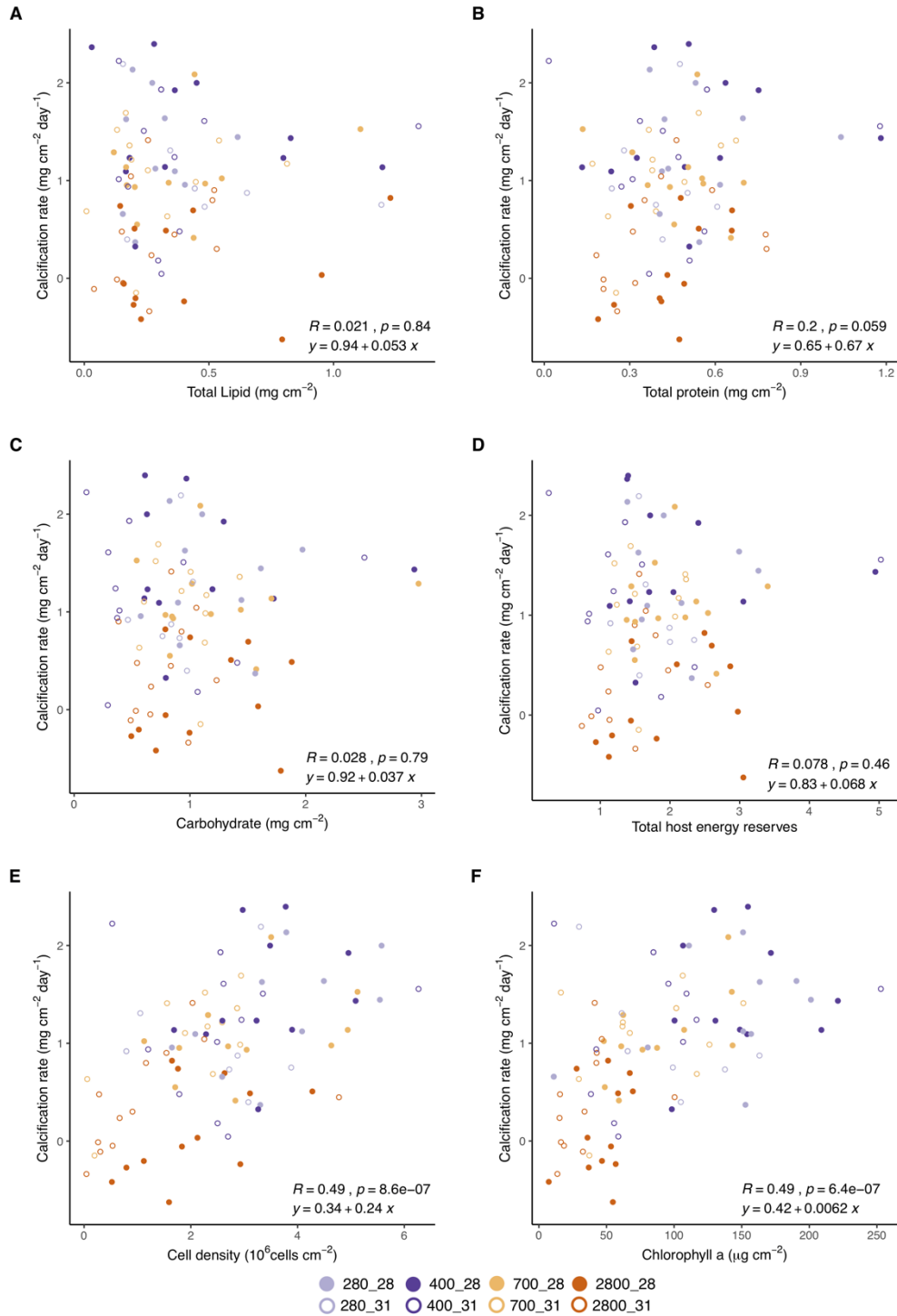


Figure S3.6 Relationship between *S. siderea* physiology and calcification rate.

Measured *S. siderea* calcification rate ($\text{mg cm}^{-2} \text{ day}^{-1}$) plotted against (A) coral host lipid (mg cm^{-2}), (B) coral host protein (mg cm^{-2}), (B) coral host carbohydrate (mg cm^{-2}), (D) coral host total energy reserves (mg cm^{-2}), (E) algal endosymbiont cell density ($10^6 \text{ cells cm}^{-2}$), and (F) algal endosymbiont chlorophyll a concentration (mg cm^{-2}). Each plot contains the corresponding R^2 , p-value, and regression equation fit to each parameter pair.

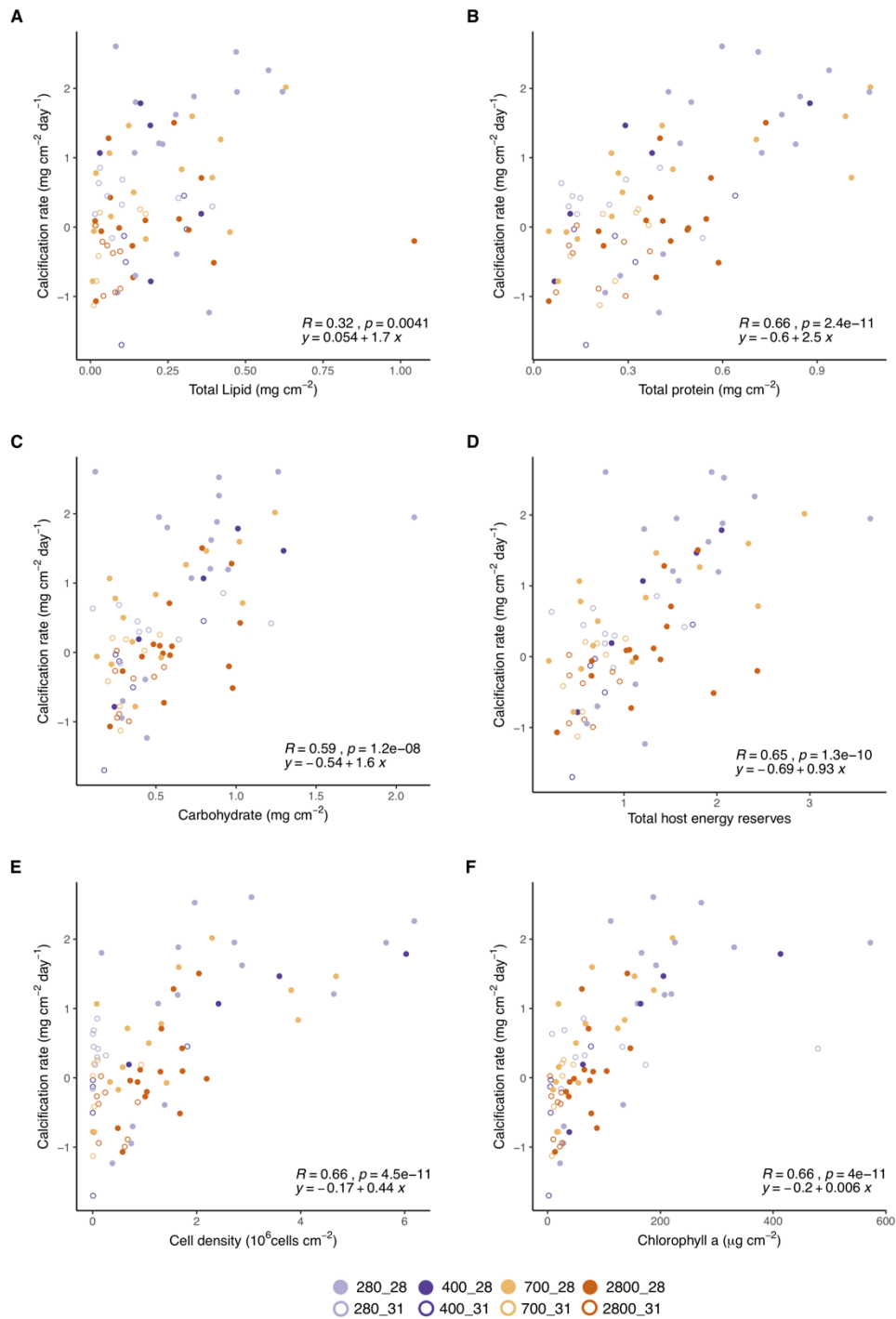


Figure S3.7 Relationship between *P. strigosa* physiology and calcification rate.

Measured *P. strigosa* calcification rate (mg cm⁻² day⁻¹) plotted against (A) coral host lipid (mg cm⁻²), (B) coral host protein (mg cm⁻²), (B) coral host carbohydrate (mg cm⁻²), (D) coral host total energy reserves (mg cm⁻²), (E) algal endosymbiont cell density (10⁶ cells cm⁻²), and (F) algal endosymbiont chlorophyll a concentration (mg cm⁻²). Each plot contains the corresponding R², p-value, and regression equation fit to each parameter pair.

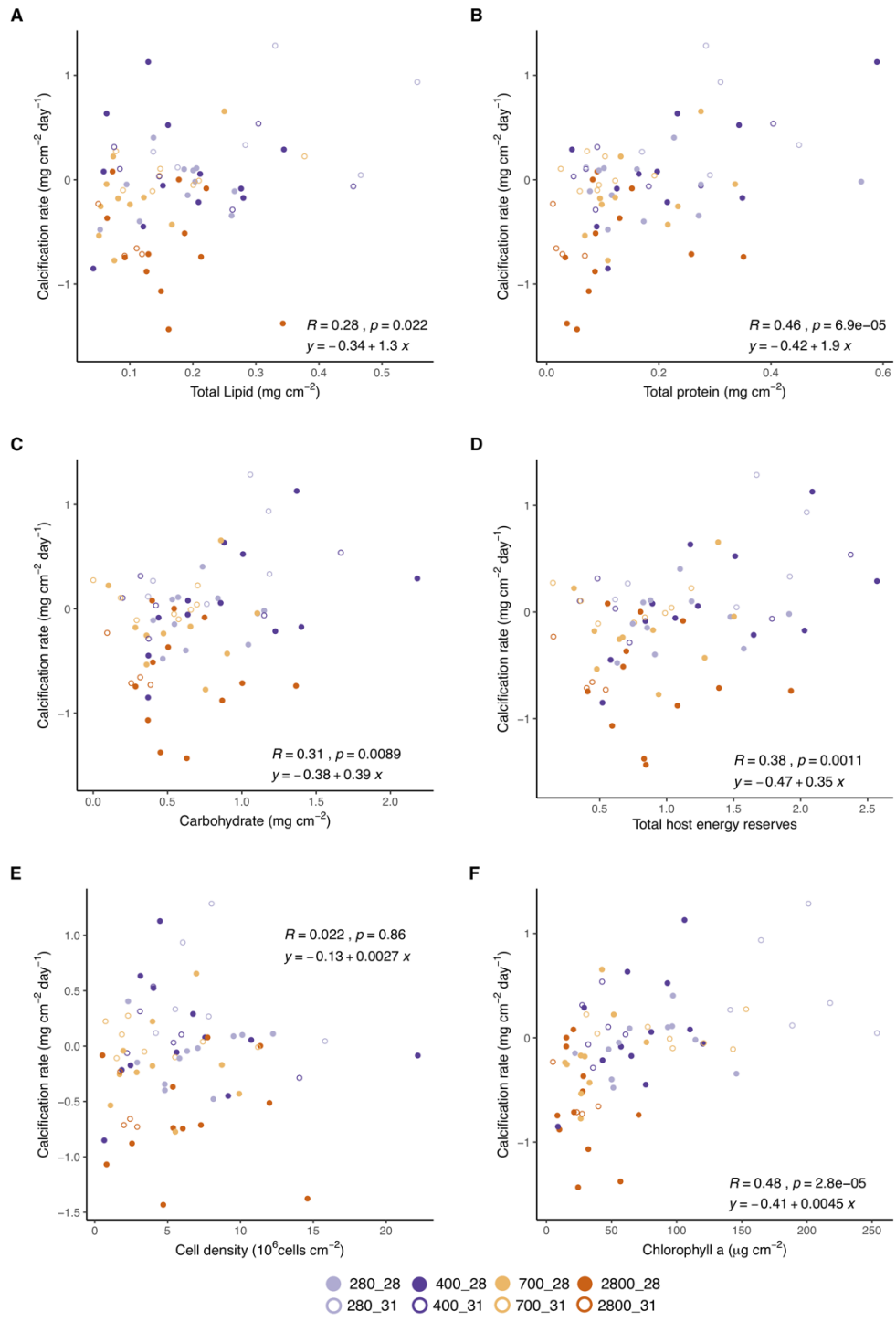
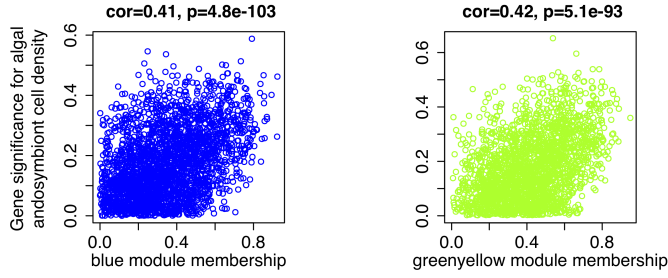


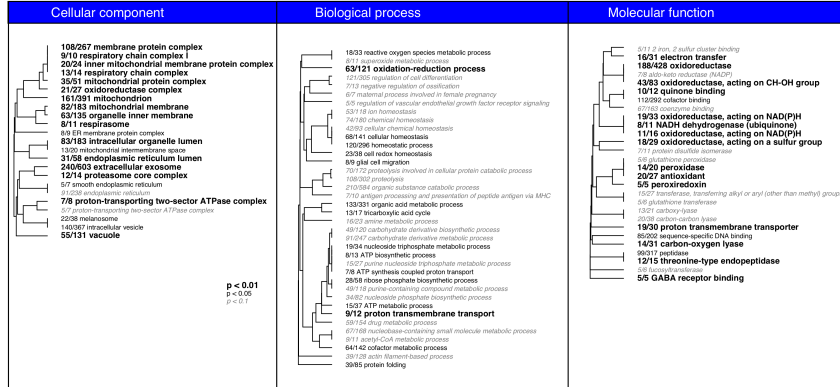
Figure S3.8 Relationship between *P. astreoides* physiology and calcification rate.

Measured *P. astreoides* calcification rate ($\text{mg cm}^{-2} \text{ day}^{-1}$) plotted against (A) coral host lipid (mg cm^{-2}), (B) coral host protein (mg cm^{-2}), (B) coral host carbohydrate (mg cm^{-2}), (D) coral host total energy reserves (mg cm^{-2}), (E) algal endosymbiont cell density ($10^6 \text{ cells cm}^{-2}$), and (F) algal endosymbiont chlorophyll a concentration ($\mu\text{g cm}^{-2}$). Each plot contains the corresponding R^2 , p-value, and regression equation fit to each parameter pair.

A



B



C

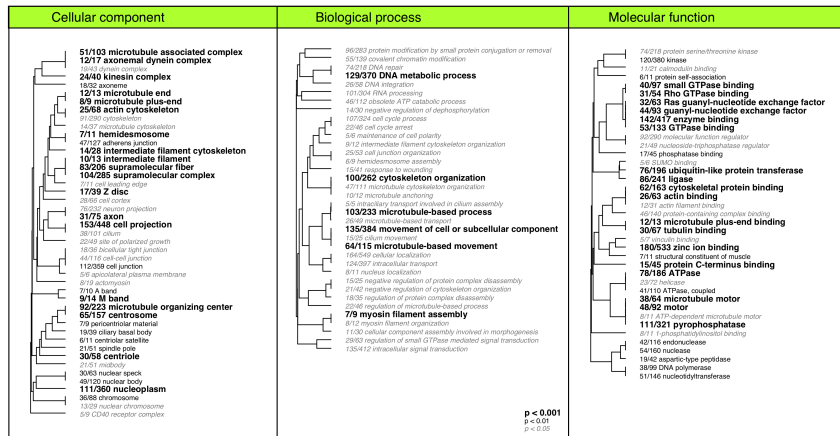
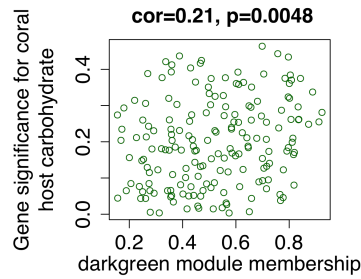


Figure S3.9 Expression modules correlated with algal endosymbiont cell density

Significantly correlated modules (“blue” and “green yellow”) with algal endosymbiont cell density values for *S. siderea*, with higher correlations indicating stronger associations between the module and cell density (A). Gene Ontology (GO) categories significantly enriched for the “blue” (B) and “green yellow” (C) modules by “cellular component” (CC), “biological process” (BP), and “molecular function” (MF). Significance (via Fisher’s exact test) of each identified pathway is denoted by text font. Each fraction denotes the number of genes within the corresponding module compared to the total number of genes within the GO category.

A



B

Cellular component	Biological process	Molecular function
<ul style="list-style-type: none"> 7/12 cytosolic small ribosomal subunit 11/24 small ribosomal subunit 11/12 cytosolic large ribosomal subunit 12/25 large ribosomal subunit 23/49 ribosomal subunit 23/195 ribonucleoprotein complex 23/61 ribosome 	<ul style="list-style-type: none"> 43/319 organonitrogen compound biosynthetic process 42/135 amide biosynthetic process 42/150 peptide metabolic process 42/112 peptide biosynthetic process 42/214 cellular amide metabolic process 	<ul style="list-style-type: none"> 43/186 structural molecule 41/86 structural constituent of ribosome 9/23 rRNA binding
<p>p < 0.001 F = 0.001 P < 0.002</p>		

Figure S3.10 Dark green module correlated with coral host carbohydrate

Significantly correlated “dark green” module with coral host algal endosymbiont concentration for *S. siderea*, with higher correlations indicating stronger associations between the module and carbohydrate content (A). Gene Ontology (GO) categories significantly enriched for the “dark green” (B) module by “cellular component” (CC), “biological process” (BP), and “molecular function” (MF). Significance (via Fisher’s exact test) of each identified pathway is denoted by text font. Each fraction denotes the number of genes within the corresponding module compared to the total number of genes within the GO category.

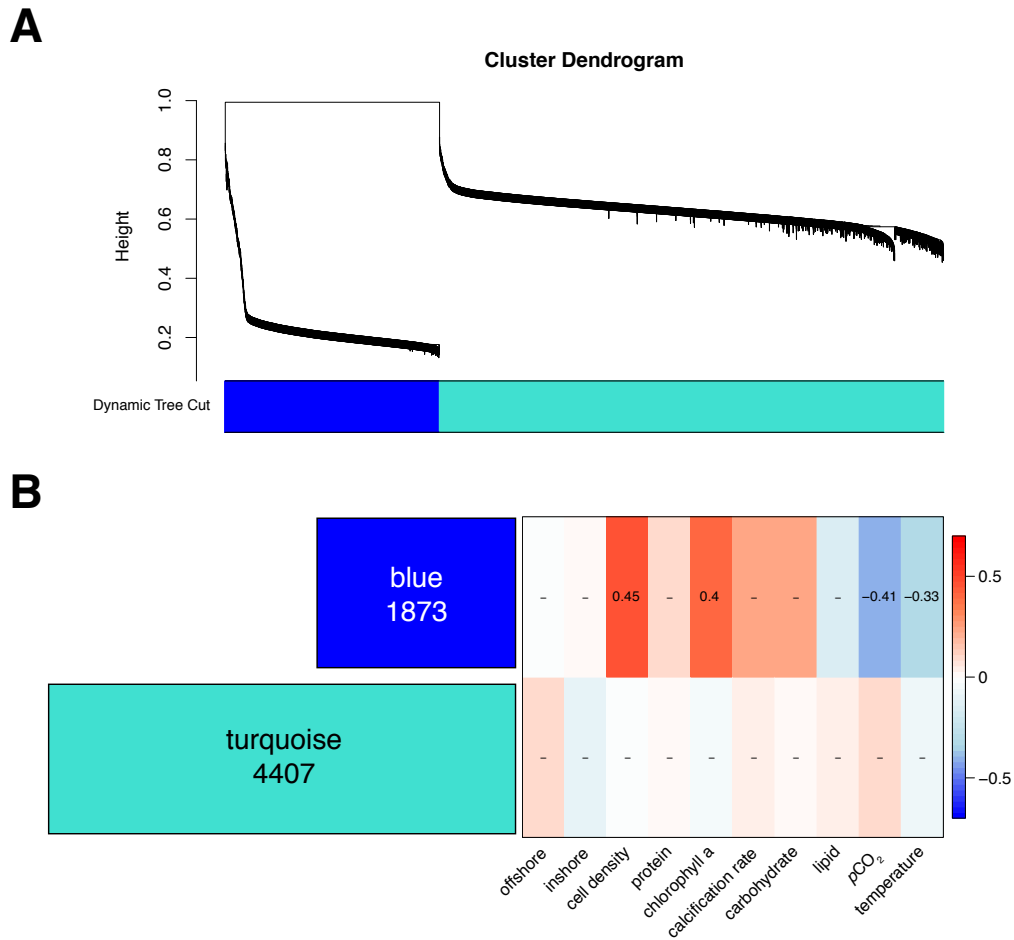


Figure S3.11 WGCNA analysis of *Siderastrea siderea* algal endosymbiont gene expression

Dendrogram of gene clustering based on similar expression patterns (B). Coloured bars in the top depict co-expression modules. Correlations between module eigengenes and treatment or physiological parameters (B). The bar graph (left) depicts the number of genes corresponding to each module. Significant modules are denoted by values for Pearson's correlation coefficients within each cell.

APPENDIX 4: SUPPLEMENTAL DESCRIPTIONS AND FIGURES – CHAPTER 4

Table S4.1 AIC model selection for corallite height. Summary of AIC and degrees of freedom (df) for all model combinations assessing corallite height. The model combination in bold is the final model used in this analysis.

Model	df	AIC
reef * $p\text{CO}_2$ * temperature	18	-25.44
reef + $p\text{CO}_2$ + temperature	8	-39.67
reef + $p\text{CO}_2$ * temperature	11	-35.76
reef * $p\text{CO}_2$ + temperature	11	-33.69
reef * temperature + $p\text{CO}_2$	9	-39.51
reef * ($p\text{CO}_2$ + temperature)	12	-33.53
$p\text{CO}_2$ * temperature	10	-37.2
$p\text{CO}_2$ + temperature	7	-41.08

Table S4.2 AIC model selection for corallite skeletal infilling. Summary of AIC and degrees of freedom (df) for all model combinations assessing corallite skeletal infilling. The model combination in bold is the final model used in this analysis.

Model	df	AIC
reef * $p\text{CO}_2$ * temperature	18	513.99
reef + $p\text{CO}_2$ * temperature	11	511.49
reef * $p\text{CO}_2$ + temperature	11	513.69
reef * ($p\text{CO}_2$ + temperature)	12	515.61
$p\text{CO}_2$ * temperature	10	509.73
$p\text{CO}_2$ + temperature	7	515.00

Table S4.3 AIC model selection for septal peak rugosity. Summary of AIC and degrees of freedom (df) for all model combinations assessing septal peak rugosity. The model combination in bold is the final model used in this analysis.

Model	df	AIC
septa * reef * $p\text{CO}_2$ * temperature	28	-823.77
septa * reef * $p\text{CO}_2$ + temperature	245	-642.98
septa * reef * temperature + $p\text{CO}_2$	137	-688.98
septa * reef * ($p\text{CO}_2$ + temperature)	304	-664.65

Table S4.4 AIC model selection for septal ridge rugosity. Summary of AIC and degrees of freedom (df) for all model combinations assessing septal ridge rugosity. The model combination in bold is the final model used in this analysis.

Model	df	AIC
septa + reef + $p\text{CO}_2$ + temperature	19	123.94
septa + reef + ($p\text{CO}_2$ * temperature)	22	110.85
septa * reef + ($p\text{CO}_2$ * temperature)	33	122.7
septa * reef * $p\text{CO}_2$ + temperature	83	164.27
septa * reef * temperature + $p\text{CO}_2$	49	158.94
septa * reef * ($p\text{CO}_2$ + temperature)	102	178.92
septa * $p\text{CO}_2$ * temperature	93	201.06
septa + $p\text{CO}_2$ + temperature	18	137.31
septa * $p\text{CO}_2$ + temperature	51	164.45
septa * temperature + $p\text{CO}_2$	29	152.99
septa * ($p\text{CO}_2$ + temperature)	62	178.06

Table S4.5 Model output of linear mixed effects model of corallite height by treatment $p\text{CO}_2$ and temperature. Summary output of the linear mixed effects model used to determine the relationship between corallite height, $p\text{CO}_2$ and temperature for *S. siderea*. Temperature and $p\text{CO}_2$ were treated as factors.

<i>Predictors</i>	<i>Estimates</i>	<i>CI</i>	<i>p</i>
(Intercept)	1.26	1.13 – 1.38	< 0.001
$p\text{CO}_2$ (669 μatm)	0.03	-0.07 – 0.13	0.542
$p\text{CO}_2$ (3297 μatm)	-0.08	-0.18 – 0.02	0.104
$p\text{CO}_2$ (426 μatm)	0	-0.10 – 0.10	0.971
Temperature (31 °C)	0.01	-0.06 – 0.07	0.838
<i>Random Effects</i>			
σ^2	0.02		
τ_{00} colony	0.03		
ICC	0.51		
N_{colony}	12		
Observations	86		
Marginal R^2 / Conditional R^2	0.036 / 0.529		

Table S4.6 Bootstrapped linear mixed effects model mean and 95% confidence interval for corallite height. Bootstrapped modelled mean corallite height for *S. siderea* in all $p\text{CO}_2$ and temperature treatments reported in mm. 95% confidence intervals (CI) are reported for each modelled mean (Figure 4.3A).

$p\text{CO}_2$	Temperature	Mean	Lower 95% CI	Upper 95% CI
299	28	1.25	1.18	1.33
299	31	1.26	1.18	1.34
3297	28	1.17	1.10	1.25
3297	31	1.18	1.11	1.25
426	31	1.26	1.18	1.33
426	28	1.25	1.18	1.33
669	28	1.29	1.21	1.36
669	31	1.29	1.22	1.37

Table S4.7 Model output of linear mixed effects model of corallite height by treatment $p\text{CO}_2$ and temperature. Summary output of the linear mixed effects model used to determine the relationship between corallite skeletal infilling, $p\text{CO}_2$ and temperature for *S. siderea*. Temperature and $p\text{CO}_2$ were treated as factors.

<i>Predictors</i>	<i>Estimates</i>	<i>CI</i>	<i>p</i>
(Intercept)	61.16	58.03 – 64.30	<0.001
$p\text{CO}_2$ (426 matm)	-9.32	-13.59 – -5.04	<0.001
$p\text{CO}_2$ (669 matm)	-0.08	-4.36 – 4.20	0.971
$p\text{CO}_2$ (3297 matm)	-15.83	-20.11 – -11.55	<0.001
Temperature (31 °C)	1.37	-3.28 – 6.02	0.564
$p\text{CO}_2$ (426 matm) : Temperature (31 °C)	6.06	-0.27 – 12.38	0.061
$p\text{CO}_2$ (669 matm) : Temperature (31 °C)	-2.75	-9.06 – 3.57	0.394
$p\text{CO}_2$ (3297 matm) : Temperature (31 °C)	-2.8	9.05 – 3.45	0.380
<i>Random Effects</i>			
σ^2	24.84		
τ_{00} colony	0.66		
ICC	0.03		
N_{colony}	12		
Observations	82		
Marginal R^2 / Conditional R^2	0.667 / 0.675		

Table S4.8 Bootstrapped linear mixed effects model mean and 95% confidence interval for corallite % skeletal infilling. Bootstrapped modelled mean corallite % skeletal infilling for *S. siderea* in all $p\text{CO}_2$ and temperature treatments. 95% confidence intervals (CI) are reported for each modelled mean (Figure 4.3B).

$p\text{CO}_2$	Temperature	Mean	Lower 95% CI	Upper 95% CI
299	28	61.08	57.99	64.11
299	31	62.54	59.16	66.10
426	28	51.81	48.77	54.76
426	31	59.25	56.25	62.42
669	28	61.09	58.12	63.92
669	31	59.72	56.54	62.93
3297	28	45.33	42.37	48.22
3297	31	43.88	40.90	46.85

Table S4.9 Model output of linear mixed effects model of septal peak rugosity by treatment $p\text{CO}_2$ and temperature. Summary output of the linear mixed effects model used to determine the relationship between septal peak rugosity, $p\text{CO}_2$, temperature, and reef environment for *S. siderea*. Temperature and $p\text{CO}_2$ were treated as factors.

<i>Predictors</i>	<i>Estimates</i>	<i>CI</i>	<i>p</i>
(Intercept)	1.17	1.05 – 1.29	< 0.001
$p\text{CO}_2$ (669 μatm)	-0.15	-0.21 – -0.08	< 0.001
param2F_peak: Inshore : $p\text{CO}_2$ (3297 μatm)	0.12	-0.01 – 0.24	0.067
$p\text{CO}_2$ (426 μatm)	0.01	-0.19 – 0.20	0.952
4 th peak : Temperature (31 °C)	0	-0.15 – 0.15	0.986
$p\text{CO}_2$ (426 μatm): Temperature (31 °C)	0.3	-0.02 – 0.63	0.069
4 th peak : Inshore	-0.06	-0.15 – 0.04	0.247
$p\text{CO}_2$ (669 μatm) : Temperature (31 °C)	0.1	0.02 – 0.19	0.021
$p\text{CO}_2$ (3297 μatm)	0.05	-0.01 – 0.11	0.119
4 th peak : $p\text{CO}_2$ (3297 μatm) : Temperature (31 °C)	-0.05	-0.17 – 0.07	0.45
Inshore : $p\text{CO}_2$ (426 μatm)	-0.15	-0.36 – 0.05	0.142
4 th peak	0.07	-0.00 – 0.14	0.059
Inshore	0.19	-0.01 – 0.38	0.067
4 th peak : $p\text{CO}_2$ (3297 μatm)	-0.04	-0.13 – 0.05	0.379
Inshore : $p\text{CO}_2$ (3297 μatm)	-0.15	-0.36 – 0.05	0.134
4 th peak : $p\text{CO}_2$ (669 μatm)	0.03	-0.06 – 0.12	0.483
Temperature (31 °C)	-0.15	-0.36 – 0.06	0.167
4 th peak : Inshore : $p\text{CO}_2$ (426 μatm) : Temperature (31 °C)	0.08	-0.10 – 0.25	0.403
4 th peak : Inshore : $p\text{CO}_2$ (426 μatm)	0.02	-0.11 – 0.14	0.786
Inshore : Temperature (31 °C)	0.08	-0.12 – 0.28	0.431
4 th peak : Inshore : Temperature (31 °C)	-0.01	-0.13 – 0.12	0.919
$p\text{CO}_2$ (3297 μatm) : Temperature (31 °C)	0.12	0.04 – 0.21	0.005
4 th peak: $p\text{CO}_2$ (426 μatm) : Temperature (31 °C)	-0.07	-0.25 – 0.11	0.436
4 th peak : $p\text{CO}_2$ (426 μatm)	-0.02	-0.11 – 0.07	0.676
Inshore : $p\text{CO}_2$ (426 μatm) : Temperature (31 °C)	-0.16	-0.39 – 0.06	0.144
4 th peak : $p\text{CO}_2$ (669 μatm) : Temperature (31 °C)	-0.03	-0.16 – 0.09	0.615
<i>Random Effects</i>			
σ^2	0.01		
τ_{00} colony	0.01		
ICC	0.42		
N_{colony}	4		
Observations	437		
Marginal R^2 / Conditional R^2	0.177 / 0.525		

Table S4.10 Bootstrapped linear mixed effects model mean and 95% confidence interval for septal peak rugosity. Bootstrapped modelled mean septal peak rugosity for *S. siderea* in all $p\text{CO}_2$ and temperature treatments. 95% confidence intervals (CI) are reported for each modelled mean (Figure 4.5). Inshore values are represented by “I” and offshore values are represented by “O.”

$p\text{CO}_2$	Temperature	Reef environment	Mean	Lower 95% CI	Upper 95% CI
299	28	O	1.18	1.12	1.24
299	28	I	1.36	1.32	1.41
299	31	I	1.30	1.26	1.34
3297	28	I	1.25	1.20	1.30
3297	28	O	1.22	1.19	1.25
3297	31	O	1.19	1.15	1.25
3297	31	I	1.30	1.25	1.36
426	31	I	1.28	1.22	1.33
426	31	O	1.33	1.27	1.39
426	28	I	1.21	1.17	1.25
426	28	O	1.18	1.14	1.22
669	28	I	1.21	1.17	1.26
669	31	I	1.26	1.21	1.30

Table S4.11 Model output of linear mixed effects model of septal ridge rugosity by treatment $p\text{CO}_2$ and temperature. Summary output of the linear mixed effects model used to determine the relationship between septal ridge rugosity, $p\text{CO}_2$, temperature, and reef environment for *S. siderea*. Temperature and $p\text{CO}_2$ were treated as factors.

<i>Predictors</i>	<i>Estimates</i>	<i>CI</i>	<i>p</i>
(Intercept)	1.79	1.18 – 2.39	<0.001
$p\text{CO}_2$ (669 μatm)	-0.51	-0.91 – -0.11	0.014
param2F_peak: Inshore : $p\text{CO}_2$ (3297 μatm)	-0.09	-0.90 – 0.71	0.824
$p\text{CO}_2$ (426 μatm)	0.58	-0.37 – 1.53	0.229
1 st peak : Temperature (31 °C)	0.2	-0.76 – 1.16	0.685
$p\text{CO}_2$ (426 μatm): Temperature (31 °C)	-0.31	-1.89 – 1.27	0.699
1 st peak : Inshore	0.03	-0.58 – 0.63	0.93
$p\text{CO}_2$ (669 μatm) : Temperature (31 °C)	0.32	-0.22 – 0.87	0.247
$p\text{CO}_2$ (3297 μatm)	0.4	-0.01 – 0.81	0.054
1 st peak: $p\text{CO}_2$ (3297 μatm) : Temperature (31 °C)	0.14	-0.62 – 0.89	0.724
Inshore : $p\text{CO}_2$ (426 μatm)	-0.48	-1.50 – -0.55	0.363
1 st peak	-0.06	-0.51 – 0.39	0.787
Inshore	0.6	-0.36 – 1.55	0.221
1 st peak: $p\text{CO}_2$ (3297 μatm)	-0.13	-0.72 – 0.46	0.665
Inshore : $p\text{CO}_2$ (3297 μatm)	0.05	-0.95 – 1.04	0.928
1 st peak: $p\text{CO}_2$ (669 μatm)	0.16	-0.42 – 0.73	0.593
Temperature (31 °C)	0.26	-0.80 – 1.32	0.631
1 st peak : Inshore : $p\text{CO}_2$ (426 μatm) : Temperature (31°C)	-0.01	-1.14 – 1.11	0.982
1 st peak: Inshore : $p\text{CO}_2$ (426 μatm)	0.29	-0.52 – 1.09	0.489
Inshore : Temperature (31 °C)	-0.17	-1.15 – 0.82	0.737
1 st peak : Inshore : Temperature (31 °C)	-0.44	-1.23 – 0.35	0.273
$p\text{CO}_2$ (3297 μatm) : Temperature (31 °C)	-0.46	-1.00 – 0.07	0.089
1 st peak : $p\text{CO}_2$ (426 μatm) : Temperature (31 °C)	0	-1.13 – 1.12	0.995
1 st peak : $p\text{CO}_2$ (426 μatm)	-0.26	-0.84 – 0.32	0.38
Inshore : $p\text{CO}_2$ (426 μatm) : Temperature (31 °C)	0.26	-0.87 – 1.39	0.655
1 st peak : $p\text{CO}_2$ (669 μatm) : Temperature (31 °C)	0.3	-0.47 – 1.08	0.446
<i>Random Effects</i>			
σ^2	0.11		
τ_{00} colony	0.12		
ICC	0.53		
N colony	4		
Observations	143		
Marginal R^2 / Conditional R^2	0.216/0.634		

Table S4.12 Bootstrapped linear mixed effects model mean and 95% confidence interval for septal ridge rugosity. Bootstrapped modelled mean septal ridge rugosity for *S. siderea* in all $p\text{CO}_2$ and temperature treatments. 95% confidence intervals (CI) are reported for each modelled mean (Figure 4.5). Inshore values are represented by “I” and offshore values are represented by “O.”

$p\text{CO}_2$	Temperature	Reef environment	Mean	Lower 95% CI	Upper 95% CI
299	28	O	2.17	1.91	2.42
299	28	I	2.46	2.21	2.70
299	31	I	2.16	1.90	2.43
3297	28	O	2.36	2.14	2.59
3297	28	I	2.65	2.38	2.94
3297	31	I	2.39	2.11	2.67
3297	31	O	1.93	1.70	2.17
426	31	O	2.02	1.75	2.29
426	31	I	2.31	2.03	2.64
426	28	I	2.41	2.19	2.64
426	28	O	2.04	1.79	2.29
669	28	I	1.87	1.59	2.15
669	31	I	2.24	1.95	2.52

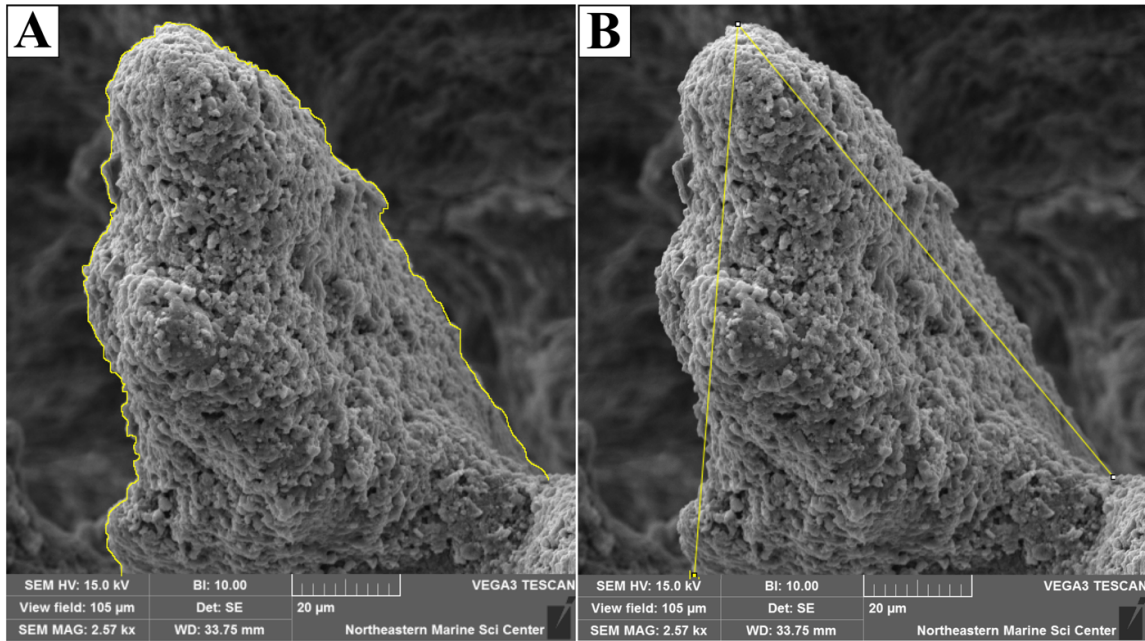


Figure S4.1 Corallite peak rugosity measurement

Example images of how septal peak rugosity was assessed. The peak outline was traced in IMAGEJ (A) and then divided by the length of the peak as quantified from the base to the top and back down (B).

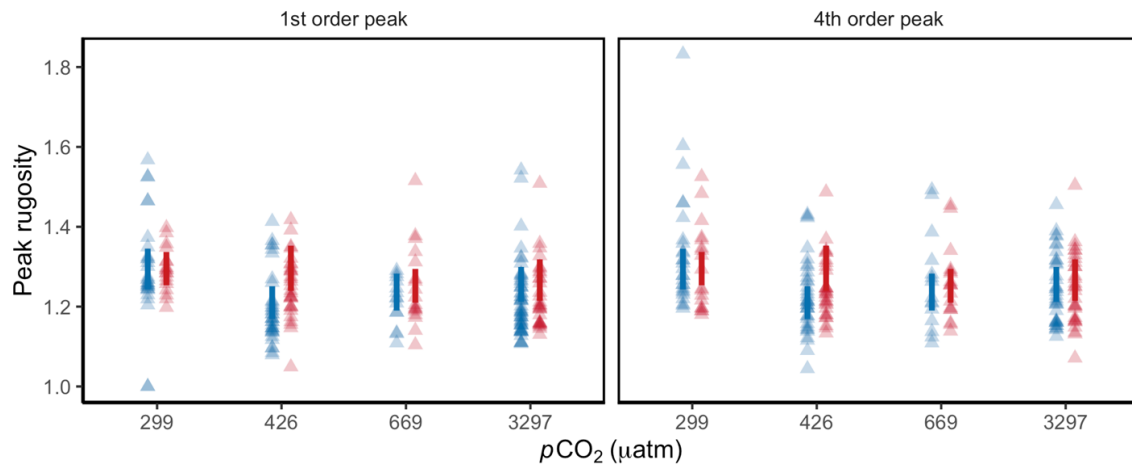


Figure S4.2 Septal peak rugosity without reef environment effects

Response of peak rugosity to temperature and $p\text{CO}_2$ treatment combined by treatment. Blue triangles represent values for fragments in the 28°C treatments and red triangles represent values for fragments in the 31°C treatments. Blue and red vertical bars represent modelled 95% confidence intervals for each $p\text{CO}_2$ treatment at 28°C and 31°C, respectively.

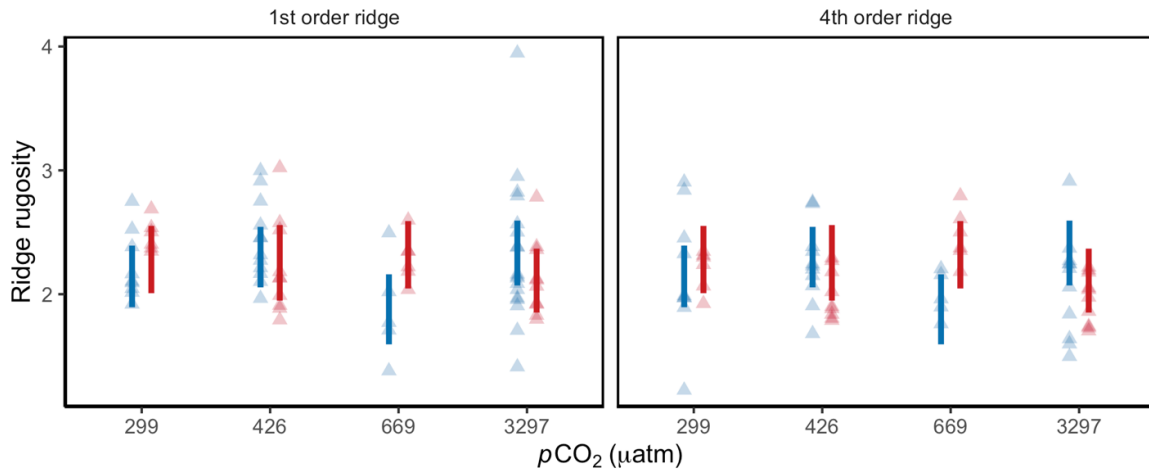


Figure S4.3 Septal ridge rugosity without reef environment effects

Response of ridge rugosity to temperature and $p\text{CO}_2$ treatment combined by treatment. Blue triangles represent values for fragments in the 28°C treatments and red triangles represent values for fragments in the 31°C treatments. Blue and red vertical bars represent modelled 95% confidence intervals for each $p\text{CO}_2$ treatment at 28°C and 31°C, respectively.

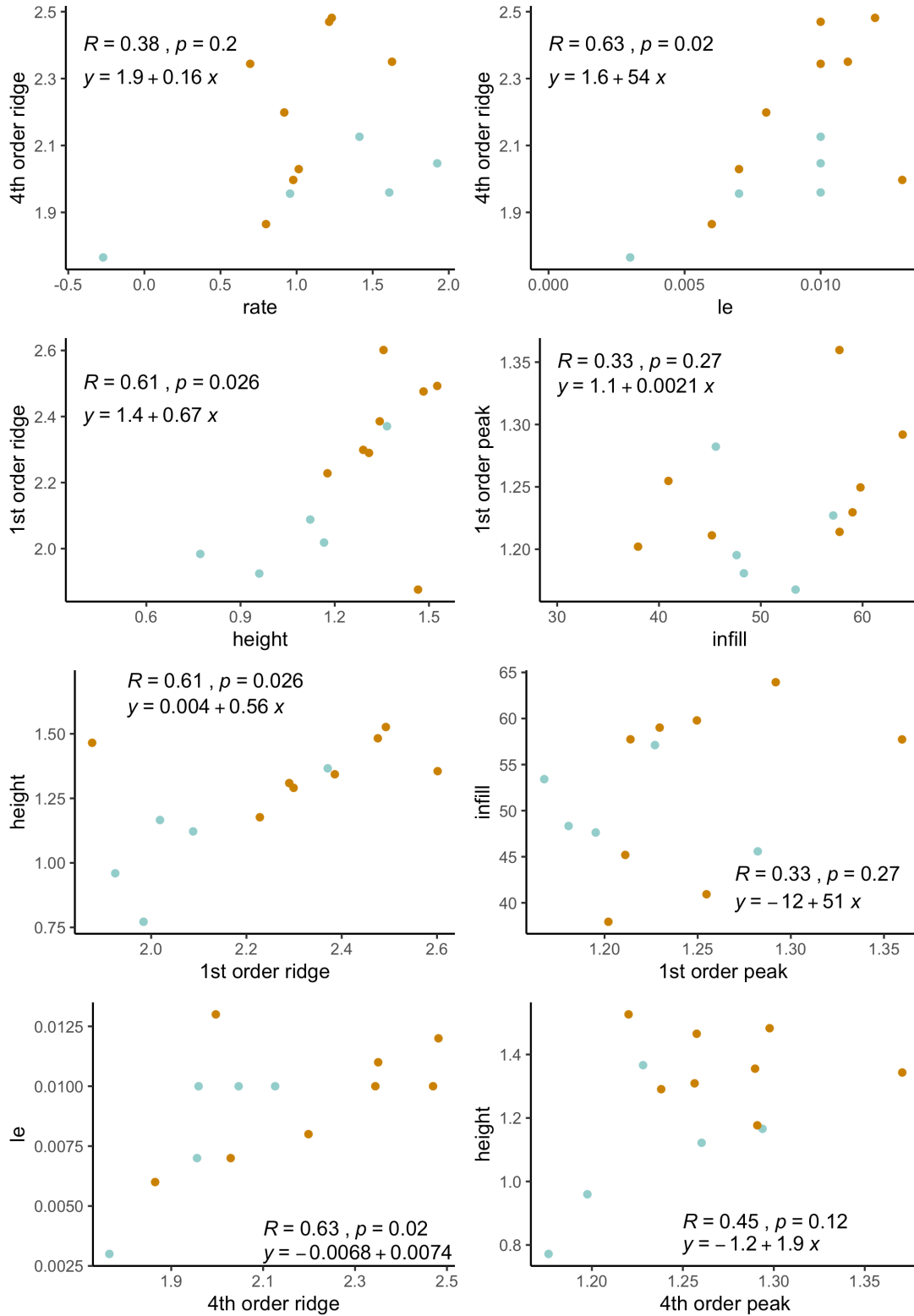


Figure S4.4 Pairwise regressions of morphological features

Preliminary assessment of pairwise comparisons between skeletal morphology and growth parameters with R^2 , p-value, and regression equations for the best comparisons as determined through AIC model selection on linear models.

REFERENCES

- Agostini, S., H. Fujimura, T. Higuchi, I. Yuyama, B. E. Casareto, Y. Suzuki, and Y. Nakano. 2013. The effects of thermal and high-CO₂ stresses on the metabolism and surrounding microenvironment of the coral *Galaxea fascicularis*. *Comptes Rendus Biologies* **336**:384-391.
- Al-Horani, F. A., S. M. Al-Moghrabi, and D. de Beer. 2003. The mechanism of calcification and its relation to photosynthesis and respiration in the scleractinian coral *Galaxea fascicularis*. *Marine Biology* **142**:419-426.
- Albright, R., L. Caldeira, J. Hoffelt, L. Kwiatkowski, J. K. Maclaren, B. M. Mason, Y. Nebuchina, A. Ninokawa, J. Pongratz, K. L. Ricke, T. Rivlin, K. Schneider, M. Sesboue, K. Shamberger, J. Silverman, K. Wolfe, K. Zhu, and K. Caldeira. 2016. Reversal of ocean acidification enhances net coral reef calcification. *Nature* **531**:362-365.
- Albright, R., and C. Langdon. 2011. Ocean acidification impacts multiple early life history processes of the Caribbean coral *Porites astreoides*. *Global Change Biology* **17**:2478-2487.
- Albright, R., Y. Takeshita, D. A. Koweek, A. Ninokawa, K. Wolfe, T. Rivlin, Y. Nebuchina, J. Young, and K. Caldeira. 2018. Carbon dioxide addition to coral reef waters suppresses net community calcification. *Nature* **555**:516-+.
- Alemu, J. I., and Y. Clement. 2014. Mass Coral Bleaching in 2010 in the Southern Caribbean. *PLoS One* **9**.
- Allemand, D., C. Ferrier-Pages, P. Furla, F. Houlbrequé, S. Puvrel, S. Reynaud, E. Tambutte, S. Tambutte, and D. Zoccola. 2004. Biomineralisation in reef-building corals: from molecular mechanisms to environmental control. *Comptes Rendus Palevol* **3**:453-467.
- Allemand, D., É. Tambutté, D. Zoccola, and S. Tambutté. 2010. Coral calcification, cells to reefs. Springer, Dordrecht, Netherlands.
- Alvarez-Filip, L., N. K. Dulvy, J. A. Gill, I. M. Cote, and A. R. Watkinson. 2009. Flattening of Caribbean coral reefs: region-wide declines in architectural complexity. *Proceedings of the Royal Society B-Biological Sciences* **276**:3019-3025.
- Anthony, K. R. N., S. R. Connolly, and O. Hoegh-Guldberg. 2007. Bleaching, energetics, and coral mortality risk: Effects of temperature, light, and sediment regime. *Limnology and Oceanography* **52**:716-726.
- Anthony, K. R. N., and K. E. Fabricius. 2000. Shifting roles of heterotrophy and autotrophy in coral energetics under varying turbidity. *Journal of Experimental Marine Biology and Ecology* **252**:221-253.

- Anthony, K. R. N., D. I. Kline, G. Diaz-Pulido, S. Dove, and O. Hoegh-Guldberg. 2008. Ocean acidification causes bleaching and productivity loss in coral reef builders. *Proceedings of the National Academy of Sciences of the United States of America* **105**:17442-17446.
- Arnott, S. A., S. Chiba, and D. O. Conover. 2006. Evolution of intrinsic growth rate: Metabolic costs drive trade-offs between growth and swimming performance in *Menidia menidia*. *Evolution* **60**:1269-1278.
- Aronson, R. B., I. G. Macintyre, W. F. Precht, T. J. T. Murdoch, and C. M. Wapnick. 2002. The expanding scale of species turnover events on coral reefs in Belize. *Ecological Monographs* **72**:233-249.
- Aronson, R. B., W. F. Precht, I. G. Macintyre, and T. J. T. Murdoch. 2000. Coral bleach-out in Belize. *Nature* **405**:36.
- Atkinson, M. J., and C. Bingman. 1997. Elemental composition of commercial seasalts. *Journal of Aquariculture and Aquatic Sciences* **8**:39-43.
- Bahr, K. D., K. S. Rodgers, and P. L. Jokiel. 2018. Ocean warming drives decline in coral metabolism while acidification highlights species-specific responses. *Marine Biology Research* **14**:924-935.
- Baird, A. H., R. Bhagooli, P. J. Ralph, and S. Takahashi. 2009. Coral bleaching: the role of the host. *Trends in Ecology & Evolution* **24**:16-20.
- Barnes, D. J., and J. M. Lough. 1993. On the nature and causes of density banding in massive coral skeletons. *Journal of Experimental Marine Biology and Ecology* **167**:91-108.
- Barott, K. L., A. A. Venn, S. O. Perez, S. Tambutte, and M. Tresguerres. 2015. Coral host cells acidify symbiotic algal microenvironment to promote photosynthesis. *Proceedings of the National Academy of Sciences of the United States of America* **112**:607-612.
- Barshis, D. J., J. T. Ladner, T. A. Oliver, F. O. Seneca, N. Traylor-Knowles, and S. R. Palumbi. 2013. Genomic basis for coral resilience to climate change. *Proceedings of the National Academy of Sciences of the United States of America* **110**:1387-1392.
- Bassim, K. M., and P. W. Sammarco. 2003. Effects of temperature and ammonium on larval development and survivorship in a scleractinian coral (*Diploria strigosa*). *Marine Biology* **142**:241-252.
- Bates, D., M. Machler, B. M. Bolker, and S. C. Walker. 2015a. Fitting Linear Mixed-Effects Models Using lme4. *Journal of Statistical Software* **67**:1-48.
- Bates, D., M. Maechler, B. Bolker, and S. Walker. 2015b. Fitting Linear Mixed-Effects Models Using lme4. *Journal of Statistical Software* **67**:1-48.

- Baumann, J. H., J. E. Townsend, T. A. Courtney, H. E. Aichelman, S. W. Davies, F. P. Lima, and K. D. Castillo. 2016. Temperature Regimes Impact Coral Assemblages along Environmental Gradients on Lagoonal Reefs in Belize. *PLoS One* **11**.
- Bedwell-Ivers, H. E., M. S. Koch, K. E. Peach, L. Joles, E. Dutra, and C. Manfrino. 2017. The role of hospite zooxanthellae photophysiology and reef chemistry on elevated pCO₂ effects in two branching Caribbean corals: *Acropora cervicornis* and *Porites divaricata*. *ICES Journal of Marine Science* **74**:1103-1112.
- Benjamini, Y., and Y. Hochberg. 1995. Controlling the false discovery rate: a practical and powerful approach to multiple testing. *Journal of the Royal Statistical Society: Series B* **57**:289–300.
- Bove, C., J. Ries, S. Davies, I. Westfield, J. Umbanhowar, and K. Castillo. 2019. Common Caribbean corals exhibit highly variable responses to future acidification and warming. *Proceedings of the Royal Society B-Biological Sciences* **286**:1-9.
- Bove, C. B., J. Umbanhowar, and K. D. Castillo. 2020. Meta-Analysis Reveals Reduced Coral Calcification Under Projected Ocean Warming but Not Under Acidification Across the Caribbean Sea. *Frontiers in Marine Science* **7**.
- Brown, B. E. 1997. Coral bleaching: causes and consequences. *Coral Reefs* **16**:S129-S138.
- Brown, D., and P. J. Edmunds. 2016. Differences in the responses of three scleractinians and the hydrocoral *Millepora platyphylla* to ocean acidification. *Marine Biology* **163**.
- Brown, N. E. M., J. R. Bernhardt, K. M. Anderson, and C. D. G. Harley. 2018. Increased food supply mitigates ocean acidification effects on calcification but exacerbates effects on growth. *Scientific Reports* **8**:1-9.
- Bürkner, P.-C. 2017. brms: An R Package for Bayesian Multilevel Models Using Stan. *Journal of Statistical Software* **80**:1-28.
- Burrows, M. T., D. S. Schoeman, L. B. Buckley, P. Moore, E. S. Poloczanska, K. M. Brander, C. Brown, J. F. Bruno, C. M. Duarte, B. S. Halpern, J. Holding, C. V. Kappel, W. Kiessling, M. I. O'Connor, J. M. Pandolfi, C. Parmesan, F. B. Schwing, W. J. Sydeman, and A. J. Richardson. 2011. The Pace of Shifting Climate in Marine and Terrestrial Ecosystems. *Science* **334**:652-655.
- Burrows, M. T., D. S. Schoeman, A. J. Richardson, J. G. Molinos, A. Hoffmann, L. B. Buckley, P. J. Moore, C. J. Brown, J. F. Bruno, C. M. Duarte, B. S. Halpern, O. Hoegh-Guldberg, C. V. Kappel, W. Kiessling, M. I. O'Connor, J. M. Pandolfi, C. Parmesan, W. Sydeman, S. Ferrier, K. J. Williams, and E. S. Poloczanska. 2014. Geographical limits to species-range shifts are suggested by climate velocity. *Nature* **507**:492-+.
- Cai, W. J., Y. Ma, B. M. Hopkinson, A. G. Grottoli, M. E. Warner, Q. Ding, X. Hu, X. Yuan, V. Schoepf, H. Xu, C. Han, T. F. Melman, K. D. Hoadley, D. T. Pettay, Y. Matsui, J. H. Baumann, S. Levas, Y. Ying, and Y. Wang. 2016. Microelectrode characterization

- of coral daytime interior pH and carbonate chemistry. *Nature Communications* **7**:11144.
- Cantin, N. E., A. L. Cohen, K. B. Karnauskas, A. M. Tarrant, and D. C. McCorkle. 2010. Ocean Warming Slows Coral Growth in the Central Red Sea. *Science* **329**:322-325.
- Carricart-Ganivet, J. P., N. Cabanillas-Teran, I. Cruz-Ortega, and P. Blanchon. 2012. Sensitivity of Calcification to Thermal Stress Varies among Genera of Massive Reef-Building Corals. *PLoS One* **7**.
- Caruso, N. M., M. W. Sears, D. C. Adams, and K. R. Lips. 2014. Widespread rapid reductions in body size of adult salamanders in response to climate change. *Global Change Biology* **20**:1751-1759.
- Castillo, K. D., and F. P. Lima. 2010. Comparison of in situ and satellite-derived (MODIS-Aqua/Terra) methods for assessing temperatures on coral reefs. *Limnology and Oceanography-Methods* **8**:107-117.
- Castillo, K. D., J. B. Ries, J. F. Bruno, and I. T. Westfield. 2014. The reef-building coral *Siderastrea siderea* exhibits parabolic responses to ocean acidification and warming. *Proceedings of the Royal Society B-Biological Sciences* **281**.
- Castillo, K. D., J. B. Ries, and J. M. Weiss. 2011. Declining Coral Skeletal Extension for Forereef Colonies of *Siderastrea siderea* on the Mesoamerican Barrier Reef System, Southern Belize. *PLoS One* **6**.
- Castillo, K. D., J. B. Ries, J. M. Weiss, and F. P. Lima. 2012. Decline of forereef corals in response to recent warming linked to history of thermal exposure. *Nature Climate Change* **2**:756-760.
- Chan, N. C. S., and S. R. Connolly. 2013. Sensitivity of coral calcification to ocean acidification: a meta-analysis. *Global Change Biology* **19**:282-290.
- Chen, H. K., L. H. Wang, W. N. U. Chen, A. B. Mayfield, O. Levy, C. S. Lin, and C. S. Chen. 2017. Coral lipid bodies as the relay center interconnecting diel-dependent lipidomic changes in different cellular compartments. *Scientific Reports* **7**.
- Cheng, Y. S., Y. Zheng, and J. S. VanderGheynst. 2011. Rapid Quantitative Analysis of Lipids Using a Colorimetric Method in a Microplate Format. *Lipids* **46**:95-103.
- Chou, W. C., P. J. Liu, Y. H. Chen, and W. J. Huang. 2020. Contrasting Changes in Diel Variations of Net Community Calcification Support That Carbonate Dissolution Can Be More Sensitive to Ocean Acidification Than Coral Calcification. *Frontiers in Marine Science* **7**.
- Chua, C. M., W. Leggat, A. Moya, and A. H. Baird. 2013. Temperature affects the early life history stages of corals more than near future ocean acidification. *Marine Ecology Progress Series* **475**:85-92.

- Cohen, A. L., and M. Holcomb. 2009. Why Corals Care About Ocean Acidification: Uncovering the Mechanism. *Oceanography* **22**:118-127.
- Cohen, A. L., and T. A. McConnaughey. 2003. Geochemical perspectives on coral mineralization. *Biom mineralization* **54**:151-187.
- Coles, S. L., and B. E. Brown. 2003. Coral bleaching - Capacity for acclimatization and adaptation. *Advances in Marine Biology*, Vol 46 **46**:183-223.
- Comeau, S., R. C. Carpenter, and P. J. Edmunds. 2013a. Coral reef calcifiers buffer their response to ocean acidification using both bicarbonate and carbonate. *Proceedings of the Royal Society B-Biological Sciences* **280**.
- Comeau, S., C. E. Cornwall, and M. T. McCulloch. 2017. Decoupling between the response of coral calcifying fluid pH and calcification to ocean acidification. *Scientific Reports* **7**.
- Comeau, S., P. J. Edmunds, N. B. Spindel, and R. C. Carpenter. 2013b. The responses of eight coral reef calcifiers to increasing partial pressure of CO₂ do not exhibit a tipping point. *Limnology and Oceanography* **58**:388-398.
- Comeau, S., P. J. Edmunds, N. B. Spindel, and R. C. Carpenter. 2014. Fast coral reef calcifiers are more sensitive to ocean acidification in short-term laboratory incubations. *Limnology and Oceanography* **59**:1081-1091.
- Conover, D. O., and E. T. Schultz. 1995. Phenotypic similarity and the evolutionary significance of countergradient variation. *Trends in Ecology & Evolution* **10**:248-252.
- Cornwall, C. E., and C. L. Hurd. 2016. Experimental design in ocean acidification research: problems and solutions. *ICES Journal of Marine Science: Journal du Conseil* **73**:572-581.
- Costanza, R., R. de Groot, P. Sutton, S. van der Ploeg, S. J. Anderson, I. Kubiszewski, S. Farber, and R. K. Turner. 2014. Changes in the global value of ecosystem services. *Global Environmental Change-Human and Policy Dimensions* **26**:152-158.
- Crain, C. M., K. Kroeker, and B. S. Halpern. 2008. Interactive and cumulative effects of multiple human stressors in marine systems. *Ecology Letters* **11**:1304-1315.
- Crawley, A., D. I. Kline, S. Dunn, K. Anthony, and S. Dove. 2010. The effect of ocean acidification on symbiont photorespiration and productivity in *Acropora formosa*. *Global Change Biology* **16**:851-863.
- Crook, E. D., A. L. Cohen, M. Rebolledo-Vieyra, L. Hernandez, and A. Paytan. 2013. Reduced calcification and lack of acclimatization by coral colonies growing in areas of persistent natural acidification. *Proceedings of the National Academy of Sciences of the United States of America* **110**:11044-11049.

- D'Angelo, C., and J. Wiedenmann. 2014. Impacts of nutrient enrichment on coral reefs: new perspectives and implications for coastal management and reef survival. *Current Opinion in Environmental Sustainability* **7**:82-93.
- Daly, R. 1915. The glacial-control theory of coral reefs. *Proceedings of the American Academy of Arts and Sciences* **51**:155-251.
- Darling, E. S., L. Alvarez-Filip, T. A. Oliver, T. R. McClanahan, and I. M. Cote. 2012. Evaluating life-history strategies of reef corals from species traits. *Ecology Letters* **15**:1378-1386.
- Davies, P. S. 1989. Short-term growth measurements of corals using an accurate buoyant weighing technique. *Marine Biology* **101**:389-395.
- Davies, S. W., A. Marchetti, J. B. Ries, and K. D. Castillo. 2016. Thermal and pCO₂ Stress Elicit Divergent Transcriptomic Responses in a Resilient Coral. *Frontiers in Marine Science* **3**.
- Davies, S. W., J. B. Ries, A. Marchetti, and K. D. Castillo. 2018. Symbiodinium Functional Diversity in the Coral *Siderastrea siderea* Is Influenced by Thermal Stress and Reef Environment, but Not Ocean Acidification. *Frontiers in Marine Science* **5**.
- De'ath, G., J. M. Lough, and K. E. Fabricius. 2009. Declining Coral Calcification on the Great Barrier Reef. *Science* **323**:116-119.
- DeCarlo, T. M., A. L. Cohen, G. T. F. Wong, K. A. Davis, P. Lohmann, and K. Soong. 2017. Mass coral mortality under local amplification of 2 degrees C ocean warming. *Scientific Reports* **7**.
- DeCarlo, T. M., S. Comeau, C. E. Cornwall, and M. T. McCulloch. 2018. Coral resistance to ocean acidification linked to increased calcium at the site of calcification. *Proceedings of the Royal Society B-Biological Sciences* **285**.
- DeCarlo, T. M., C. L. Ross, and M. T. McCulloch. 2019. Diurnal cycles of coral calcifying fluid aragonite saturation state. *Marine Biology* **166**.
- Doney, S. C., V. J. Fabry, R. A. Feely, and J. A. Kleypas. 2009. Ocean Acidification: The Other CO₂ Problem. *Annual Review of Marine Science* **1**:169-192.
- Drury, C. 2019. Resilience in reef-building corals: The ecological and evolutionary importance of the host response to thermal stress. *Molecular Ecology*.
- Eakin, C. M., J. A. Morgan, S. F. Heron, T. B. Smith, G. Liu, L. Alvarez-Filip, B. Baca, E. Bartels, C. Bastidas, C. Bouchon, M. Brandt, A. W. Bruckner, L. Bunkley-Williams, A. Cameron, B. D. Causey, M. Chiappone, T. R. L. Christensen, M. J. C. Crabbe, O. Day, E. de la Guardia, G. Diaz-Pulido, D. DiResta, D. L. Gil-Agudelo, D. S. Gilliam, R. N. Ginsburg, S. Gore, H. M. Guzman, J. C. Hendee, E. A. Hernandez-Delgado, E. Husain, C. F. G. Jeffrey, R. J. Jones, E. Jordan-Dahlgren, L. S. Kaufman, D. I. Kline,

- P. A. Kramer, J. C. Lang, D. Lirman, J. Mallela, C. Manfrino, J. P. Marechal, K. Marks, J. Mihaly, W. J. Miller, E. M. Mueller, E. M. Muller, C. A. O. Toro, H. A. Oxenford, D. Ponce-Taylor, N. Quinn, K. B. Ritchie, S. Rodriguez, A. R. Ramirez, S. Romano, J. F. Samhuri, J. A. Sanchez, G. P. Schmahl, B. V. Shank, W. J. Skirving, S. C. C. Steiner, E. Villamizar, S. M. Walsh, C. Walter, E. Weil, E. H. Williams, K. W. Roberson, and Y. Yusuf. 2010. Caribbean Corals in Crisis: Record Thermal Stress, Bleaching, and Mortality in 2005. *PLoS One* **5**.
- Edmunds, P. J. 2011. Zooplanktivory ameliorates the effects of ocean acidification on the reef coral *Porites* spp. *Limnology and Oceanography* **56**:2402-2410.
- Edmunds, P. J. 2012. Effect of pCO₂ on the growth, respiration, and photophysiology of massive *Porites* spp. in Moorea, French Polynesia. *Marine Biology* **159**:2149-2160.
- Edmunds, P. J., D. Brown, and V. Moriarty. 2012. Interactive effects of ocean acidification and temperature on two scleractinian corals from Moorea, French Polynesia. *Global Change Biology* **18**:2173-2183.
- Elizalde-Rendon, E. M., G. Horta-Puga, P. Gonzalez-Diaz, and J. P. Carricart-Ganivet. 2010. Growth characteristics of the reef-building coral *Porites astreoides* under different environmental conditions in the Western Atlantic. *Coral Reefs* **29**:607-614.
- Enochs, I. C., D. P. Manzello, R. Carlton, S. Schopmeyer, R. van Hooidek, and D. Lirman. 2014. Effects of light and elevated pCO₂ on the growth and photochemical efficiency of *Acropora cervicornis*. *Coral Reefs* **33**:477-485.
- Enochs, I. C., D. P. Manzello, G. Kolodziej, S. H. C. Noonan, L. Valentino, and K. E. Fabricius. 2016. Enhanced macroboring and depressed calcification drive net dissolution at high-CO₂ coral reefs. *Proceedings of the Royal Society B-Biological Sciences* **283**.
- Feder, M. E., and G. E. Hofmann. 1999. Heat-shock proteins, molecular chaperones, and the stress response: Evolutionary and ecological physiology. *Annual Review of Physiology* **61**:243-282.
- Fitt, W. K., F. K. McFarland, M. E. Warner, and G. C. Chilcoat. 2000. Seasonal patterns of tissue biomass and densities of symbiotic dinoflagellates in reef corals and relation to coral bleaching. *Limnology and Oceanography* **45**:677-685.
- Fitt, W. K., H. J. Spero, J. Halas, M. W. White, and J. W. Porter. 1993. Recovery of the coral *Montastrea annularis* in the Florida Feys after the 1987 Caribbean bleaching event. *Coral Reefs* **12**:57-64.
- Fitter, A. H., and R. S. R. Fitter. 2002. Rapid changes in flowering time in British plants. *Science* **296**:1689-1691.
- Folch, J., M. Lees, and G. Sloane-Stanley. 1956. A simple method for isolation and purification of total lipids from animal tissue. *Journal of Biological Chemistry* **226**:497-509.

- Foster, A. B. 1979. Phenotypic plasticity in the reef corals *Montastraea-annularis* (Ellis and Solander) and *Siderastrea-siderea* (Ellis and Solander). *Journal of Experimental Marine Biology and Ecology* **39**:25-54.
- Foster, A. B. 1980. Environmental variation in skeletal morphology within the Caribbean reef corals *Montastraea annularis* and *Siderastrea siderea*. *Bulletin of Marine Science* **30**:678-709.
- Foster, T., J. L. Falter, M. T. McCulloch, and P. L. Clode. 2016. Ocean acidification causes structural deformities in juvenile coral skeletons. *Science Advances* **2**.
- Gattuso, J. P., O. Hoegh-Guldberg, and H. O. Pörtner. 2014. Cross-chapter box on coral reefs. Cambridge University Press, Cambridge, United Kingdom and New York, NY, USA.
- GIMP Development Team. 2019. GIMP.
- Glynn, P. W. 1991. Coral-reef bleaching in the 1980s and possible connections with global warming. *Trends in Ecology & Evolution* **6**:175-179.
- Glynn, P. W. 1996. Coral reef bleaching: Facts, hypotheses and implications. *Global Change Biology* **2**:495-509.
- Granados-Cifuentes, C., A. J. Bellantuono, T. Ridgway, O. Hoegh-Guldberg, and M. Rodriguez-Lanetty. 2013. High natural gene expression variation in the reef-building coral *Acropora millepora*: potential for acclimative and adaptive plasticity. *Bmc Genomics* **14**.
- Green, D. H., P. J. Edmunds, and R. C. Carpenter. 2008. Increasing relative abundance of *Porites astreoides* on Caribbean reefs mediated by an overall decline in coral cover. *Marine Ecology Progress Series* **359**:1-10.
- Gregoire, V., F. Schmacka, M. A. Coffroth, and U. Karsten. 2017. Photophysiological and thermal tolerance of various genotypes of the coral endosymbiont *Symbiodinium* sp (Dinophyceae). *Journal of Applied Phycology* **29**:1893-1905.
- Greve, P., L. Gudmundsson, and S. I. Seneviratne. 2018. Regional scaling of annual mean precipitation and water availability with global temperature change. *Earth System Dynamics* **9**:227-240.
- Grottoli, A. G., L. J. Rodrigues, and C. Juarez. 2004. Lipids and stable carbon isotopes in two species of Hawaiian corals, *Porites compressa* and *Montipora verrucosa*, following a bleaching event. *Marine Biology* **145**:621-631.
- Grottoli, A. G., L. J. Rodrigues, and J. E. Palardy. 2006. Heterotrophic plasticity and resilience in bleached corals. *Nature* **440**:1186-1189.

- Grottoli, A. G., M. E. Warner, S. J. Levas, M. D. Aschaffenburg, V. Schoepf, M. McGinley, J. Baumann, and Y. Matsui. 2014. The cumulative impact of annual coral bleaching can turn some coral species winners into losers. *Global Change Biology* **20**:3823-3833.
- Guest, J. R., A. H. Baird, J. A. Maynard, E. Muttaqin, A. J. Edwards, S. J. Campbell, K. Yewdall, Y. A. Affendi, and L. M. Chou. 2012. Contrasting Patterns of Coral Bleaching Susceptibility in 2010 Suggest an Adaptive Response to Thermal Stress. *PLoS One* **7**.
- Gunderson, A. R., and J. H. Stillman. 2015. Plasticity in thermal tolerance has limited potential to buffer ectotherms from global warming. *Proc Biol Sci* **282**:20150401.
- Gurevitch, J., and L. V. Hedges. 1999. Statistical issues in ecological meta-analyses. *Ecology* **80**:1142-1149.
- Halpern, B. S., K. A. Selkoe, F. Micheli, and C. V. Kappel. 2007. Evaluating and ranking the vulnerability of global marine ecosystems to anthropogenic threats. *Conservation Biology* **21**:1301-1315.
- Harvey, B. P., D. Gwynn-Jones, and P. J. Moore. 2013. Meta-analysis reveals complex marine biological responses to the interactive effects of ocean acidification and warming. *Ecology and Evolution* **3**:1016-1030.
- Hii, Y.-S., A. M. A. Bolong, T.-T. Yang, and H.-C. Liew. 2009. Effect of Elevated Carbon Dioxide on Two Scleractinian Corals: *Porites cylindrica* (Dana, 1846) and *Galaxea fascicularis* (Linnaeus, 1767). *Journal of Marine Biology*:1-7.
- Hoadley, K. D., A. M. Lewis, D. C. Wham, D. T. Pettay, C. Grasso, R. Smith, D. W. Kemp, T. C. LaJeunesse, and M. E. Warner. 2019. Host-symbiont combinations dictate the photo-physiological response of reef-building corals to thermal stress. *Scientific Reports* **9**.
- Hoegh-Guldberg, O., and J. F. Bruno. 2010. The Impact of Climate Change on the World's Marine Ecosystems. *Science* **328**:1523-1528.
- Hoegh-Guldberg, O., D. Jacob, M. Taylor, M. Bindi, S. Brown, I. Camilloni, A. Diedhiou, R. Djalante, K. Ebi, F. Engelbrecht, J. Guiot, Y. Hijioka, S. Mehrotra, A. Payne, S. Seneviratne, A. Thomas, R. Warren, and G. Zhou. 2018. Global Warming of 1.5°C. An IPCC Special Report on the impacts of global warming of 1.5°C above pre-industrial levels and related global greenhouse gas emission pathways, in the context of strengthening the global response to the threat of climate change, sustainable development, and efforts to eradicate poverty World Meteorological Organization, Geneva.
- Hoegh-Guldberg, O., D. Jacob, M. Taylor, T. G. Bolanos, M. Bindi, S. Brown, I. A. Camilloni, A. Diedhiou, R. Djalante, K. Ebi, F. Engelbrecht, J. Guiot, Y. Hijioka, S. Mehrotra, C. W. Hope, A. J. Payne, H. O. Portner, S. I. Seneviratne, A. Thomas, R. Warren, and G. Zhou. 2019. The human imperative of stabilizing global climate change at 1.5 degrees C. *Science* **365**:1263-+.

- Hoegh-Guldberg, O., P. J. Mumby, A. J. Hooten, R. S. Steneck, P. Greenfield, E. Gomez, C. D. Harvell, P. F. Sale, A. J. Edwards, K. Caldeira, N. Knowlton, C. M. Eakin, R. Iglesias-Prieto, N. Muthiga, R. H. Bradbury, A. Dubi, and M. E. Hatziolos. 2007. Coral reefs under rapid climate change and ocean acidification. *Science* **318**:1737-1742.
- Holcomb, M., A. L. Cohen, R. I. Gabbitov, and J. L. Hutter. 2009. Compositional and morphological features of aragonite precipitated experimentally from seawater and biogenically by corals. *Geochimica et Cosmochimica Acta* **73**:4166-4179.
- Holcomb, M., A. A. Venn, E. Tambutte, S. Tambutte, D. Allemand, J. Trotter, and M. McCulloch. 2014. Coral calcifying fluid pH dictates response to ocean acidification. *Scientific Reports* **4**.
- Honisch, B., A. Ridgwell, D. Schmidt, E. Thomas, S. Gibbs, A. Sluijs, R. Zeebe, L. Kump, R. Martindale, S. Greene, W. Kiessling, J. Ries, J. Zachos, D. Royer, S. Barker, T. Marchitto, R. Moyer, C. Pelejero, P. Ziveri, G. Foster, and B. Williams. 2012. The Geological Record of Ocean Acidification. *Science* **335**:1058-1063.
- Horvath, K. M., K. D. Castillo, P. Armstrong, I. T. Westfield, T. Courtney, and J. B. Ries. 2016. Next-century ocean acidification and warming both reduce calcification rate, but only acidification alters skeletal morphology of reef-building coral *Siderastrea siderea*. *Sci Rep* **6**:29613.
- Hughes, T. P., A. H. Baird, D. R. Bellwood, M. Card, S. R. Connolly, C. Folke, R. Grosberg, O. Hoegh-Guldberg, J. B. C. Jackson, J. Kleypas, J. M. Lough, P. Marshall, M. Nystrom, S. R. Palumbi, J. M. Pandolfi, B. Rosen, and J. Roughgarden. 2003. Climate change, human impacts, and the resilience of coral reefs. *Science* **301**:929-933.
- Hughes, T. P., M. L. Barnes, D. R. Bellwood, J. E. Cinner, G. S. Cumming, J. B. C. Jackson, J. Kleypas, I. A. van de Leemput, J. M. Lough, T. H. Morrison, S. R. Palumbi, E. H. van Nes, and M. Scheffer. 2017a. Coral reefs in the Anthropocene. *Nature* **546**:82-90.
- Hughes, T. P., J. T. Kerry, M. Alvarez-Noriega, J. G. Alvarez-Romero, K. D. Anderson, A. H. Baird, R. C. Babcock, M. Beger, D. R. Bellwood, R. Berkelmans, T. C. Bridge, I. R. Butler, M. Byrne, N. E. Cantin, S. Comeau, S. R. Connolly, G. S. Cumming, S. J. Dalton, G. Diaz-Pulido, C. M. Eakin, W. F. Figueira, J. P. Gilmour, H. B. Harrison, S. F. Heron, A. S. Hoey, J. P. A. Hobbs, M. O. Hoogenboom, E. V. Kennedy, C. Y. Kuo, J. M. Lough, R. J. Lowe, G. Liu, M. T. M. Cculloch, H. A. Malcolm, M. J. McWilliam, J. M. Pandolfi, R. J. Pears, M. S. Pratchett, V. Schoepf, T. Simpson, W. J. Skirving, B. Sommer, G. Torda, D. R. Wachenfeld, B. L. Willis, and S. K. Wilson. 2017b. Global warming and recurrent mass bleaching of corals. *Nature* **543**:373-+.
- Hughes, T. P., J. T. Kerry, A. H. Baird, S. R. Connolly, A. Dietzel, C. M. Eakin, S. F. Heron, A. S. Hoey, M. O. Hoogenboom, G. Liu, M. J. McWilliam, R. J. Pears, M. S. Pratchett, W. J. Skirving, J. S. Stella, and G. Torda. 2018. Global warming transforms coral reef assemblages. *Nature* **556**:492-+.

- Hyde, K. J. W., J. E. O'Reilly, and C. A. Oviatt. 2007. Validation of SeaWiFS chlorophyll a in Massachusetts Bay. *Continental Shelf Research* **27**:1677-1691.
- IPCC. 2014. *Climate Change 2014: Synthesis Report. Contribution of Working Groups I, II and III to the Fifth Assessment Report of the Intergovernmental Panel on Climate Change*. Geneva, Switzerland.
- IPCC. 2019. *Technical Summary*.
- Jokiel, P. L., and S. L. Coles. 1977. Effects of temperature on mortality and growth of Hawaiian reef corals. *Marine Biology* **43**:201-208.
- Jones, R. J. 1997. Changes in zooxanthellar densities and chlorophyll concentrations in corals during and after a bleaching event. *Marine Ecology Progress Series* **158**:51-59.
- Jury, C. P., R. F. Whitehead, and A. M. Szmant. 2010. Effects of variations in carbonate chemistry on the calcification rates of *Madracis auretenra* (= *Madracis mirabilis* sensu Wells, 1973): bicarbonate concentrations best predict calcification rates. *Global Change Biology* **16**:1632-1644.
- Kaniewska, P., P. R. Campbell, D. I. Kline, M. Rodriguez-Lanetty, D. J. Miller, S. Dove, and O. Hoegh-Guldberg. 2012. Major Cellular and Physiological Impacts of Ocean Acidification on a Reef Building Coral. *PLoS One* **7**.
- Kelley, A. L., and J. J. Lunden. 2017. Meta-analysis identifies metabolic sensitivities to ocean acidification *Aims Environmental Science* **4**:709-729.
- Kenkel, C. D., A. T. Almanza, and M. V. Matz. 2015. Fine-scale environmental specialization of reef-building corals might be limiting reef recovery in the Florida Keys. *Ecology* **96**:3197-3212.
- Kenkel, C. D., G. Goodbody-Gringley, D. Caillaud, S. W. Davies, E. Bartels, and M. V. Matz. 2013a. Evidence for a host role in thermotolerance divergence between populations of the mustard hill coral (*Porites astreoides*) from different reef environments. *Molecular Ecology* **22**:4335-4348.
- Kenkel, C. D., E. Meyer, and M. V. Matz. 2013b. Gene expression under chronic heat stress in populations of the mustard hill coral (*Porites astreoides*) from different thermal environments. *Molecular Ecology* **22**:4322-4334.
- Kleypas, J. A., J. W. McManus, and L. A. B. Menez. 1999. Environmental limits to coral reef development: Where do we draw the line? *American Zoologist* **39**:146-159.
- Knowlton, N. 2001. The future of coral reefs. *Proceedings of the National Academy of Sciences of the United States of America* **98**:5419-5425.
- Kornder, N. A., B. M. Riegl, and J. Figueiredo. 2018. Thresholds and drivers of coral calcification responses to climate change. *Global Change Biology* **24**:5084-5095.

- Krief, S., E. J. Hendy, M. Fine, R. Yam, A. Meibom, G. L. Foster, and A. Shemesh. 2010. Physiological and isotopic responses of scleractinian corals to ocean acidification. *Geochimica et Cosmochimica Acta* **74**:4988-5001.
- Kroeker, K. J., R. L. Kordas, R. Crim, I. E. Hendriks, L. Ramajo, G. S. Singh, C. M. Duarte, and J. P. Gattuso. 2013. Impacts of ocean acidification on marine organisms: quantifying sensitivities and interaction with warming. *Global Change Biology* **19**:1884-1896.
- Kroeker, K. J., R. L. Kordas, R. N. Crim, and G. G. Singh. 2010. Meta-analysis reveals negative yet variable effects of ocean acidification on marine organisms. *Ecology Letters* **13**:1419-1434.
- LaJeunesse, T. C. 2002. Diversity and community structure of symbiotic dinoflagellates from Caribbean coral reefs. *Marine Biology* **141**:387-400.
- LaJeunesse, T. C., J. E. Parkinson, P. W. Gabrielson, H. J. Jeong, J. D. Reimer, C. R. Voolstra, and S. R. Santos. 2018. Systematic Revision of Symbiodiniaceae Highlights the Antiquity and Diversity of Coral Endosymbionts. *Current Biology*:2570-2580.
- Langdon, C., and M. J. Atkinson. 2005. Effect of elevated pCO₂ on photosynthesis and calcification of corals and interactions with seasonal change in temperature/irradiance and nutrient enrichment. *Journal of Geophysical Research-Oceans* **110**:16.
- Langfelder, P., and S. Horvath. 2008. WGCNA: an R package for weighted correlation network analysis. *BMC Bioinformatics* **9**.
- Leggat, W., F. Seneca, K. Wasmund, L. Ukani, D. Yellowlees, and T. D. Ainsworth. 2011. Differential Responses of the Coral Host and Their Algal Symbiont to Thermal Stress. *PLoS One* **6**.
- Leong, W., and J. R. Pawlik. 2010. Evidence of a resource trade-off between growth and chemical defenses among Caribbean coral reef sponges. *Marine Ecology Progress Series* **406**:71-78.
- Lesser, M. P. 1997. Oxidative stress causes coral bleaching during exposure to elevated temperatures. *Coral Reefs* **16**:187-192.
- Lewis, J. B., and W. S. Price. 1975. Feeding mechanisms and feeding strategies of Atlantic reef corals. *Journal of Zoology* **176**:527-544.
- Lough, J. M., and D. J. Barnes. 2000. Environmental controls on growth of the massive coral *Porites*. *Journal of Experimental Marine Biology and Ecology* **245**:225-243.
- Love, M. I., W. Huber, and S. Anders. 2014. Moderated estimation of fold change and dispersion for RNA-seq data with DESeq2. *Genome Biology* **15**:550.

- Lugo-Fernandez, A., H. H. Roberts, and J. N. Suhayda. 1998. Wave transformations across a Caribbean fringing-barrier Coral Reef. *Continental Shelf Research* **18**:1099-1124.
- Manzello, D., R. Berkelmans, and J. Hendee. 2007. Coral bleaching indices and thresholds for the Florida Reef Tract, Bahamas, and St. Croix, US Virgin Islands. *Marine Pollution Bulletin* **54**:1923-1931.
- Manzello, D. P., I. C. Enochs, G. Kolodziej, and R. Carlton. 2015. Coral growth patterns of *Montastraea cavernosa* and *Porites astreoides* in the Florida Keys: The importance of thermal stress and inimical waters. *Journal of Experimental Marine Biology and Ecology* **471**:198-207.
- Manzello, D. P., I. C. Enochs, N. Melo, D. K. Gledhill, and E. M. Johns. 2012. Ocean Acidification Refugia of the Florida Reef Tract. *PLoS One* **7**.
- Maor-Landaw, K., S. Karako-Lampert, H. W. Ben-Asher, S. Goffredo, G. Falini, Z. Dubinsky, and O. Levy. 2014. Gene expression profiles during short-term heat stress in the red sea coral *Stylophora pistillata*. *Global Change Biology* **20**:3026-3035.
- Marshall, P. A., and A. H. Baird. 2000. Bleaching of corals on the Great Barrier Reef: differential susceptibilities among taxa. *Coral Reefs* **19**:155-163.
- Marubini, F., C. Ferrier-Pages, and J. P. Cuif. 2003. Suppression of skeletal growth in scleractinian corals by decreasing ambient carbonate-ion concentration: a cross-family comparison. *Proceedings of the Royal Society B-Biological Sciences* **270**:179-184.
- Mason, R. A. B. 2018. Decline in symbiont densities of tropical and subtropical scleractinian corals under ocean acidification. *Coral Reefs* **37**:945-953.
- Masuko, T., A. Minami, N. Iwasaki, T. Majima, S. I. Nishimura, and Y. C. Lee. 2005. Carbohydrate analysis by a phenol-sulfuric acid method in microplate format. *Analytical Biochemistry* **339**:69-72.
- Mauritsen, T., and R. Pincus. 2017. Committed warming inferred from observations. *Nature Climate Change*.
- Mayfield, A. B., Y. Y. Hsiao, T. Y. Fan, C. S. Chen, and R. D. Gates. 2010. Evaluating the temporal stability of stress-activated protein kinase and cytoskeleton gene expression in the Pacific reef corals *Pocillopora damicornis* and *Seriatopora hystrix*. *Journal of Experimental Marine Biology and Ecology* **395**:215-222.
- McCulloch, M., J. Falter, J. Trotter, and P. Montagna. 2012. Coral resilience to ocean acidification and global warming through pH up-regulation. *Nature Climate Change* **2**:623-633.
- Melendez, M., and J. Salisbury. 2017. Impacts of Ocean Acidification in the Coastal and Marine Environments of Caribbean Small Island Developing States (SIDS). *Caribbean Marine Climate Change Report Card: Science Review* 2017:31-30.

- Metcalf, N. B., and P. Monaghan. 2001. Compensation for a bad start: grow now, pay later? *Trends in Ecology & Evolution* **16**:254-260.
- Mollica, N. R., W. F. Guo, A. L. Cohen, K. F. Huang, G. L. Foster, H. K. Donald, and A. R. Solow. 2018. Ocean acidification affects coral growth by reducing skeletal density. *Proceedings of the National Academy of Sciences of the United States of America* **115**:1754-1759.
- Moya, A., L. Huisman, E. E. Ball, D. C. Hayward, L. C. Grasso, C. M. Chua, H. N. Woo, J. P. Gattuso, S. Foret, and D. J. Miller. 2012. Whole Transcriptome Analysis of the Coral *Acropora millepora* Reveals Complex Responses to CO₂-driven Acidification during the Initiation of Calcification. *Molecular Ecology* **21**:2440-2454.
- Mucci, A. 1983. The solubility of calcite and aragonite in seawater at various salinities, temperatures, and one atmosphere total pressure. *American Journal of Science* **283**:780-799.
- Muehllehner, N., and P. Edmunds. 2008. Effects of ocean acidification and increased temperature on skeletal growth of two scleractinian corals, *Pocillopora meandrina* and *Porites rus*. *Proceedings of the 11th International Coral Reef Symposium*.
- Muscatine, L., and E. Cernichiaro. 1969. Assimilation of photosynthetic products of zooxanthellae by a reef coral. *Biological Bulletin* **137**:506-+.
- Muscatine, L., L. R. McCloskey, and R. E. Marian. 1981. Estimating the daily contribution of carbon from zooxanthellae to coral animal respiration. *Limnology and Oceanography* **26**:601-611.
- Nagelkerken, I., and S. D. Connell. 2015. Global alteration of ocean ecosystem functioning due to increasing human CO₂ emissions. *Proceedings of the National Academy of Sciences of the United States of America* **112**:13272-13277.
- Neal, B. P., A. Khen, T. Treibitz, O. Beijbom, G. O'Connor, M. A. Coffroth, N. Knowlton, D. Kriegman, B. G. Mitchell, and D. I. Kline. 2017. Caribbean massive corals not recovering from repeated thermal stress events during 2005-2013. *Ecology and Evolution* **7**:1339-1353.
- Neves, E., F. Silveira, and R. Johnsson. 2016. Cnidaria, Scleractinia, Siderastreidae, *Siderastrea siderea* (Ellis and Solander, 1786): Hartt Expedition and the first record of a Caribbean siderastreid in tropical Southwestern Atlantic. *Check List* **6**:505-510.
- Norstrom, A. V., M. Nystrom, J. Lokrantz, and C. Folke. 2009. Alternative states on coral reefs: beyond coral-macroalgal phase shifts. *Marine Ecology Progress Series* **376**:295-306.
- Okazaki, R. R., E. K. Towle, R. van Hooidonk, C. Mor, R. N. Winter, A. M. Piggot, R. Cuning, A. C. Baker, J. S. Klaus, P. K. Swart, and C. Langdon. 2017. Species-specific

- responses to climate change and community composition determine future calcification rates of Florida Keys reefs. *Global Change Biology* **23**:1023-1035.
- Oliver, T. A., and S. R. Palumbi. 2011. Do fluctuating temperature environments elevate coral thermal tolerance? *Coral Reefs* **30**:429-440.
- Orr, J. C., V. J. Fabry, O. Aumont, L. Bopp, S. C. Doney, R. A. Feely, A. Gnanadesikan, N. Gruber, A. Ishida, F. Joos, R. M. Key, K. Lindsay, E. Maier-Reimer, R. Matear, P. Monfray, A. Mouchet, R. G. Najjar, G. K. Plattner, K. B. Rodgers, C. L. Sabine, J. L. Sarmiento, R. Schlitzer, R. D. Slater, I. J. Totterdell, M. F. Weirig, Y. Yamanaka, and A. Yool. 2005. Anthropogenic ocean acidification over the twenty-first century and its impact on calcifying organisms. *Nature* **437**:681-686.
- Pacifici, M., P. Visconti, S. H. M. Butchart, J. E. M. Watson, F. M. Cassola, and C. Rondinini. 2017. Species' traits influenced their response to recent climate change. *Nature Climate Change* **7**:205-+.
- Pandolfi, J. M., R. H. Bradbury, E. Sala, T. P. Hughes, K. A. Bjorndal, R. G. Cooke, D. McArdle, L. McClenachan, M. J. H. Newman, G. Paredes, R. R. Warner, and J. B. C. Jackson. 2003. Global trajectories of the long-term decline of coral reef ecosystems. *Science* **301**:955-958.
- Parsons, T., Y. Maita, and C. M. Lalli. 1984. *A Manual of Chemical & Biological Methods for Seawater Analysis*. First edition. Pergamon Press, Oxford; New York, NY.
- Pecl, G. T., M. B. Araujo, J. D. Bell, J. Blanchard, T. C. Bonebrake, I. C. Chen, T. D. Clark, R. K. Colwell, F. Danielsen, B. Evengard, L. Falconi, S. Ferrier, S. Frusher, R. A. Garcia, R. B. Griffis, A. J. Hobday, C. Janion-Scheepers, M. A. Jarzyna, S. Jennings, J. Lenoir, H. I. Linnertved, V. Y. Martin, P. C. McCormack, J. McDonald, N. J. Mitchell, T. Mustonen, J. M. Pandolfi, N. Pettorelli, E. Popova, S. A. Robinson, B. R. Scheffers, J. D. Shaw, C. J. B. Sorte, J. M. Strugnell, J. M. Sunday, M. N. Tuanmu, A. Verges, C. Villanueva, T. Wernberg, E. Wapstra, and S. E. Williams. 2017. Biodiversity redistribution under climate change: Impacts on ecosystems and human well-being. *Science* **355**:1389-+.
- Perry, C. T., G. N. Murphy, P. S. Kench, S. G. Smithers, E. N. Edinger, R. S. Steneck, and P. J. Mumby. 2013. Caribbean-wide decline in carbonate production threatens coral reef growth. *Nature Communications* **4**.
- Pierrot, D., E. Lewis, and D. Wallace. 2006. MS Excel Program Developed for CO₂ System Calculations. Carbon Dioxide Information Analysis Center, Oak Ridge National Laboratory. U.S Department of Energy, Oak Ridge, Tennessee, ORNL/CDIAC-105a.
- Portner, H. O., A. F. Bennett, F. Bozinovic, A. Clarke, M. A. Lardies, M. Lucassen, B. Pelster, F. Schiemer, and J. H. Stillman. 2006. Trade-offs in thermal adaptation: The need for a molecular to ecological integration. *Physiological and Biochemical Zoology* **79**:295-313.

- Prada, F., E. Caroselli, S. Mengoli, L. Brizi, P. Fantazzini, B. Capaccioni, L. Pasquini, K. E. Fabricius, Z. Dubinsky, G. Falini, and S. Goffredo. 2017. Ocean warming and acidification synergistically increase coral mortality. *Sci Rep* **7**:40842.
- Pratte, Z. A., and L. L. Richardson. 2014. Impacts of temperature increase and acidification on thickness of the surface mucopolysaccharide layer of the Caribbean coral *Diploria* spp. *Coral Reefs* **33**:487-496.
- Prezelin, B. 1987. Photosynthetic physiology of dinoflagellates. Pages 174–223 *in* T. FJR, editor. *The biology of dinoflagellates*. Blackwell Scientific Publishers, Oxford.
- Putnam, H. M., K. L. Barott, T. D. Ainsworth, and R. D. Gates. 2017. The Vulnerability and Resilience of Reef-Building Corals. *Current Biology* **27**:R528-R540.
- R Core Development Team. 2016. R: A language and environment for statistical computing. R Foundation for Statistical Computing, Vienna, Austria.
- Raftery, A. E., A. Zimmer, D. M. W. Frierson, R. Startz, and P. Liu. 2017. Less than 2 °C warming by 2100 unlikely. *Nature Climate Change*.
- Reynaud, S., N. Leclercq, S. Romaine-Lioud, C. Ferrier-Pages, J. Jaubert, and J. P. Gattuso. 2003. Interacting effects of CO₂ partial pressure and temperature on photosynthesis and calcification in a scleractinian coral. *Global Change Biology* **9**:1660-1668.
- Ries, J. B. 2011. A physicochemical framework for interpreting the biological calcification response to CO₂-induced ocean acidification. *Geochimica et Cosmochimica Acta* **75**:4053-4064.
- Ries, J. B., A. L. Cohen, and D. C. McCorkle. 2009. Marine calcifiers exhibit mixed responses to CO₂-induced ocean acidification. *Geology* **37**:1131-1134.
- Ries, J. B., A. L. Cohen, and D. C. McCorkle. 2010. A nonlinear calcification response to CO₂-induced ocean acidification by the coral *Oculina arbuscula*. *Coral Reefs* **29**:661-674.
- Ries, J. B., M. N. Ghazaleh, B. Connolly, I. Westfield, and K. D. Castillo. 2016. Impacts of seawater saturation state ($\Omega_A=0.4-4.6$) and temperature (10, 25 °C) on the dissolution kinetics of whole-shell biogenic carbonates. *Geochimica et Cosmochimica Acta* **192**:318-337.
- Rinkevich, B. 1996. Do reproduction and regeneration in damaged corals compete for energy allocation? *Marine Ecology Progress Series* **143**:297-302.
- Rippe, J. P., J. H. Baumann, D. N. De Leener, H. E. Aichelman, E. B. Friedlander, S. W. Davies, and K. D. Castillo. 2018. Corals sustain growth but not skeletal density across the Florida Keys Reef Tract despite ongoing warming. *Global Change Biology* **24**:205-5217.

- Rivest, E. B., M. W. Kelly, M. B. DeBiasse, and G. E. Hofmann. 2018. Host and Symbionts in *Pocillopora damicornis* Larvae Display Different Transcriptomic Responses to Ocean Acidification and Warming. *Frontiers in Marine Science* **5**.
- Robbart, M. L., P. Peckol, S. P. Scordilis, H. A. Curran, and J. Brown-Saracino. 2004. Population recovery and differential heat shock protein expression for the corals *Agaricia agaricites* and *A-tenuifolia* in Belize. *Marine Ecology Progress Series* **283**:151-160.
- Rodolfo-Metalpa, R., F. Houlbreque, E. Tambutte, F. Boisson, C. Baggini, F. P. Patti, R. Jeffree, M. Fine, A. Foggo, J. P. Gattuso, and J. M. Hall-Spencer. 2011. Coral and mollusc resistance to ocean acidification adversely affected by warming. *Nature Climate Change* **1**:308-312.
- Rodolfo-Metalpa, R., S. Martin, C. Ferrier-Pages, and J. P. Gattuso. 2010. Response of the temperate coral *Cladocora caespitosa* to mid- and long-term exposure to pCO₂ and temperature levels projected for the year 2100 AD. *Biogeosciences* **7**:289-300.
- Rodrigues, L. J., and A. G. Grottoli. 2007. Energy reserves and metabolism as indicators of coral recovery from bleaching. *Limnology and Oceanography* **52**:1874-1882.
- Roy, R. N., L. N. Roy, K. M. Vogel, C. Porter Moore, T. Pearson, C. E. Good, F. J. Millero, and D. M. Campbell. 1993. The dissociation-constants of carbonic-acid in seawater at salinities 5 to 45 and temperatures 0-degrees-C to 45-degrees-C. *Marine Chemistry* **44**:249-267.
- Sabine, C. L., R. A. Feely, N. Gruber, R. M. Key, K. Lee, J. L. Bullister, R. Wanninkhof, C. S. Wong, D. W. R. Wallace, B. Tilbrook, F. J. Millero, T. H. Peng, A. Kozyr, T. Ono, and A. F. Rios. 2004. The oceanic sink for anthropogenic CO₂. *Science* **305**:367-371.
- Scheufen, T., W. E. Kramer, R. Iglesias-Prieto, and S. Enriquez. 2017. Seasonal variation modulates coral sensibility to heat-stress and explains annual changes in coral productivity. *Scientific Reports* **7**.
- Schindelin, J., I. Arganda-Carreras, E. Frise, V. Kaynig, M. Longair, T. Pietzsch, S. Preibisch, C. Rueden, S. Saalfeld, B. Schmid, J.-Y. Tinevez, D. J. White, V. Hartenstein, K. Eliceiri, P. Tomancak, and A. Cardona. 2012. Fiji: an open-source platform for biological-image analysis. *Nature Methods* **9**:676-682.
- Schneider, K., and J. Erez. 2006. The effect of carbonate chemistry on calcification and photosynthesis in the hermatypic coral *Acropora eurystoma*. *Limnology and Oceanography* **51**:1284-1293.
- Schoepf, V., A. G. Grottoli, M. E. Warner, W. J. Cai, T. F. Melman, K. D. Hoadley, D. T. Pettay, X. Hu, Q. Li, H. Xu, Y. Wang, Y. Matsui, and J. H. Baumann. 2013. Coral energy reserves and calcification in a high-CO₂ world at two temperatures. *PLoS One* **8**:e75049.

- Schoepf, V., C. P. Jury, R. J. Toonen, and M. T. McCulloch. 2017. Coral calcification mechanisms facilitate adaptive responses to ocean acidification. *Proceedings of the Royal Society B-Biological Sciences* **284**.
- Schutte, V. G. W., E. R. Selig, and J. F. Bruno. 2010. Regional spatio-temporal trends in Caribbean coral reef benthic communities. *Marine Ecology Progress Series* **402**:115-122.
- Seemann, J., R. Carballo-Bolaños, K. L. Berry, C. T. González, C. Richter, and R. R. Leinfelder. 2012. Importance of heterotrophic adaptations of corals to maintain energy reserves. *Proceedings of the 12th International Coral Reef Symposium, Cairns, Australia*:9-13.
- Silbiger, N. J., G. Goodbody-Gringley, J. F. Bruno, and H. M. Putnam. 2019. Comparative thermal performance of the reef-building coral *Orbicella franksi* at its latitudinal range limits. *Marine Biology* **166**:1-14.
- Solomon, S., G. K. Plattner, R. Knutti, and P. Friedlingstein. 2009. Irreversible climate change due to carbon dioxide emissions. *Proceedings of the National Academy of Sciences of the United States of America* **106**:1704-1709.
- Somero, G. N. 2010. The physiology of climate change: how potentials for acclimatization and genetic adaptation will determine 'winners' and 'losers'. *J Exp Biol* **213**:912-920.
- Soto, I., S. Andrefouet, C. Hu, F. E. Muller-Karger, C. C. Wall, J. Sheng, and B. G. Hatcher. 2009. Physical connectivity in the Mesoamerican Barrier Reef System inferred from 9 years of ocean color observations. *Coral Reefs* **28**:415-425.
- Stocker, T. F., D. Qin, G.-K. Plattner, M. Tignor, S. K. Allen, J. Böschung, A. Natels, Y. Via, V. Bex, and P. M. Midgley. 2013. *Climate Change 2013: The Physical Science Basis. Contribution of Working Group I to the Fifth Assessment Report of the Intergovernmental Panel on Climate Change*. Cambridge University Press, Cambridge, United Kingdom and New York, New York, USA.
- Stoltenberg, L., K. G. Schulz, T. Cyronak, and B. D. Eyre. Seasonal variability of calcium carbonate precipitation and dissolution in shallow coral reef sediments. *Limnology and Oceanography* **9999**:1-16.
- Stuart-Smith, R. D., G. J. Edgar, N. S. Barrett, S. J. Kininmonth, and A. E. Bates. 2015. Thermal biases and vulnerability to warming in the world's marine fauna. *Nature* **528**:88-+.
- Suggett, D. J., L. F. Dong, T. Lawson, E. Lawrenz, L. Torres, and D. J. Smith. 2013. Light availability determines susceptibility of reef building corals to ocean acidification. *Coral Reefs* **32**:327-337.

- Suggett, D. J., M. E. Warner, D. J. Smith, P. Davey, S. Hennige, and N. R. Baker. 2008. Photosynthesis and production of hydrogen peroxide by Symbiodinium (Pyrrophyta) phylotypes with different thermal tolerances. *Journal of Phycology* **44**:948-956.
- Szmant, A. M. 1986. Reproductive ecology of Caribbean reef corals. *Coral Reefs* **5**:43-53.
- Szmant, A. M., and N. J. Gassman. 1990. The effects of prolonged bleaching on the tissue biomass and reproduction of the reef coral *Montastrea annularis*. *Coral Reefs* **8**:217-224.
- Tambutte, E., A. A. Venn, M. Holcomb, N. Segonds, N. Techer, D. Zoccola, D. Allemand, and S. Tambutte. 2015. Morphological plasticity of the coral skeleton under CO₂-driven seawater acidification. *Nature Communications* **6**.
- Tans, P., and R. Keeling. 2017. Recent Monthly Average Mauna Loa CO₂. NOAA/ESRL and Scripps Institution of Oceanography, San Diego, California, USA.
- Therneau, T. M. 2015a. *coxme: Mixed Effects Cox Models*.
- Therneau, T. M. 2015b. *A Package for Survival Analysis in S*.
- Thornhill, D. J., R. D. Rotjan, B. D. Todd, G. C. Chilcoat, R. Iglesias-Prieto, D. W. Kemp, T. C. LaJeunesse, J. M. Reynolds, G. W. Schmidt, T. Shannon, M. E. Warner, and W. K. Fitt. 2011. A Connection between Colony Biomass and Death in Caribbean Reef-Building Corals. *PLoS One* **6**.
- Towle, E. K., I. C. Enochs, and C. Langdon. 2015. Threatened Caribbean coral is able to mitigate the adverse effects of ocean acidification on calcification by increasing feeding rate. *PLoS One* **10**:e0123394.
- Urban, M. C. 2015. Accelerating extinction risk from climate change. *Science* **348**:571-573.
- Venn, A. A., E. Tambutte, M. Holcomb, J. Laurent, D. Allemand, and S. Tambutte. 2013. Impact of seawater acidification on pH at the tissue-skeleton interface and calcification in reef corals. *Proceedings of the National Academy of Sciences of the United States of America* **110**:1634-1639.
- Venti, A., A. Andersson, and C. Langdon. 2014. Multiple driving factors explain spatial and temporal variability in coral calcification rates on the Bermuda platform. *Coral Reefs* **33**:979-997.
- Veron, J. E. N. 2000. *Corals of the world*. Australian Institute of Marine Science, Townsville, Australia.
- Viechtbauer, W. 2010. Conducting meta-analyses in R with the metafor package. *Journal of Statistical Software* **36**:1-48.

- Von Euw, S., Q. H. Zhang, V. Manichev, N. Murali, J. Gross, L. C. Feldman, T. Gustafsson, C. Flach, R. Mendelsohn, and P. G. Falkowski. 2017. Biological control of aragonite formation in stony corals. *Science* **356**:933-+.
- Weis, V. M. 2010. The susceptibility and resilience of corals to thermal stress: adaptation, acclimatization or both? *Molecular Ecology* **19**:1515-1517.
- Widdicombe, S., S. Dupont, and M. Thorndyke. 2010. Laboratory experiments and benthic mesocosm studies. Publications Office of the European Union, Luxembourg.
- Wilcox, R. R. 2010. *Fundamental of Modern Statistical Methods: Substantially Improving Power and Accuracy, Second Edition*. Fundamental of Modern Statistical Methods: Substantially Improving Power and Accuracy, Second Edition:1-249.
- Winston, J. E. 1983. The Atlantic barrier-reef ecosystem at Carrie Bow Cay, Belize 1. Structure and communities. *Ecology* **64**:612-612.
- Yamashiro, H., H. Oku, and K. Onaga. 2005. Effect of bleaching on lipid content and composition of Okinawan corals. *Fisheries Science* **71**:448-453.
- Zeebe, R., and D. Wolf-Gladrow. 2001. *CO₂ in seawater: equilibrium, kinetics, and isotopes*. 1st edition. Elsevier Science, Amsterdam, Netherlands.